The role of RNA Polymerase III in the ageing process

Zhe Wang BSc MSc

SUBMITTED IN FULFILMENT OF THE REQUIREMENTS FOR THE DEGREE OF DOCTOR OF PHILOSOPHY

SCHOOL OF MOLECULAR BIOSCIENCES

COLLEGE OF MEDICAL, VETERINARY AND LIFE SCIENCES
UNIVERSITY OF GLASGOW

DECEMBER 2025

ABSTRACT

Ageing arises from the gradual accumulation of molecular and cellular damage that affects tissues in different ways and increases disease susceptibility. Nutrient-sensing pathways that regulate protein synthesis influence the rate of ageing, and studies in invertebrates have shown that reducing RNA Polymerase III (Pol III) activity can improve lifespan and stress tolerance. Reducing Pol III altered translational capacity in both invertebrate and vertebrate models. However, far less is known about how a reduction in Pol III activity influences mammalian physiology. This thesis addresses this gap using mice heterozygous for *Polr3b* (*Polr3b*$^{+/-}$) to achieve a partial loss-of-function in Pol III and examine how reduced Pol III activity affects molecular readouts of its function, reproductive performance, immune balance, and tissue integrity in age-associated contexts.

The first part of the thesis investigates molecular features associated with Pol III function across liver, brain, skeletal muscle, and primary dermal fibroblasts. *Polr3b* heterozygosity alters protein synthesis and the expression of Pol III components and regulators in a manner that is tissue- and sex-dependent, with effects observed in liver, brain, and dermal fibroblasts but not in skeletal muscle.

Phenotypic analyses reveal that reduced Pol III activity has systemic consequences. *Polr3b*$^{+/-}$ mice showed increased litter size at birth but impaired postnatal survival, including increased pre-weaning mortality and reduced male pup weight. Change in endocrine gene expression suggests altered ovarian function, supported by reduced *Cype19a1* expression in *Polr3b*$^{+/-}$ ovaries. In parallel, a retrospective cohort analysis identifies increased susceptibility to idiopathic dermatitis in *Polr3b*$^{+/-}$ females, accompanied by elevated circulating IL-6, splenomegaly, altered inflammatory gene expression, and changes in dermal composition, despite largely preserved skin structure.

The final experimental chapter examines liver physiology. Despite reduced *Polr3b* expression, no overt structural or pathological changes are observed. Instead, mild alterations in inflammatory gene expression suggest a role for Pol III in maintaining hepatic immune balance.

Together, these findings indicate that reduced Pol III activity in mammals produces subtle, tissue- and context-dependent effects rather than widespread dysfunction. While core tissue structure is largely preserved, Pol III activity influences reproductive outcomes, as well as protein synthesis and immune regulation in some tissues, highlighting its role as a regulator of metabolic and immune homeostasis *in vivo*. These findings provide evidence that modulation of Pol III-dependent translational capacity contributes to mammalian ageing and disease susceptibility.

TABLE OF CONTENTS

LIST OF FIGURES

LIST OF TABLES

ACKNOWLEDGEMENTS

First and foremost, I would like to express my sincere gratitude to my primary supervisor, Professor Colin Selman, for his guidance, encouragement, and support throughout my PhD. His professionalism, deep understanding of science, and the many discussions we had helped me develop my understanding of research and scientific thinking. I am also deeply grateful for the considerable time and effort he devoted to reading, correcting, and improving my thesis and other written work. Beyond the science, I am especially grateful for his patience, kindness, and understanding over the years. During periods when motivation was low, experiments were not going as planned, or personal circumstances affected my studies, he consistently offered support and encouragement. His willingness to listen, provide guidance, and help me work through challenges made a tremendous difference throughout my PhD journey.

I would also like to thank my secondary supervisor, Dr Ian Salt, for his expertise and valuable advice throughout this project. His insight, particularly in the areas of cellular and signalling biology, strengthened my understanding of the scientific questions explored in this thesis. I am deeply grateful to Dr Gillian Borland, a former member of the laboratory, for her support during my PhD study. Much of my laboratory training came from Gillian, and she played a major role in helping me develop the practical and analytical skills needed for research. Beyond teaching experimental techniques, she taught me how to approach troubleshooting logically and systematically, a skill that has remained invaluable throughout my PhD. I would also like to thank Mrs Jackie Thomson for her technical assistance. I am particularly grateful for her help with cell culture techniques and for her willingness to offer support whenever it was needed.

The most important people I would like to thank are my beloved mum and dad, Mrs Shie Liu and Mr Kezhao Wang, who have supported, encouraged, and believed in me throughout every stage of my life, including this PhD journey.

Mum and Dad, no words can truly express how grateful I am for everything you have given me. The love, care, and sacrifices you have made for our family are beyond measure. I have always known that I am fortunate to have parents who love me unconditionally and selflessly, and I will never take that for granted.

One of the reasons I chose to study ageing and longevity during my PhD is because of a simple wish: I hope that both of you can enjoy long, healthy, and happy lives, and remain by my side for a little longer. As my studies progressed, I came to realise that living beyond one hundred years in perfect health is an ambitious goal. Nevertheless, my wish remains unchanged. More than anything else, I hope you both enjoy many years of good health, happiness, and fulfilment in the future.

Mommy, you have always been my superhero. From my earliest memories, you devoted yourself to every aspect of my upbringing. You cared for me, encouraged me to stay active, taught me good manners, and together with Dad guided me in my studies throughout my school years. More importantly, you guided me through every stage of growing up. I greatly admire your insight into the world. Beyond that, you taught me many of the life skills that cannot be learned in a classroom: how to communicate with people, how to approach challenges thoughtfully, and how to navigate the world with confidence and kindness. To this day, I still admire your wisdom, determination, and ability to overcome any challenge that comes your way.

Daddy, you have always been the steady mountain behind our family. While Mum guided me through daily life, you provided us with security, protection, and unwavering support. I know that the responsibilities and pressures you carried over the years were really tough, and I have seen how hard you worked to provide opportunities and support for our family. I have always known how deeply you love and care for me. You and Mum have always been the best parents I could have wished for. Your strength, reliability, and constant belief in me have given me confidence throughout my life.

Dad and Mum, I am incredibly proud to be your daughter. Of all the things I could be grateful for in life, being raised by the two of you is one of the greatest blessings. Thank you for everything you have done for me. More than any achievement in my academic or future career, my greatest wish is that you both enjoy continued good health and many happy years ahead.

Also, to my little sister, Athena Wang, it is hard to believe how quickly you have grown up, I wish you all the happiness in the world as you become whoever you

want to be. Finally, without my family, I would not be where I am today. Their love and support have shaped the person I have become ☺

Apart from my supervisors and the lab group members for their academic support, I would also like to express my gratitude to several people in the school. Dr Paul Johnson, who helped me with my GLMM analysis in the fecundity chapter. Mr Cameron Thomson, who was very welcoming and offered me help with Masson Trichrome staining analysis. Dr Wai Kwong Lee from the School of Cardiovascular & Metabolic Health, who gave me access to their qPCR machine. As well as all the members of Biological Services for help with animal housing and routine checks.

Lastly, but certainly no less importantly, I want to thank all my besties and friends for their tremendous emotional support throughout my PhD journey. I love you all 🥰

AUTHOR'S DECLARATION

I confirm that the work presented within the thesis is my own. Information which is obtained from other sources has been referenced appropriately, and experiments which have been performed by others or as part of a collaboration have been clearly indicated.

Zhe Wang

DEFINITIONS/ABBREVIATIONS

AFAs	Antimicrobial fatty acids
AGC kinases	A highly conserved family of protein kinases which comprise cAMP-dependent protein kinase A, cGMP-dependent protein kinase G, and phospholipid-dependent protein kinase C
AMPs	Antimicrobial peptides
AMPK	AMP-activated protein kinase
ATP	Adenosine triphosphate
BCA	Bicinchoninic acid
CRAMP	Cathelicidin
CRISPR	Clustered Regularly Interspaced Short Palindromic Repeats
CV	Central vein (liver)
DSE	Distal sequence element
dWAT	dermal white adipose tissue
ECM	Extracellular matrix
EVs	Extracellular vesicles
FBS	Fetal bovine serum
FKBP12	FK506-binding protein 12
FOXC2	Forkhead box protein C2
GATA	GATA-binding proteins
GATA1	GATA-binding factor 1
H&E	Haematoxylin and Eosin
HGPS	Hutchinson-Gilford progeria syndrome
HLD8	Hypomyelinating leukodystrophy 8

HSP	Heat shock protein
ID	Idiopathic dermatitis
IIS	Insulin/IGF-1 signalling or Insulin/insulin-like growth factor signalling
InR	Insulin-like receptor
IRF	Interferon Regulatory Factors
IRS1	Insulin receptor substrate-1
KO	Knockout
LL-37	Human cathelicidin peptide
OXPHOS	Oxidative phosphorylation
PBS	Phosphate-buffered saline
PCR	Polymerase Chain Reaction
PKA	Protein kinase A
POLR3a	Polymerase (RNA) III (DNA directed) polypeptide A
POLR3b	Polymerase (RNA) III (DNA directed) polypeptide B
PP4	Protein phosphatase 4
Pph3	The catalytic subunit of the PP4 complex
Pre-rRNAs	Precursor ribosomal RNAs
Pre-tRNAs	Precursor transfer RNAs
PSE	Proximal sequence element
PT	Portal triad (liver)
PTEN	Phosphatase and tensin homolog
Q-Q plot	Quantile-quantile plot
ROS	Reactive oxygen species
RT-qPCR	Reverse Transcriptase quantitative PCR
SA-ß-gal	Senescence-associated ß-galactosidase

SASP	Senescence-associated secretory phenotype
SDS-PAGE	Sodium dodecyl sulfate-polyacrylamide gel electrophoresis
SEM	Standard error of the mean
S6K	Ribosomal protein S6 kinase
S6K1	Ribosomal protein S6 kinase 1
TBK1	TANK-binding kinase 1
TNF	Tumour necrosis factor
TOR	Target of rapamycin
mTOR	Mammalian target of rapamycin
TORC1	TOR complex 1
mTORC1	mTOR complex 1
mTORC2	mTOR complex 2
TSLP	Thymic stromal lymphopoietin
WT	Wild type
4H	Hypomyelination, Hypodontia and Hypogonadotropic Hypogonadism

Chapter 1: General Introduction

1.1 AGEING

1.1.1 Ageing and age-related diseases

Ageing is a complex and inevitable process marked by the gradual accumulation of cellular damage, molecular alterations, and functional decline over time (Lopez-Otin et al., 2013). These changes lead to reduced reproductive capacity, impaired homeostasis, and an increased likelihood of death in most living organisms (Lopez-Otin et al., 2013; Partridge, 2010). In humans, it is believed that ageing arises from the combined influence of intrinsic and extrinsic factors, including damage accumulation (e.g., DNA damage, oxidative damage, mitochondrial damage, and telomere shortening), environmental exposures, and lifestyle choices (Antell & Taczanowski, 1999; de Magalhães, 2025; Lopez-Otin et al., 2013).

At the organismal level, ageing phenotypes are highly complex and variable. Within a single tissue, multiple forms of molecular and cellular damage accumulate with age, and the spectrum and types of these changes differ across tissues and individuals (Finch & Kirkwood, 2000; Partridge, 2010). For example, even within one organism, not all tissues age in the same way. The skin ages due to intrinsic and extrinsic factors such as UV light exposure, leading to decreased skin thickness, collagen, and elasticity; the lungs suffer from pollution and ages lead to widening of alveolar ducts, reduced elasticity, and increased fibrosis; the liver accumulates metabolic stress, which leads to impaired metabolic pathways, hepatic cirrhosis, and fibrosis; and the brain experiences oxidative stress and protein aggregation (Hunt et al., 2019; Hwang et al., 2011; Schulte et al., 2019). These differences arise because each tissue has a different structure and function, therefore, encounters different forms of damage and pathology during ageing. Moreover, the diverse phenomena observed during ageing have contributed to the view that ageing does not represent a single linear process, but rather the outcome of numerous independent and stochastic mechanisms of damage accumulation that occur in parallel, each contributing to functional

decline in different ways (Finch & Kirkwood, 2000; Partridge, 2010). These cumulative changes lead to physiological deterioration and increase vulnerability to age-related diseases such as cancers, cardiovascular disorders, and neurodegeneration (Fabbri & Rabe, 2007).

Age-related conditions rarely occur in isolation. It is estimated that more than half of individuals aged ≥70 in the UK live with multimorbidity, defined as having two or more long-term conditions (Valabhji et al., 2024). Meanwhile, life expectancy has also risen markedly over the decades due to improvements in public health, particularly attributed to clean water, immunisation, and antibiotics (Partridge, 2010). In the UK, the life expectancy increased from 70.8 years in 1980 to 78.8 years in 2024 for men, and from 76.8 to 82.8 years for women over the same period (**Figure 1-1**) (Office for National Statistics, 2025). However, while life expectancy has increased, healthspan - the years lived free from age-related disease - has not increased at a comparable rate. This makes the 'ageing society' a defining feature of most developed and some developing countries. For example, the UK population grew by 8% between the 2011 and 2021 censuses, but the proportion aged ≥65 years rose to 19% in 2022, compared with only 13% in 1972 (Barton et al., 2024). This demographic shift highlights that ageing population is becoming a central social and health challenge.

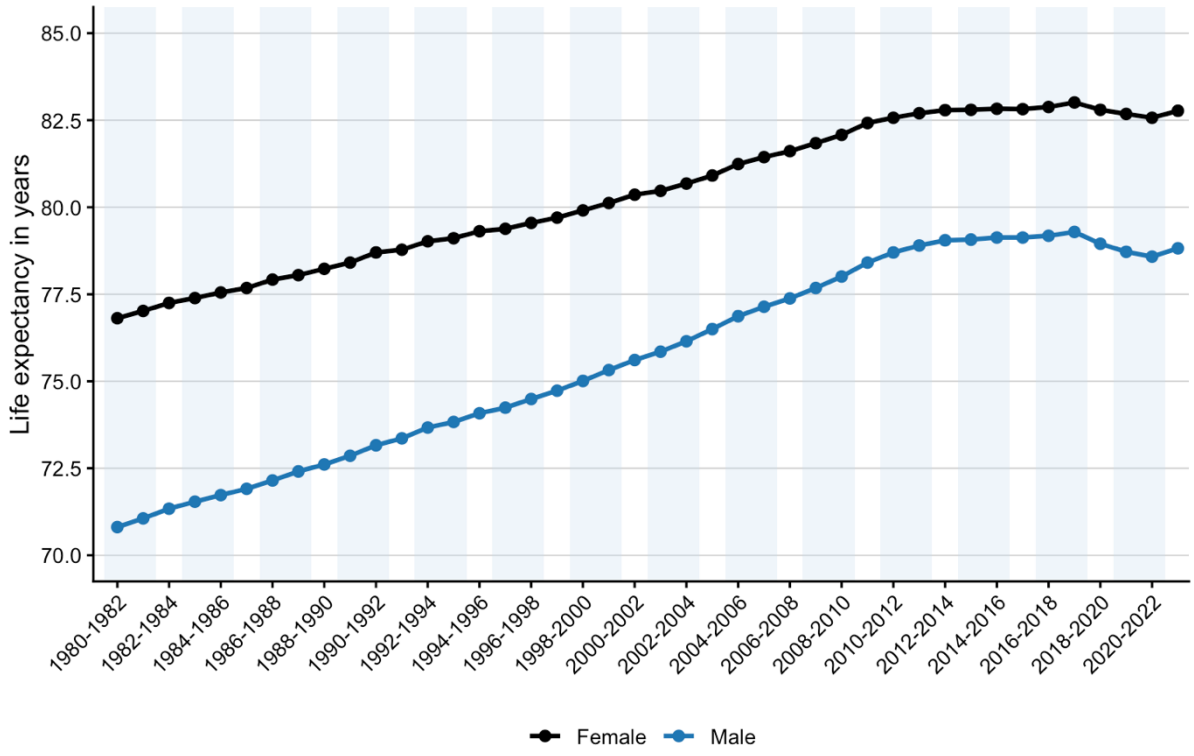

Figure 1-1 Life expectancy at birth in the United Kingdom (1980-2023) for males and females

Life expectancy at birth for males and females in the United Kingdom from 1980 to 2023. Values are derived from the ONS National Life Tables, which estimate period life expectancy using three-year aggregated mortality and population data. Source data contains public sector information licensed under the Open Government Licence v3.0.

1.1.2 Hallmarks of ageing in mammals

To understand how the diverse organismal and tissue-level changes arise in the ageing process, the cellular and molecular mechanisms of ageing are commonly considered through the framework of the hallmarks of ageing.

In mammals, ageing is proposed to involve a set of interconnected cellular and molecular processes (Guo et al., 2022; Lopez-Otin et al., 2013). Genomic instability, telomere attrition, epigenetic alterations, loss of proteostasis, deregulated nutrient sensing, mitochondrial dysfunction, cellular senescence, stem cell exhaustion, and altered intercellular communication are the main hallmarks that together drive physiological and functional decline during ageing.

Genomic instability arises from lifelong exposure to endogenous and exogenous DNA-damaging agents such as reactive oxygen species (ROS), DNA replication errors, and environmental genotoxins (Hoeijmakers, 2009; Lopez-Otin et al., 2013). Reinforcing DNA repair pathways or maintaining nuclear architecture integrity has been shown to delay progeroid phenotypes in animal models, highlighting their role in ageing (Guo et al., 2022; Lopez-Otin et al., 2013).

Telomere attrition, the progressive shortening of chromosome ends due to incomplete replication, limits cellular replicative capacity and promotes cellular senescence and apoptosis (Blackburn et al., 2006; Blasco, 2007). The role of telomere attrition in the ageing process has been demonstrated (Jaskelioff et al., 2011; Mojiri et al., 2021). Restoration of telomerase activity in mice reverted degenerative phenotypes across tissues (Jaskelioff et al., 2011). Overexpression of telomerase mRNA decreased inflammation and DNA damage markers in endothelial cells across various organs and increased the lifespan of progeria mice with Hutchinson-Gilford progeria syndrome (HGPS) (Mojiri et al., 2021). These studies demonstrate that telomere damage is a driver of age-related decline and disease risk.

Epigenetic alterations accumulate with age and include global DNA hypomethylation, locus-specific hypermethylation, and histone modification changes (Lopez-Otin et al., 2013). Reversion of epigenetic changes such as the sirtuin family (SIRT1, SIRT6) and H4 acetylation, can improve age-related

memory impairment in mice and ameliorate the premature phenotypes as well as the lifespan in the progeroid mice, respectively (Krishnan et al., 2011; Peleg et al., 2010). Suggesting that re-establishing youthful epigenetic states may be therapeutically beneficial.

Loss of proteostasis, which is the impairment in protein homeostasis, results from reduced chaperone activity, impaired proteasome and autophagy function, and accumulation of misfolded or aggregated proteins (Lopez-Otin et al., 2013; Powers et al., 2009). This contributes to neurodegenerative diseases such as Alzheimer's and Parkinson's, and other age-related diseases, including cataracts (Lopez-Otin et al., 2013; Powers et al., 2009). Interventions that enhance autophagy (e.g. mTOR inhibitor rapamycin, spermidine) or chaperone activity and delay age-associated pathology and extend lifespan in model organisms (Hipp et al., 2019; Lopez-Otin et al., 2013).

Deregulated nutrient-sensing pathways involve the disruption of key metabolic signalling networks, including insulin/insulin-like growth factor-1 (IIS), mammalian target of rapamycin (mTOR), and AMP-activated protein kinase (AMPK), which coordinate nutrient availability with cellular energy status (Guo et al., 2022; Lopez-Otin et al., 2013). In mammals, the mammalian TOR (mTOR) signalling is sensitive to nutrients and integrates environmental inputs to regulate growth, metabolism, protein synthesis, and autophagy (Willis & Moir, 2018). mTOR kinase consists of two distinct protein complexes: mTOR complex 1 (mTORC1) and mTOR complex 2 (mTORC2). Of these, mTORC1 enhances the initiation of translation and coordinates anabolic and catabolic balance in response to environmental stimuli including nutrients (Saxton & Sabatini, 2017). On the other hand, IIS integrates hormonal cues with metabolic state through PI3K-Akt signalling, which in turn modulates the tuberous sclerosis complex (TSC) 1/TSC2 complex and thereby regulates mTORC1 activity (Templeman & Murphy, 2018). mTORC1 is stimulated by nutrient availability and promotes anabolic processes such as protein, lipid and nucleotide synthesis, while simultaneously suppressing catabolic pathways including autophagy (González & Hall, 2017). In contrast, AMPK is activated when cellular energy levels fall and inhibits mTORC1 to conserve resources, highlighting the opposing roles of these pathways in nutrient sensing and growth control (Guo et al., 2022). Reduced IIS, mTOR activity, or the mTORC1 substrate S6K1 activity extends lifespan across

model organisms, whereas excessive anabolic signalling accelerates ageing (Fontana et al., 2010; Harrison et al., 2009; Lopez-Otin et al., 2013; Selman et al., 2009). These findings together highlight links between nutrient availability, energy perception, and longevity.

Mitochondrial dysfunction manifests as reduced respiratory efficiency, increased ROS generation, and impaired mitophagy, which eventually cause the ageing of the organism (Guo et al., 2022). Mitochondria are the main sites of oxidative phosphorylation, where nutrients are converted into adenosine triphosphate (ATP), providing the energy required for normal cellular functions (Davis et al., 2013). Persistent and severe mitochondrial damage disrupts mitochondrial dynamics, including fusion, fission, and mitophagy, which are essential for maintaining neuronal homeostasis, synaptic transmission, and cell survival, thereby promoting inflammation, metabolic impairment, and neurodegeneration (Bustamante-Barrientos et al., 2023; Haigis & Yankner, 2010; Lopez-Otin et al., 2013).

In contrast, mild mitochondrial stress can elicit an adaptive response known as mitohormesis, whereby low levels of mitochondrial perturbation promote cellular resilience and improved organismal health (Barcena et al., 2018; Ristow & Schmeisser, 2014). This concept reflects a biphasic response in which sublethal stress enhances stress resistance and metabolic adaptation, while excessive stress remains detrimental. Mitohormesis is often mediated by transient increases in mitochondrial ROS and associated signalling pathways, which activate protective mechanisms including antioxidant responses, metabolic rewiring such as mTOR, and stress-response pathways, and in some contexts, extend healthspan and lifespan in some organisms (Barcena et al., 2018; Cheng et al., 2023).

Cellular senescence is a stable cell-cycle arrest that can have both detrimental and beneficial effects, and is triggered by telomere erosion, DNA damage, or oncogenic stress (Lopez-Otin et al., 2013). Senescent cells remain metabolically active; they exhibit irregular nuclear size with the loss of expression of the nuclear lamina protein lamin B1, and are coupled to the accumulation of defective organelles including mitochondria, endoplasmic reticulum, and lysosomes (B. Wang et al., 2024). They also secrete a variety of pro-

inflammatory cytokines, growth factors, and matrix-remodelling enzymes - collectively known as the senescence-associated secretory phenotype (SASP) - which alter the tissue microenvironments and promote inflammation (Campisi & d'Adda di Fagagna, 2007; Lopez-Otin et al., 2013; B. Wang et al., 2024). Manipulation of key senescence regulators, such as $p16^{Ink4a}$ and the tumour suppressor p53, has shown that both excessive and insufficient senescence can be harmful; modulation of these pathways, either decreased or mildly increased the activity, can both alleviate age-related dysfunction or extend lifespan in mice, supporting the dual and context-dependent role of cellular senescence in ageing (Lopez-Otin et al., 2013).

Stem cell exhaustion reflects the gradual loss of regenerative capacity in self-renewing tissues such as marrow, muscle, and skin (Lopez-Otin et al., 2013). Accumulated DNA damage, telomere shortening, and niche deterioration all contribute (Lopez-Otin et al., 2013). The pharmacological interventions, particularly mTORC1 inhibition with rapamycin, have been found to improve stem cell function in the epidermis (Castilho et al., 2009).

Finally, **altered intercellular communication** encompasses chronic, low-grade inflammation (termed inflammaging), disrupted neuroendocrine signalling, and impaired neurohormonal signalling (Lopez-Otin et al., 2013). Beyond cytokine-driven inflammation, senescent cells also modify their local environment through SASP factors and extracellular vesicles (EVs), which transfer tRNAs, proteins, lipids, and other stress signals to neighbouring or distant cells, and these processes collectively reinforce senescence and contribute to broader functional decline across the organism (Guo et al., 2022). Altogether, these hallmarks form an interconnected network of damage responses that collectively drive organismal ageing and highlight the difficulty of disentangling the mechanistic basis for the ageing process.

Notably, several of these hallmarks are directly implicated in **reproductive ageing**, and in many cases manifest earlier or more prominently in reproductive tissues, suggesting that reproductive decline represents a sensitive readout of systemic ageing processes (S. Wang et al., 2024). For instance, stem cell exhaustion/deterioration in the ovary and testis contributes to reduced oocyte and sperm quality, leading to age-related infertility in mice (Ryu et al., 2006;

Sharma & Bhartiya, 2022). Mitochondrial dysfunction disrupts energy metabolism and oxidative balance, contributing to diminished oocyte quality and impaired follicle development (Somasundaram et al., 2024; Zhang et al., 2025). Accumulated DNA damage, compromised DNA repair systems, and a range of epigenetic changes are observed in oocytes of older females (Chamani & Keefe, 2019; Wu et al., 2025). In males, ageing is associated with changes in DNA methylation and histone modifications in sperm, affecting reproduction and offspring health (Ajayi et al., 2024). Moreover, deregulated nutrient-sensing pathways, including insulin/IGF-1 and mTOR signalling, impair reproductive function across model organisms (Filer et al., 2017; Yuan et al., 2023). Together, these observations indicate that the molecular hallmarks of ageing converge on the reproductive system, where their cumulative effects contribute to a progressive decline in fertility and reproductive capacity, positioning reproductive ageing as an early and integrative biomarker of organismal ageing.

Since many of these ageing hallmarks were defined and tested through experimental systems, the choice of model organism is central to how ageing mechanisms are identified and interpreted.

1.1.3 Model organisms in ageing research

The discovery of long-lived *Caenorhabditis elegans* strains more than forty years ago marked a turning point in ageing research (Klass, 1983). In this study, Klass isolated several mutant lines with a significantly extended lifespan using a mutagenesis screen in a temperature-sensitive sterile background. Some mutants showed reduced pharyngeal pumping and lower food intake, and their extended lifespan was closely associated with the degree of reduced feeding. Other exhibited traits similar to the dauer stage, a semi-quiescent, stress-resistant larval state in which growth, development, and feeding stop, while mobility and chemotactic responses are maintained. Klass also noted that screening approximately eight thousand mutagenized genomes did not reveal mutants that extended lifespan through a single specific mechanism, suggesting that longevity is influenced by multiple biological processes rather than controlled by a single gene. Since this work, *C. elegans* (worm), *Drosophila melanogaster* (fruit fly),

and *Mus musculus* (house mouse) have become the key model organisms in the ageing field, valued for their relatively short lifespans, ease of husbandry, rapid generation times, high-quality sequencing data, and well-annotated genomic resources (Holtze et al., 2021). Although these organisms have been central to ageing research, studies based solely on them have important limitations. Their biological features differ in fundamental ways from those of longer-lived species, which means that some findings may not translate directly to humans. Partridge and Gems (2002) emphasised that organisms age for different biological reasons because they live different lives, and this variation can shape both the pace and the mechanisms of ageing. Reliance on a narrow set of species may therefore overlook forms of longevity adaptation that arise under different ecological or physiological conditions. Important longevity adaptations present in other species may be missed if the field remains centred on these classical models.

These limitations therefore provide a rationale for extending ageing research into mammalian systems. This is particularly important for pathways such as Pol III, where invertebrate studies have identified clear links with lifespan, but mammalian studies show more complex and tissue-specific outcomes (Borland et al., 2024; Filer et al., 2017; Malik, Goncalves Silva, et al., 2024). Studying Pol III in mammals therefore helps determine whether mechanisms first identified in classical model organisms are conserved, modified, or reversed in longer-lived vertebrate physiology. This need to compare mechanisms across species is particularly relevant when considering interventions that modify conserved growth and nutrient-sensing pathways.

1.1.4 Dietary, genetic, and pharmacological means to extend longevity

Despite these species differences, many molecular changes associated with ageing, including IIS, mTOR, AMPK and adrenergic signalling, are conserved across evolution (Khan et al., 2019). Ageing itself is also plastic and can be shaped in model organisms by nutrient, genetic, and pharmacological interventions, as discussed below, which demonstrates that trajectories of decline are not fixed (Blasimme, 2021)

Dietary means to extend longevity

Dietary and nutrient-based approaches to extend lifespan date back to the early work of McCay, who showed that reducing the amount of food available to young rats, which lowered overall calorie intake, slowed growth and extended lifespan, with more pronounced effects in males (McCay et al., 1935). Following McCay's work, it became clear that the effects of dietary restriction extend well beyond simple reductions in energy intake. Studies in rodents have shown that altering the balance of dietary protein, specific amino acids, or fat can influence lifespan and later-life function (healthspan) independently of total calories, and that changes in feeding patterns can produce additional benefits (Selman, 2024). Experimental work across different mouse strains demonstrates that dietary restriction improves metabolic flexibility, lowers circulating insulin and IGF-1, modulates mTORC1 and downstream anabolic signalling, and reduces age-associated impairments in glucose homeostasis and cardiac and hepatic function (Selman, 2024). The variations of these responses depend on genetic background, sex, age of intervention, and the severity of restriction (Selman, 2024).

Genetic means to extend longevity

In addition to dietary interventions, genetic studies have provided direct evidence that ageing can be modified by altering conserved signalling pathways. In the early 1990s, independent studies in *C. elegans* first revealed that single-gene mutations can dramatically extend lifespan. For example, worms with loss-of-function mutations in *daf-2*, which encodes an insulin/IGF-1-like receptor, lived more than twice as long as normal (Kenyon, 2005). This discovery foreshadowed similar phenomena in other organisms. In *D. melanogaster*, reducing insulin/IGF signalling likewise promotes longevity. Clancy et al. (2001) found that mutation of *chico*, which encodes an insulin receptor substrate (IRS) protein, extended the flies' median lifespan by up to 48%. Tatar et al. (2001) further reported that a hypomorphic mutation in the insulin-like receptor (InR) gene, which is the insulin/IGF receptor homolog in *D. melanogaster*, produced smaller adults with as much as an 85% increase in longevity. Building on these

invertebrate findings, mammalian studies showed that suppressing the IGF-1 signalling axis can similarly delay ageing.

Notably, unlike worms and flies, mice have separate insulin and IGF-1 receptors. Holzenberger et al. (2003) demonstrated that *Igf1r*$^{+/-}$ mice lived about 26% longer than wild-type controls, with lifespan extension most pronounced in females. Likewise, Selman et al. (2008) reported that mice lacking *Irs1* (insulin receptor substrate-1) (*Irs1*$^{-/-}$) were long-lived and showed delayed age-related decline, whereas deletion of Irs2 did not extend lifespan (Selman et al., 2008). Together, these findings established that reduced insulin/IGF-1 signalling by single-gene mutations can extend lifespan and slow ageing across evolutionarily distant species.

Furthermore, the TOR kinase functions as a central nutrient and amino acid sensor that promotes anabolic processes, including protein and lipid synthesis, while inhibiting catabolic pathways such as autophagy under nutrient-rich condition (Laplante & Sabatini, 2012; Saxton & Sabatini, 2017). Inhibiting the TOR pathway by gene modulation also increases lifespan in many species (Kaeberlein et al., 2005; Kapahi et al., 2004; Vellai et al., 2003). Notably, one study by Bonawitz and colleagues found that deleting the TOR1 gene in yeast extended chronological lifespan mainly by increasing the translation of mitochondrial DNA-encoded oxidative phosphorylation complex subunits (Bonawitz et al., 2007). A study by Wu and colleagues demonstrated that mice with reduced mammalian TOR (mTOR) activity, which had increased lifespan, showed no changes in food intake, glucose homeostasis, or metabolic rate while exhibiting a reduction in several ageing tissue biomarkers (Wu et al., 2013). Additionally, deletion of the ribosomal protein S6 kinase 1 (*S6k1*$^{-/-}$), a key downstream effector of mTOR, also increased lifespan and improved late-life health in mice (Selman et al., 2009).

More recently, studies in worms and flies identified RNA polymerase III (Pol III) as a downstream effector of TORC1 in longevity regulation (Filer et al., 2017; Malik, Goncalves Silva, et al., 2024). Borland and colleagues additionally found that mice heterozygous for the Pol III subunit *Polr3b* (*Polr3b*$^{+/-}$) displayed some sex- and organ-specific benefits for late-life health (Borland et al., 2024). Not only that, deletion of Maf1, a global repressor of Pol III, also showed extended

lifespan in *D. melanogaster* and *M. musculus*, and the long-lived *Maf1*$^{-/-}$ mice exhibited improvements in metabolic health (Bonhoure et al., 2015; Bonhoure et al., 2020; Xu et al., 2025).

Pharmacological means to extend longevity

The identification of the above nutrient- and growth-regulatory pathways has also enabled pharmacological approaches to target ageing mechanisms. One of the most studied is rapamycin, a macrocyclic lactone produced by the bacterium *Streptomyces hygroscopicus* (Sehgal et al., 1975). Rapamycin was initially found to bind to FKBP12 in *Saccharomyces cerevisiae*, and this rapamycin-FKBP12 complex was subsequently found to inhibit TOR (Brown et al., 1994; Cafferkey et al., 1993; Sabatini et al., 1994). Rapamycin treatment reduces phosphorylation of S6 by mTORC1 and extends lifespan (Bjedov et al., 2010; Harrison et al., 2009; Zhang et al., 2014). This supports the idea that rapamycin promotes longevity primarily through inhibition of mTORC1 (Lamming et al., 2013). Other compounds have also shown effects. Trametinib, a Ras inhibitor, extends fly lifespan by ~10% by blocking Ras-Erk signalling downstream of IIS (Slack et al., 2015). Combining interventions can be synergistic: trametinib, rapamycin, and lithium (a drug which offsets some negative effects of TOR and IIS inhibition) act additively to extend lifespan in flies (Castillo-Quan et al., 2019). More recently, combined trametinib and rapamycin treatment has also shown longevity benefits in mice (Gkioni et al., 2025).

1.2 RNA POLYMERASE III

1.2.1 Eukaryotic RNA polymerases and core functions of Pol III

In eukaryotic cells, transcription is carried out by three nuclear RNA polymerases (Kulaberoglu et al., 2021). RNA polymerase I (Pol I) transcribes most ribosomal RNAs (rRNAs) except 5S rRNA; RNA polymerase II (Pol II) transcribes all protein-coding messenger RNAs (mRNAs) and several small nuclear non-coding RNAs (snRNAs); RNA polymerase III (Pol III) is the largest and most complex of the three enzymes, responsible for transcribing a diverse set of short non-coding

RNAs, including 5S rRNA, tRNAs, 7SL RNA, 7SK RNA, U6 type snRNAs, Alu RNA, H1 RNA, RNase MRP RNA, Y RNA, and vault RNAs (Kulaberoglu et al., 2021; Lesniewska & Boguta, 2017; Schramm & Hernandez, 2002; Yee et al., 2007).

The major Pol III products are tRNAs and 5S rRNA, which directly support protein synthesis. tRNAs deliver amino acids to the ribosome during translation, whereas 5S rRNA forms part of the large ribosomal subunit and contributes to ribosome structure and function (Moir & Willis, 2013). Together, 5S rRNA and tRNAs represent around 15% of total cellular RNAs by weight, reflecting their abundance (Moir & Willis, 2013). Pol III also produces several short non-coding RNAs with more specialised roles. For example, 7SL RNA forms the scaffold of the signal recognition particle, directing nascent polypeptides into the endoplasmic reticulum (Marshall & White, 2008; Moir & Willis, 2013); H1 RNA is the RNA subunit of RNase P, which is required for pre-tRNA processing (Jarrous, 2017); and 7SL RNA forms the scaffold of the signal recognition particle, which directs nascent polypeptides into the endoplasmic reticulum (Moir & Willis, 2013). Some transcripts, such as Y RNAs or vault RNAs, remain less well understood but are implicated in processes ranging from RNA stability to stress responses. The wide range of roles that the Pol III transcripts play highlight their essential contributions not only to translation, but also RNA maturation, protein targeting, gene regulation, and stress-related cellular functions. At the same time, Pol III activity is energetically costly. The tight regulation of these products is thought to conserve metabolic resources and optimise energy allocation, particularly under nutrient stress or other unfavourable conditions (Willis & Moir, 2018). Importantly, the functional diversity of Pol III transcripts depends on a specialised transcriptional machinery, which is organised according to promoter type.

1.2.2 Structure and transcriptional regulation of RNA Polymerase III

In mammals, Pol III genes are classified into three main types based on the promoter architecture, and the components of this system are evolutionarily conserved throughout the eukaryotic kingdom. All three types require TFIIIB, comprising the B double prime 1 (BDP1), TATA-box binding protein (TBP), and B-

related factor 1 (BRF1; for type I and type II promoters) or BRF2 (for type III promoters), to recruit Pol III complex onto DNA upstream of the transcription start site (TSS) (Park et al., 2017; Willis & Moir, 2018). **Figure 1-2** illustrates the machinery of Pol III based on the three promoter types. In detail, promoter in type I (currently restricted to 5S rRNA, therefore the Pol III type I promoter is also known as 5S promoter) and type II (various tRNAs) are gene-internal, in which TFIIIC, that binds intragenic promoter elements A box, IE, and C box (for type I) or A box and B box (for type II) recruit TFIIIB to the site to start the transcription (Lesniewska & Boguta, 2017; Park et al., 2017). It is known that the C box is conserved in the 5S promoters of different species; therefore, the encoding of the small ribosomal RNA is highly conserved and consistent across eukaryotic species. Type III (such as U6 snRNA, 7SK RNA, H1 RNA), with a gene-external promoter, possesses a core promoter consisting of TATA-box, proximal sequence element (PSE), and an enhanced promoter distal sequence element (DSE), alternatively (Park et al., 2017; Schramm & Hernandez, 2002). Besides, the TATA-box is not exclusive to type III promoter, it is also found in some hybrid Pol III promoters (yeast US snRNA) (Brow & Guthrie, 1990; Eschenlauer et al., 1993). The diverse promoter types, resulting from different protein-protein or protein-DNA interactions within the promoter elements, allow Pol III to regulate a wide array of non-coding RNAs with roles in translation, RNA processing, and gene regulation in eukaryotic cells. This promoter organisation provides the basis for Pol III transcription, but Pol III output is also strongly controlled by nutrient- and growth-responsive signalling pathways.

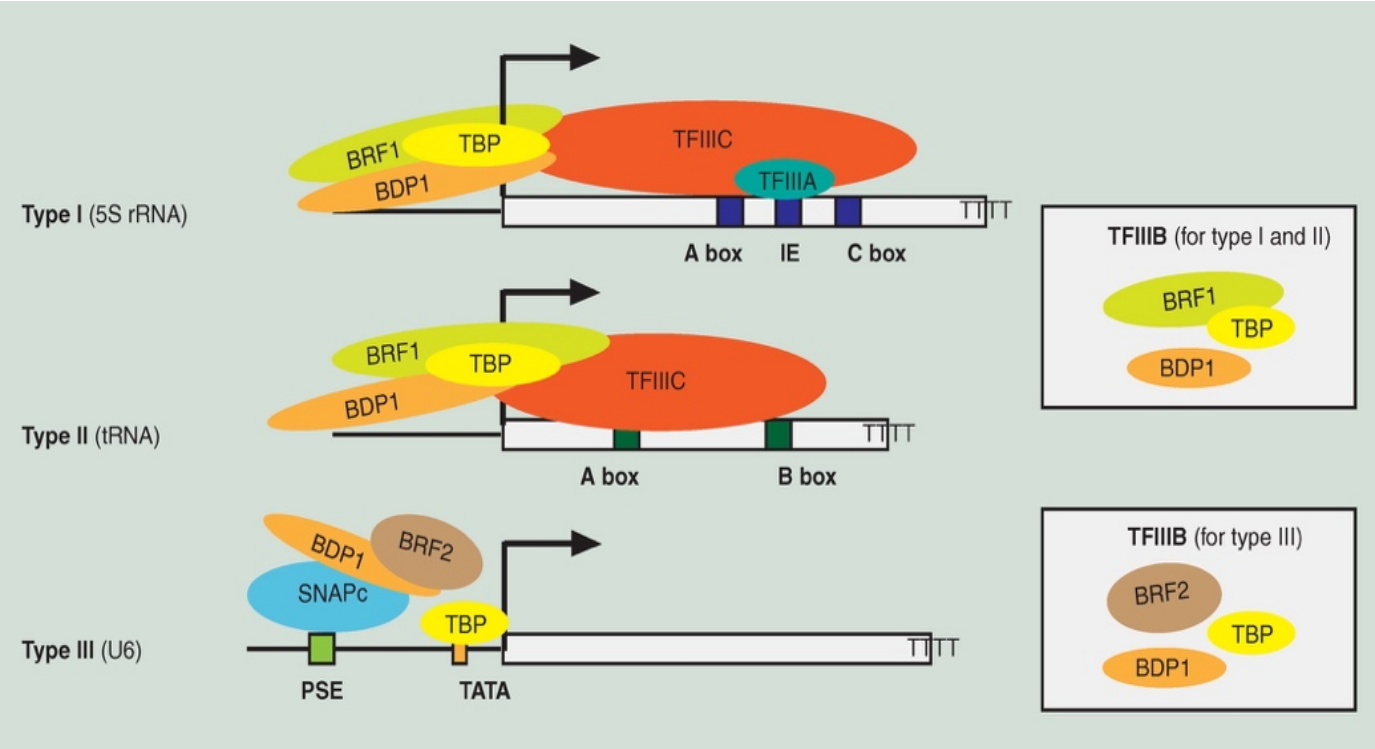

Figure 1-2 Illustration of the machinery of Pol III based on the three promoter types

Pol III promoters are classified into three types. Type I (5S rRNA genes): internal promoters containing A and C boxes; Type II (tRNA genes): Internal promoters containing A and B boxes; Type III (U6, 7SK, H1 RNA, etc.): External promoters with TATA-box, proximal sequence element (PSE), and distal sequence element (DSE). The relative positions of BDP1 and BRF1 are based on a ChIP-seq experiment in human cells, as reported in a study by Canella et al. (2010). Diagram reproduced from Park et al. (2017) under the Creative Commons Attribution-NonCommercial-NoDerivatives 4.0 International License (CC BY-NC-ND 4.0). No changes were made.

1.2.3 The TOR-Maf1-Pol III pathway and longevity

The connection between Pol III transcription and nutrient signalling was first established through studies of TOR-dependent transcriptional control. Work in yeast in the late 1990s first showed that inhibition of TOR signalling suppressed the transcription of ribosomal RNA (Pol I), ribosomal protein genes (Pol II), and Pol III-transcribed genes 5S rRNA and tRNAs (Li et al., 2000; Nierras & Warner, 1999; Powers & Walter, 1999; Zaragoza et al., 1998). More recent studies demonstrated that partial inhibition of Pol III increased chronological lifespan in *S. cerevisiae*, and extended the lifespan of *C. elegans* and *D. melanogaster* (Filer et al., 2017; Malik, Goncalves Silva, et al., 2024), In pioneering studies, Filer et al. (2017) demonstrated that conditional degradation of the largest Pol III subunit (C160/RPC160) led to improved survival during stationary phase (chronological lifespan) in *S. cerevisiae*. Similarly, knockdown of *rpc-1* (the worm Pol III largest subunit gene) by RNAi in adult *C. elegans* extended their lifespan. In *D. melanogaster*, heterozygous mutation of another Pol III subunit (dC53 gene) reduced Pol III expression and significantly increased female fly lifespan. These interventions did not drastically impair development or fertility when applied in adulthood, yet they showed a clear longevity benefit, implying that normal Pol III activity levels promote ageing in these organisms.

Notably, lifespan extension by rapamycin is not additive with Pol III knockdown (gut-specific dC160 RNAi) in flies, and rapamycin feeding inhibited phosphorylation of S6K as well as reproduction, while dC160 RNAi flies did not have these effects. These consequences together indicate that Pol III mediates the ageing process downstream of TORC1 (Filer et al., 2017). Similar observations have been made in *C. elegans*, where Malik, Goncalves Silva, et al. (2024) reported that the contribution of Pol III to longevity depends on the timing of TORC1 inhibition. In adults, TORC1 inhibition extends lifespan only if Pol III activity is reduced, and inhibiting TORC1 or Pol III both impaired reproduction, indicating that Pol III and TORC1 act on the same pathways in longevity and reproduction, and Pol III is a necessary downstream effector of adult TORC1 signalling in *C. elegans*. However, when TORC1 is suppressed during development, lifespan extension occurs independently of Pol III, revealing developmental mechanisms that do not require Pol III downregulation.

MAF1, a general repressor of Pol III transcription, is a key mediator of the TORC1-Pol III axis. Under nutrient-rich, growth-promoting conditions, TORC1 phosphorylates MAF1 to inactivate it, thereby relieving Pol III from MAF1 suppression to start the transcription (Wei et al., 2009). Conversely, when TORC1 is inhibited by starvation or rapamycin, MAF1 rapidly dephosphorylates and relocates to the nucleus to inhibit Pol III transcription (Shor et al., 2010). Detailed mechanisms of MAF1 are shown in **Chapter 3 of Figure 3-1**. This TOR-MAF1-Pol III signalling module is highly conserved. It was first mechanically characterised in *S. cerevisiae* (Pluta et al., 2001; Upadhya et al., 2002). Mammalian studies confirmed that mTORC1 phosphorylates MAF1 at conserved sites and that active mTORC1 is necessary to keep Pol III active (Shor et al., 2010). The same regulation of MAF1 by TOR signalling on the Pol III activity was also observed in *D. melanogaster* (Marshall et al., 2012; Sriskanthadevan-Pirahas et al., 2018). Together, these studies show that the TOR-MAF1-Pol III signalling module is highly conserved from yeast to mammals. In detail, the tuberous sclerosis complex TSC1 and TSC2 that located upstream of TORC1 acts as an important negative regulator of mTORC1 activity. Growth factor signalling through PI3K-Akt inhibits the TSC1/TSC2 complex, thereby allowing Rheb-dependent activation of mTORC1 (Dibble & Cantley, 2015). When nutrients and growth signals are abundant, activated mTORC1 promotes anabolic metabolism and phosphorylates downstream targets including S6K1 and 4E-BP1, while also phosphorylating MAF1 and reducing its ability to repress Pol III transcription (Battaglioni et al., 2022; Michels et al., 2010). In this state, Pol III-dependent production of tRNAs and 5S rRNA supports increased translational capacity and growth. Conversely, nutrient limitation, stress, or rapamycin-mediated TORC1 inhibition promotes MAF1 dephosphorylation and nuclear localisation, leading to repression of Pol III transcription (Michels et al., 2010; Moir & Willis, 2013). Overactivation of mTORC1, such as through impaired TSC1/TSC2 function, is associated with excessive anabolic signalling, reduced autophagy, altered proteostasis, and tissue dysfunction, all of which are relevant to ageing biology (Guillen & Benito, 2018; Panwar et al., 2023). Therefore, the TSC1/TSC2-mTORC1-MAF1-Pol III axis links nutrient sensing to RNA production, protein synthesis, cellular growth, and ageing-related stress responses.

Given that Pol III inhibition promotes longevity in invertebrate animal models, one might expect that increasing Pol III activity would accelerate ageing. Surprisingly, the opposite was observed in certain mammalian settings. Bonhoure et al. (2015) generated whole-body Maf1-knockout mice that showed elevated Pol III-dependent transcription (Bonhoure et al., 2020) to examine the effects of elevated Pol III activity on mammals. Rather than suffering from over-growth or early ageing, these *Maf1*$^{-/-}$ mice displayed metabolic inefficiency and resistance to diet-induced obesity. They ate slightly less and expended more energy than their wild-type littermates, resulting in a lean phenotype and protection from diet-induced fatty liver disease. They also exhibited a significant increase in lifespan, an effect most pronounced in female mice. Mechanistically, loss of MAF1 causes unchecked and elevated Pol III activity, leading to higher energy expenditure and accelerated turnover/degradation of pre-tRNAs. These mice also showed metabolic shifts, including the accumulation of the polyamine spermidine, which in turn induces autophagy. Enhanced autophagy is thought to underlie the improved healthspan and longevity of these MAF1-deficient mice, consistent with the pro-longevity role of autophagy observed in other model organisms (Eisenberg et al., 2009). These findings suggest that Pol III upregulation via loss of MAF1 can also produce pro-longevity metabolic phenotypes, likely by triggering compensatory stress responses such as autophagy through an energetically wasteful overproduction of pre-mature tRNAs. To better interpret these apparently contrasting findings, it is important to consider the diversity of experimental models used to study Pol III function *in vivo*. Differences in genetic manipulations, species, and developmental timing can lead to distinct phenotypic outcomes, particularly for essential processes such as transcription, translation, and growth regulation. Animal models of Pol III dysfunction therefore provide a useful framework to examine how altered Pol III activity influences development, metabolism, and tissue homeostasis (**Table 1-1**). Together, the animal models summarised in **Table 1-1** illustrate that the physiological consequences of altered Pol III activity depend on genetic context, tissue specificity, and the nature of the perturbation.

Table 1-1 Animal models of Pol III dysregulation and associated phenotypes

Model	Genetic context	Perturbation	Key phenotype(s)	Reference
C. elegans	*rpc-1*	Adult RNAi knockdown	Increased lifespan; reduced age-associated intestinal pathology	(Filer et al., 2017)
D. melanogaster	$dC53^{EY/+}$	Heterozygous partial loss-of-function	Increased lifespan	(Filer et al., 2017)
Mouse ($Maf1^{-/-}$)	Global *Maf1* loss	Constitutive knockout; increased Pol III occupancy	Lean, obesity-resistant phenotype; female lifespan extension on chow diet	(Bonhoure et al., 2015; Bonhoure et al., 2020)
Mouse ($Polr3b^{+/-}$)	Reduced *Polr3b* dosage	Heterozygous partial loss-of-function	No lifespan extension; sex- and organ-associated ageing phenotypes	(Borland et al., 2024)
Mouse ($Polr3b^{loxP/loxP}$)	Intestinal epithelial *Polr3b* deletion	Conditional hypomorphic/partial loss-of-function	Reduced survival and growth; impaired crypt proliferation; increased crypt apoptosis	(Kieckhaefer et al., 2016)
Mouse ($Polr3b^{R103H/R103H}$)	POLR3-HLD *Polr3b* p.Arg103His	Homozygous disease-associated knock-in	Embryonic lethality at day 9.5; impaired Pol III complex biogenesis	(Choquet, Pinard, et al., 2019)
Mouse ($Polr3a^{KI/+}$)	Olig2-lineage *Polr3a* knockin	Conditional disease-associated knock-in	Growth delay; neurobehavioural deficits; cerebral and spinal hypomyelination	(Merheb et al., 2021)
Danio rerio (*slim jim* mutation)	*polr3b* splice-site mutation	Partial loss-of-function	Intestinal and exocrine pancreatic hypoplasia; reduced progenitor-cell proliferation	(Yee et al., 2007)

From what is described above, it is now known that the role of Maf1 and Pol III longevity is complex and is model and context dependent. Conversely to some of the previous studies mentioned above, Borland et al. (2024) using the Polr3b$^{+/-}$ heterozygous mutant found that *Polr3b*$^{+/-}$ mice did not live longer than wild-type controls in either sex. At the same time, these mice displayed both beneficial and detrimental phenotypes affecting healthspan, with effects varying by organ and sex. These effects included smaller body mass and improved gut barrier integrity (the opposite of females) found in the *Polr3b*$^{+/-}$ males, and better bone health found in the *Polr3b*$^{+/-}$ females. Collectively, research across model systems identified the TOR-MAF1-Pol III axis as an evolutionarily conserved mechanism linking growth control to ageing. In lower organisms, reducing Pol III activity promotes longevity. However, in mammals, the results become complicated, as both Pol III inhibition and Pol III hyperactivation (via MAF1 loss) have been reported to extend life or health spans in different models. This paradox highlights the still-emerging understanding of how cellular translational capacity interfaces with ageing biology, and it suggests that the downstream consequences of Pol III activity, from proteostasis, energy utilisation to stress signalling, can shift the balance toward longevity or pathology depending on physiological context.

1.2.4 Pol III-RIG-I innate immune signalling pathway

Beyond its role in growth and translational control, Pol III also contributes to innate immune signalling (**Figure 1-3**), providing another route through which Pol III activity may influence ageing-related tissue phenotypes. In addition to transcribing endogenous short non-coding RNAs, Pol III transcribes cytosolic AT-rich DNA, including DNA derived from some viruses, and transcribes it into 5'-triphosphate RNA (Ablasser et al., 2009; Hornung & Latz, 2010). These RNA intermediates are recognised by retinoic acid-inducible gene I (RIG-I), which signals through mitochondrial antiviral-signalling protein (MAVS) to activate downstream TBK1/IRF3 and NF-κB pathways (Ablasser et al., 2009; Rehwinkel & Gack, 2020). This induces type I interferon and inflammatory gene expression (Ablasser et al., 2009; Cavlar et al., 2012; Naesens et al., 2023). Therefore, Pol III can act as a bridge between cytosolic DNA detection and RNA-sensing antiviral

pathways. This function is relevant to ageing because chronic or dysregulated innate immune activation contributes to inflammation, tissue dysfunction, and altered intercellular communication, which are key features of age-related decline (Lopez-Otin et al., 2013).

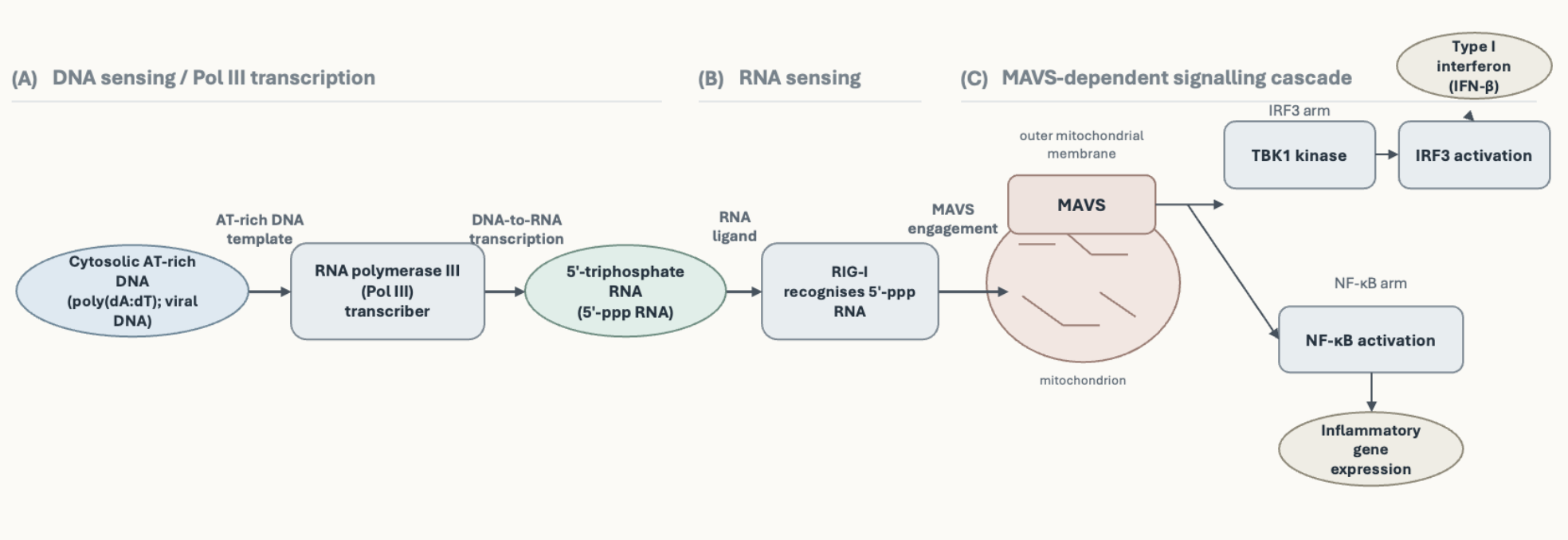

Figure 1-3 RNA polymerase III-RIG-I innate immune signalling pathway

RNA polymerase III transcribes cytosolic AT-rich DNA into 5'-triphosphate RNA, which activates RIG-I signalling through MAVS, leading to IRF3 and NF-κB activation and induction of type I interferon and inflammatory gene expression, respectively. Thereinto, cytosolic AT-rich DNA is converted into an RNA ligand for RIG-I, linking DNA exposure to antiviral and inflammatory transcriptional outputs. Adapted from Ablasser et al. (2009); Rehwinkel and Gack (2020).

Together, the roles of Pol III in transcription, nutrient-responsive growth regulation, autophagy, metabolism, and innate immune signalling provide the rationale for examining Pol III in mammalian tissues. Because Pol III regulates short non-coding RNA production and contributes to translational capacity and nutrient-dependent growth signalling, changes in Pol III activity may influence tissue maintenance during ageing (Filer et al., 2017; Willis & Moir, 2018). Pol III activity has also been linked to autophagy and metabolic regulation through the TOR-MAF1 pathway, and to innate immune responses via the RIG-I signalling axis (Ablasser et al., 2009; Bonhoure et al., 2015; Bonhoure et al., 2020; Moir & Willis, 2013; Naesens et al., 2023). The skin and liver are particularly relevant in this context. Skin is a highly regenerative barrier tissue that depends on keratinocyte turnover, fibroblast activity, extracellular matrix remodelling, adipose signalling, and immune defence (Simmons & Gallo, 2024; Takeo et al., 2015). The liver is a central metabolic and detoxifying organ with high biosynthetic demand and strong regenerative capacity (Hunt et al., 2019; Trefts et al., 2017). Therefore, analysing skin and liver provides an opportunity to investigate whether Pol III-related pathways contribute to ageing phenotypes in tissues with distinct physiological functions.

1.3 SKIN STRUCTURE AND FUNCTION

1.3.1 Murine skin architecture and general functions

The skin is the largest organ in animals and serves as a multifunctional barrier against environmental insults such as ultraviolet radiation, pathogens, chemicals, mechanical stress, and water loss (Takeo et al., 2015). In mice, the skin is organised into three main layers: a stratified epidermis, a supportive dermis, and a hypodermis composed of adipose tissue and muscle (**Figure 1-3** (a)). The epidermis is the outermost layer of the skin, with the stratum basale at its base. As basal keratinocytes divide and differentiate, they migrate upward to form the suprabasal cells, then into the granular layer, and finally into enucleated corneocytes that form the stratum corneum (**Figure 1-3 (b)**) (Takeo et al., 2015). This stratification establishes a robust physical barrier. Beneath the epidermis, the dermis provides mechanical strength, elasticity, and

nourishment to the skin (Lee & Sacks, 2024). It contains fibroblasts, extracellular matrix (ECM) components, hair follicles, sebaceous glands, and immune cells (Takeo et al., 2015). Fibroblasts in particular are critical to dermal structure and also give rise to adipocytes of the hypodermis during development (Driskell et al., 2013). Below the dermis lies the adipose layer, composed of dermal white adipose tissue (dWAT) and connecting to the panniculus carnosus muscle (Takeo et al., 2015). This layer cushions the skin, stores energy, and provides insulation. Together, the three layers enable skin to function as a physical, metabolic, and immunological barrier. The contribution of each skin layer to barrier function and repair is therefore important for interpreting age-associated changes in skin structure.

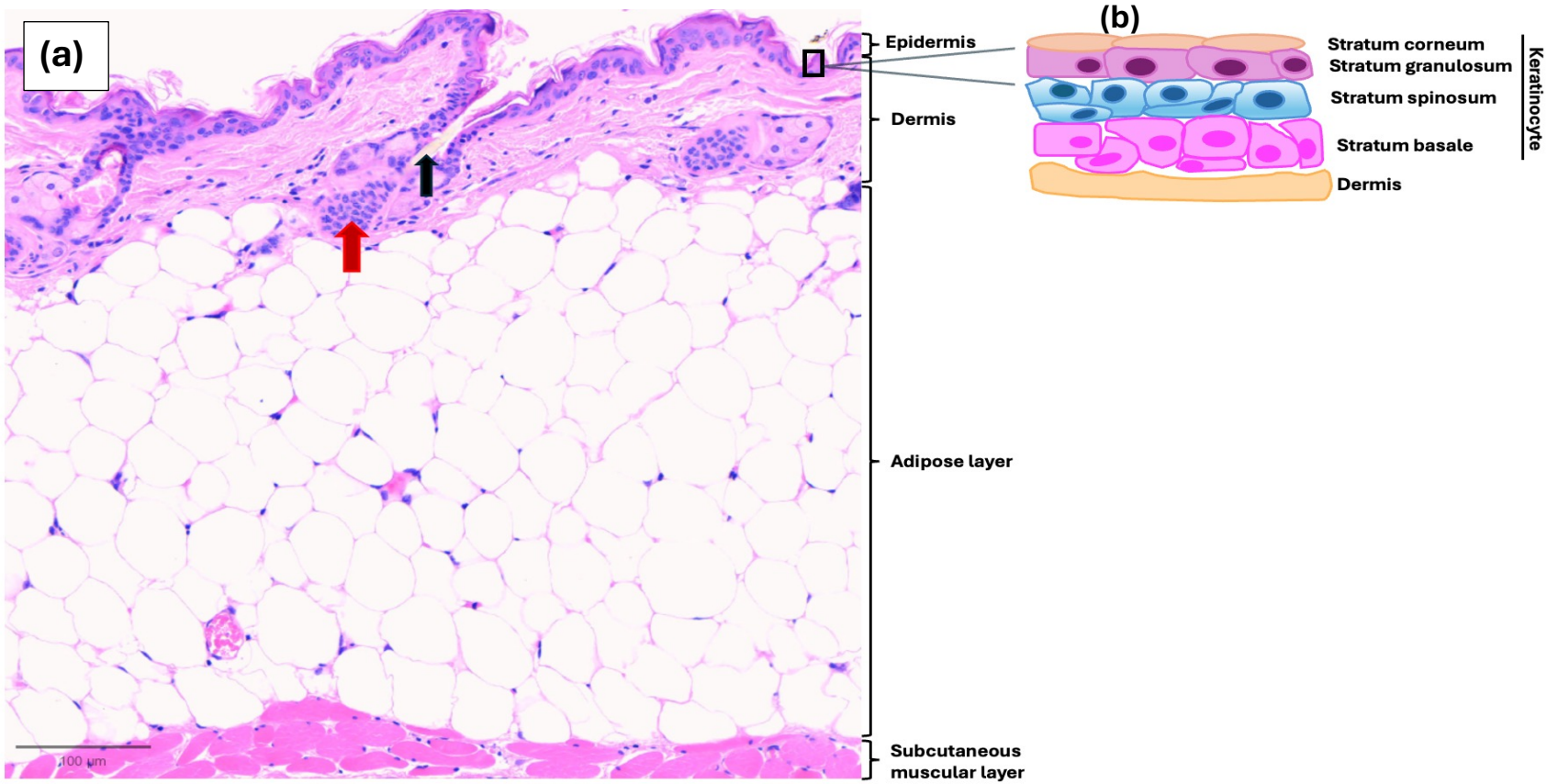

Figure 1-4 SKIN STRUCTURE OF MICE

Histological section of mouse skin (H&E) showing epidermis, dermis, and hypodermis, with hair follicle (black arrow) and sebaceous gland (red arrow) in dermis, scale bar 100 μm (a). Diagram of the epidermis showing stratum basale, spinosum, granulosum, and corneum. Keratinocytes are the predominant cell type of the epidermis (b).

1.3.2 Function of each skin layer

Epidermal defence and immune regulation

Keratinocytes are the primary structural and functional cells of the epidermis, playing a vital role in maintaining the skin's barrier and supporting tissue repair (Ye & Lai, 2025). Beyond their structural role, keratinocytes also participate in processes such as wound closure, cutaneous immune activation, neuroimmune communication, and the initiation of itch responses (Simmons & Gallo, 2024; Trier et al., 2019; Ye & Lai, 2025). Upon skin injury, keratinocytes rapidly express antimicrobial peptides (AMPs) and antimicrobial fatty acids (AFAs), which form an immediate defence against microbes and pathogenic infections (Simmons & Gallo, 2024). The structural properties of these antimicrobials dictate their selectivity against Gram-positive and Gram-negative bacteria, fungi, and viruses (Dorschner et al., 2001; Lopez-Garcia et al., 2005). Among them, the most prominent and impactful keratinocyte-derived products are cathelicidin (LL-37 in humans and CRAMP in mice), β-defensins, and members of the S100 protein family (Simmons & Gallo, 2024). Keratinocytes also produce cytokines such as interleukins, chemokines, tumour necrosis factor (TNF), interferons, and thymic stromal lymphopoietin (TSLP). These proinflammatory cytokines recruit immune cells to sites of injury or infection and are either released rapidly from ruptured cells or regulated through transcriptional pathways (Simmons & Gallo, 2024). With age, epidermal keratinocyte proliferation decreases while keratinocyte apoptosis increases, resulting in a measurable decrease in epidermal thickness (Wang et al., 2020). Keratinocytes in elderly skin also exhibit slower turnover and differentiation than in young skin, reflecting a decline in the regenerative capacity of epidermal stem cells (Strbo et al., 2025).

Role of dermal fibroblasts in extracellular matrix synthesis, skin repair and ageing

Beneath the epidermis, dermal fibroblasts are central to maintaining the extracellular matrix and mechanical properties of the skin. Fibroblasts are the

dominant cell type in the dermis, they are responsible for the synthesis and deposition of extracellular matrix (ECM) components, producing collagen and elastic fibres that provide mechanical strength and elasticity to the skin. During embryonic development, dermal fibroblasts also generate adipocytes of the hypodermis (Driskell et al., 2013; Jacob et al., 2023; Kalluri & Zeisberg, 2006). During wound healing, collagen degradation generates fragments that stimulate fibroblast proliferation and ECM remodelling (Mathew-Steiner et al., 2021).

Collagen is the major component of the dermal ECM. It maintains tissue integrity by providing structural support, acting as a scaffold for cell adhesion and migration, and regulates cell phenotypes such as proliferation, differentiation, and polarisation (Jurgensen et al., 2020). The fibril-forming collagens type I, III, and V are the most abundant in skin, especially type I collagen, which represents 80%-90% of the total dermal collagen (David & Jennifer, 2021; Mathew-Steiner et al., 2021). Collagen composition changes dynamically during tissue repair (Mathew-Steiner et al., 2021). Type III collagen, due to its hydrophilic structure, is the first to be synthesised in wound healing, and it is then replaced by type I collagen in later stages to restore tensile strength (Mathew-Steiner et al., 2021; Singh et al., 2023). Dysregulated collagen turnover can impair repair. For example, Staphylococcus aureus infection upregulates the collagenolytic enzyme MMP-2, sharply decreasing the collagen I/collagen III ratio and compromising the biomechanical properties of the repaired skin, thereby potentially increasing the risk of chronic wound recurrence (Roy et al., 2020). Collagen ratios also shift during ageing. Studies have shown that the ratio of type I and type III collagen declines with age, and this is associated with impaired collagen synthesis as a result of the increased ECM degradation (Lovell et al., 1987; Nizar et al., 2021). These changes highlight the importance of collagen balance for skin integrity across the lifespan.

Role of dermal adipose tissue in skin physiology and ageing

In addition to epidermal and dermal compartments, the adipose layer contributes to skin homeostasis through metabolic and paracrine functions. In mouse skin, the adipose compartment comprises a layer of adipocytes known as

dWAT, which lies between the dermis and the subcutaneous muscle layer. The adipose layer in the skin plays multiple roles in skin homeostasis. dWAT has been shown to participate in hair follicle cycling, wound healing, skin thermoregulation, defence against infection, and fibrotic responses (Kruglikov & Scherer, 2016). dWAT is not a passive fat store but a metabolically active layer that communicates with neighbouring cells. During skin injury, dermal adipocytes undergo lipolysis, releasing fatty acids that contribute to fibroblast metabolism and support efficient tissue repair (Shook et al., 2020; Z. Zhang et al., 2021). Changes in dWAT are also observed under environmental stress and during ageing. Extrinsic insults, such as near-infrared and UVR irradiation, can transiently increase adipocyte number (in the near-infrared irradiation study only) before reducing dWAT volume and promoting fibrosis (Mitani et al., 1999; Tanaka et al., 2011). With age, dermal adipocytes exhibit altered lipid metabolism and expansion, which are linked to fibroblast reprogramming, enhanced fatty acid oxidation, and increased fibrotic remodelling (Kruglikov et al., 2022). Recapitulating, these findings highlight dWAT as a dynamic component of skin, contributing to both homeostasis and age-associated changes in tissue structure.

Together, these features make skin a useful tissue for assessing whether altered Pol III activity is associated with changes in barrier maintenance, inflammation, and age-related remodelling.

1.4 MURINE LIVER STRUCTURE AND FUNCTION

1.4.1 Liver architecture and general functions

The liver is the largest internal organ and performs diverse physiological roles. In mice, its organisation resembles that of other mammals (Baratta et al., 2009). Structurally, the mouse liver is divided into lobes, each composed of repeating functional units called lobules (Baratta et al., 2009). Each lobule is centred on a central vein and bordered by portal triads, which contain a branch of the portal vein, a branch of the hepatic artery, and bile duct (**Figure 1-4**). In general, for each of the lobular units, liver cells (hepatocytes) are arranged in cords or

plates that radiate from the regions of the central vein (CV) to the portal areas (PTs). The cords or plates of cells are separated by sinusoidal capillaries (Baratta et al., 2009; Gebhardt, 1992). This arrangement, known as hepatic zonation, allows the liver to integrate blood from both systemic and portal circulation to the central venules. After processing, the blood flows out of the liver via the hepatic veins. This hepatic zonation arrangement also supports liver metabolic functions, such as drug activation and detoxification (Schenk et al., 2017). Additionally, the bile canaliculi collect bile from hepatocytes and deliver it to the bile ducts in the portal triads, from where it enters the gallbladder and intestine (Boyer, 2013).

Functionally, the liver plays a central role in detoxification, and it is also a metabolic powerhouse, regulating carbohydrates, fats, and protein metabolism (Mohallem et al., 2025). Although the liver shows impressive resilience throughout ageing, increasing evidence indicates it exhibits all the cellular hallmarks of ageing, leading to the risk of liver and systemic diseases (Hunt et al., 2019). For instance, the liver of aged mice showed downregulation of protein phosphorylation, impaired metabolic pathways, as well as age-related changes in a wide range of proteome and phosphoproteome, including a decline in mitochondrial function and oxidative phosphorylation (OXPHOS) (Mohallem et al., 2025; Williams et al., 2022). At the cellular level, a reduction in the number of hepatocytes with larger nuclei, a higher degree of hepatic cirrhosis and fibrosis, release of more cytokines (such as IL-6, TNF-α) from the senescent hepatocytes, a decline in mitochondrial biogenesis, and increased accumulation of ROS in hepatocytes, as well as impaired cellular proteolysis and hydrolysis of lipid stores and glycogen, are often observed in the aged mouse liver (Hunt et al., 2019). Understanding the main hepatic cell types is therefore necessary for interpreting how age-related changes in liver structure relate to metabolic and inflammatory function.

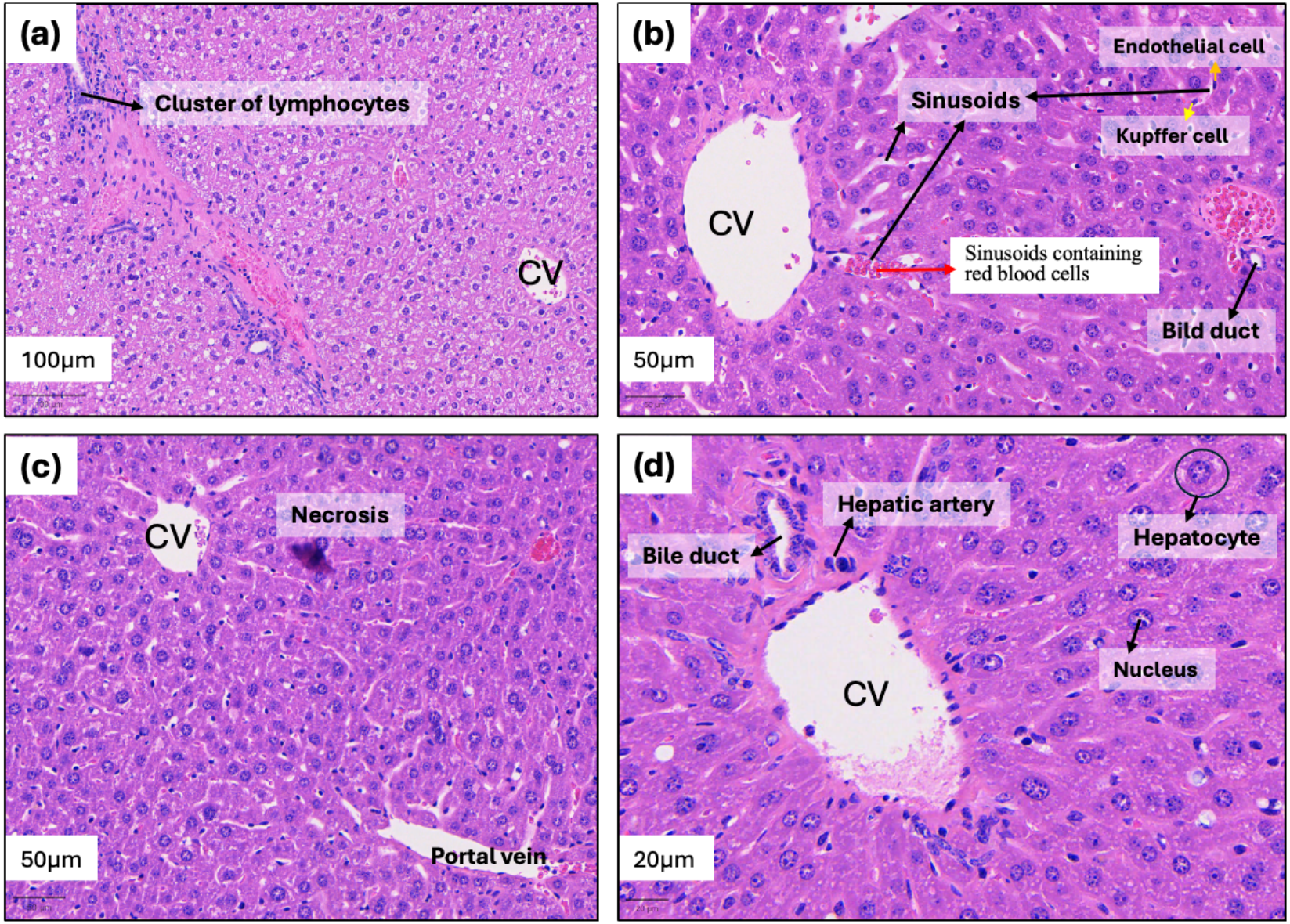
(a)
Cluster of lymphocytes
CV
100µm
(b)
Endothelial cell
Sinusoids
Kupffer cell
CV
Sinusoids containing red blood cells
Bild duct
50µm
(c)
CV
Necrosis
50µm
Portal vein
(d)
Hepatic artery
Hepatocyte
Bile duct
Nucleus
CV
20µm

Figure 1-5 ARCHITECTURE OF MOUSE LIVER

Histology liver section of mice (H&E) showing central vein (CV) and portal triads (PT). PTs containing portal vein, hepatic artery, and bile duct. Due to the plane of the section, the PT structures could not always be detected. The hepatic artery and portal vein are lined by endothelial cells. The hepatic artery is small with thick walls (d), while the portal vein is large with thin walls (c). The bile duct is roughly the same size as the hepatic artery and is lined by a single layer of square-shaped epithelium (b,d). Plates of hepatocytes radiate out from the CV toward the PTs (b-c). The CV drains blood coming from the PT via the sinusoids that are lined by the endothelial and Kupffer cells; therefore, sometimes red blood cells can be observed in sinusoids (b). Bile is transported from the CV to the PTs (b,d). In addition to the above structures, (a) also shows a cluster of lymphocytes, (b) shows a regular oval-shaped endothelial cell, and an irregular-shaped Kupffer cell (macrophage) that protrudes into the sinusoids (b), (c) shows necrosis of the hepatocytes, and (d) shows a typical hepatocyte with a nucleus.

1.4.2 Cellular components of the liver and their functions

Hepatocytes and metabolic regulation

Hepatocytes are the predominant cell type in the liver and carry out most of its metabolic tasks. They regulate glycogen storage and mobilisation, and control lipid, carbohydrate, and protein metabolism (Klover & Mooney, 2004; Trefts et al., 2017). In addition, hepatocytes synthesise bile and secrete proteins (e.g. pro-inflammatory cytokines) that influence systemic physiology, including acute-phase proteins and clotting factors (J. Gong et al., 2022; Kalra et al., 2023). Together with Kupffer cells, hepatocytes contribute to hepatic detoxification, where Kupffer cells remove pathogens and debris by phagocytosis, while hepatocytes metabolise drugs and xenobiotics through Phase I and II enzymatic pathways (Blondet et al., 2018).

During ageing, hepatocytes display features of cellular senescence, reduced proliferative capacity, and nuclear enlargement with chromatin alterations reflecting genomic instability (Dai et al., 2024; Hunt et al., 2019; Ledda-Columbano et al., 2004). They also show mitochondrial dysfunction and impaired lipid metabolism, changes that predispose to liver fibrosis, insulin resistance, steatosis, and cancer (Aravinthan et al., 2015; Dai et al., 2024; Hunt et al., 2019; Ogrodnik et al., 2017).

Cholangiocytes and bile transport

Although hepatocytes account for most liver metabolic activity, non-parenchymal and epithelial cell populations also contribute to liver homeostasis and disease. Cholangiocytes are epithelial cells that line the bile ducts. They participate in the formation and transport of bile with the help of transmembrane molecules within these cells (Baiocchi et al., 2021; Yoo et al., 2016). These transmembrane molecules include water channels, glucose transporters, and exchangers (such as the Cl/HCO3- exchanger); impairing these molecules could lead to cholestasis (Yoo et al., 2016). With ageing, increased biliary senescence resulting from, for example, telomere shortening, may

contribute to chronic liver disease and fibrosis progression (Baiocchi et al., 2021; Sasaki et al., 2010). Ageing also contributes to cholestatic disorders and is associated with the development of cholangiocarcinoma, a primary liver cancer of the bile ducts (Labib et al., 2019; Pinto et al., 2021).

1.5 AIMS

Partial inhibition of RNA Polymerase III has been shown to extend lifespan in yeast, worms, and flies, acting downstream of TORC1 through the conserved repressor MAF1 (Bonhoure et al., 2020; Filer et al., 2017; Malik, Goncalves Silva, et al., 2024). Pol III transcribes 5S rRNA and tRNAs required for ribosome assembly, protein synthesis, and cellular adaptation to metabolic and environmental cues (Moir & Willis, 2013). While these studies have firmly established a role for Pol III in the regulation of lifespan and stress resilience in invertebrates, far less is known about how reductions in Pol III signalling influence mammalian physiology, healthspan, or tissue integrity.

This thesis uses C57BL/6N mice heterozygous for *Polr3b* (*Polr3b*$^{+/-}$), which exhibit a reduction in Pol III activity, to explore how Pol III insufficiency affects molecular signalling pathways, reproductive function, inflammatory regulation, tissue structure, and age-associated pathology. By adopting a multi-organ, multi-phenotype approach, this work aims to clarify whether reduced Pol III output produces beneficial or detrimental consequences across the ages and whether these effects display tissue- or sex-specificity. The objective of this thesis was to define the physiological impact of reduced Pol III signalling in mammals. To address this, the thesis investigates the following questions:

How does Polr3b heterozygosity influence Pol III-related signalling and protein synthesis in key tissues?

In Chapter 3 I examined molecular indices of Pol III function across liver, brain, skeletal muscle, and primary dermal fibroblasts from *Polr3b*$^{+/-}$ mice. This included quantifying Pol III-related mRNA and protein expression (*Polr3a, Polr3b, Maf1*), assessing phosphorylation of ribosomal protein S6 as an index of mTORC1 activity, evaluating global protein synthesis via puromycin incorporation, and measuring mitochondrial chaperones HSP60 and HSP90. The aim was to determine whether partial loss of *Polr3b* alters Pol III-associated molecular and translational processes in tissues where Pol III expression is high. Given that Pol III activity supports tRNA and 5S rRNA synthesis required for protein translation,

it was hypothesised that *Polr3b*$^{+/-}$ mice would exhibit reduced *Polr3b* expression and a corresponding decrease in global protein synthesis. Changes in *Maf1*, markers linked to mTORC1 signalling, and cellular stress responses (including phosphorylation of S6 and expression of HSP60 and HSP90) were explored to assess whether reduced Pol III activity is associated with broader alterations in these pathways.

Does reduced Pol III signalling affect fecundity, fertility, and reproductive endocrine pathways in mice?

In Chapter 4, I investigated whether *Polr3b*$^{+/-}$ mice display altered reproductive performance, given the known links between growth, protein synthesis, and reproductive ageing. Measures included: time to first litter as an index of fecundity, litter size, pre-weaning pup survival, offspring weight, and gonadal morphology. Expression of Pol III-related and hormone-related genes (*Cyp19a1, Fshr, Lhcgr)* was quantified to determine whether changes in Pol III signalling influence ovarian or testicular endocrine pathways. This chapter aimed to clarify whether Pol III activity contributes to the coordination between reproduction and lifespan. I expected that reproductive performance to be impaired in *Polr3b*$^{+/-}$ mice, reflecting reduced biosynthetic and protein synthesis capacity associated with decreased Pol III activity.

Does reduced Pol III activity alter susceptibility to idiopathic dermatitis and skin inflammatory phenotypes during ageing?

Chapter 5 used a retrospective cohort analysis to explore the unexpectedly high incidence of idiopathic dermatitis observed in female *Polr3b*$^{+/-}$ mice. The study quantified disease onset, seasonal patterns, splenomegaly, and circulating IL-6, and assessed skin architecture, mast cell degranulation, collagen content, and wound-healing capacity. Inflammatory gene expression in skin tissue was analysed to determine whether reduced Pol III activity affects cutaneous immune homeostasis. Given the role of Pol III in innate immune signalling and

cellular homeostasis, reduced Pol III activity may be associated with dysregulated inflammatory responses and impaired maintenance of skin integrity during ageing.

How does *Polr3b* heterozygosity influence liver structure, inflammatory homeostasis, and age-related pathology?

In Chapter 6 I examined whether reduced Pol III activity influences hepatic ageing, focusing on liver-to-body weight ratios, tumour incidence, histopathology (including lipid accumulation, nuclear morphology, polyploidy, fibrosis, and inflammatory foci), and expression of senescence- and inflammation-related genes (*p16, p21, Il1α, Il6, Tnfα, Il17α, Il22, Il23α, Ccl20, Jam-a*). This chapter aimed to determine whether Pol III reduction disrupts hepatic integrity or immune regulation, and whether these effects differ between sexes. Given the role of Pol III in regulating translational capacity and metabolic signalling pathways, reduced Pol III activity may influence liver integrity, contributing to changes in age-associated pathology, including inflammation, cellular senescence, and tissue remodelling. Therefore, it was hypothesised that *Polr3b*$^{+/-}$ mice would exhibit alterations in hepatic structure and inflammatory homeostasis during ageing.

Together, these chapters aimed to provide a comprehensive assessment of how partial reduction in Pol III signalling shapes mammalian physiology across molecular, reproductive, immunological and structural domains.

Chapter 2: Methods and Materials

2.1 RNA Polymerase III heterozygous knock-out animal model and husbandry

Mice were obtained from the same source as described in Borland et al. (2024) and were housed and maintained according to the same husbandry protocols. In detail, the *Polr3b* wild-type (*Polr3b*$^{+/+}$) and *Polr3b* heterozygous mutant mice (*Polr3b*$^{+/-}$) were derived from C57BL/6N background mice, where the *Polr3b*$^{+/-}$ mouse line introduced a heterozygous mutation (Polr3b$^{em7(IMPC)Tcp/Tcp}$) before birth, resulting in a frameshift and early truncation in the sequence of the *Polr3b* gene. This mouse line C57BL/6NCrl-Polr3b$^{em7(IMPC)Tcp/Tcp}$ was generated using genome editing based on the Clustered Regularly Interspaced Short Palindromic Repeats (CRISPR)-Cas9 system derived from the adaptive immune system of prokaryotes. Genome editing technology based on this system allows more precise introduction of mutation on the target DNA sequences (Lee et al., 2020). The mouse line was made as part of the NorCOMM2 project funded by Genome Canada and the Ontario Genomics Institute (OGI-051) at the Toronto Centre for Phenogenomics (http://phenogenomics.ca), and it was obtained from the Canadian Mouse Mutant Repository as part of the Knockout Mouse Program (KOMP2) (Lloyd, 2011). *Polr3b*$^{+/-}$ were bred in-house with non-transgenic C57BL/6N wild-type mice to maintain the line on a heterozygous background. The International Mouse Phenotyping Consortium (IMPC; Toronto Centre for Phenogenomics) has reported that homozygous *Polr3b* knockout results in complete preweaning lethality in both female and male mice, based on a viability primary screen (IMPC, 2024). Experimental *Polr3b*$^{+/-}$ mice were generated by mating *Polr3b*$^{+/-}$ mice with C57BL/6N mice; to avoid any potential carry-over effect in experimental mice, experimental WT mice were generated by mating WT mice generated from *Polr3b*$^{+/-}$ x C57BL/6N matings with C57BL/6N mice.

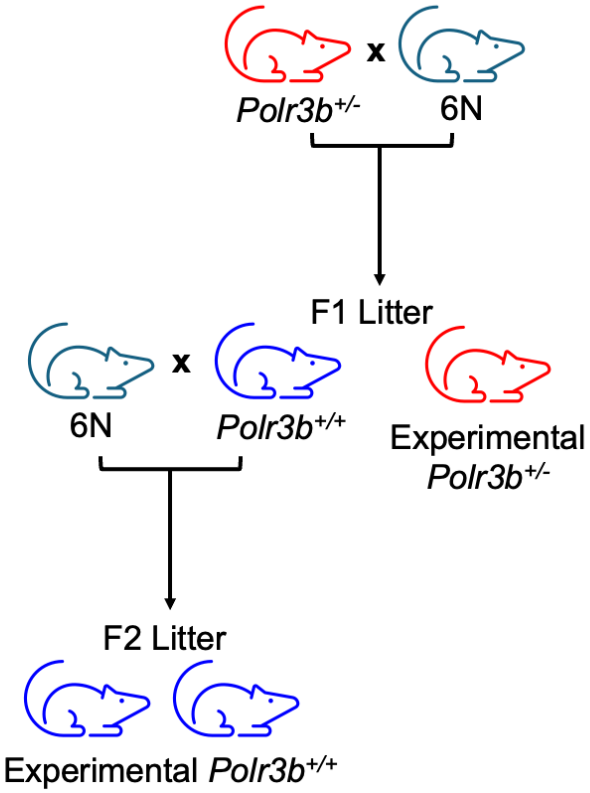

Figure 2-1 Breeding strategy for generating experimental *Polr3b*$^{+/-}$ and *Polr3b*$^{+/+}$ (WT) mice

Experimental *Polr3b*$^{+/-}$ mice were generated by mating *Polr3b*$^{+/-}$ breeders with C57BL/6N mice, producing F1 litters containing both *Polr3b*$^{+/-}$ and *Polr3b*$^{+/+}$ offspring. F1 *Polr3b*$^{+/-}$ mice were used directly as the heterozygous experimental group. F1 *Polr3b*$^{+/+}$ offspring from these matings were further outcrossed to C57BL/6N mice, and the resulting F2 progeny were all *Polr3b*$^{+/+}$ and used as the experimental WT group.

Mice were maintained in Emerald line IVC EM500 (Tecniplast, Italy) under a housing temperature of 22±2°C and a 12L/12D photoperiod (lights on 7.00 am-7.00 pm). Mice were given *ad libitum* access to both water and standard chow diet (CRM(P), Research Diets Services, LBS Biotech, UK; Atwater Fuel Energy-protein 22%, carbohydrate 69%, fat 9%). All animal experiments were undertaken following The University of Glasgow Animal Welfare and Ethical Review Board, under project licenses PDBDC7568, PP2141975, and personal license I01541544 from the UK Home Office and following the "principles of laboratory animal care" (NIH Publication No. 86–23, revised 1985).

2.2 Routine check, ante- and post-mortem evaluation

Routine checks and ante- and post-mortem evaluations were performed as described in Borland et al. (2024). Specifically, mice were routinely examined daily for general condition and weighed monthly (weekly for mice after reaching 12 months of age) using an Ohaus CX221 portable balance. Any mice aged after 12 months or showing signs of pathology (e.g. presence of tumours/dermatitis, piloerection, ophthalmia) or acute weight loss were subject to enhanced monitoring, which involved daily checks and evaluation using a scoring system to measure cumulative harm from normal age-related changes and pathological changes (**Appendix 2**). Mice were scored on general physical appearance (e.g. presence of tumours/dermatitis, piloerection), breathing, activity, changes in body mass and changes in body condition. Mice identified with ID received standard treatment: the lesions were treated with green clay (montmorillonite) daily and their nails were cut by the animal technician. Mice were weighed and their ID was monitored daily until they either recovered or reached the humane endpoints (**Appendix 2**). Specifically, euthanasia was performed by the Schedule 1 standard method of humane killing if any of the following criteria were met: mouse reached a threshold score; mouse with severe dermatitis not respond to treatment; mouse unable to bear weight on hind limbs, impacting the ability to feed or drink normally; mouse with a tumour that caused rapid loss of body mass or condition, or that was ulcerated, or that interfered with normal movement or behaviour; mouse with gasping or rapid breathing; mouse with recent weight loss exceeding 20%, or more than 10% with no response to the treatment; mouse with

a body condition score of 1. Post-mortem examinations were performed on mice that were euthanised or died spontaneously (undertaken by Dr Gillian Borland, Prof Colin Selman, Dr Stephen E. Wilkie, or Zhe Wang).

2.3 DNA extraction and Polymerase Chain Reaction (PCR)

Mice were genotyped from ear biopsies either in-house by PCR (**Figure 2-2**), or by qPCR using an external provider (Transnetyx Inc, Cordova, TN, USA). For in-house PCR, mice were genotyped from either ear or tail biopsies. Genomic DNA was extracted from mouse tissue samples using a proteinase K digestion method. In detail, samples were incubated in 500 µL of lysis buffer (100 mM Tris-HCl, 5 mM EDTA, 0.2% SDS, 200 mM NaCl; pH 8.5) supplemented with 10 µL proteinase K (25 mg/mL) for 3 h at 55°C to ensure complete tissue digestion. Following incubation, lysates were centrifuged at 13,000 × g for 20 min at 4°C to pellet debris. The resulting supernatant was carefully transferred to a fresh microcentrifuge tube containing 500 µL of ice-cold isopropanol and mixed gently by inversion to precipitate DNA. Samples were then centrifuged at 13,000 × g for 20 min at 4°C, yielding a visible DNA pellet. The supernatant was discarded, and the pellet was washed with 500 µL of 70% ethanol to remove residual impurities. After a subsequent centrifugation step at 13,000 × g for 5 min at 4°C, the ethanol was removed and the pellet was air-dried for approximately 3 h. The dried DNA pellet was resuspended in 100 µL TE buffer (10 mM Tris-HCl, 1 mM EDTA; pH 8.0) and incubated at 37°C for 30 min to facilitate dissolution. DNA samples were stored at 4°C until further use. Prior to PCR genotyping, DNA was diluted 1:10 in nuclease-free water.

For PCR, each PCR contained 12.5 µL DreamTaq Green (ThermoFisher, Inchinnan, UK), 2.5 µL each primer, 0.75 µL genomic DNA in a total volume of 25 µL. Amplification was carried out in a MiniAmp Plus thermal cycler (ThermoFisher, Inchinnan, UK) using the following conditions: 95°C for 10 minutes; 35 cycles of 95°C for 30 seconds, 53°C for 35 seconds and 72°C for 65 seconds; 72°C for 5 minutes. PCR products were run on a 2% agarose gel and visualised using a BioRad Gel Doc XR+ (BioRad, Watford, UK). Primer sequences are in **Table 2-1**.

Table 2-1 Primer sequences used in PCR experiments

Gene	Forward primer	Reverse primer	Expected band size (bp)
Polr3b WT	5'- AGGCTGCTGTGCACTGTATT-3'	5'-GACGGCACTGGAGCAGAAT-3'	82
Polr3b KO	5'- TCAGTGGGGAAAGTTCAGGC-3'	5'- TCAGACGGACACTGGACACT-3'	110

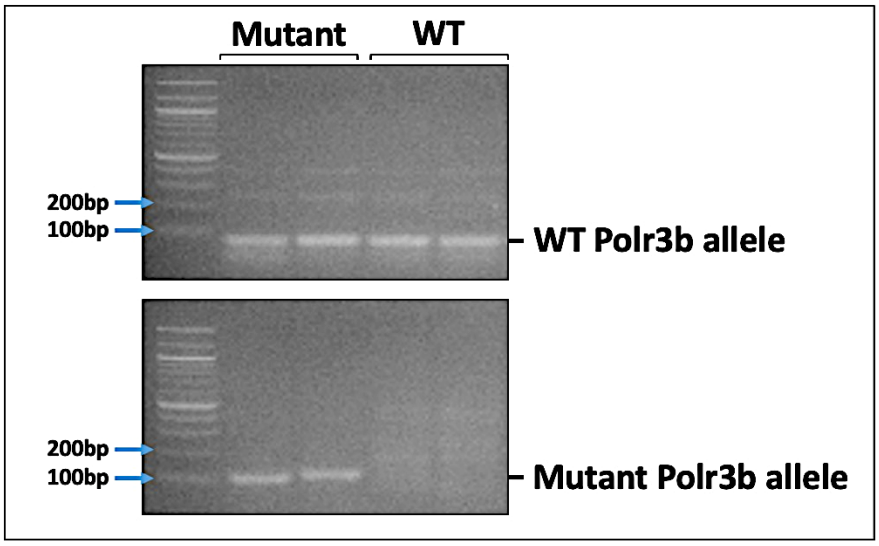

Figure 2-2 Representative genotyping PCR of Polr3b$^{+/+}$ and Polr3b$^{+/-}$ mouse. The top panel shows the results of the WT Polr3b allele. The bottom panel shows the result for the heterozygous mutant Polr3b allele.

2.4 Cell culture for dermal fibroblasts

Dermal fibroblasts were isolated and cultured using standard procedures adapted from our laboratory's primary cell isolation protocol. In detail, ear tissues were collected from 5-month-old female WT and *Polr3b*$^{+/-}$ mice immediately following the Schedule 1 standard method of humane killing. Tissues were briefly rinsed in 70% ethanol, then transferred to sterile Petri dishes (Corning, NY, USA) and finely diced using a sterile blade. To remove residual ethanol, diced tissue was washed in serum-free Dulbecco's Modified Eagle Medium (DMEM; ThermoFisher, Paisley, UK) supplemented with 1% Penicillin-Streptomycin (v/v; ThermoFisher, Grand Island, USA) and 0.2% Primocin (v/v; InvivoGen, Toulouse, France). For enzymatic digestion, tissue fragments were incubated overnight at 37°C in serum-free medium containing 0.25% (v/v) sterilised-filtered collagenase under continuous humidified conditions (5% CO_2 in air). Following digestion, samples were centrifuged to pellet cells and undigested debris was removed by aspiration of the supernatant. The pellet was resuspended in complete medium composed of DMEM supplemented with 10% heat-inactivated fetal bovine serum (v/v; FBS; ThermoFisher, Paisley, UK), 1% (v/v) Penicillin-Streptomycin and 0.2% (v/v)

Primocin. Culture medium was replaced every 3 days. Once fibroblasts reached 80%-90% confluence, cells were passaged (designated first-passage cells) using trypsin-EDTA (ThermoFisher, Paisley, UK) for 3-5 mins at 37°C in an incubator. Trypsinisation was halted by adding an excess volume of complete medium. At the end of the second passage, confluent cells were cryopreserved in freezing medium containing complete DMEM supplemented with 20% (v/v) FBS and 10% (v/v) dimethyl sulfoxide (DMSO). Cells were gradually cooled (-1°C/min) prior to storage at -70°C and subsequently transferred to long-term storage in liquid nitrogen. Frozen cells were stored until further use for RNA extraction, wound healing and RT-qPCR.

2.5 Reverse Transcriptase quantitative-PCR (RT-qPCR)

2.5.1 RNA extraction

For ovary and testis, total RNA was isolated using QIAzol Lysis Reagent (Qiagen, Maryland, USA) and purified with a RNeasy Mini Kit (Qiagen, Hilden, Germany) including on-column DNase I digestion (Qiagen, Manchester, UK), followed by column-based purification. 25-50 mg of snap-frozen tissue was homogenised in 700 µL QIAzol using a motorised homogeniser. After adding 140 µL chloroform (Sigma-Aldrich, St. Louis, MO, USA), samples were shaken vigorously and centrifuged at 12,000 x *g* for 15 minutes at 4°C to isolate the aqueous phase. The aqueous phase was mixed with 1.5 volumes of absolute ethanol, followed by purification using the RNeasy Mini Kit. RNA was eluted in RNase-free H_2O (Qiagen, Hilden, Germany).

For dorsal skin, liver and cultured dermal fibroblasts, total RNA was extracted using a RNeasy Mini Kit (Qiagen, Manchester, UK), following the manufacturer's protocols for animal tissues and cultured cells, respectively. For skin and liver tissues, 20-30 mg of frozen sample was homogenised in Buffer RLT using a 20-gauge needle fitted to an RNase-free syringe. Homogenates were mixed with 70% ethanol and processed using spin columns. For dermal fibroblasts, the frozen cells obtained from **Section 2.4** were re-grown from cryopreserved vials and harvested at passage 3 by trypsinisation. The cell pellet was resuspended in Buffer RLT and processed following the vacuum/spin protocol for animal cells. In both cases, on-column DNase digestion was performed using the RNase-Free DNase Set (Qiagen, Manchester, UK), as described in Appendix D of the RNeasy Mini Handbook, to remove genomic DNA contamination. After washing steps with RW1 and RPE buffers, RNA was eluted in RNase-free H_2O. RNA concentration and purity were assessed using a NanoDrop® Spectrophotometer ND-1000 (ThermoFisher, Wilmington, DE, USA).

2.5.2 cDNA synthesis and RT-qPCR

For each sample, 2 µg of total RNA was reverse transcribed using M-MLV Reverse Transcriptase (ThermoFisher, Carlsbad, CA, USA). RNA was combined with 1 µL Random Hexamers (ThermoFisher, Carlsbad, CA, USA) and 1 µL 10 mM dNTP mix (New England Biolabs, Ipswich, MA, USA), and the volume was adjusted to 12 µL with nuclease-free H_2O (ThermoFisher, Vilnius, Lithuania). Samples were incubated at 65°C for 5 minutes and immediately placed on ice to prevent secondary structure reformation. A 7 µL master mix containing 4 µL of 5x First Strand Buffer (ThermoFisher, Carlsbad, CA, USA), 2 µL of 100 mM DTT, and 1 µL 40 U/µL RNaseOUT™ Recombinant Ribonuclease Inhibitor (Carlsbad, CA, USA) was then added to each reaction. Following brief incubation at 70°C for 15 minutes to inactivate reverse transcriptase and the resulting cDNA was diluted in PCR-grade nuclease-free H_2O (ThermoFisher, Vilnius, Lithuania) to 12.5 ng/µL.

Quantitative PCR was carried out on 1 µL cDNA, 10 µL Applied Biosystems Fast Sybr Green Master Mix (ThermoFisher, Inchinnan, UK), 0.5 µL of a 10 µM stock of each primer and 8 µL of PCR-grade H_2O per well. Amplification using primer sets was carried out on a 7500 Fast Real Time PCR system (ThermoFisher, Inchinnan, UK) using the following cycling conditions: 95°C for 10 min; 40 cycles of 95°C for 15 seconds, 60°C for 60 sec, 72°C for 60 sec; and followed by a standard melt curve. Expression was calculated using the $2^{\wedge DDCt}$ method (Borland et al., 2024). Ct values were normalised to housekeeping genes selected based on low variability across samples and the absence of genotype-associated shifts in Ct values within each tissue. Candidate reference genes included *B2m*, *Hmbs*, *Ppia*, *Rplp0*, and *Ywhaz*. For each tissue, housekeeping genes were used if their expression showed no significant difference between WT and *Polr3b*$^{+/-}$ mice (details on housekeeping gene selection for each tissue are provided in the Methods section of the corresponding result chapters). The geometric mean of Ct values from the selected reference genes was used to calculate DCt values for each target gene. DDCt was then calculated relative to the WT group mean, and results were expressed as fold change (2^{-DDCt}), normalised such that the WT group was centred at 1. Primer sequences are shown in **Table 2-2**.

Table 2-2 Primer sequences used in RT-qPCR experiments

Gene	Forward primer	Reverse primer
B2m	5'-CATGGCTCGCTCGGTGAC-3'	5'-CAGTTCAGTATGTTCGGCTTCC-3'
Hmbs	5'-ATGAGGGTGATTCGAGTGGG-3'	5'-TTGTCTCCCGTGGTGGACATA-3'
Ppia	5'-GGCAAATGCTGGACCAAAC-3'	5'-CATTCCTGGACCCAAAACG-3'
Rplp0	5'-TTATAACCCTGAAGTGCTCGAC-3'	5'-CGCTTGTACCCATTGATGATG-3'
Ywhaz	5'-GAAAAGTTCTTGATCCCCAATGC-3'	5'-TGTGACTGGTCCACAATTCCTT-3'
Ccl20	5'-GGTACTGCTGGCTCACCTCT-3'	5'-TGTACGAGGGGCAACAGTCG-3'
Col1a1	5'-AGGCGAACAAGGTGACAGAGG-3'	5'-GGAGAACCAGGAGAACCAGGAG-3'
Col3a1	5'-TCCAGGTCCTCCAGGTTCTCC -3'	5'-ATGTGGTCCAACTGGTCCTCT-3'
Cxcl15	5'-TCCTGCTGGCTGTCCTTAACC-3'	5'-TTCCTGAATACACAGACATCGTAGC-3'
Cyp19a1	5'- CGAAGCAGCAATCCTGAAGGAG-3'	5'- CCAAGTCCACAACAGGCTGGTA-3'
Fshr	5'-GAGGCAGATGTGTTCTCCAACC-3'	5'- TCGGAGACTGGGAAGATTCTGG-3'
Il6	5'- CTGCAAGAGACTTCCATCCAG-3'	5'- AGTGGTATAGACAGGTCTGTTGG-3'
Il1α	5'-CTGAAGAAGAGACGGCTGAGTTTC-3'	5'-TCTGGTAGGTGTAAGGTGCTGATC-3'
Il1β	5'- GAAATGCCACCTTTTGACAGTG-3'	5'- TGGATGCTCTCATCAGGACAG-3'
Il17α	5'-TCCAGGGAGAGCTTCATCTGTGTC-3'	5'-TTGGACACGCTGAGCTTTGAGG-3'
Il22	5'-GTGCGATCTCTGATGGCTGTC-3'	5'-AGGGCAATGAGAAGCAGGCA-3'
Il23α	5'-TCCAGTGTGAAGATGGTTGTGAC-3'	5'-TTGCAAGCAGAACTGGCTGTTG-3'
Lhcgr	5'- AGCCACTGCTGTGCTTTCAG-3'	5'- AAAGATGGCAGAATAAAGCGTCTC-3'
Maf1	5'-GACTATGACTTCAGCACAGCC-3'	5'-CTGGGTTATAGCTGTAGATGTCAC-3'
Polr3a	5'- GCTTGCCAGATCATCGCTTCAATAC-3'	5'- GTCCACAGGGTGACAGGCTTTA-3'
Polr3b	5'-TTGGAGCCTCAGTTACCAGC-3'	5'-GAATCGACCCTGTTTCACGG-3'
Tnfα	5'-GTCCCCAAAGGGATGAGAAGT-3'	5'-TTTGCTACGACGTGGGCTAC-3'

Abbreviations: *B2m: Beta-2 microglobulin; Hmbs: Hydroxymethylbilane synthase; Ppia: Peptidylprolyl isomerase A; Rplp0: Ribosomal protein lateral stalk subunit P0; Ywhaz: Tyrosine 3-monooxygenase/tryptophan 5-monooxygenase activation protein zeta polypeptide; Ccl20: C-C Motif Chemokine Ligand 20; Col1a1: Collagen Type I Alpha 1; Col3a1: Collagen Type III Alpha 1; Cxcl15: C-X-C motif chemokine ligand 15; Cyp19a: Cytochrome P450 family 19 subfamily A member 1; Fshr: Follicle stimulating hormone receptor; Il6: Interleukin 6; Il1α: Interleukin 1 Alpha; Il1β: Interleukin 1 Beta; Il17α: Interleukin 17 Alpha; Il22: Interleukin 22; Il23α: Interleukin 23 Alpha; Lhcgr: Luteinizing hormone/choriogonadotropin receptor; Maf1: Mucosa-Associated Lymphoid Tissue Lymphoma Translocation gene 1; Polr3a: Polymerase (RNA) III (DNA directed) polypeptide A; Polr3b: Polymerase (RNA) III (DNA directed) polypeptide B; Tnfα: Tumour Necrosis Factor alpha.*

2.6 Western blotting

2.6.1 Protein lysate extracts and Western blotting

Protein lysates were extracted with RIPA buffer containing phosphatase (Roche, Germany) and cOmplete™, mini, EDTA-free protease (Roche, Germany) inhibitors from mice liver, brain, duodenum or dermal fibroblasts. Lysates were then incubated at 4°C with agitation with tissues for 1 hour or with fibroblasts for 30 mins. Lysates were then spun at 13K rpm for 20 mins at 4°C, and the interphase was transferred to a new tube. Protein concentration was determined by carrying out BCA assay according to the manual of the Pierce™ BCA Protein Assay Kit (ThermoFisher Scientific, USA). Lysates were diluted in SDS-PAGE sample buffer and RIPA buffer to 2-6 mg/ml final concentration, separated by SDS-PAGE of Mini-PROTEAN® TGX™ Precast Gels (Bio-Rad, USA) at 200V for 30 mins, and transferred to nitrocellulose at 100V for 1 hour. Membranes were blocked with 5% milk in TBST for 1 hour at room temperature. The protein concentrations were normalised by Li-Cor Revert 700 total protein staining (Li-Cor, USA). The membranes were then imaged with the Li-Cor Odyssey® imaging system. The use of antibodies listed below (**Table 2-3**).

Table 2-3 Antibodies used in western blotting

Full Name	Company	Catalogue Number	Expected Band size (kDa)	Dilution
Anti-**MAF1** antibody	Abcam	ab230499	45	1:1000
Fluorescent TrueBlot Anti Mouse Ig Dylight 800	Rockland	18-4517-32		1:1000
Goat Anti-Rabbit IgG H&L (Alexa Fluor® 680) preabsorbed	Abcam	ab186696		1:10,000
POLR3A (D5Y2D) Rabbit mAb	Cell Signaling Technology	12825	165	1:1000
POLR3B Polyclonal Antibody	Invitrogen	PA5-39141	128	1:1000
anti-Puromycin, Clone 12D10 (mouse monoclonal)	EMD Millipore Corporation	3682529		1:25,000
Phospho-S6 Ribosomal Protein (Ser235/236) (D57.2.2E) XP® Rabbit mAb	Cell Signaling Technology	4858	32	1:2000
S6 Ribosomal Protein (5G10) Rabbit mAb	Cell Signaling Technology	2217	32	1:1000

2.6.2 Intraperitoneal (IP) injection of mice with puromycin as a protein synthesis reporter

Mice aged 4.4 ± 0.2 months (mean ± SEM) were intraperitoneally injected with puromycin dihydrochloride (ThermoFisher Scientific, USA) under license at 0.04 µmol/gram body weight, dissolved in PBS and sterile-filtered immediately before use. Mice were fed *ad libitum* as usual until injection and remained in a sterile cage for a 30-minute labelling period. This dose is sufficient to label nascent polypeptide chains while being ~30-fold lower than the lethal dose (720 mg/kg). Puromycin incorporates into elongating polypeptide chains, causing premature termination and accumulation of puromycin-conjugated peptides. These peptides can be detected by anti-puromycin antibody and used as an indicator for *in vivo* protein synthesis rates. At the end of this period, mice were euthanised, and organs of interest were rapidly harvested and snap-frozen in liquid nitrogen. Samples were stored at -72°C until analysis. Tissue lysates were later prepared for RT-qPCR, protein quantification, and western blotting.

2.7 Histological processing

2.7.1 Tissue collection, processing for histology, and image analysis

Skin (dorsal neck region) or liver samples were collected *post-mortem* immediately following euthanasia by the Schedule 1 standard method of humane killing. For the skin samples, before dissection, overlying hair was removed using electric clippers to expose the skin surface, then a rectangular section of dorsal skin (approximately 2 cm x 1 cm) was excised and placed flat into a plastic histology tissue cassette, epidermis side up. For the liver samples, the left lateral and median lobes were dissected to ensure consistency across animals. Samples were immediately submerged in 10% (v/v) neutral buffered formalin (NBF) and fixed at room temperature for 24-48 hours. Following fixation, the cassettes were transferred into 70% (v/v) ethanol and submitted to the Histology Research Service (HRS) at the University of Glasgow for embedding and staining. Paraffin-embedded tissue blocks were sectioned at approximately 4 µm thickness using a microtome prior to mounting on glass slides. Whole-slide

images of skin and liver sections were acquired using a digital slide scanner at stain-dependent magnifications. Haematoxylin & eosin and Masson's trichrome-stained sections were scanned at x40 magnification (0.2609 µm/pixel), whereas toluidine blue-stained sections were scanned at x80 magnification (0.1289 µm/pixel) to enable high-resolution visualisation of mast cell granules. Digital images were analysed using QuPath (version 0.5.0) and Fiji/ImageJ (version 2.16.0). Regions of interest were defined randomly, and stain-specific analyses were conducted using standardised workflows, including colour-based thresholding and cell detection algorithms, depending on the staining modality. Detailed descriptions of specific quantification approaches for each staining method are provided in the corresponding Results chapters. Detailed staining protocols for each histological method are provided in the subsequent sections.

2.7.2 Haematoxylin and Eosin staining

For haematoxylin and eosin (H&E) staining, skin or liver transverse sections were dewaxed in Histo-Clear for 4 minutes then rehydrated through descending ethanol concentrations (100%, 95%, 75%) into distilled water. Sections were then stained with Gill's haematoxylin for 5 minutes to label nuclei. Following a rinse in distilled water, sections were differentiated in 1% acid ethanol (1% HCI in 70% ethanol) to enhance nuclear contrast, then rinsed again in distilled water. Nuclei were subsequently blued by immersion in Scott's tap water substitute (STWS). Sections were counterstained with eosin for 5 minutes to highlight cytoplasmic and extracellular components, followed by a brief rinse in distilled water to remove excess eosin. Finally, sections were dehydrated again through 70%, 95%, and 100% ethanol, cleared in Histo-Clear, and mounted with coverslips. After staining, nuclei appeared blue, while other tissue components displayed varying shades of red and pink. The H&E staining procedure was conducted using an Epredia Gemini AS automated stainer.

2.7.3 Toluidine blue staining

For Toluidine blue staining, skin sections were dewaxed in Histo-Clear for 4 minutes and then rehydrated through descending ethanol concentrations (100%, 95%, 75%) into distilled water. Sections were subsequently rinsed in distilled water to remove ethanol. The sections were then stained in Toluidine blue for 1 minute, followed by a rinse in distilled water. After staining, tissue sections were dehydrated through 70%, 95%, and 100% ethanol, cleared in Histo-Clear, and mounted with a coverslip. Mast cell granules were visualised as purple, while other tissue components appeared blue.

2.7.4 Masson's trichrome staining

For Masson's trichrome staining, skin or liver sections were dewaxed in Histo-Clear for 4 minutes then rehydrated through descending ethanol concentrations (100%, 95%, 75%) into distilled water. Sections were then fixed in Bouin's solution at 57°C for 1 hour. After fixation, the sections were rinsed in distilled water for 10 minutes. The sections were then stained in Weigert's solution for 10 minutes, followed by a 10-minute rinse in distilled water. Sections were then immersed in a 2:1 solution of 1% Ponceau in 1% acetic acid and 1% acid fuchsin in 1% acetic acid for 15 minutes. The sections were then rinsed in distilled water and were treated in a 1:1 solution of 1% phosphotungstic acid (PTA) and 1% paramethoxy aniline (PMA) for 10 minutes to remove cytoplasmic stain (differentiation step), then rinsed again in distilled water. The tissue was then stained in 2.5% aniline blue in 2% acetic acid for 5 minutes, followed by a rinse in distilled water and a brief immersion in 1% acetic acid for 3 minutes. The sections were then dehydrated through 70%, 95%, and 100% ethanol, cleared in Histo-Clear, and mounted with a coverslip. The Masson's trichrome staining was performed on an Epredia Gemini AS automatic stainer.

2.8 Statistical and data analysis

All data analyses were performed using Prism 9.3.1 (GraphPad Software, LLC., 2021), SPSS 29.0.2.0 (20) (Armonk, NY: IBM Corp), and R 4.1.3 (GUI 1.77 Big Sur ARM build, ©R Foundation for Statistical Computing, 2021). Data were first analysed by the ROUT outlier test with Q set to 1%, after that, all data were tested for normality. Any removed outliers are noted in the figure legends. The specific statistical tests are noted in the figure legends. For the t-test, datasets with groups of equal variances (p-value of F-test>0.050) used a normal unpaired t-test; datasets with groups of unequal variances (p-value of F-test <0.050) used an unpaired t-test with Welch's correction.

In the case of 2-way ANOVA, the approach examined genotype (*Polr3b*$^{+/-}$, wild-type), sex (female, male) or age (14 months, 20 months) as main (fixed) factors, also testing interaction effects. In all cases where non-significant interaction effects (*p>0.05*) were identified, these were subsequently removed, and the analysis was rerun with main effects to obtain the best-fit model. Statistical tests used exclusively within individual results chapters are described in the corresponding chapter-specific Methods sections.

Effects and differences were considered significant if the p-value <0.05, where * denotes a p-value of <0.050, ** denotes a p-value of <0.010, and *** denotes a p-value of <0.001. Any significant main or interaction effects are noted in the figures.

Chapter 3: The impact of *Polr3b* heterozygosity on RNA polymerase III signalling

3.1 INTRODUCTION

3.1.1 RNA polymerase III and its signalling cascades

Eukaryotic cells contain three RNA polymerases; of these, RNA Polymerase III (Pol III) is the largest, comprising 17 subunits and responsible for transcribing short non-coding RNAs such as 5S rRNA and tRNAs (Dieci et al., 2007; Willis & Moir, 2018). Together with RNA polymerases I and II, Pol III supports ribosome assembly and protein synthesis, thereby linking transcriptional activity to cellular growth and metabolic status (Liu & Sabatini, 2020; Schramm & Hernandez, 2002). Because of its central role in biosynthetic output, Pol III transcription is tightly regulated by target of rapamycin complex 1 (TORC1), a major controller of anabolic metabolism (Filer et al., 2017).

TORC1 regulates Pol III activity through MAF1, a conserved repressor of Pol III transcription (Moir & Willis, 2013). **Figure 3-1** illustrates how TORC1 regulates Pol III by MAF1. It has been found that both the yeast and mammalian MAF1 proteins are negatively regulated by phosphorylation at seven serine residues, six of which correspond to consensus PKA/Sch9 sites (Moir & Willis, 2013). Under nutrient-rich conditions, TORC1 is active and maintains MAF1 in a phosphorylated state through direct and indirect mechanisms: TORC1 can directly phosphorylate MAF1, and it also activates downstream kinase Sch9 in yeast, which further phosphorylates MAF1 at the consensus sites (Moir & Willis, 2013; Turowski & Tollervey, 2016). The phosphorylated MAF1 therefore remains in the cytoplasm and is unable to bind Pol III, allowing active transcription of tRNAs and 5S rRNA (Moir & Willis, 2013). When TORC1 activity declines during nutrient starvation or rapamycin treatment, phosphorylation of MAF1 at the PKA/Sch9 consensus sites is reduced. Under these conditions, Sch9 activity decreases, along with the dephosphorylation of MAF1 by the PP4 phosphatase complex, whose catalytic subunit Pph3 directly associates with MAF1 and is required for efficient dephosphorylation and repression of Pol III (Moir & Willis,

2013). PP2A can also contribute to MAF1 dephosphorylation, but its role becomes apparent mainly when PP4 is impaired (Moir & Willis, 2013). These phosphatases dephosphorylate MAF1 by removing the phosphate groups from the protein (Turowski & Tollervey, 2016). Dephosphorylated MAF1 subsequently accumulates in the nucleus and nucleolus, where it binds TFIIIB and Pol III and inhibits transcription initiation (Boguta, 2013; Moir & Willis, 2013; Upadhya et al., 2002). This mechanism appears to be conserved in eukaryotes and enables cells to conserve energy under nutrient stress by reducing the synthesis of energetically costly Pol III transcripts (Willis & Moir, 2018). It is worth noting that ribosomal protein S6 kinase 1 (S6K1) is the functional mammalian homolog of yeast Sch9, as both are TORC1-regulated AGC kinases that promote protein synthesis and growth; however, unlike Sch9, S6K1 does not phosphorylate MAF1 (Moir & Willis, 2013).

In mammalian cells, protein synthesis is a major energy-demanding process regulated by the mTORC1 pathway (Liu & Sabatini, 2020). Upon activation, mTORC1 phosphorylates two major translational effectors: the eukaryotic translation repressor 4E-binding proteins (4E-BPs) and S6K1 (Liu & Sabatini, 2020). Phosphorylated S6K1 subsequently phosphorylates ribosomal protein S6 (rpS6), resulting in the translation of 5'TOP mRNAs that encode ribosomal proteins and translation factors, thereby promoting ribosome biogenesis and protein synthesis (Magnuson et al., 2012). Phosphorylated S6 therefore serves as a surrogate marker for mTORC1 activity (Chowdhury & Kohler, 2015). Through this pathway, the mTORC1-S6K1-rpS6 axis couples nutrient and growth signals to translational capacity. In cancer cells, expression of a constitutively active S6K1 mutant can alleviate PTEN-mediated repression of Pol III-dependent transcripts $tRNA^{Leu}$ and 7SL RNA, suggesting that the mTOR-S6K1 axis is capable of modulating Pol III output under certain conditions (Woiwode et al., 2008). However, immune-purified S6K1 fails to phosphorylate human MAF1 in vitro, and MAF1 phosphorylation to mTORC1 inhibition is preserved in S6K1/2-deficient cells (Moir & Willis, 2013). These findings indicate that, unlike in yeast, in mammalian cells, mTORC1 might predominantly regulate Pol III transcription through direct phosphorylation of MAF1 rather than via S6K1 (yeast homolog Sch9).

Reduced Pol III activity extends lifespan in *S. cerevisiae, C. elegans,* and *D. melanogaster* (Filer et al., 2017; Malik, Goncalves Silva, et al., 2024). In *Drosophila*, gut-specific reduction of Pol III activity decreases pre-tRNA levels and is accompanied by a decline in protein synthesis within the intestine (Filer et al., 2017). Comparable assays of protein synthesis have not been conducted in other organism models; however, the conserved longevity phenotype across species indicates that reduced Pol III activity enhances longevity through mechanisms linked to nutrient signalling, translational output, and tissue-specific maintenance, including improved gut and muscle function as reported in *D. melanogaster* and *C. elegans*, and organ-specific effects on bone and intestinal integrity in mice (Borland et al., 2024; Filer et al., 2017; Malik, Goncalves Silva, et al., 2024).

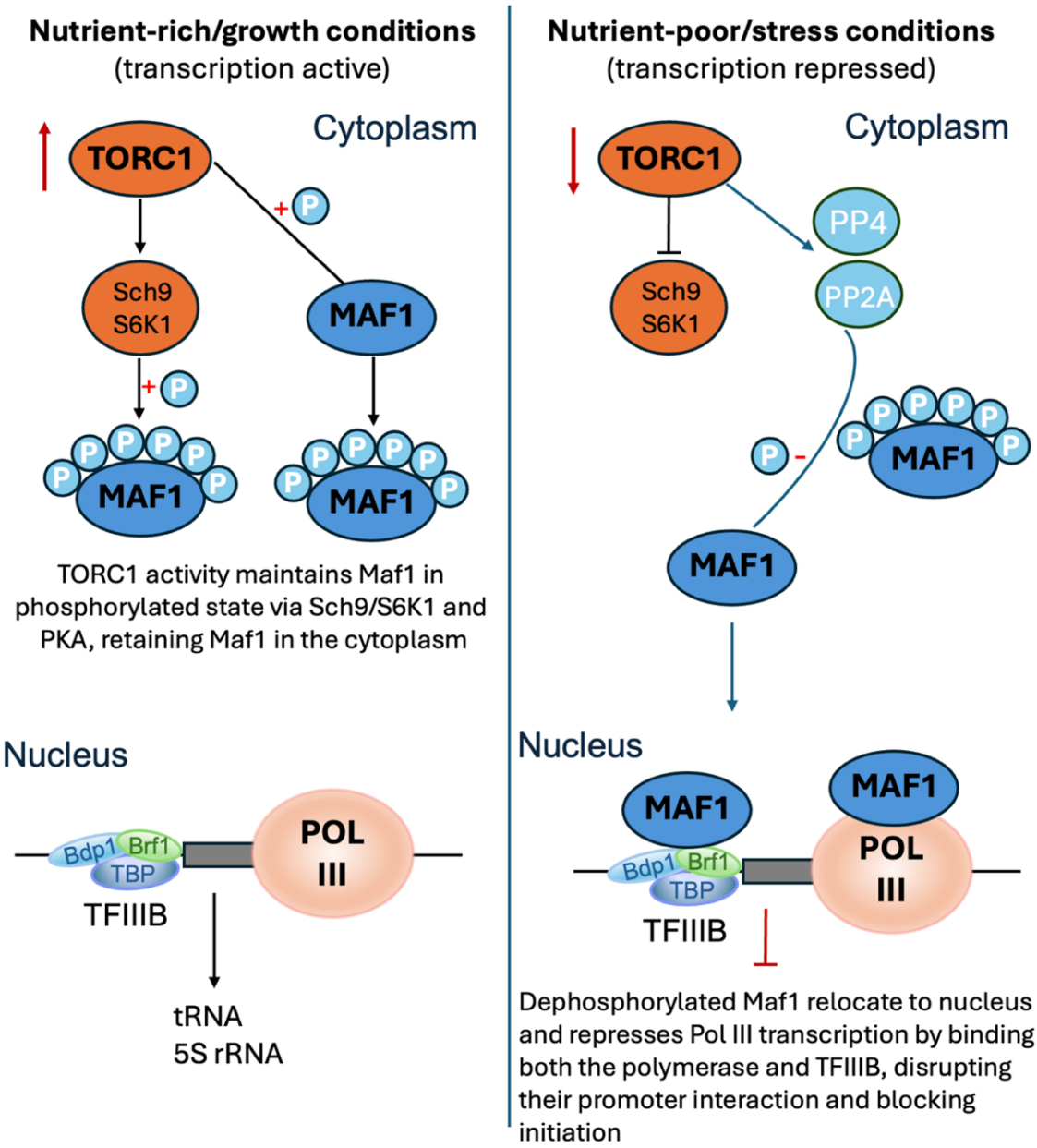

Figure 3-1 Regulation of RNA Polymerase III by the TORC1-MAF1 pathway

Under nutrient-rich conditions, TORC1 is active and maintains MAF1 in a phosphorylated form through direct phosphorylation and through activation of the downstream kinase Sch9 in yeast. Phosphorylated MAF1 is retained in the cytoplasm and cannot associate with Pol III, allowing Pol III promoter TFIIIB complex to initiate transcription of tRNAs, 5S rRNA, and other short non-coding RNAs. When nutrients become limited or TORC1 is inhibited, TORC1 signalling decreases. The kinases that normally phosphorylate MAF1 are inactivated, while protein phosphatases such as PP4 and PP2A remove phosphate groups from MAF1. Dephosphorylated MAF1 moves into the nucleus and nucleolus, where it binds Pol III and represses transcription initiation.

3.1.2 RNA polymerase III, proteostasis, and heat shock proteins

Polypeptides synthesised by RNA polymerases, including Pol III, must acquire proper three-dimensional conformations to become functional (Cooper, 2000). This process depends on molecular chaperones, including the heat shock protein (HSP) families, which assist in nascent protein folding, complex assembly, and degradation of misfolded proteins to maintain proteostasis and coordinate cellular stress responses (Cooper, 2000; Hu et al., 2022). During stress conditions such as heat shock, nutrient deprivation, or oxidative challenge, global translation is typically repressed, whereas HSPs and other chaperones are either upregulated or downregulated to preserve proteostasis (Hu et al., 2022; Moura et al., 2018). The major HSP families, including HSP70, HSP60, and HSP90, are highly conserved across all domains of life and are required for cellular survival under proteotoxic or metabolic stress (Richter et al., 2010). Beyond their cytoplasmic folding roles, HSPs also stabilise nuclear and transcriptional complexes. HSP90, for example, assists in the assembly or turnover of RNA polymerase complexes in the cytoplasm, buffering imbalances in subunit stoichiometry - that is, the precise ratio of subunits required for proper complex formation, and ensuring correct complex formation (Boulon et al., 2010; Tian et al., 2023). These findings demonstrate that chaperone capacity is also closely linked to polymerase-dependent biosynthetic status.

3.1.3 RNA polymerase III subunit B (Polr3b)

In *Homo sapiens*, the *Polr3b* gene encodes the second-largest subunit of Pol III (**Figure 3-2**). In *Mus musculus*, the orthologous gene encodes POLR3B, which together with POLR3A forms the catalytic active centre of Pol III. **Table 3-1** summarises Pol III subunit mutations and associated human diseases. In terms of the *Polr3b* mutations associated diseases, despite not having been systematically examined, clinical case studies in humans have shown that mutations in *Polr3b* have been associated with diverse conditions, including premature ageing (Wu et al., 2021), hypomyelination (Verberne et al., 2020), RNA splicing dysregulation, impaired protein synthesis and neuronal function (Saghi et al., 2022). Specifically, heterozygous *Polr3b* variants have been identified in individuals

with Wiedemann-Rautenstrauch syndrome (WRS), a rare disorder characterised by premature ageing (Wu et al., 2021). Loss-of-function mutations in *Polr3b* are associated with autosomal recessive hypomyelinating leukodystrophy 8 (HLD8), a disease affecting oligodendroglia cells by impairing the morphological differentiation of the cells (Sawaguchi et al., 2022). Oligodendroglia are responsible for myelin formation in the central nervous system in humans (Daoud et al., 2013; Saitsu et al., 2011), and their differentiation involves the dynein cofactor NDE1 (Shimizu et al., 2018). Homozygous missense *Polr3b* mutations have also been found in individuals with intellectual disability (ID), a neurodevelopmental disorder characterised by transcription factors such as FOXC2 and GATA1 (Saghi et al., 2022). Additionally, in individuals with ID with *Polr3b* mutation, dysregulation and upregulation of genes involved in tumour progression and metastasis, the immune system function, and the nervous system function have been observed (Saghi et al., 2022). Furthermore, a study in the *Danio rerio* (zebrafish) model has demonstrated that *Polr3b* is also essential for the growth of tissue progenitor cells in the digestive system (Yee et al., 2007). Collectively, these studies underscore the tightly regulated nature of Pol III subunits, and as the crucial catalytic subunit of Pol III, POLR3b plays important roles in gene transcription, cell growth, myelination, immune function, and neurodevelopment, highlighting its emerging role in ageing research.

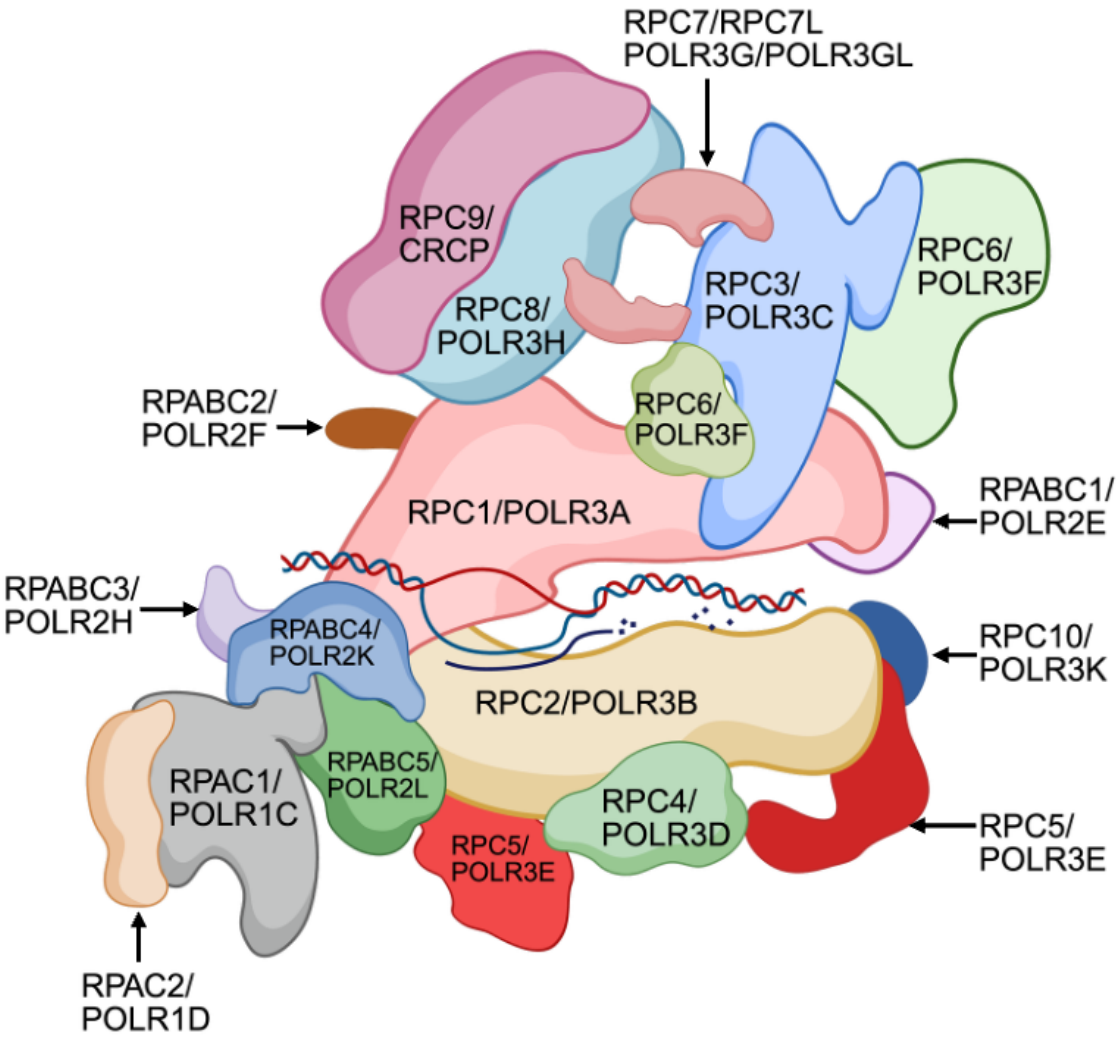

Figure 3-2 Subunits of human RNA Polymerase III

Pol III is composed of 17 subunits; it is the most complex enzyme in eukaryotic cells in terms of protein composition. This figure displays all seventeen subunits. Among these subunits, the RPC1/RPC2 complex is the core subunit; the RPC4/RPC5 complex is required for termination and reinitiation, and the RPC3/RPC6/RPC7 complex is required for transcription initiation. Diagram modified from Lata et al. (2021) and Girbig et al. (2021).

Table 3-1 Pol III subunit mutations and associated human diseases

Gene/subunit	Principal associated disease(s)	Core clinical features	Key references
POLR3A / RPC1	POLR3-related hypomyelinating leukodystrophy (4H spectrum); Wiedemann-Rautenstrauch syndrome (WRS) associated with biallelic loss-of-function variants	Childhood-onset diffuse hypomyelination with cerebellar motor dysfunction, dental anomalies, endocrine abnormalities and progressive myopia; WRS presents with prenatal or postnatal growth failure and neonatal progeroid features.	(Bernard et al., 2011; Wambach et al., 2018; Wolf et al., 2014)
POLR3B / RPC2	POLR3-related hypomyelinating leukodystrophy	Diffuse hypomyelination with cerebellar dysfunction, delayed dentition or hypodontia, and variable endocrine involvement; POLR3B-associated disease is often comparatively milder than POLR3A-associated disease.	(Tetreault et al., 2011; Wolf et al., 2014)
POLR1C / RPAC1	POLR3-related hypomyelinating leukodystrophy; autosomal-recessive Treacher Collins syndrome (TCS)	Some individuals with TCS show craniofacial abnormalities consistent with mandibulofacial dysostosis.	(Dauwerse et al., 2011; Thiffault et al., 2015)
POLR3K / RPC10	POLR3-related hypomyelinating leukodystrophy	Developmental delay, diffuse hypomyelination, cerebellar atrophy and variable extraneurological involvement, including gastrointestinal dysfunction in early reports.	(Dorboz et al., 2018; Perrier et al., 2024)
POLR3GL	POLR3GL-related disorder with endosteal hyperostosis and oligodontia; Wiedemann-Rautenstrauch-like neonatal progeroid syndrome	Short stature, oligodontia, axial endosteal hyperostosis and mild facial dysmorphism; progeroid presentations include severe growth restriction, apparent macrocephaly and lipodystrophy.	(Beauregard-Lacroix et al., 2020; Terhal et al., 2020)

In this chapter, Pol III-related gene expression and protein abundance were examined in *Polr3b*$^{+/-}$ mice to determine how partial loss of the RNA Polymerase III catalytic subunit *Polr3b* influences the related signalling cascades and stress responses. Analyses included the catalytic subunits POLR3B and POLR3A, the transcriptional repressor MAF1, the mTORC1 effector ribosomal protein S6 and its phosphorylated form, which indicates the mTOR activity, overall protein synthesis, and the molecular chaperones HSP60 and HSP90. Both female and male mice were studied to identify potential sex-dependent effects. Tissue analyses focused on the liver, brain, and skeletal muscle, where *Polr3b* expression is relatively high. Primary dermal fibroblasts were also assessed. These experiments were designed to confirm the efficacy of heterozygous *Polr3b* deletion in these mice and to characterise the impact of reduced Pol III activity on translational capacity and proteostatic regulation across tissues and primary dermal fibroblasts.

3.2 AIMS AND OBJECTIVES

Aims: Partial knockdown of RNA Polymerase III has been shown to extend the lifespan from yeast to flies, with its transcription negatively regulated by MAF1 repressor and acting on lifespan downstream of TORC1 (Bonhoure et al., 2020; Filer et al., 2017). Pol III transcribes 5S rRNA and tRNAs required for ribosome assembly and protein synthesis - processes essential for cell growth, proliferation, and cell development. Using C57BL/6N mice heterozygous for *Polr3b* (*Polr3b*$^{+/-}$), this chapter aims to investigate how the absence of one allele of *Polr3b* influences Pol III-related cascade kinases, protein synthesis, and heat shock protein levels in selected tissues and primary dermal fibroblasts. The liver and brain were selected for detailed study because *Polr3b* is reported to be highly expressed in these tissues according to the Mouse Genome Informatics Database (The Jackson Laboratory, 2025).

Objective 1: Quantify mRNA expression of Pol III-related genes (*Polr3b, Polr3a, Maf1*) in liver, brain, and skeletal muscle from *Polr3b*$^{+/-}$ mice, compared to wild-type controls.

Objective 2: Assess protein abundance of POLR3B, POLR3A, and MAF1, and quantify phosphorylation of ribosomal protein S6 (total S6 and phospho-S6) in liver, brain, skeletal muscle (for POLR3B only), and primary dermal fibroblast cells from *Polr3b*$^{+/-}$ mice compared to wild-type controls.

Objective 3: Assess protein synthesis by measuring the levels of puromycin-conjugated peptide abundance via western blotting in liver and brain from *Polr3b*$^{+/-}$ mice compared to wild-type controls.

Objective 4: Determine HSP60 and HSP90 protein levels in the liver of the *Polr3b*$^{+/-}$ mice, compared to wild-type controls.

3.3 METHODS

3.3.1 Mouse model and husbandry

Polr3b wild-type (*Polr3b*$^{+/+}$) and heterozygous mutant (*Polr3b*$^{+/-}$) mice on a C57BL/6N background were used. Experimental animals were generated as described in **Chapter 2, Section 2.1**. Mice were housed under standard conditions with *ad libitum* access to water and standard mouse chow. All procedures were approved by the University of Glasgow Animal Welfare and Ethical Review Board and conducted under UK Home Office project licences. Full details are provided in Chapter 2.

3.3.2 Intraperitoneal (IP) injection of mice with puromycin as a protein synthesis reporter

Mice aged 4.4 ± 0.2 months (mean ± SEM) were intraperitoneally injected with puromycin dihydrochloride (0.04 µmol/g body weight; ThermoFisher Scientific), dissolved in PBS and sterile-filtered prior to use. Mice were maintained under *ad libitum* feeding conditions and returned to a sterile cage for a 30-minute labelling period. Following labelling, mice were euthanised, and tissues were rapidly harvested and snap-frozen in liquid nitrogen. Samples were stored at -72°C until further analysis. Full details are provided in **Chapter 2, Section 2.6.2**.

3.3.3 Cell culture for dermal fibroblasts

Primary dermal fibroblasts were isolated from ear tissue of 5-month-old female WT and *Polr3b*$^{+/-}$ mice and cultured under standard conditions. Cells were passaged and cryopreserved prior to downstream applications. Full details of the tissue processing, digestion, culture conditions and cryopreservation procedures are provided in **Chapter 2, Section 2.4.**

3.3.4 Protein lysates extraction and western blot analysis

Protein lysates were extracted from tissues or cells and analysed by SDS-PAGE and Western blotting. Protein levels were normalised using total protein staining. The antibodies used are listed on **Table 2-3**. Full details are provided in **Chapter 2, Section 2.6.1**.

3.3.5 Reverse Transcriptase quantitative-PCR (RT-qPCR)

RNA extraction and quality assessment were performed as described in Chapter 2 (**Section 2.5**). For each sample, 2 µg of total RNA was reverse-transcribed using M-MLV Reverse Transcriptase with random hexamers. The resulting cDNA was diluted to 12.5 ng/µL in nuclease-free water.

Quantitative PCR was performed using SYBR Green chemistry. Each reaction contained cDNA, SYBR Green Master Mix, primers, and PCR-grade water. Reference genes *B2m* and *Ywhaz* were selected based on expression stability within each tissue. Cycling conditions were followed by a standard melt-curve analysis. Primer sequences are shown in **Table 4-1**.

Relative expression was calculated by the 2^{-DDCt} method. normalised to the geometric mean of reference genes, and expressed relative to the WT group.

Table 3-2 Primer sequences used in RT-qPCR experiments

Gene	Forward primer	Reverse primer
B2m	5'-CATGGCTCGCTCGGTGAC-3'	5'-CAGTTCAGTATGTTCGGCTTCC-3'
Ywhaz	5'-GAAAAGTTCTTGATCCCCAATGC-3'	5'-TGTGACTGGTCCACAATTCCTT-3'
Maf1	5'-GACTATGACTTCAGCACAGCC-3'	5'-CTGGGTTATAGCTGTAGATGTCAC-3'
Polr3a	5'- GCTTGCCAGATCATCGCTTCAATAC-3'	5'- GTCCACAGGGTGACAGGCTTTA-3'
Polr3b	5'-TTGGAGCCTCAGTTACCAGC-3'	5'-GAATCGACCCTGTTTCACGG-3'

Abbreviations: *B2m: Beta-2 microglobulin; Ywhaz: Tyrosine 3-monooxygenase/tryptophan 5-monooxygenase activation protein zeta polypeptide; Polr3a: Polymerase (RNA) III (DNA directed) polypeptide A; Polr3b: Polymerase (RNA) III (DNA directed) polypeptide B.*

3.3.6 Statistics and data analysis

All analyses were performed using Prism 10.4.2 (GraphPad Software, LLC., 2025). Data were first analysed by the ROUT outlier test with Q set to 1%; after that, all data were tested for normality. Any removed outliers are noted in the figure legends. The specific statistical tests are noted in the figure legends. For data with one independent variable, the unpaired t-test or non-parametric Mann-Whitney U test was used. For assessing the equality of variance, datasets with groups of the same equal variances (p-value of F-test >0.050) used a normal unpaired t-test; datasets with groups of unequal variances (p-value of F-test <0.050) used an unpaired t-test with Welch's correction.

For all analyses, effects and differences were considered significant if the p-value <0.05, where * denotes a p-value of <0.050, ** denotes a p-value of <0.010, and *** denotes a p-value of <0.001. Any significant main or interaction effects are noted in the figure.

3.4 RESULTS

3.4.1 Reduced *Polr3b* mRNA expression in liver and brain of male, but not female, *Polr3b*$^{+/-}$ mice

Polr3b mRNA expression was measured in liver, brain, and skeletal muscle tissues of *Polr3b*$^{+/-}$ and WT mice. In females, no significant differences were detected in liver (*t=1.696, p=0.062*, **Figure 3-3 (a)**) or brain (*t=0.413, p=0.344*, **Figure 3-3 (b)**) between genotypes. In males, *Polr3b*$^{+/-}$ mice showed significantly lower *Polr3b* expression in the liver (*t=2.747, p=0.010*, **Figure 3-3 (d)**) and brain (*t=3.504, p=0.003*, **Figure 3-3 (e)**) compared with WT controls. No genotypic differences were observed in the skeletal muscle in either sex (female *t=0.508, p=0.311*, **Figure 3-3 (c)**; male *t=0.560, p=0.311*, **Figure 3-3 (f)**).

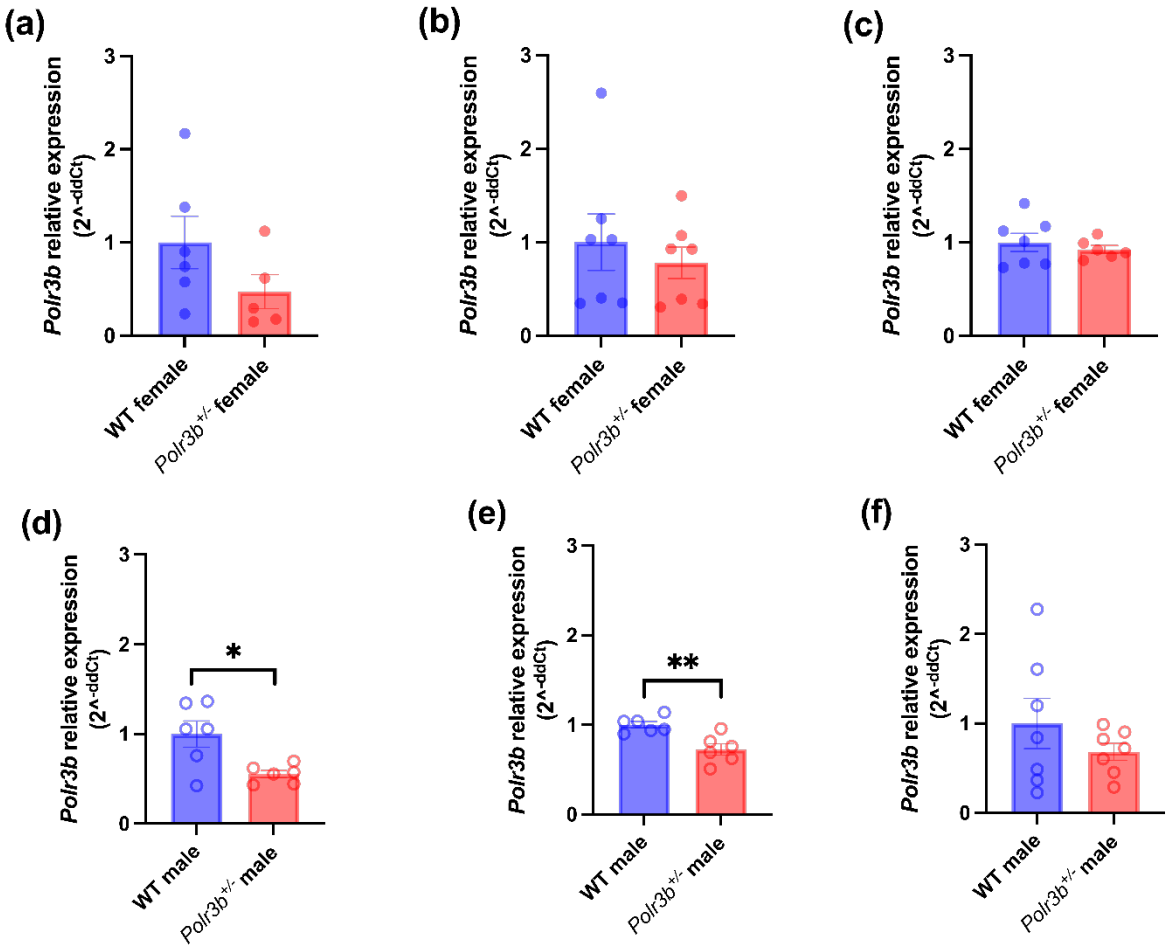

Figure 3-3 mRNA expression of *Polr3b* in liver, brain, and skeletal muscles of 4-month-old WT and *Polr3b*$^{+/-}$ mice

*Polr3b mRNA expression in liver (a,d), brain (b,e) and skeletal muscle (c,f) of 4-month-old female and male mice. Histograms denote means ± SEM, with sample sizes indicated by individual points within each group. An unpaired t-test was used to test for genotype differences. *=p<0.050, **=p<0.010.*

3.4.2 *Polr3a* mRNA expression is unaffected by genotype in liver, brain, and skeletal muscle

mRNA expression of *Polr3a*, which encodes the largest subunit of Pol III, was examined in liver, brain, and skeletal muscle tissues. No significant genotypic differences were detected in the liver (female *t=0.622, p=0.541*, **Figure 3-4 (a)**; male *t=1.783, p=0.105*, **Figure 3-4 (d)**), brain (female *t=0.704, p=0.495*, **Figure 3-4 (b)**; male *t=1.402, p=0.189*, **Figure 3-4 (e)**), or skeletal muscle (female *t=0.680, p=0.511*, **Figure 3-4 (c)**; male *t=0.023, p=0.982*, **Figure 3-4 (f)**) in either sex.

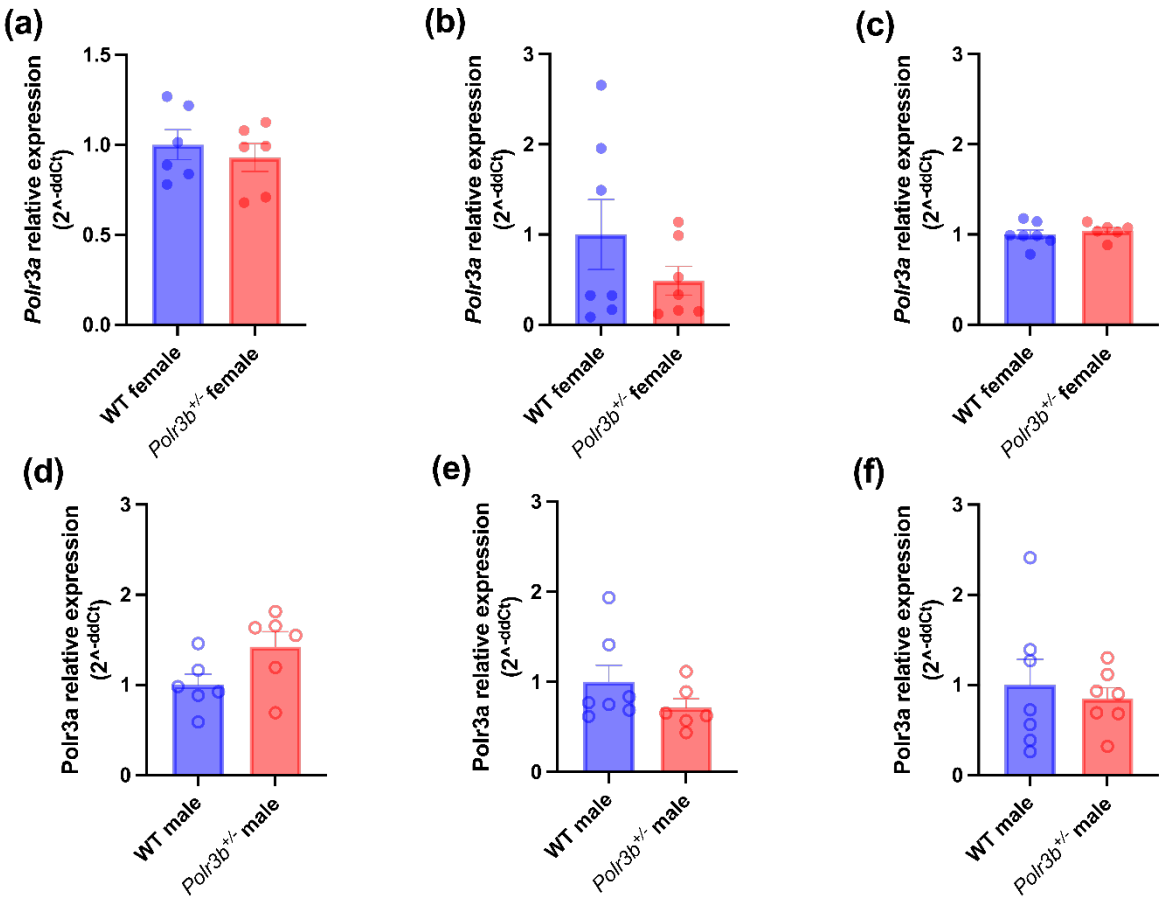

Figure 3-4 mRNA expression of *Polr3a* in liver, brain, and skeletal muscles in WT and *Polr3b*$^{+/-}$ mice

Polr3a mRNA expression in liver (a,d), brain (b,e) and skeletal muscle (c,f) of female and male mice. Histograms denote means ± SEM, with sample sizes indicated by individual points within each group. ROUT outlier tests were performed and one outlier was removed from (e) of Polr3b$^{+/-}$ *group. Unpaired t-test was used to test for genotype differences. All comparisons were non-significant.*

3.4.3 Increased *Maf1* expression in liver of the *Polr3b*$^{+/-}$ male mice

MAF1 is known for the central inhibitor of Pol III. Therefore, *Maf1* expression was also examined across tissues in WT and *Polr3b*$^{+/-}$ mice. No genotypic difference of *Maf1* expression was seen in female liver (*t=1.596*, *p=0.142*, **Figure 3-5 (a)**); however, higher *Maf1* expression was found in the liver of *Polr3b*$^{+/-}$ male mice compared to WT males (*t=2.631*, *p=0.025*, **Figure 3-5 (d)**). No genotypic differences were observed in brain (female *t=1.456*, *p=0.171*, **Figure 3-5 (b)**; male *t=0.690*, *p=0.*504, **Figure 3-5 (e)**) or skeletal muscle (female *t=1.952*, *p=0.077*, **Figure 3-5 (c)**) in either sex.

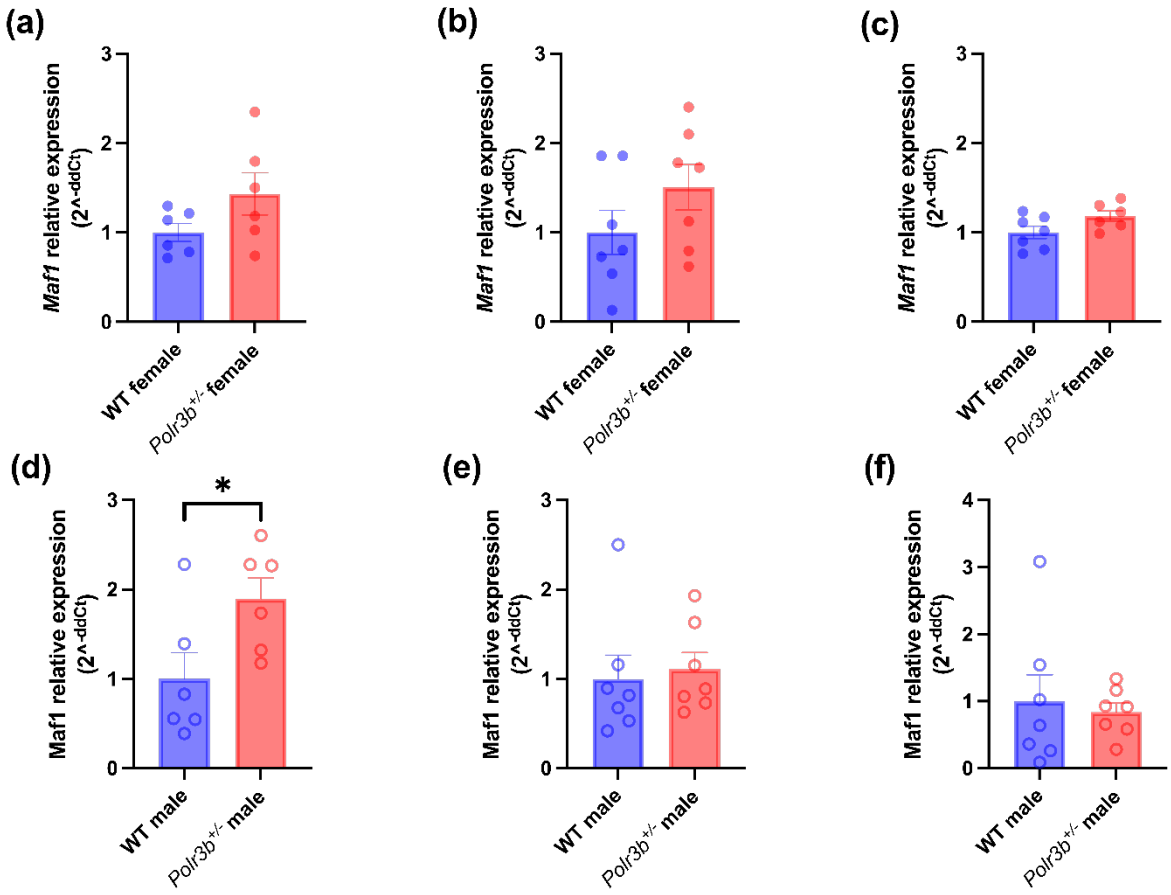

Figure 3-5 Expression of *Maf1* in liver, brain, and skeletal muscle in WT and *Polr3b*$^{+/-}$ mice

*Maf1 mRNA expression in liver (a,d), brain (b,e) and skeletal muscle (c,f) of female and male mice. Histograms denote means ± SEM, with sample sizes indicated by individual points within each group. Unpaired t-test was used to test for genotype differences. *=p<0.050.*

3.4.4 Reduced hepatic POLR3b protein levels in female *Polr3b*$^{+/-}$ mice

A significant reduction in POLR3b protein was observed in the liver of female *Polr3b*$^{+/-}$ mice compared with WT controls (*t=2.720, p=0.009*; **Figure 3-6 (a)**). In contrast, male mice showed no difference in hepatic POLR3b levels (*t=1.034, p=0.162*, **Figure 3-6 (b)**). POLR3b abundance in the brain and skeletal muscle did not differ between genotypes in either sex (female brain *t=0.737, p=0.238*, **Figure 3-7 (a)**; male brain *t=1.085, p=0.150*, **Figure 3-7 (b)**; female muscle *t=1.771, p=0.052*, **Figure 3-8 (a)**; male muscle *t=1.422, p=0.093*, **Figure 3-8 (b)**). Similarly, POLR3b protein levels in primary dermal fibroblasts were unchanged by genotype in both sexes (female *t=0.299 p=0.385*, **Figure 3-9 (a)**; male *t=0.279, p=0.394*, **Figure 3-9 (b)**).

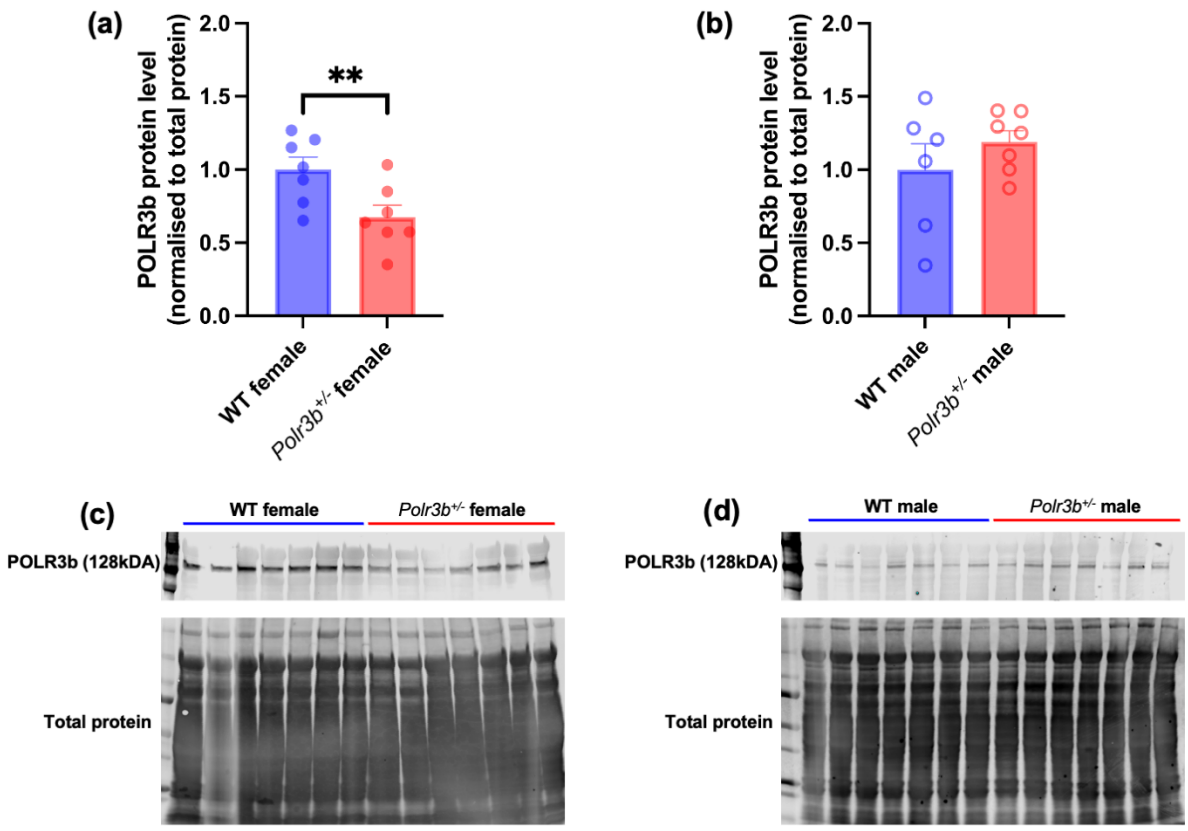

Figure 3-6 POLR3b protein levels in the livers of 4-month-old WT and *Polr3b*$^{+/-}$ mice

POLR3b protein levels in liver lysates of WT and Polr3b$^{+/-}$ *female (a) and male (b) mice. Histograms denote means ± SEM, with sample sizes indicated by individual points within each group. One WT male sample was excluded due to imaging artefacts that prevented accurate quantification. Panels (c-d) show the corresponding immunoblots of POLR3b along with REVERT total protein-stained membranes. Quantification was normalised to total protein. **=p<0.010.*

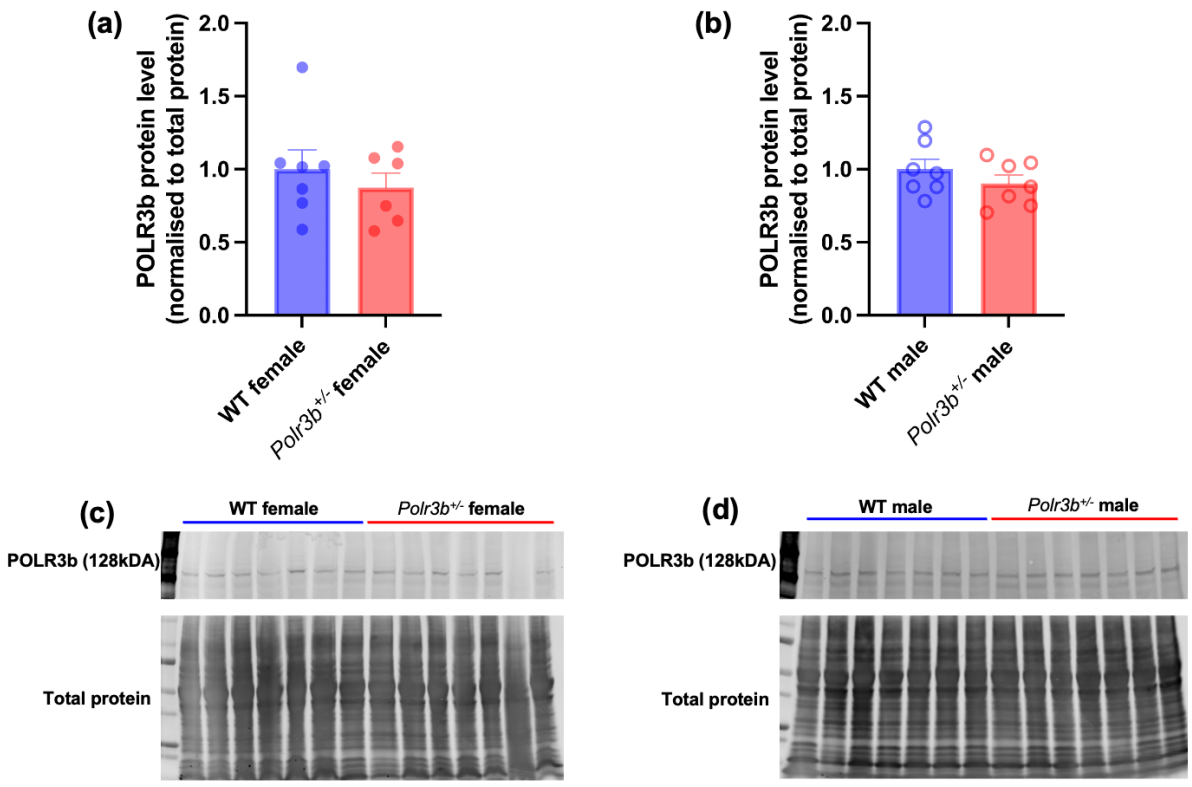

Figure 3-7 POLR3b protein levels in the brain of 4-month-old WT and *Polr3b*$^{+/-}$ mice

POLR3b protein levels in brain lysates of WT and Polr3b$^{+/-}$ *female (a) and male (b) mice. Histograms denote means ± SEM, with sample sizes indicated by individual points within each group. One Polr3b*$^{+/-}$ *female sample was excluded due to imaging artefacts that prevented accurate quantification. Panels (c-d) show the corresponding immunoblots of POLR3b along with REVERT total protein-stained membranes. Quantification was normalised to total protein.*

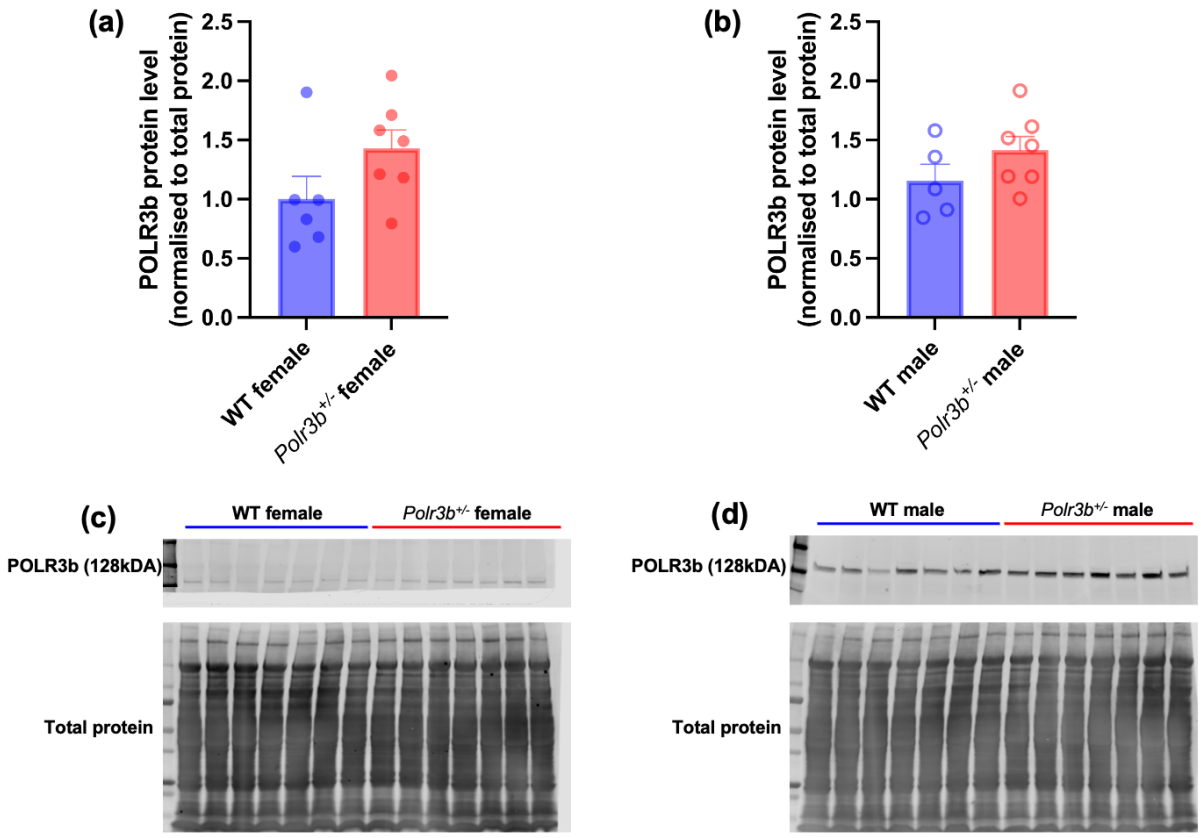

Figure 3-8 POLR3b protein levels in the skeletal muscle of 4-month-old WT and *Polr3b*$^{+/-}$ mice

POLR3b protein levels in skeletal muscle lysates of WT and Polr3b$^{+/-}$ *female (a) and male (b) mice. Histograms denote means ± SEM, with sample sizes indicated by individual points within each group. One WT female and one WT male sample were excluded due to quantification artefacts, including imaging issues and undetectable signals. Panels (c-d) show the corresponding immunoblots of POLR3b along with REVERT total protein-stained membranes. Quantification was normalised to total protein.*

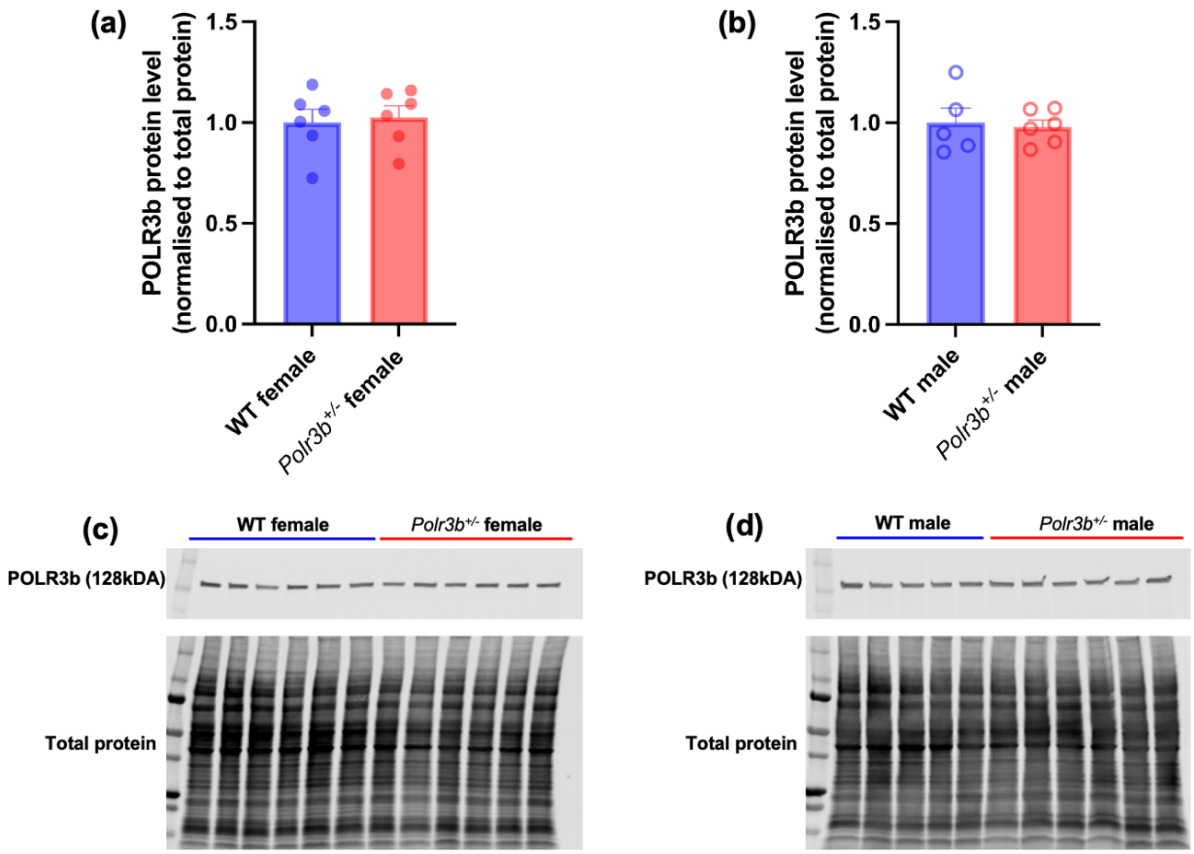

Figure 3-9 POLR3b protein levels in primary dermal fibroblasts of 5-month-old WT and *Polr3b*$^{+/-}$ mice

POLR3b protein levels were measured in dermal fibroblast lysates from WT and Polr3b$^{+/-}$ *female (a) and male (b) mice. Histograms denote means ± SEM, with sample sizes indicated by individual points within each group. Panels (c-d) show the corresponding immunoblots for POLR3b, alongside REVERT total protein-stained membranes. Quantification was normalised to total protein.*

3.4.5 No differences in POLR3a protein levels between WT and *Polr3b*$^{+/-}$ mice

POLR3a protein levels were examined in tissues and primary dermal fibroblasts of the *Polr3b*$^{+/-}$ mice. No genotypic differences were detected in liver (female *t=1.930, p=0.078*, **Figure 3-10 (a)**; male *t=0.809, p=0.436*, **Figure 3-10 (b)**), brain (female *t=1.501, p=0.161*, **Figure 3-11 (a)**; male *t=0.948, p=0.362*, **Figure 3-11 (b)**) and dermal fibroblasts (female *t=0.388, p=0.706*, **Figure 3-12 (a)**; male *t=0.872, p=0.406*, **Figure 3-12 (b)**) of WT and *Polr3b*$^{+/-}$ mice in either sex.

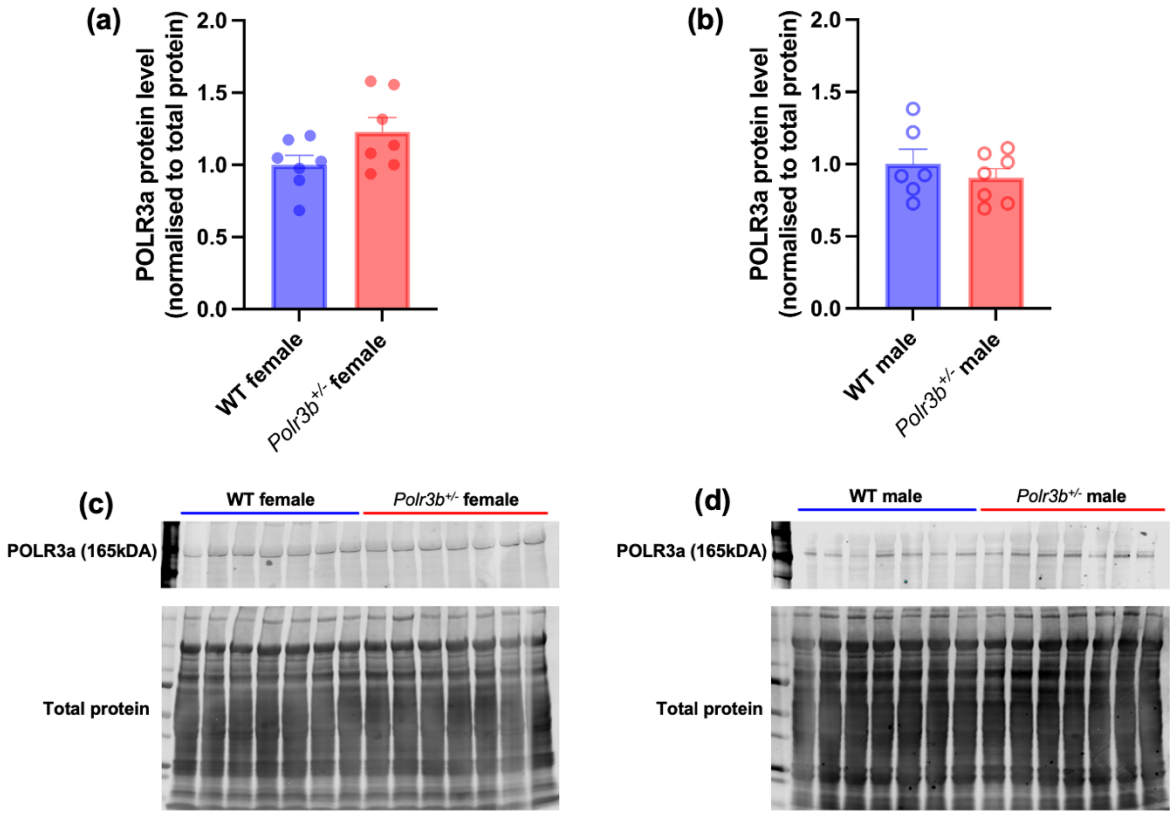

Figure 3-10 POLR3a protein levels in liver of WT and *Polr3b*$^{+/-}$ mice

POLR3a protein levels in liver lysates of 4-month-old WT and Polr3b$^{+/-}$ *female (a) and male (b) mice. Histograms denote means ± SEM, with sample sizes indicated by individual points within each group. One WT male sample was excluded due to spots overlapping that prevented accurate quantification. Panels (c-d) show the corresponding immunoblots of POLR3a along with REVERT total protein-stained membranes. Quantification was normalised to total protein.*

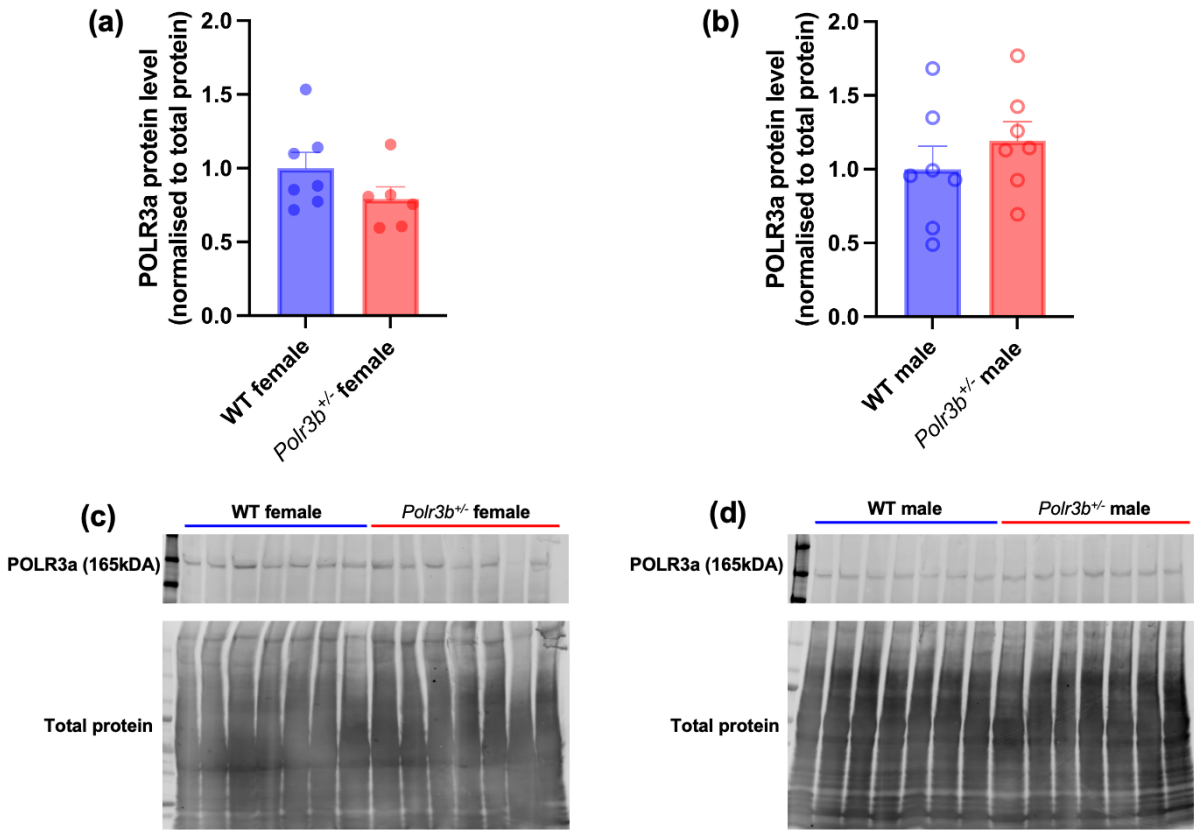

Figure 3-11 POLR3a protein levels in brain of WT and *Polr3b*$^{+/-}$ mice

POLR3a protein levels in brain lysates of WT and Polr3b$^{+/-}$ *female (a) and male (b) mice. Histograms denote means ± SEM, with sample sizes indicated by individual points within each group. One Polr3b*$^{+/-}$ *female was excluded due to quantification artefacts of undetectable signals. Panels (c-d) show the corresponding immunoblots of POLR3a along with REVERT total protein-stained membranes. Quantification was normalised to total protein. Unpaired two-tailed t-tests were used to test for genotype differences.*

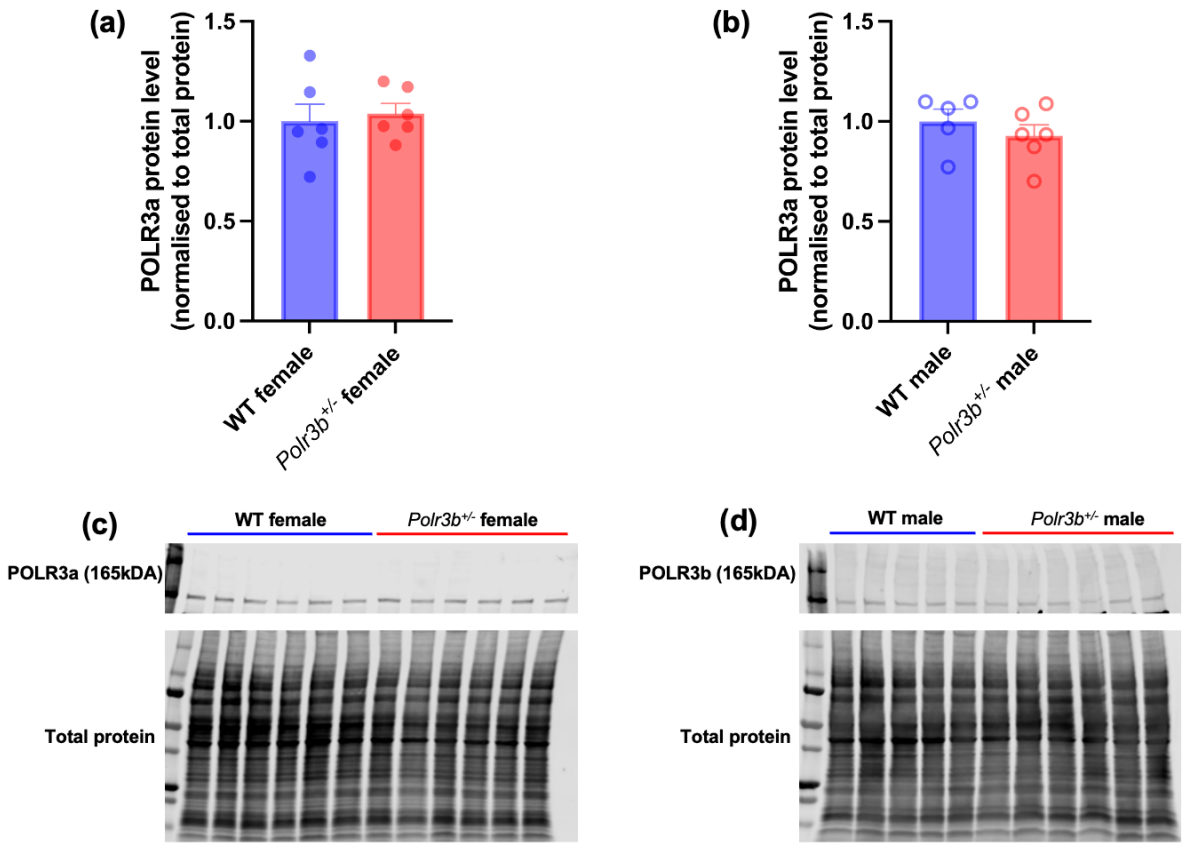

Figure 3-12 POLR3a protein levels in primary dermal fibroblasts of WT and *Polr3b*$^{+/-}$ mice

POLR3a protein levels were measured in dermal fibroblast lysates from WT and Polr3b$^{+/-}$ *female (a) and male (b) mice. Histograms denote means ± SEM, with sample sizes indicated by individual points within each group. Panels (c-d) show the corresponding immunoblots for POLR3a, alongside REVERT total protein-stained membranes. Quantification was normalised to total protein. Unpaired two-tailed t-tests were used to test for genotype differences.*

3.4.6 Reduced MAF1 protein level in dermal fibroblasts of *Polr3b*$^{+/-}$ mice

No significant genotypic differences were found in liver and brain of WT and *Polr3b*$^{+/-}$ mice in either sex (female liver tissues *t=0.338, p=0.742*, **Figure 3-13 (a)**; male liver tissues *t=1.590, p=0.142*, **Figure 3-13 (b)**; female brain tissues *t=0.970, p=0.351*, **Figure 3-14 (a)**; male brain tissues *t=1.669, p=0.516*, **Figure 3-14 (b)**). A reduction in MAF1 protein levels was detected in dermal fibroblasts of *Polr3b*$^{+/-}$ mice in both sexes (female *t=3.416, p=0.007*, **Figure 3-15 (a)**; male *t=2.963, p=0.016*, **Figure 3-15 (b)**).

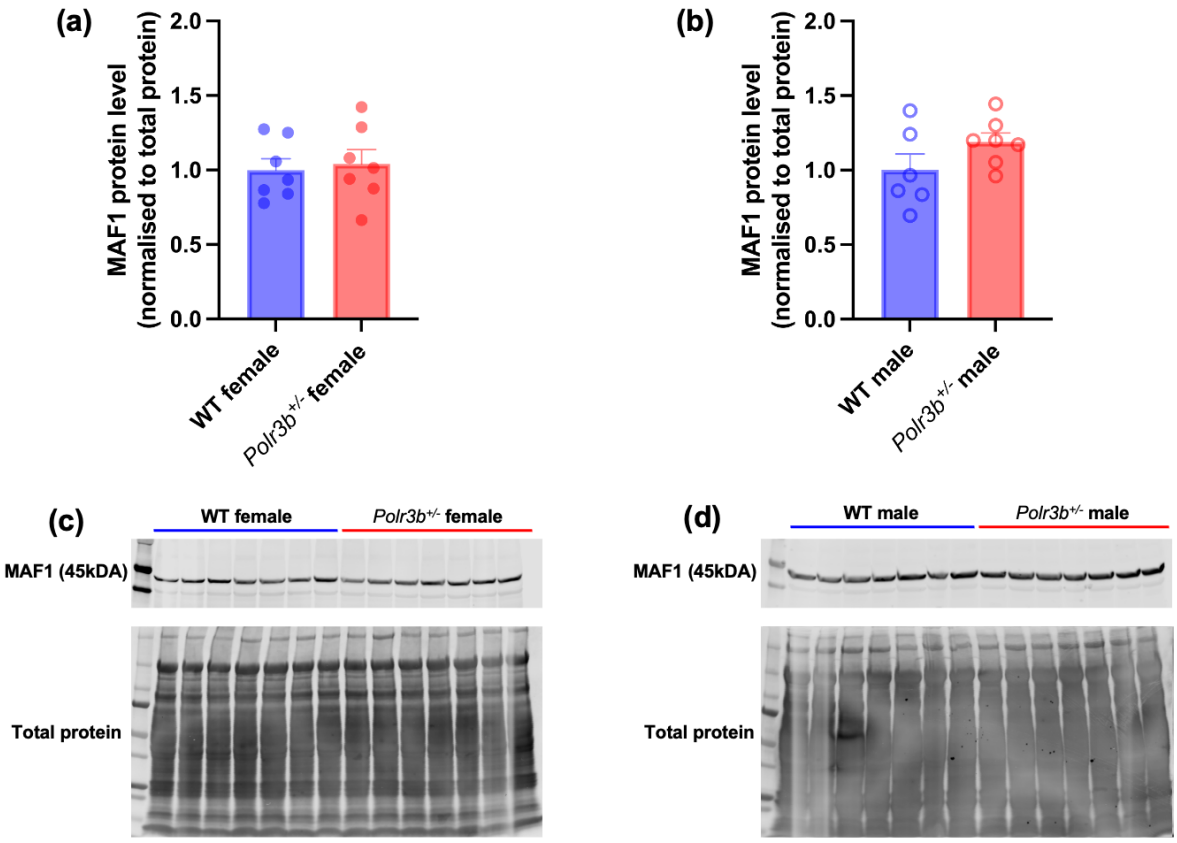

Figure 3-13 MAF1 protein levels in the livers of WT and *Polr3b*$^{+/-}$ mice

MAF1 protein levels in liver lysates of WT and Polr3b$^{+/-}$ *female (a) and male (b) mice. Histograms denote means ± SEM, with sample sizes indicated by individual points within each group. One WT male sample was excluded due to imaging artefacts that prevented accurate quantification. Panels (c-d) show the corresponding immunoblots of MAF1 along with REVERT total protein-stained membranes. Quantification was normalised to total protein.*

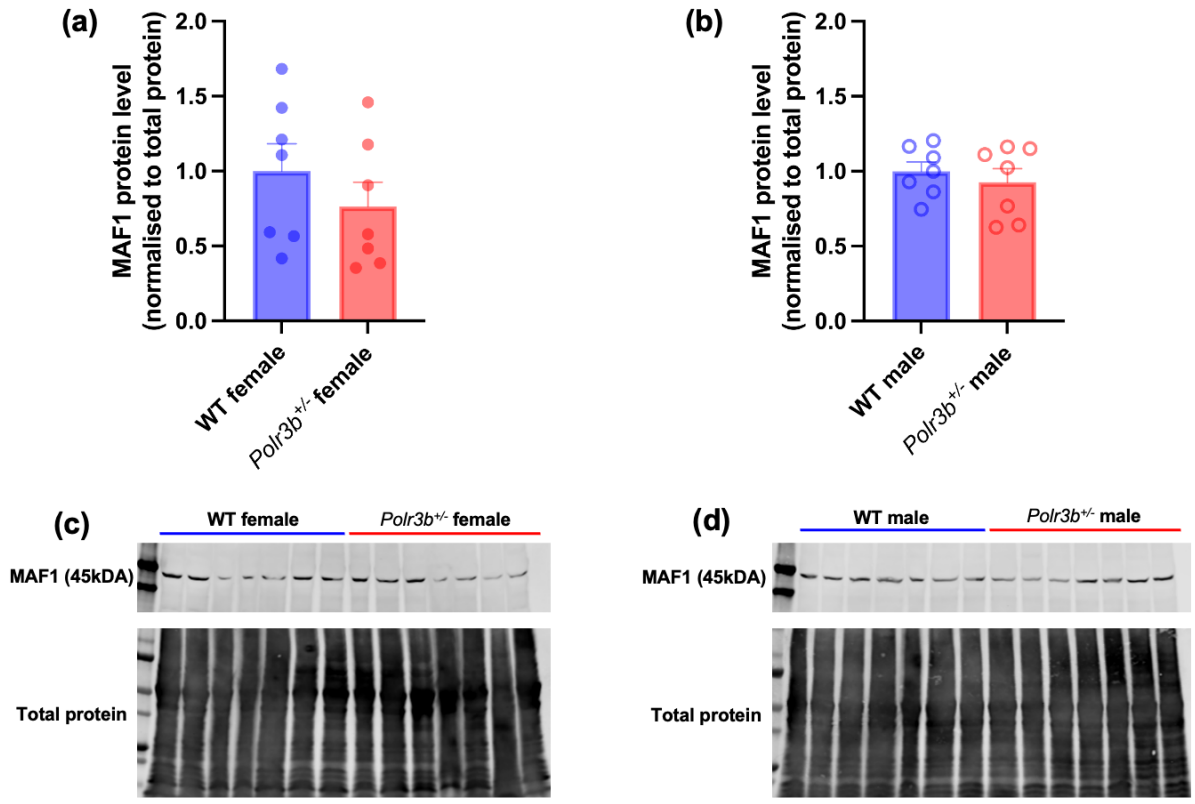

Figure 3-14 MAF1 protein levels in the brain of WT and *Polr3b*$^{+/-}$ mice

MAF1 protein levels in brain lysates of WT and Polr3b$^{+/-}$ *female (a) and male (b) mice. Histograms denote means ± SEM, with sample sizes indicated by individual points within each group. Panels (c-d) show the corresponding immunoblots of MAF1 along with REVERT total protein-stained membranes. Quantification was normalised to total protein. Unpaired two-tailed t-tests were used to test for genotype differences.*

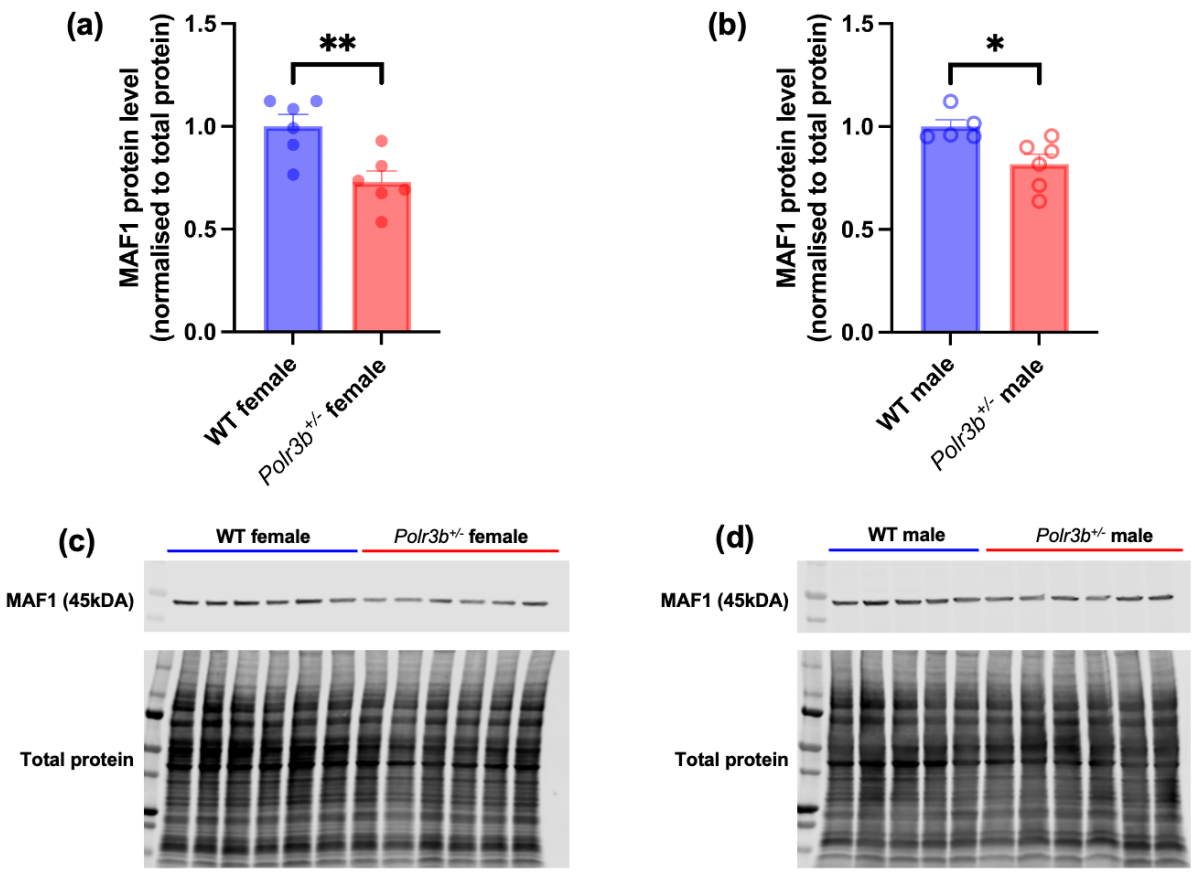

Figure 3-15 MAF1 protein levels in the primary dermal fibroblasts of WT and *Polr3b*$^{+/-}$ mice

*MAF1 protein levels were measured in dermal fibroblast lysates from WT and Polr3b$^{+/-}$ female (a) and male (b) mice. Histograms denote means ± SEM, with sample sizes indicated by individual points within each group. Panels (c-d) show the corresponding immunoblots for MAF1, alongside REVERT total protein-stained membranes. Quantification was normalised to total protein. Unpaired two-tailed t-tests were used to test for genotype differences. *=p<0.050, **=p<0.010.*

3.4.7 No differences in S6 phosphorylation levels in liver, brain, and dermal fibroblasts of WT and *Polr3b*$^{+/-}$ mice

S6 is a surrogate for TORC1 activity as it measures the activity of S6K, which is regulated by TORC1. To assess potential changes in TORC1 activity, the total and phosphorylated S6 protein levels were measured in liver, brain, and primary dermal fibroblasts of WT and *Polr3b*$^{+/-}$ mice. The amount of p-S6 was expressed relative to total S6 protein for each sample. No genotypic differences were detected in the liver (female *t=0.575, p=0.577*, **Figure 3-16 (a)**; male *t=1.505, p=0.158*, **Figure 3-16 (b)**), brain (female *t=1.510, p=0.157*, **Figure 3-17 (a)**; male *t=1.478, p=0.165*, **Figure 3-17 (b)**), and dermal fibroblasts (female *t=1.032, p=0.344*, **Figure 3-18 (a)**; male *t=1.823, p=0.102*, **Figure 3-18 (b)**) of WT and *Polr3b*$^{+/-}$ mice in either sex.

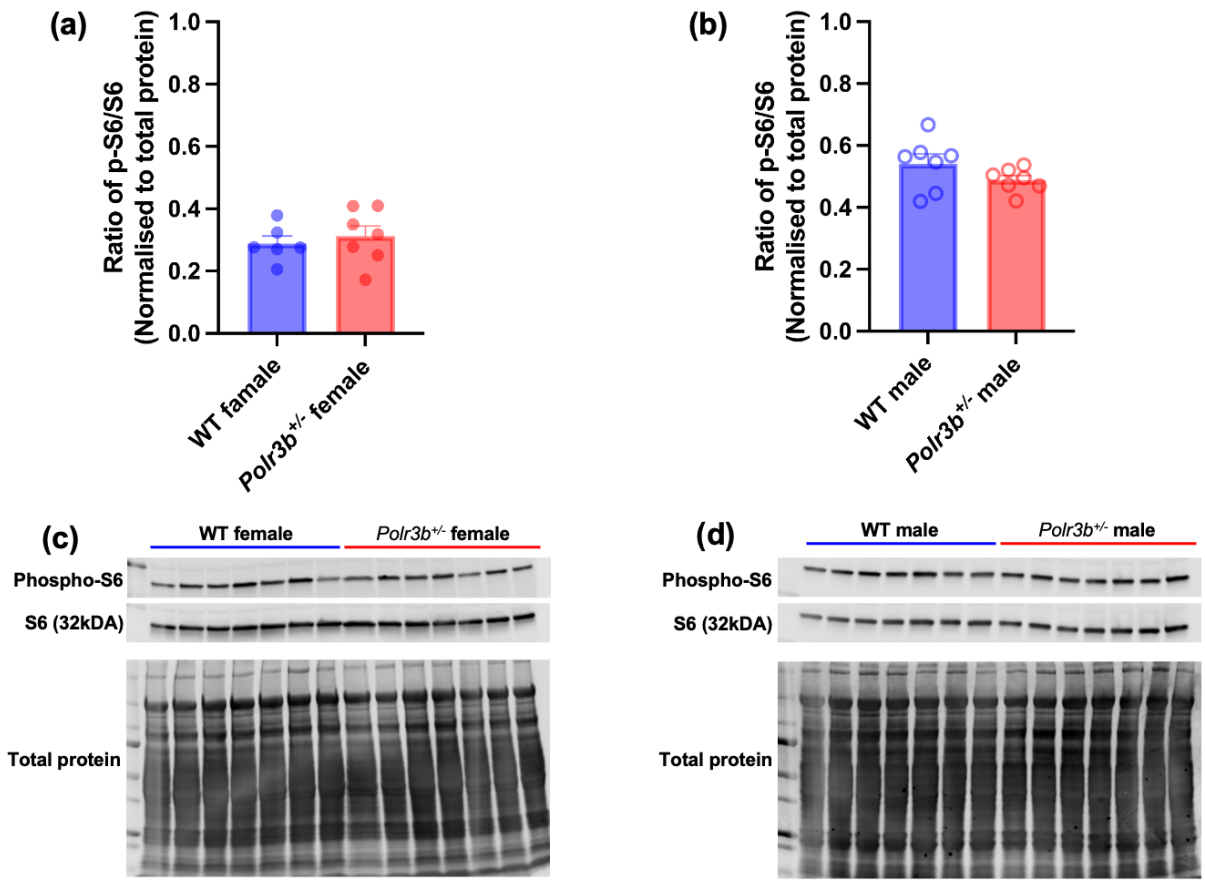

Figure 3-16 Phospho-S6 relative to total S6 protein in the liver of WT and *Polr3b*$^{+/-}$ mice

Phospho-S6 relative to total S6 protein in liver lysates of WT and Polr3b$^{+/-}$ *female (a) and male (b) mice. Histograms denote means ± SEM, with sample sizes indicated by individual points within each group. Panels (c-d) show the corresponding immunoblots of phospho-S6 and total S6, along with REVERT total protein-stained membranes. Phospho-S6 and total S6 bands were normalised to total-protein staining, and phosphorylation was expressed as the phospho-S6/total S6 ratio.*

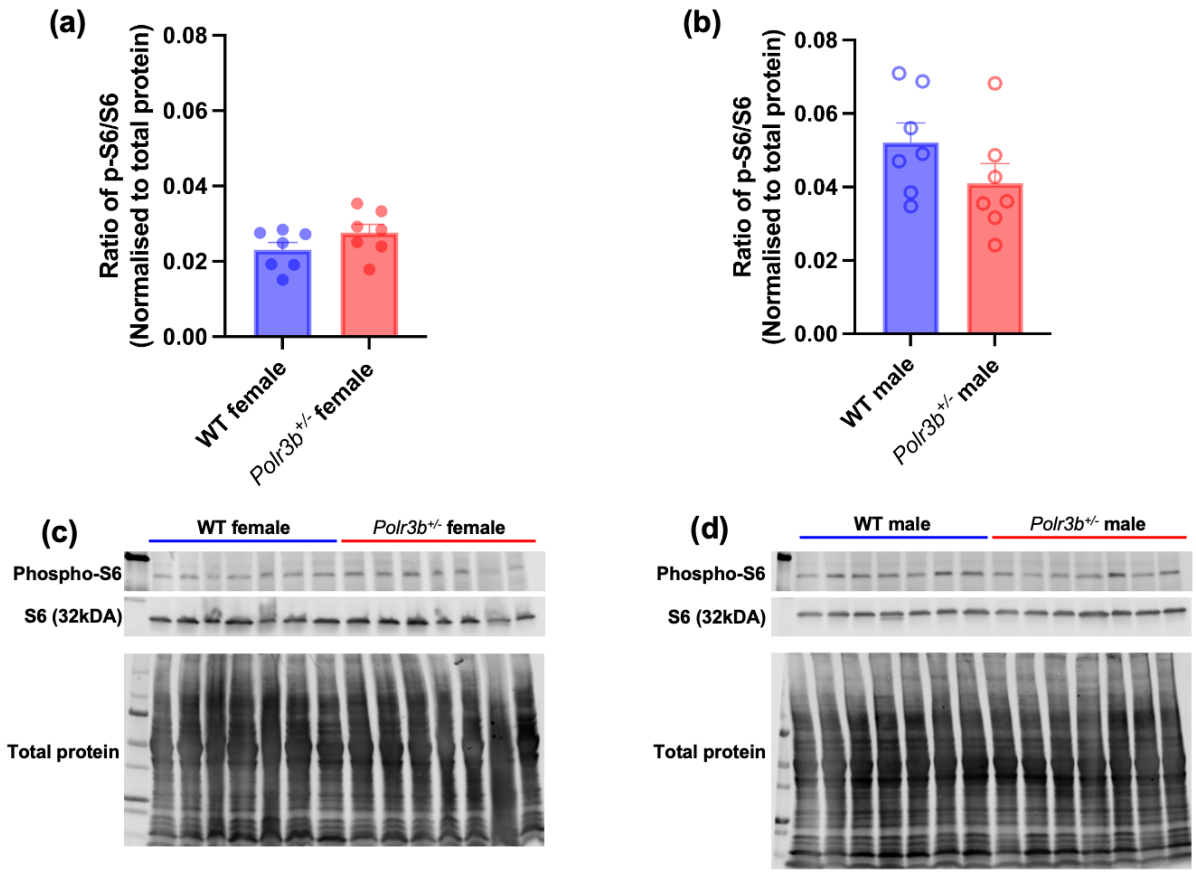

Figure 3-17 Phospho-S6 relative to total S6 protein in the brain of WT and *Polr3b*$^{+/-}$ mice

Phospho-S6 relative to total S6 protein in brain lysates of WT and Polr3b$^{+/-}$ *female (a) and male (b) mice. Histograms denote means ± SEM, with sample sizes indicated by individual points within each group. Panels (c-d) show the corresponding immunoblots of phospho-S6 and total S6, along with REVERT total protein-stained membranes. Phospho-S6 and total S6 bands were normalised to total-protein staining, and phosphorylation was expressed as the phospho-S6/total S6 ratio.*

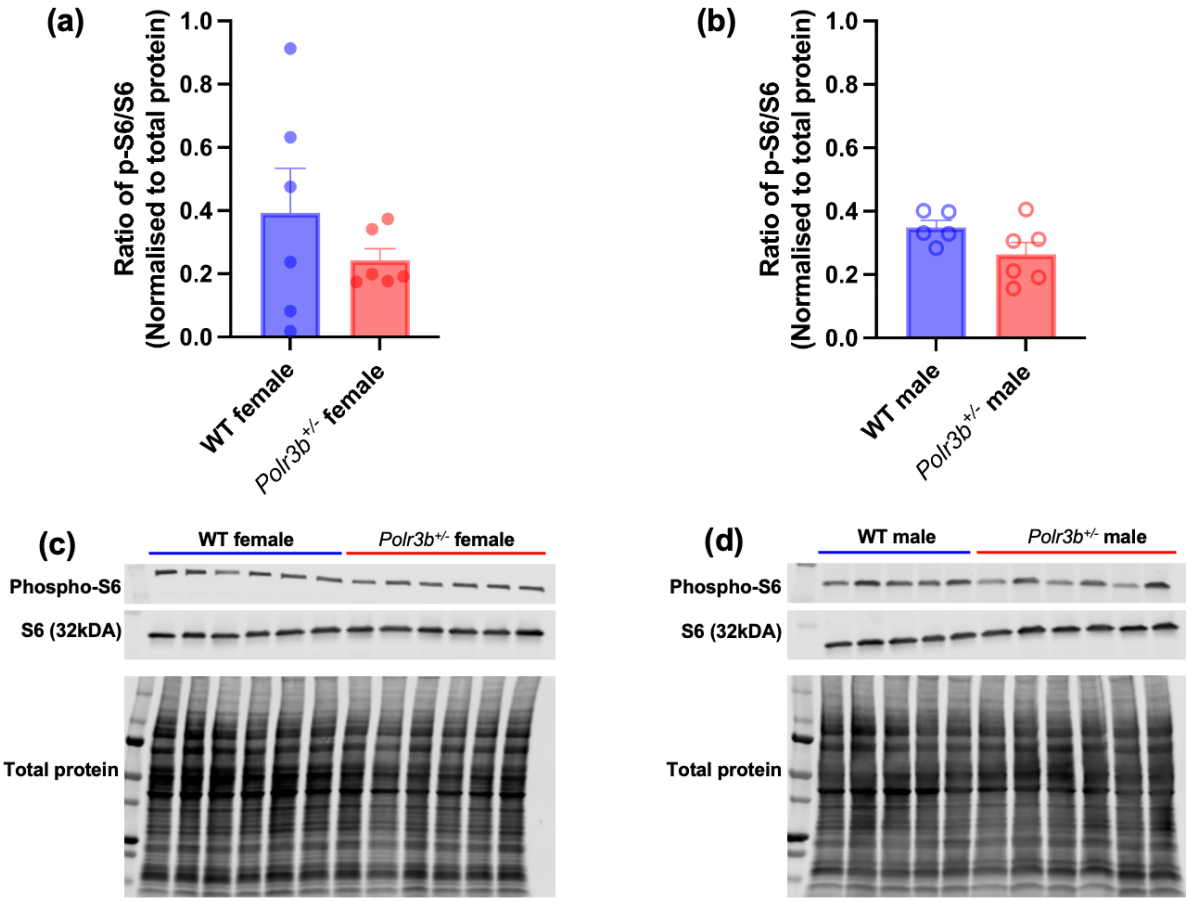

Figure 3-18 Phospho-S6 relative to total S6 protein in primary dermal fibroblasts of WT and *Polr3b*$^{+/-}$ mice

Phospho-S6 relative to total S6 protein in primary dermal fibroblasts of WT and Polr3b$^{+/-}$ *female (a) and male (b) mice. Histograms denote means ± SEM, with sample sizes indicated by individual points within each group. Panels (c-d) show the corresponding immunoblots of phospho-S6 and total S6, along with REVERT total protein-stained membranes. Phospho-S6 and total S6 bands were normalised to total-protein staining, and phosphorylation was expressed as the phospho-S6/total S6 ratio.*

3.4.8 Female *Polr3b*$^{+/-}$ exhibited lower protein synthesis in the brain

Protein synthesis was assessed in liver and brain tissue of *Polr3b*$^{+/-}$ and WT mice using puromycin incorporation, where lower puromycin labelling indicates reduced translational activity. No differences were detected in the liver of either sex (female *t=1.139, p=0.294*, **Figure 3-19 (a)**; male *t=1.563, p=0.149*, **Figure 3-19 (b)**). In the brain, however, female *Polr3b*$^{+/-}$ mice exhibited reduced protein synthesis compared with WT controls (*t=2.343, p=0.044*, **Figure 3-20 (a)**), whereas no difference was observed in males (*t=0.911, p=0.382*, **Figure 3-20 (b)**).

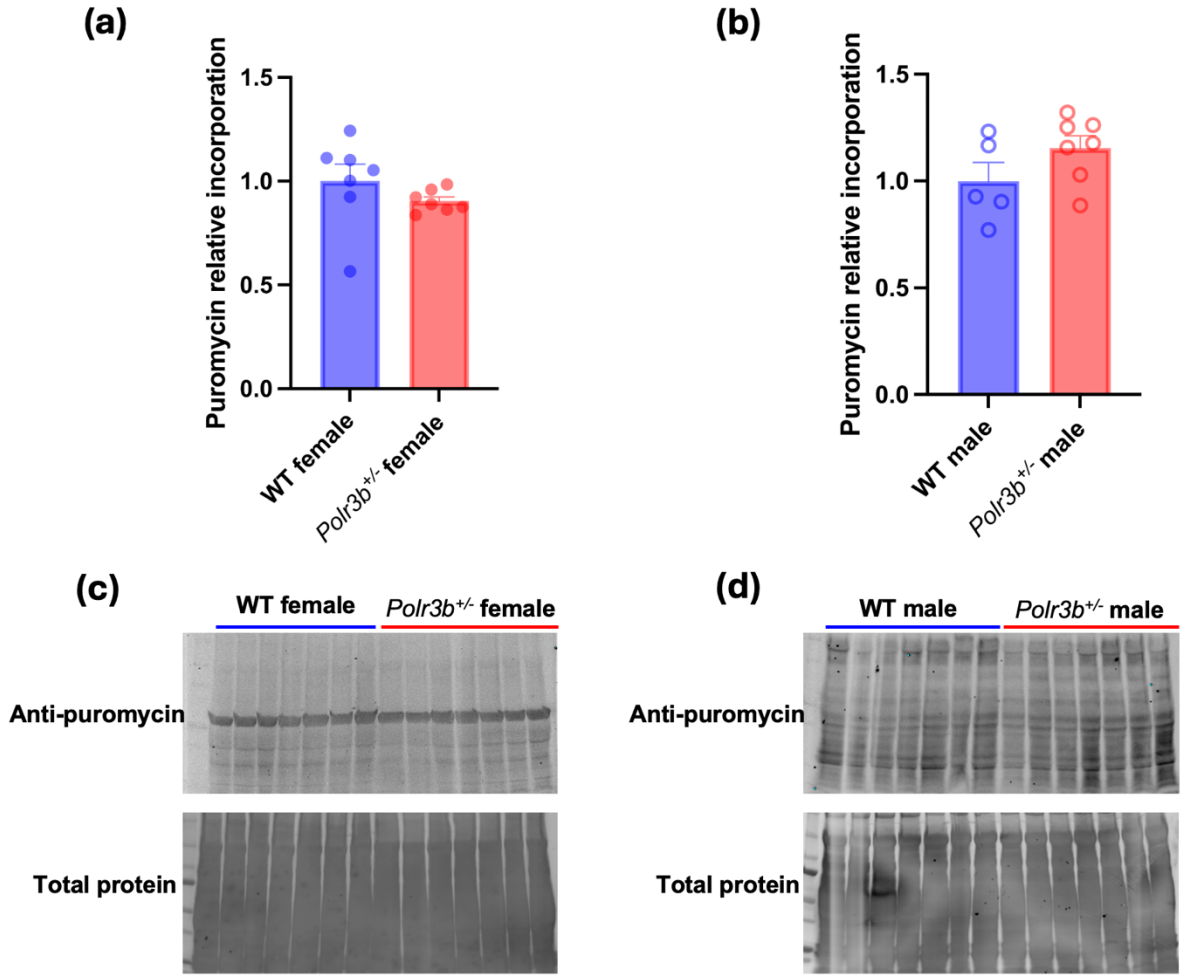

Figure 3-19 Protein synthesis (quantified by puromycin incorporation) in the liver of WT and *Polr3b*$^{+/-}$ mice

Puromycin-conjugated peptide levels in liver lysates of WT and Polr3b$^{+/-}$ *female (a) and male (b) mice. Histograms denote means ± SEM, with sample sizes indicated by individual points within each group. Two WT male samples were excluded due to imaging artefacts that prevented accurate quantification. Panels (c-d) show the corresponding immunoblots of puromycin-conjugated peptides along with REVERT total protein-stained membranes. Quantification was normalised to total protein.*

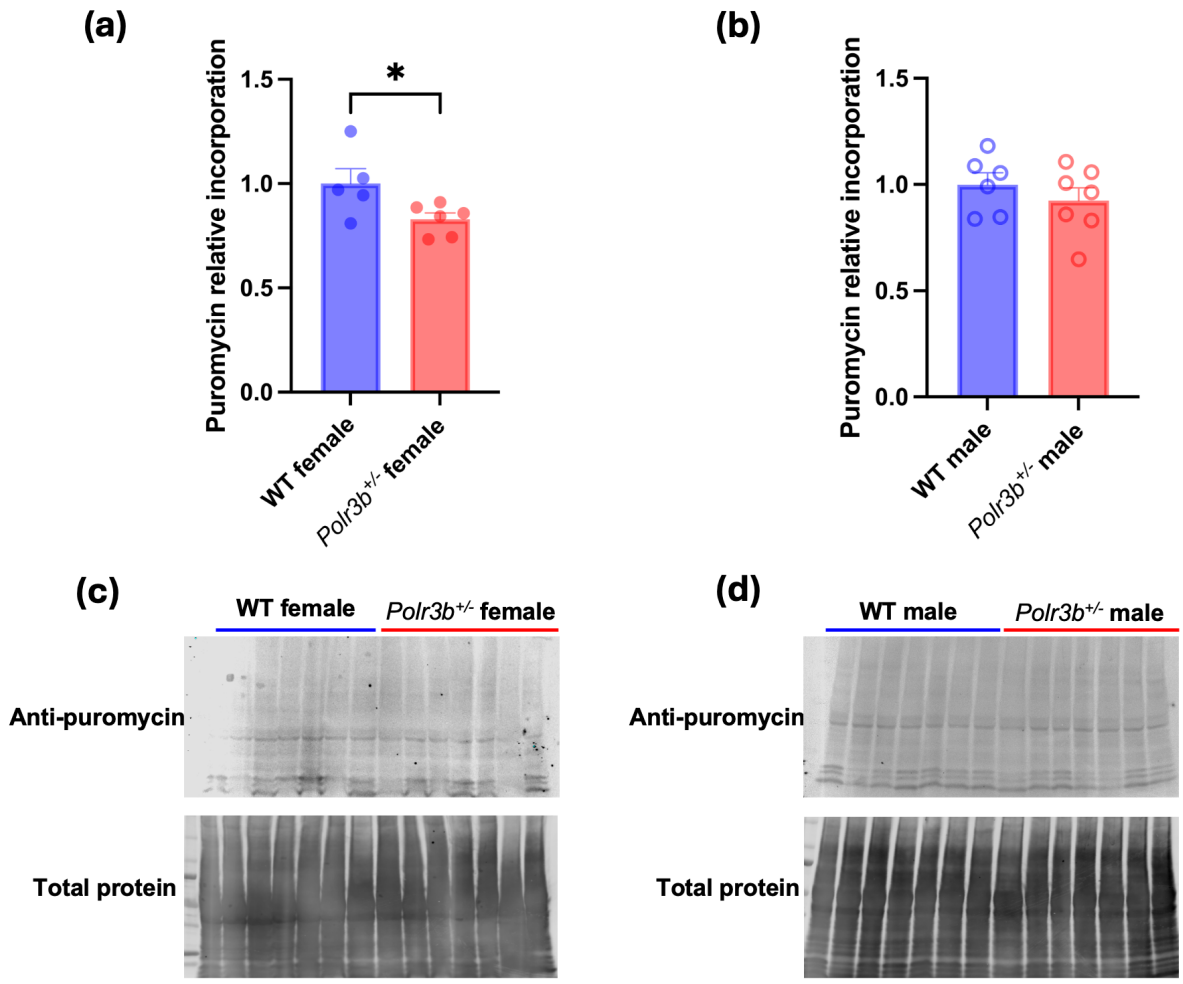

Figure 3-20 protein synthesis (quantified by puromycin incorporation) in the brain of WT and *Polr3b*$^{+/-}$ mice

*Puromycin-conjugated peptide levels in brain lysates of WT Polr3b$^{+/-}$ female (a) and male (b) mice. Histograms denote means ± SEM, with sample sizes indicated by individual points within each group. Two WT female, one Polr3b$^{+/-}$ female, and one WT male samples were excluded due to quantification artefacts, including imaging issues and undetectable signals. Panels (c-d) show the corresponding immunoblots of puromycin-conjugated peptides along with REVERT total protein-stained membranes. Quantification was normalised to total protein. *=p<0.050.*

3.4.9 Hepatic HSP60 protein levels reduced in female *Polr3b*$^{+/-}$ mice

Heat shock proteins HSP60 and HSP90 were measured in the liver of *Polr3b*$^{+/-}$ and WT mice. Lower HSP60 levels were observed in the female *Polr3b*$^{+/-}$ liver compared to WT controls (*t=3.900, p=0.002*, **Figure 3-21 (a)**), although no difference was detected in males (*t=0.132, p=0.899*, **Figure 3-21 (b)**).

No genotypic differences in hepatic HSP90 levels were detected in the liver of either female or male mice (female *t=0.708, p=0.493*, **Figure 3-22 (a)**; male *0.131, p=0.898*, **Figure 3-22 (b)**).

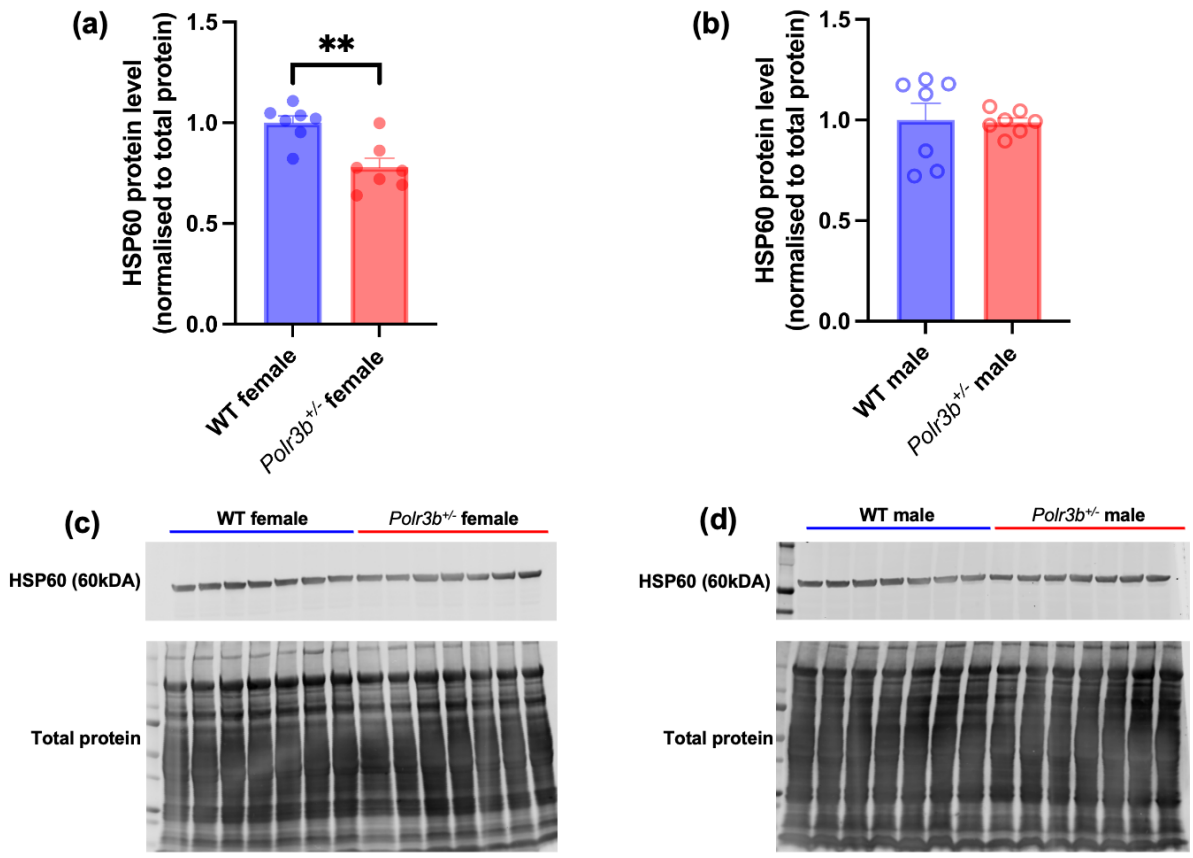

Figure 3-21 HSP60 protein levels in the liver of WT and Polr3b+/- mice

*HSP60 protein levels were measured in liver lysates of WT and Polr3b$^{+/-}$ female (a) and male (b) mice. Histograms denote means ± SEM, with sample sizes indicated by individual points within each group. Panels (c-d) show the corresponding immunoblots for HSP60, alongside REVERT total protein-stained membranes. Quantification was normalised to total protein. Unpaired two-tailed t-tests were used to test for genotype differences. **=p<0.010.*

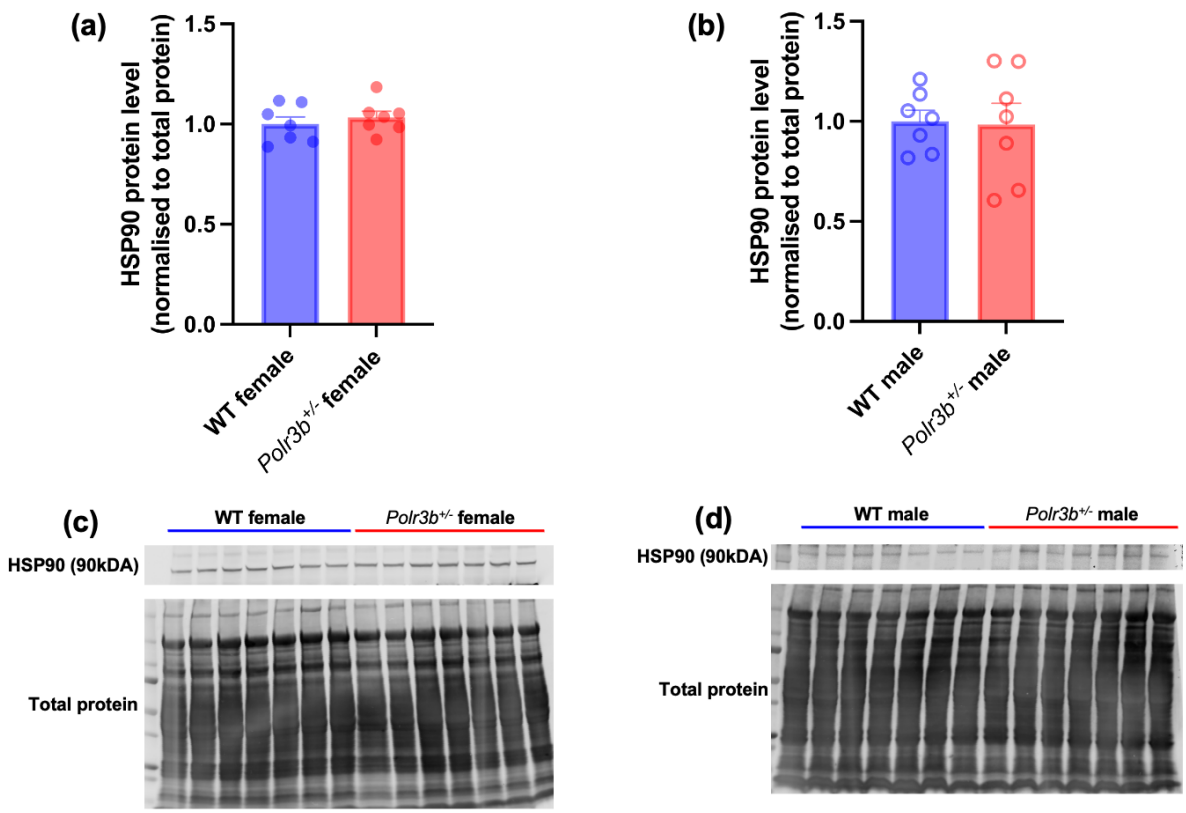

Figure 3-22 HSP90 protein levels in the liver of WT and *Polr3b*$^{+/-}$ mice

HSP90 protein levels were measured in liver lysates of WT and Polr3b$^{+/-}$ *female (a) and male (b) mice. Histograms denote means ± SEM, with sample sizes indicated by individual points within each group. Panels (c-d) show the corresponding immunoblots for HSP90, alongside REVERT total protein-stained membranes. Quantification was normalised to total protein. Unpaired two-tailed t-tests were used to test for genotype differences.*

3.5 DISCUSSION

Pol III, negatively regulated by MAF1 downstream of mTORC1, transcribes short non-coding RNAs such as 5S rRNA and tRNAs that are essential for ribosome assembly and translation (Moir & Willis, 2013; Pluta et al., 2001; Upadhya et al., 2002). In *D. melanogaster*, partial inhibition of Pol III activity through heterozygous mutation of Pol III subunit or tissue-specific RNAi knockdown reduces Pol III-dependent transcription and global protein synthesis, leading to extended lifespan (Filer et al., 2017). Pol III functions downstream of mTORC1, a central nutrient-sensing pathway that promotes anabolic metabolism. mTORC1 directly phosphorylates S6K1 (Magnuson et al., 2012), and a previous study showed that rapamycin-induced TORC1 inhibition decreases S6K phosphorylation in *D. melanogaster* (Filer et al., 2017). Moreover, protein synthesis itself is regulated by mTORC1 through phosphorylation of S6K1 and its substrate ribosomal protein S6, where phosphorylation of S6 reflects the activation state of mTORC1 (Magnuson et al., 2012). In addition, HSPs have been implicated in both protein folding and RNA polymerase complex assembly or turnover (Boulon et al., 2010; Hu et al., 2022; Tian et al., 2023). This chapter, therefore, aimed to examine whether reduced Pol III activity affects the abundance of the Pol III subunits POLR3B and POLR3A and its repressor MAF1, as well as the ratio of phosphorylated to total S6 across tissues and dermal fibroblasts. Measuring the phospho-S6/S6 ratio, rather than phosphorylated S6 alone, allows a more accurate assessment of S6 phosphorylation relative to total protein abundance and thus provides a reliable marker of mTORC1 activity. In addition, protein synthesis levels and the levels of major chaperones HSP60 and HSP90 were examined to evaluate whether reduced Pol III output impacts translational or proteostatic capacity.

The current study revealed a tissue- and sex-specific reduction of *Polr3b* in both mRNA and protein levels, with *Polr3b* mRNA expression being reduced in the male liver and brain, whereas POLR3b protein level was lower in the female liver. No changes were found in the skeletal muscle. Consistent with this, Borland et al. (2024) reported that *Polr3b*$^{+/-}$ mice exhibit sex- and tissue-specific changes in *Polr3b* expression and physiological outcomes, suggesting that partial Pol III reduction in this *Polr3b*$^{+/-}$ mouse model does not apply to all tissues consistently. The lack of consistent reduction across mRNA and protein levels in

this *Polr3b*$^{+/-}$ mouse model in the current study may explain the tissue- and sex-specific inconsistent responses, such as the changes in protein synthesis and HSP levels across tissues and sexes. Moreover, the mismatch between transcript and protein levels suggests the involvement of post-transcriptional regulatory mechanisms rather than direct transcriptional effects alone. It is well established that mRNA abundance does not always correlate with protein levels due to differences in translation efficiency, protein stability, and degradation rates (Liu et al., 2016). In addition, sex-specific hormonal regulation, particularly via oestrogen signalling, can influence protein turnover and mTOR-associated protein synthesis pathways, contributing to sexually dimorphic gene expression outcomes across tissues (Tao & Cheng, 2023; Wolff et al., 2021). Therefore, the observed divergence between mRNA and protein levels in *Polr3b*$^{+/-}$ mice likely reflects the combined effects of post-transcriptional regulation and sex-dependent modulation of protein homeostasis, rather than a simple gene dosage effect. Furthermore, as highlighted by Watt et al. (2023), different tissues and cell types exhibit various expression of Pol III-dependent transcripts and Pol III subunits, and evidence from pathogenic contexts indicates that disruptions to Pol III transcription can trigger tissue-specific responses (Watt et al., 2023). Collectively, a more robust or tissue-targeted knockout strategy would be required to achieve a more consistent reduction in Pol III activity.

As a phosphoprotein inhibitor, MAF1 is required for the mediation of Pol III transcriptional repression, and its role on Pol III is conserved from yeast to humans (Goodfellow et al., 2008; Pluta et al., 2001; Upadhya et al., 2002). The current study found an increase in *Maf1* expression in the liver of the *Polr3b*$^{+/-}$ male, where reduced *Polr3b* expression was also observed. Physical interaction of MAF1 and Pol III complexes and Pol III-dependent transcripts may explain the changes: MAF1 was found to physically interact with Pol III subunit *RPC160* (homologous to mouse *Polr3a*), and Pol III promoter subunits *Brf1* and *Brf2* (Goodfellow et al., 2008; Park et al., 2017). On the other hand, previous literature also showed that MAF1 regulation involves mTORC1-dependent phosphorylation and phosphatase-mediated dephosphorylation, which drives its nuclear translocation and subsequent repression of Pol III transcription (Goodfellow et al., 2008) (**Figure 3-1**). These processes are energy-consuming, requiring ATP for phosphorylation reactions and energy-dependent transport for

nuclear import (Cohen, 2002). Recent transcriptomic analyses further suggest that Pol III activity indirectly supports ATP generation, as genes sensitive to Pol III are enriched for mitochondrial oxidative phosphorylation and ATP synthesis pathways (Rajendra et al., 2024). When Pol III activity is reduced, reduced mitochondrial metabolism together with altered tRNA pools may modify the energetic environment that governs MAF1 activation (Bonhoure et al., 2015; Malik, Goncalves Silva, et al., 2024; Willis & Moir, 2018). Further investigation into the molecular mechanisms underlying this potential regulation is warranted, such as to investigate the dephosphorylation ratio of Maf1 (for example, to measure the levels of serine and alanine residues) (Noguchi et al., 2021) when Pol III activity is reduced.

In mammalian cells, mTORC1 is known to regulate protein synthesis through phosphorylation of S6K1, and phosphorylated S6 is widely used as a surrogate indicator of mTORC1 activity (Chowdhury & Kohler, 2015; Liu & Sabatini, 2020). To determine whether reduced Pol III activity influences this pathway, the abundance of phospho-S6 relative to total S6 was assessed in *Polr3b*$^{+/-}$ tissues and dermal fibroblasts. The phospho-S6/S6 ratio did not differ between genotypes; however, this measure represents an indirect readout of translational control. Phosphorylation of S6 reflects S6K1 activity downstream of mTORC1 but does not directly quantify global protein synthesis, and S6 phosphorylation has been shown to be dispensable for bulk translation under certain conditions (Magnuson et al., 2012; Ruvinsky & Meyuhas, 2006). Therefore, the absence of differences in phospho-S6/S6 does not exclude potential changes in translational output, as also suggested by the reduction in puromycin incorporation observed in the female brain. In addition, without pathway activation controls, the absolute level of mTORC1 activity cannot be inferred. In fibroblast assays, for example, insulin treatment is widely used as a positive control to activate the mTORC1-S6K axis and induce robust S6 phosphorylation (Sancak et al., 2007; Scott et al., 1998; Um et al., 2006). The absence of equivalent controls in the current study, therefore, limits interpretation of baseline S6 phosphorylation. Nevertheless, the unchanged phospho-S6/S6 ratio in *Polr3b*$^{+/-}$ mouse is consistent with findings in *D. melanogaster*, that TORC1 inhibition reduces S6K phosphorylation, whereas reduced Pol III activity does not alter S6K or S6 phosphorylation (Filer et al., 2017). Together, these findings indicate that Pol III

acts downstream of TORC1 and Pol III reduction does not feed back to modify mTORC1-S6K activity.

To provide a more comprehensive assessment of mTORC1-dependent translational regulation, additional markers such as 4E-BP1 phosphorylation should be considered. mTORC1 promotes cap-dependent translation by phosphorylating 4E-BP1, leading to its dissociation from elF4E and enabling translation initiation (Liu & Sabatini, 2020). Unlike S6 phosphorylation, which reflects S6K1 activity, 4E-BP1 phosphorylation more directly regulates translation initiation. Therefore, future studies incorporating 4E-BP1 phosphorylation alongside S6K/S6 measurements would provide a more complete evaluation of mTORC1-driven translational control in *Polr3b*$^{+/-}$ model.

Changes in protein synthesis were also examined to determine whether *Polr3b*$^{+/-}$ mutation affects translational output, because Pol III produces tRNAs and 5S rRNA that are required for ribosome assembly and protein synthesis (Dieci et al., 2007; Schramm & Hernandez, 2002; Willis & Moir, 2018). Consistent with the variable reduction of *Polr3b* across tissues and sexes, protein synthesis was unchanged in liver but reduced in the female brain. This pattern suggests that the *Polr3b*$^{+/-}$ mutation in this mouse model does not consistently influence translation output across tissues and that the effect depends on the extent of Polr3b reduction within each tissue. Findings in *D. melanogaster* have shown that tissue-specific reduction of Pol III activity can lower pre-tRNA abundance and diminish protein synthesis in a tissue-dependent manner, and the present data are consistent with this finding (Filer et al., 2017). In addition, a lower HSP60 protein level was detected in the liver of *Polr3b*$^{+/-}$ female mice. Members of the HSP family assist in the folding of nascent polypeptides and support the maturation and stability of protein complexes under both basal and stress conditions (Cooper, 2000; Hu et al., 2022; Richter et al., 2010). Although direct evidence linking HSP60 to Pol III assembly is currently lacking, reduced chaperone capacity could indirectly impair the folding or stability of Pol III subunits, particularly under conditions where subunit stoichiometry is already perturbed by *Polr3b* haploinsufficiency. Importantly, HSP90, but not HSP60, has been directly implicated in RNA polymerase assembly including Pol III, and no change in HSP90 levels was detected in this study (Boulon et al., 2010; Tian et al., 2023). While reduced HSP60 may indicate altered proteostatic capacity in

female liver, its functional impact on Pol III assembly remains speculative and requires direct experimental validation. For example, examining Pol III subunit assembly after controlled manipulation of HSP60 or mapping chaperone interactions with Pol III, would help clarify whether the reduction in HSP60 observed in this study has causal consequences for Pol III (Boulon et al., 2010; Tian et al., 2023).

3.6 CONCLUSION

In summary, *Polr3b*$^{+/-}$ mice exhibited tissue- and/or sex-specific alterations in *Polr3b* mRNA and protein levels, MAF1 protein level, protein synthesis, and HSP protein level, while POLR3A and phospho-S6 remained unchanged. This study demonstrates that Pol III activity is differentially regulated across tissues. Future work using tissue-specific or conditional *Polr3b* knockouts will be essential to dissect whether its modulation can influence nutrient-sensing and proteostatic pathways in *vivo*.

Chapter 4: The role of RNA Polymerase III in reproduction

4.1 INTRODUCTION

4.1.1 Reproduction in *Mus musculus*

Reproduction is a fundamental biological process that ensures the survival and continuation of a species (Sadler, 2012). It involves complex physiological mechanisms regulated by the endocrine system, ensuring successful gamete production, fertilisation, and offspring development (Norris & Carr, 2023). Mice exhibit a polyoestrous cycle, meaning they undergo recurring oestrous cycles throughout the year (Nelson, 2011). Unlike species with induced ovulation, such as rabbits (*Oryctolagus cuniculus*), where ovulation is triggered by copulation, mice experience spontaneous ovulation (Laurie & Goodrich, 1946). The mouse reproductive cycle is controlled by the hypothalamic-pituitary-gonadal (HPG) axis, which secretes gonadotropin-releasing hormone (GnRH) (Nelson, 2011). This, in turn, triggers the release of fluctuating levels of luteinizing hormone (LH) and follicle-stimulating hormone (FSH) from the pituitary cells, regulating follicular development, ovulation, and pregnancy maintenance (Conti et al., 2012; Laurie & Goodrich, 1946). Reproductive capacity in mice follows a well-defined timeline, reaching sexual maturity between 45 and 65 days of age, a reproductive lifespan of approximately 210 to 270 days, and gestation lasting between 19 and 21 days (Nilsson & Skinner, 2024). There is a lack of evidence to suggest major differences exist in reproductive ability between the C57BL/6 substrains, with both C57BL/6N and C57BL/6J mice showing similar superovulation responses, suggesting similar hypothalamus-pituitary-ovarian axis activity (Shindo et al., 2021).

4.1.2 Reproduction and ageing

Ageing is a complex, multifactorial process and is characterised by such features as reduced reproductive capacity, genomic instability, epigenetic alterations, proteostasis instability, deregulated nutrient sensing, and cellular senescence (Lopez-Otin et al., 2013; Templeman & Murphy, 2018). Reproductive ageing in laboratory mice resembles that of humans and is characterised by a midlife loss of fertility cycles, which is a canonical feature of ageing (Finch & Kirkwood, 2000). In humans, fertility begins to decline with age in both sexes, but the trajectory is far more pronounced in females, in whom reproductive capacity starts to diminish earlier and more abruptly (Mason et al., 2022). Unlike men, who have relatively infinitive sperms, women have few primary follicles that begin to decline since birth (Park et al., 2021). The end of reproductive function in women occurs with menopause, typically around 51 years of age, and this transition is accompanied by a sharp increase in disease risk due to the loss of ovarian-dependent endocrine support (Broekmans et al., 2009; Mason et al., 2022). Unlike women, female mice do not undergo a defined menopause but instead experience a relatively progressive ovarian ageing that begins around 7 to 8 months of age (Lambert, 2007; Van Kempen et al., 2011). Female reproductive ageing in mice is characterised by a progressive decline in ovarian function, including depletion of the follicle pool and disruption of hypothalamic-pituitary-ovarian hormonal signalling (Balough et al., 2024; Park et al., 2021). Ageing females show prolonged gestation and parturition, and produce smaller litters (Patel et al., 2017). Age-related declines in the number of eggs ovulated and in oocyte quality, including the defects in oocyte spindle structure, chromosome cohesion, and mitochondrial function, reduce the capacity for egg activation and impair early embryo development (Balough et al., 2024). These oocyte abnormalities contribute to the reproductive phenotypes observed in aged females, including prolonged gestation, reduced litter size, and reduced offspring viability (Balough et al., 2024; Patel et al., 2017). Ageing additionally leads to structural and functional changes in the uterus, and reductions in ovarian reserve and ovulation frequency (Balough et al., 2024). Male reproductive ageing in mice is characterised by reductions in sperm quantity and quality, including decreased sperm concentration, motility and viability, as well as increased morphological abnormalities (Ozawa et al., 2023). These changes

arise from age-associated declines in spermatogenic activity and disruptions in testicular microvascular function, including endothelial cell senescence and reduced vascular density, which impair support for sperm production (Ozawa et al., 2023). Ageing males also show delays in pre-implantation embryo development, a phenotype linked to declines in sperm motility, viability, morphology and concentration, and associated with reduced foetal growth, higher postnatal mortality and delayed locomotor development in offspring (Stábile et al., 2025). Together, these age-related defects in sperm production and sperm integrity contribute to impaired fertilising capacity and poorer outcomes in offspring.

The relationship between reproduction and longevity has long been recognised. The disposable soma theory, developed from antagonistic pleiotropy (Williams, 1957), argues that organisms have finite energetic resources that must be divided between reproduction and somatic maintenance (Kirkwood, 1977). When more is contributed to growth and reproduction, less is available for repair, allowing damage to accumulate with age (Kirkwood, 1977). This general pattern is reflected in dietary restriction (DR), where reduced energy intake reliably extends lifespan while suppressing growth and reproductive output in rodents (Holliday, 1989; Shanley & Kirkwood, 2000; Yuan et al., 2023). Mechanistic work in rodents shows that ageing is accompanied by a gradual decline in protein synthesis, ribosomal capacity and overall protein turnover, pointing to a broad reduction in cellular maintenance (Lewis et al., 1985). In *ad libitum*-fed rats, both fractional protein synthesis and degradation decreased with age, and the RNA-to-protein ratio also decreased. Chronic DR slows these age-related declines, that the DR animals maintain higher fractional protein synthesis and degradation rates into later life and show a smaller reduction in ribosomal capacity than age-matched controls (Lewis et al., 1985). By limiting growth and cellular proliferation, DR reduces the energetic cost of continued growth and allows resources to be redirected towards the replacement of damaged proteins, which is thought to help sustain somatic maintenance and contribute to the longer lifespan observed under restricted diets (Lewis et al., 1985; Merry & Holehan, 1979). Together, these findings show how changes in energy allocation shape the balance between reproduction, growth, and somatic maintenance across the lifespan. Another perspective on the ageing process comes from the

quasi-programmed theory of senescence, which builds on the idea that ageing can arise from the continued activity of developmental or reproductive programmes beyond the period in which they are adaptive (Blagosklonny, 2006; Gems, 2022). This theory argues that ageing does not arise solely from accumulated damage but can also emerge when growth-promoting pathways that support development and reproduction in early life continue to operate beyond maturity (Blagosklonny, 2006; Gems, 2022). When these pathways are not down-regulated, processes that are beneficial during development and reproductive function may generate harmful effects in later life (Blagosklonny, 2006; Gems, 2022). Specifically, genes involved in anabolic processes such as growth and reproduction may become deleterious when their activity remains unchecked post-maturation. Key examples are the IIS and TOR pathways, which promote cellular growth and metabolism in early life, and contribute to ageing later in life (Blagosklonny, 2006; de Magalhaes & Church, 2005). Consistent with this view, reduced activity in these pathways, including their specific downstream effectors such as IRS1 or S6K1, has been shown to extend lifespan in animals from yeast to mice (Clancy et al., 2001; Filer et al., 2017; Kenyon, 2005; Piper et al., 2008; Powers et al., 2006; Selman et al., 2008; Selman et al., 2009). To further illustrate whether extending longevity may affect reproduction, **Table 4-1** lists long-lived mutant mice with impaired mTOR or IGF-1 activity and their effects on reproduction. In summary, some but not all long-lived strains exhibited impaired reproduction. These findings would be consistent with the notion that while lifespan extension is often associated with reduced reproductive output, this trade-off is not universal and may depend on the genetic pathway involved. Given that Pol III functions downstream of mTOR and is known to influence both growth and reproductive processes in invertebrate models (Filer et al., 2017), Pol III represents a compelling target for exploring how partial Pol III reduction affects reproduction.

Table 4-1 Reproduction effects of long-lived mutant mice

Strain	Gene	Reproduction	Reference
Dgat1$^{-/-}$	*Dgat1* (acyl CoA:diacylglycerol acyltransferase 1)	reduced (smaller litter size)	(Streeper et al., 2012)
Igfr$^{+/-}$	*Igf-1r* (insulin-like growth factor type 1 receptor)	unaffected (sexual maturation age, litter size, frequency of pregnancies, number of live newborns, oestrus cycle length, and ovarian capacity unchanged)	(Holzenberger et al., 2003)
Klotho (overexpressed)	*Klotho*	reduced (fewer offspring per breeder pair in 12 months while litter size unchanged)	(Kurosu et al., 2005)
Myc$^{+/-}$	*Myc*	unaffected (litter size, lifetime fecundity, reproductive longevity unchanged)	(Hofmann et al., 2015)
Ames dwarf	*Prop-1* (Prophet of Pit-1)	almost infertile	(Bartke, 2000; Brown-Borg et al., 1996; Sornson et al., 1996)
Little	*Ghrhr* (GH releasing hormone receptor)	impaired fertility (fewer litters produced)	(Eicher & Beamer, 1976)
Snell dwarf	*Pit1* (pituitary-specific transcriptional factor)	impaired, retarded postnatal growth	(Flurkey et al., 2001; Liu et al., 2022)

4.1.3 Endocrine control of reproductive function

Reproductive performance is regulated by key gonadotropins, primarily FSH and LH. FSH supports ovarian follicle development, while LH is essential for triggering ovulation and regulating sex steroid hormone synthesis in both sexes (Oduwole et al., 2021; Qiao & Han, 2019). Both FSH and LH are heterodimeric glycoproteins composed of a common α-subunit and a unique ß-subunit that confers receptor specificity (Choi & Smitz, 2014). Their actions are mediated through their respective receptors, FSH receptors (FSHRs), and luteinizing hormone/choriogonadotropin receptors (LHCGRs), which are expressed primarily in the gonads (Segaloff & Ascoli, 2013). Notably, LHCGR binds both LH and choriogonadotropin (CG), a placental hormone structurally similar to LHß, and is therefore named for both ligands.

Reproductive hormone signalling is further mediated through the transcription and function of key regulatory genes. The *Cyp19a1* gene encodes aromatase, a cytochrome P450 enzyme that converts androgens into oestrogens, primarily producing 17ß-oestradiol (E2), the most abundant circulating oestrogen in both humans and mice (Hammes & Levin, 2019; Hussain & Gilloteaux, 2020). Oestrogens act via oestrogen receptors to regulate reproductive organ development, ovulation, and inhibit the secretion of FSH through feedback mechanisms (Horstman et al., 2012).

Fshr encodes FSH receptor, which is expressed on ovarian granulosa cells and is essential for follicular development and ovarian function in females (Hunzicker-Dunn & Maizels, 2006; Raju et al., 2013; Simoni et al., 1997). Reduced *Fshr* expression has been associated with oocyte depletion and elevated serum FSH levels (Danilovich & Sairam, 2002; Vihko, 1996). *Lhcgr* encodes LHCG receptor, a key mediator of LH- and CG-dependent signalling in both the ovary and testis (Segaloff & Ascoli, 2013). In males, LHCGR activation stimulates testosterone production during foetal development and post-puberty, promoting male sex differentiation (Danilovich & Sairam, 2002; Vihko, 1996). In females, it contributes to ovulation and corpus luteum maintenance (Mann et al., 2022; Narayan & Puett, 2003). Impaired *Lhcgr* function disrupts gonadal steroidogenesis and ovulation, contributing to reproductive decline in both mice and humans (Mann et al., 2022; Narayan & Puett, 2003).

4.1.4 Reproduction in the context of Pol III-mediated pathways

Pol III supports anabolic activity through the transcription of small non-coding RNAs, including tRNAs and 5S rRNA, which are required for ribosome biogenesis and protein synthesis (Goodfellow & White, 2007; Moir & Willis, 2013; Willis & Moir, 2018). These processes underpin cell growth, germ cell development, and early embryogenesis, and all of these are necessary for reproductive function (Malik, Goncalves Silva, et al., 2024; Ni & Buszczak, 2023; Willis & Moir, 2018). Pol III activity is positively regulated by mTORC1 through TFIIIB activation and MAF1 inhibition (Filer et al., 2017; Marshall et al., 2012; Shor et al., 2010; Upadhya et al., 2002; Urena et al., 2024). This connection is notable given the role of mTOR signalling in follicle growth, oocyte maturation, ovarian somatic cell proliferation, steroidogenesis, and early embryo development (Guo & Yu, 2019).

Across model organisms, altering Pol III activity affects both lifespan and reproduction. Reduced Pol III activity extends lifespan in S. cerevisiae, *D. melanogaster*, and *C. elegans* (Filer et al., 2017; Hammerquist & Curran, 2020; Khanna et al., 2014). In *D. melanogaster*, lifespan extension occurs without a reduction in egg production (Filer et al., 2017), whereas in *C. elegans*, changes in Pol III activity have also been found to have an impact on reproduction (Hammerquist & Curran, 2020; Khanna et al., 2014; Malik, Goncalves Silva, et al., 2024). Mutations affecting ribosome biogenesis in *D. melanogaster* also impair reproduction and slow the development (Marygold et al., 2007), highlighting the sensitivity of reproductive output to changes in translational capacity.

Although direct studies in mammals are limited, existing evidence from mammals also supports a role for Pol III signalling in reproductive function. *Maf1*$^{-/-}$ mice, which lack the central repressor of Pol III, show elevated precursor tRNA synthesis and broad metabolic alterations, including increased energy expenditure and resistance to diet-induced obesity (Bonhoure et al., 2015; Bonhoure et al., 2020). These mice exhibit extended lifespan and reduced reproductive output, that female *Maf1*$^{-/-}$ mice produce smaller litters and have longer intervals between litters than the wild-type controls (Bonhoure et al., 2015). Together, these findings suggest that the mTORC1 effector Pol III, may

influence reproductive performance. This raises the possibility that partial reductions in Pol III activity, as in *Polr3b*$^{+/-}$ mice, could have an impact on reproduction.

4.1.5 Measuring reproductive performance in mice

Reproductive performance is a key indicator of biological fitness and is tightly regulated by physiological and genetic factors. In laboratory mice, mating trials are commonly used to evaluate reproductive performance, with established parameters including time to first litter, interbirth intervals, litter size, pup weight, and pre-weaning mortality (Berndtson et al., 1997; Handelsman et al., 2020; Knecht et al., 2015). To assess whether partial reduction in Pol III activity affects reproduction, this chapter evaluated four key reproductive parameters: time to first litter, litter size at birth, pup weight at weaning (postnatal day 21), and pre-weaning mortality rate, across four reciprocal breeding pairs of a total of 20 *Polr3b*$^{+/-}$ and WT mice (**Figure 4-1**). These traits were chosen for their relevance to both reproductive efficiency and developmental outcomes. For instance, litter size is not only a direct measure of female fecundity but also influences per-pup resource allocation, with larger litters typically associated with lower individual pup weights and increased mortality due to higher competition for maternal care (Hudson & Trillmich, 2008; Kounig et al., 1988). In addition to offspring-based measures, parental reproductive organs were analysed morphologically, and expression levels of three key reproductive hormone-related genes (*Cyp19a1*, *Fshr*, *Lhcgr*) were quantified to evaluate potential molecular mechanisms underpinning phenotypic effects.

4.2 AIMS AND OBJECTIVES

Aims:

Partial knockdown of RNA polymerase III has been shown to extend the lifespan in yeast, worms and flies (Filer et al., 2017). RNA polymerase III enzyme functions in the transcription of 5S rRNA and tRNAs for ribosome and protein synthesis. As reproduction and longevity are intricately related, the current chapter, using *Polr3b*$^{+/-}$ mice with a global partial reduction in Pol III signalling, aims to investigate the role of RNA Pol III in the reproductive performance in mice.

Objectives:

Objective 1: To assess the fecundity of the *Polr3b*$^{+/-}$ mice compared to wild-type (WT) mice.

Fecundity is defined as an individual's potential to conceive and produce offspring, measured in this study by the duration it takes for a female to achieve her first birth from the introduction of a male.

Objective 2: To evaluate the fertility of the *Polr3b*$^{+/-}$ mouse by measuring the number of offspring produced (litter size), compared to WT mice.

Objective 3: To measure the weight of the offspring at weaning age and assess the pre-weaning mortality rate among the offspring of the *Polr3b*$^{+/-}$ mice relative to WT mice.

Objective 4: To analyse the morphological characteristics of the gonads for *Polr3b*$^{+/-}$ and wild-type mice.

Objective 5: To investigate the expression of Pol III-related (*Polr3b, Polr3a, Maf1*) and sex hormone-related genes (*Cyp19a1*, *Fshr, Lhcgr*) in the gonads of the female and male *Polr3b*$^{+/-}$ mice relative to WT mice.

4.3 METHODS

4.3.1 Mouse model and husbandry

Polr3b wild-type (*Polr3b*$^{+/+}$) and heterozygous mutant (*Polr3b*$^{+/-}$) mice on a C57BL/6N background were used. Experimental animals were generated as previously described. Mice were housed under standard conditions with *ad libitum* access to water and standard mouse chow. All procedures were approved by the University of Glasgow Animal Welfare and Ethical Review Board and conducted under UK Home Office project licences. Full details are provided in **Chapter 2, Section 2.1**.

For the fecundity experiment, a single female and a single male mouse were housed in pair to breed until four consecutive litters were produced. Pups from heterozygous breeding pairs were genotyped from either ear or tail biopsies in-house by PCR. Each PCR contained 12.5 µL DreamTaq Green (ThermoFisher, Inchinnan, UK), 2.5 µL each primer, and 0.75 µL genomic DNA in a total volume of 25 µL. Amplification was carried out in a MiniAmp Plus thermal cycler (ThermoFisher, Inchinnan, UK) using the following conditions: 95°C for 10 minutes; 35 cycles of 95°C for 30 seconds, 53°C for 35 seconds and 72°C for 65 seconds; 72°C for 5 minutes. PCR products were run on a 2% agarose gel and visualised using a BioRad Gel Doc XR+ (BioRad, Watford, UK). Primer sequences are in **Table 4-3**. Mice were maintained in Emerald line IVC EM500 (Tecniplast, Italy) under a housing temperature of 22±2°C and a 12L/12D photoperiod (lights on 7.00 am-7.00 pm). Mice were given *ad libitum* access to both water and standard chow diet (CRM(P), Research Diets Services, LBS Biotech, UK; Atwater Fuel Energy-protein 22%, carbohydrate 69%, fat 9%). All animal experiments were undertaken following the University of Glasgow Animal Welfare and Ethical Review Board, under a project license PDBDC7568 and personal license I01541544 from the UK Home Office and following the "principles of laboratory animal care" (NIH Publication No. 86–23, revised 1985).

4.3.2 Design of the fecundity experiment

A total of 20 breeding pairs were established to assess reproductive performance across genotypes and sexes. Each pair consisted of one female and one male, housed together continuously to produce four consecutive litters. The breeding groups included five pairs per combination: ♀*Polr3b*$^{+/+}$ x ♂C57BL/6N, ♀*Polr3b*$^{+/-}$ x ♂C57BL/6N, ♀C57BL/6N x ♂ *Polr3b*$^{+/+}$, and ♀C57BL/6N x ♂*Polr3b*$^{+/-}$. This reciprocal crossing design enabled the assessment of parental genotype and sex as independent variables affecting fecundity (**Figure 4-1**). In litters produced by heterozygous *Polr3b*$^{+/-}$ parents, both WT (*Polr3b*$^{+/+}$) and *Polr3b*$^{+/-}$ pups were present (**Figure 4-1**). For consistency across all breeding groups, mean pup weight per litter was calculated without separating pups by genotype. As a result, litter-level weight values from *Polr3b*$^{+/-}$ crosses reflect the average of a mixed-genotype population. At the start of the experiment, female mice were 92.7 ± 4.8 (mean ± SEM) days old (range: 85-107), and male mice were 99.7 ± 1.0 (mean ± SEM) days old (range: 85-106). Pups remained in the same cage as their parents and were euthanised at weaning (postnatal day 21). No subsequent litters were born before pups from the previous litter were weaned, ensuring that reproductive performance was not confounded by overlapping litters.

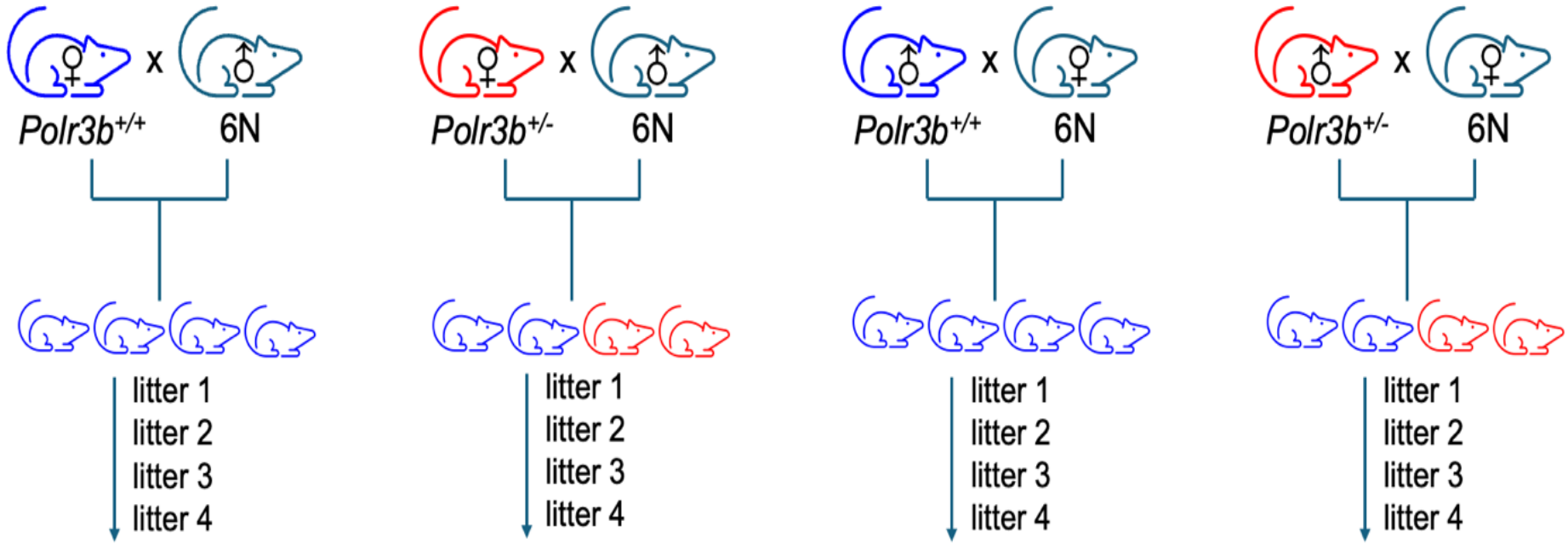

Figure 4-1 Crossing scheme for the fecundity experiment

Either Polr3b$^{+/+}$ (WT) *or Polr3b$^{+/-}$ (blue and red, respectively) mice, of each sex, were bred with C57BL/6N mice to produce four consecutive litters. Pups born from Polr3b$^{+/-}$ breeding pairs consist of both Polr3b$^{+/+}$ and Polr3b$^{+/-}$ mice. Pups were euthanised at weaning (postnatal day 21).*

4.3.3 Assessment of reproductive outcomes

To evaluate the reproductive performance of each breeding pair, several metrics were recorded: time to first litter, litter size at birth, pup body weight at weaning, and pre-weaning pup survival. The time to first litter was defined as the number of days between the initial mating cage setup and the date of birth of the first litter. Litter size was determined on the day of birth, and stillborn pups were included in the count to reflect total parturition output. The number of dead pups was recorded daily from birth to weaning (postnatal day 21), and the pre-weaning survival rate was calculated as the proportion of live-born pups that survived to weaning for each litter. At weaning, pups were weighed using an Ohaus CX221 portable balance to one decimal point and subsequently euthanised; the mean pup weight per litter was calculated to estimate growth performance under maternal care. Although pup weight at weaning does not directly quantify fecundity, it provides an indirect indicator of postnatal maternal investment and offspring viability under standardised rearing conditions (Kounig et al., 1988).

In addition to offspring measures, gross reproductive organ morphology was assessed in parental mice *post-mortem* at the completion of the breeding experiment (Mean age when culled for assessment: 7.85 ± 0.176 months). The ovaries, uteri, testes, *Ductus deferens*, and *Cauda epididymides* were dissected, and the weight, vertical length (measured along the longest axis), and horizontal length (measured along the widest axis) were recorded. These anatomical parameters were used to evaluate potential morphological correlates of reproductive output.

4.3.4 Tissue collection and processing for RT-qPCR

Ovary and testis samples were collected from 3-month-old non-breeding female and male WT and *Polr3b*$^{+/-}$ mice immediately following Schedule 1 killing. Tissues were placed into sterile cryotubes, snap-frozen in liquid nitrogen, and stored at -70°C until RNA extraction for RT-qPCR analysis.

4.3.5 Reverse Transcriptase quantitative-PCR (RT-qPCR)

RNA extraction and quality assessment were performed as described in Chapter 2 (**Section 2.5**). For each sample, 2 µg of total RNA was reverse-transcribed using M-MLV Reverse Transcriptase with random hexamers. The resulting cDNA was diluted to 12.5 ng/µL in nuclease-free water.

Quantitative PCR was performed on a 7500 Fast Real-Time PCR system using SYBR Green chemistry. Each reaction contained cDNA, SYBR Green Master Mix, primers, and PCR-grade water. Candidate reference genes included *B2m*, *Hmbs*, *Ppia*, *Rplp0*, and *Ywhaz*. For each tissue, housekeeping genes were retained only if their expression (CT values) showed no significant difference ($p>0.05$) between WT and *Polr3b*$^{+/-}$ groups (**Table 4-2**). Cycling conditions were followed by a standard melt-curve analysis. Primer sequences are shown in **Table 4-4**.

Relative expression was calculated using the $2^{\wedge -DDCt}$ method, normalised to the geometric mean of selected reference genes, and expressed relative to the WT group. Full details are provided in **Chapter 2, Section 2.**5.

Table 4-2 Housekeeping gene validation summary

Tissue	Housekeeping Gene(s) Used	Validation Method	Specific note
Ovary	*Hmbs, B2m, Ywhaz*	No significant difference in Ct between WT and *Polr3b*$^{+/-}$ when perform reference gene tests with fewer samples (unpaired t-test)	For *Polr3b* and *Maf1*, *B2m* and *Hmbs* retained based on uniformity; For *Polr3a, Cyp19a1, Fshr, and Lhcgr*, *B2m* and *Ywhaz* retained based on uniformity.
Testis	*Ppia, Rplp0, Ywhaz*	No significant difference in Ct between WT and *Polr3b*$^{+/-}$ when perform reference gene tests with fewer samples (unpaired t-test)	For *Polr3b* and *Maf1*, *Ywhaz* retained as the rest two housekeeping genes display significant difference between genotype groups when all sample included; For *Polr3a, Cyp19a1, Fshr, and Lhcgr*, *Ppia* and *Rplp0* retained based on uniformity.

Abbreviations: *B2m: Beta-2 microglobulin; Hmbs: Hydroxymethylbilane synthase; Ppia: Peptidylprolyl isomerase A; Rplp0: Ribosomal protein lateral stalk subunit P0; Ywhaz: Tyrosine 3-monooxygenase/tryptophan 5-monooxygenase activation protein zeta polypeptide*

Table 4-3 Primer sequences used in PCR experiments

Gene	Forward primer	Reverse primer	Expected band size (bp)
Polr3b WT	5'- AGGCTGCTGTGCACTGTATT-3'	5'-GACGGCACTGGAGCAGAAT-3'	82
Polr3b KO	5'- TCAGTGGGGAAAGTTCAGGC-3'	5'- TCAGACGGACACTGGACACT-3'	110

Table 4-4 Primer sequences used in RT-qPCR experiments

Gene	Forward primer	Reverse primer
B2m	5'-CATGGCTCGCTCGGTGAC-3'	5'-CAGTTCAGTATGTTCGGCTTCC-3'
Hmbs	5'-ATGAGGGTGATTCGAGTGGG-3'	5'-TTGTCTCCCGTGGTGGACATA-3'
Ppia	5'-GGCAAATGCTGGACCAAAC-3'	5'-CATTCCTGGACCCAAAACG-3'
Rplp0	5'-TTATAACCCTGAAGTGCTCGAC-3'	5'-CGCTTGTACCCATTGATGATG-3'
Ywhaz	5'-GAAAAGTTCTTGATCCCCAATGC-3'	5'-TGTGACTGGTCCACAATTCCTT-3'
Cyp19a1	5'- CGAAGCAGCAATCCTGAAGGAG-3'	5'- CCAAGTCCACAACAGGCTGGTA-3'
Fshr	5'-GAGGCAGATGTGTTCTCCAACC-3'	5'- TCGGAGACTGGGAAGATTCTGG-3'
Lhcgr	5'- AGCCACTGCTGTGCTTTCAG-3'	5'- AAAGATGGCAGAATAAAGCGTCTC-3'
Maf1	5'-GACTATGACTTCAGCACAGCC-3'	5'-CTGGGTTATAGCTGTAGATGTCAC-3'
Polr3a	5'- GCTTGCCAGATCATCGCTTCAATAC-3'	5'- GTCCACAGGGTGACAGGCTTTA-3'
Polr3b	5'-TTGGAGCCTCAGTTACCAGC-3'	5'-GAATCGACCCTGTTTCACGG-3'

Abbreviations: *Cyp19a: Cytochrome P450 family 19 subfamily A member 1; Fshr: Follicle stimulating hormone receptor; Lhcgr: Luteinizing hormone/choriogonadotropin receptor; Polr3a: Polymerase (RNA) III (DNA directed) polypeptide A; Polr3b: Polymerase (RNA) III (DNA directed) polypeptide B*

4.3.6 Statistics and data analysis

All data analyses were performed using Prism 10.4.2 (GraphPad Software, LLC., 2025), SPSS Statistics 29.0.2.0 (IBM Corp., 2023), and RStudio 2024.09.0+375 (Posit Software, PBC., 2024). For dataset excluded factor of litter number, data were first analysed by ROUT outlier test with Q set to 1%, after that all data were tested for normality with Shapiro-Wilk test, followed by Q-Q plot and boxplot for skewness confirmation especially when the sample size was too small such that a normality test might not be stable (Ghasemi & Zahediasl, 2012). Any removed outliers are noted in figure legends. Non-normal distributed data were either analysed using nonparametric tests or log-transformed, based on the outcomes of detailed normality assessments. For data with one independent variable, unpaired t-test or non-parameter Mann-Whitney U test was used. For assessing the equality of variance, datasets with groups of the equal variances (p-value of F test>0.050) used a normal unpaired t-test; datasets with groups of unequal variances (p-value of F test<0.050) used unpaired t-test with Welch's correction. For data with two independent variables, 2-way ANOVA was used. In the case of 2-way ANOVA, the approach examined genotype (*Polr3b*$^{+/-}$, wild-type), sex (female, male) as main (fixed) factors, also testing interaction effects. In all cases where non-significant interaction effects (p>0.05) were identified, these were subsequently removed, and the analysis was re-run with main effects to obtain the best-fit model.

For datasets involving repeated measures from four consecutive litters per breeding pair: litter size, mean pup weight per litter at weaning, and pre-weaning mortality rate, generalised linear mixed models (GLMMs) were used to test the fixed effects included parental genotype, litter number (parity order), and, where applicable, parental sex and its interaction with genotype. Breeding pair identity (parent.ID) was included as a random intercept to account for repeated litters from the same breeding pair.

Litter size was analysed using Gaussian GLMM (package 'lmerTest' version 3.1.3) (Kuznetsova et al., 2017) due to the normal distribution of the data. Model residuals and diagnostic plots confirmed the suitability of the Gaussian error structure over a Poisson alternative (package 'lme4' version 1.1.35.3) (Bates et al., 2015). Mean pup weight datasets were treated as a continuous outcome as

well as a normally distributed response therefore analysed using a GLMM with Gaussian errors as well. Pre-weaning mortality data, comprising counts of dead versus surviving pups at 21 days, were modelled using a binomial error structure with a logit link function (package 'lme4' version 1.1.35.3) (Bates et al., 2015).

The general model structures were:

$$y \sim \text{genotype} + \text{litter number} + \text{parent ID}$$

for analyses stratified by parental genotype only, and:

$$y \sim \text{genotype x sex} + \text{litter number} + \text{parent ID}$$

for analyses stratified by both parental genotype and sex, where y represents the trait of interest (e.g., litter size, mean pup weight per litter, or pup pre-weaning mortality rate), litter number was included to assess parity effects across four consecutive litters per breeding pair, and parent.ID denotes a random intercept allowing for litter-level variation across breeding pairs.

For each dataset, model fit and validation performed through following tests. Residual structures were assessed using the 'DHARMa' package (version 0.4.6) (Hartig, 2024) including checks for normality, dispersion, residual-vs-predicted patterns. Homoscedasticity was assessed by comparing the standard deviation of observed and simulated residuals using the apply() function across traits and simulation columns. Comparable standard deviation values between observed and simulated data were taken as evidence of acceptable variance structure. Moreover, to evaluate model structure, likelihood ratio tests (LRTs) were performed via the drop1() function, testing whether the inclusion of each fixed effect significantly improved model fit. P-values for fixed and/or interaction effects were obtained using t-test (data stratified by parental genotype only), or Type III F-test (data stratified by parental genotype and sex) with Satterthwaite approximations, except for the pre-weaning mortality dataset, where p-values were obtained using Type III Wald X^2 tests for fixed effects. Outliers were checked via residual diagnostics (package 'DHARMa' v0.4.6) (Hartig, 2024). All GLMM analyses were implemented in RStudio 2024.09.0+375 (Posit Software, PBC., 2024).

For all analyses, effects and differences were considered significant if $p<0.05$, where * denotes a p-value of <0.050, ** denotes a p-value of <0.010, and *** denotes a p-value of <0.001. Any significant main or interaction effects are noted in the figures.

4.4 RESULTS

4.4.1 Lower *Polr3b* expression in testes of the *Polr3b*$^{+/-}$ mice

Polr3b, *Polr3a* and *Maf1* expression in the ovary and testis tissues were examined to confirm Pol III reduction in the *Polr3b*$^{+/-}$ mice. No difference was found for the *Polr3b* expression in the ovary tissues (*t=0.923, p=0.373*) (**Figure 4-2(a)**), and the insignificant result may be due to the large intra-group variation found in the ovary tissues. Lower expression of *Polr3b* was found in the testis tissues of the *Polr3b*$^{+/-}$ mice, compared to their WT counterparts (*t=7.246, p=1.021e-05*) (**Figure 4-2(d)**). There were also no genotypic differences for the *Polr3a* and *Maf1* expression in the ovary and testis tissues (*Polr3a* in ovary tissues: *t=0.286, p=0.779*; *Maf1* in ovary tissues *t=0.252, p=0.805*; *Polr3a* in testis tissues: *t=0.475, p=0.643*; *Maf1* in testis tissues *t=1.883, p=0.084*) (**Figure 4-2**).

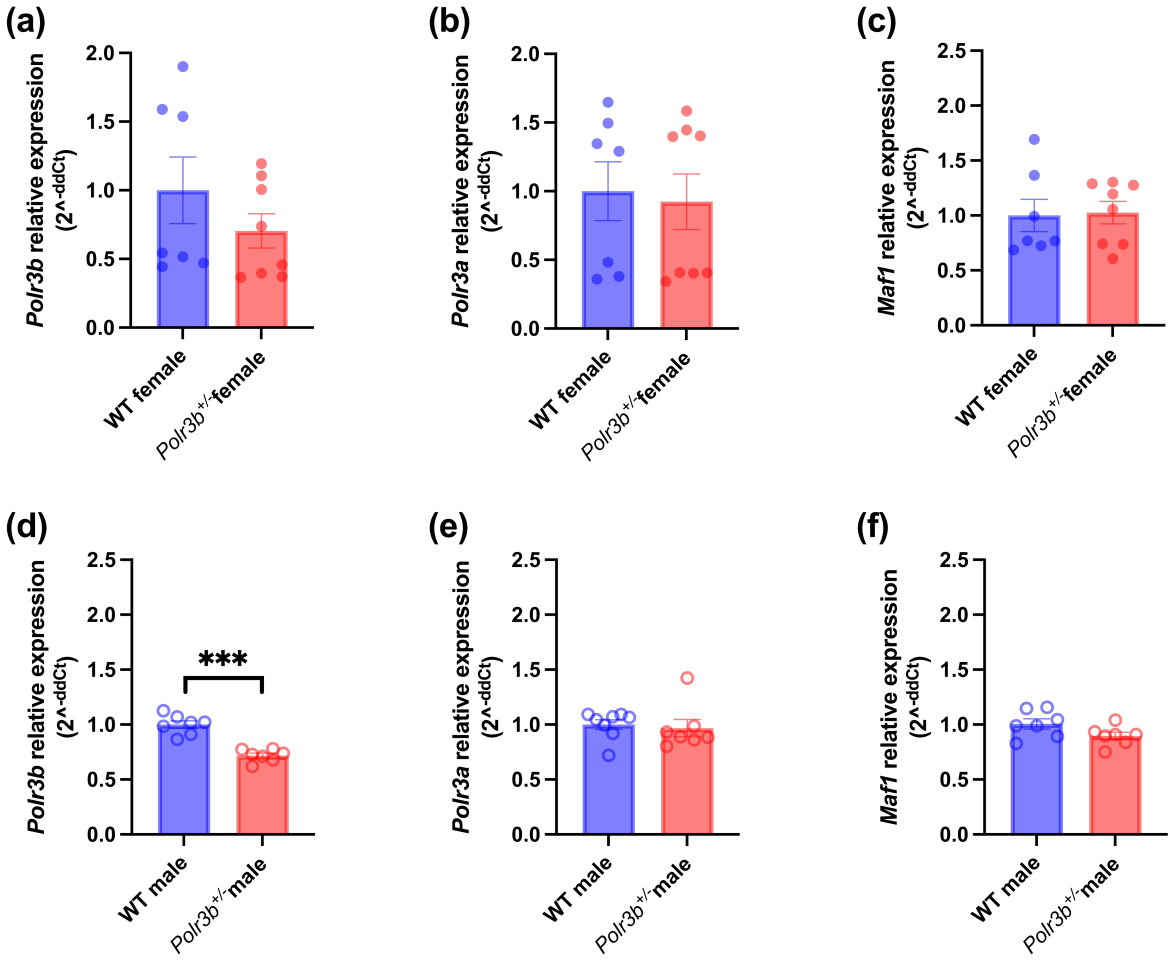

Figure 4-2 Expression of Pol III-related genes *Polr3b*, *Polr3a*, and *Maf1* in ovaries and testes of 3-month-old WT and *Polr3b*$^{+/-}$ mice

*Polr3b, Polr3a, and Maf1 mRNA expression in ovary (a-c) and testis (d-f) of 3-month-old female and male mice. Histograms denote means ± SEM, with sample sizes indicated by individual points within each group. An unpaired t-test was used to test for genotype differences. ***=p<0.001.*

4.4.2 No difference in time from mating to first litter between *Polr3b*$^{+/-}$ and WT mice

For all the following reproductive performance metrics, in order to assess the effect of maternal and paternal *Polr3b*$^{+/-}$ genotype, *Polr3b*$^{+/-}$ or WT mice were bred with C57BL/6N partners of the opposite sex. The time from cage setup (mating date) to first birth was recorded. **Figure 4-3(a)** indicated no significant differences in the interval from mating to the birth of the first litter between the two genotypes (*Mann-Whitney U=45.500, p=0.750*).

When all reciprocal breeding pairs were assessed individually, there was no effect of genotype or sex on interval from mating date to the birth of first litter (genotype *F=1.940, p=0.184*; sex *F=1.705, p=0.211*; genotype*sex interaction *F=3.747, p=0.072*). Note: data were log-transformed prior to ANOVA due to lack of normality.

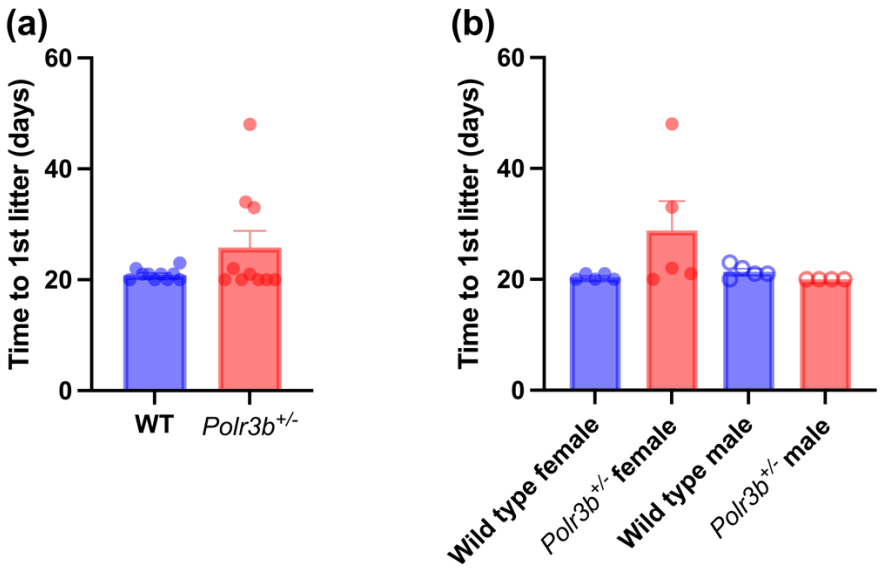

Figure 4-3 Time to first litter in WT and *Polr3b*$^{+/-}$ breeding pairs

Time from mating to first birth in WT and Polr3b$^{+/-}$ *breeding pairs (blue and red, respectively) (a), and separated by all four reciprocal breeding combinations based on genotype and sex of the breeding parent (b). Histograms present means ± SEM, with sample sizes indicate by individual points within a group. Due to skewed distribution, a nonparametric Mann-Whitney U test (a) and log-transform following two-way ANOVA (b) were used for statistical analysis.*

4.4.3 *Polr3b*$^{+/-}$ mice produced larger litters

To compare litter sizes produced by *Polr3b*$^{+/-}$ or WT mice, breeding pairs were set up by mating each genotype to C57BL/6N mice, and litter sizes from four consecutive litters were recorded. A generalised linear mixed model (GLMM) was used to account for fixed effects including litter number as a continuous variable, as well as a possible random effect for breeding pair identity. The analysis showed that *Polr3b*$^{+/-}$ mice produced significantly larger litters than WT controls across all four litters (*estimate=1.449, t=2.396, p=0.019*) (**Figure 4-4(a)**). Moreover, litter size showed a trend of decreasing over time across *Polr3b*$^{+/-}$ and WT breeding groups (*estimate=-0.521, t=-1.897, p=0.062*) (**Figure 4-4(c)**). When the analysis was expanded to consider both genotype and sex of the parent, genotypic effect was again observed (*F=5.752, p=0.019*), there was no effect of sex (*F=0.003, p=0.954*) nor was there a significant interaction between genotype and sex (*F=3.659, p=0.060*) on the litter size (**Figure 4-4(b)**). Altogether, *Polr3b*$^{+/-}$ breeders produced larger litters than WT breeders.

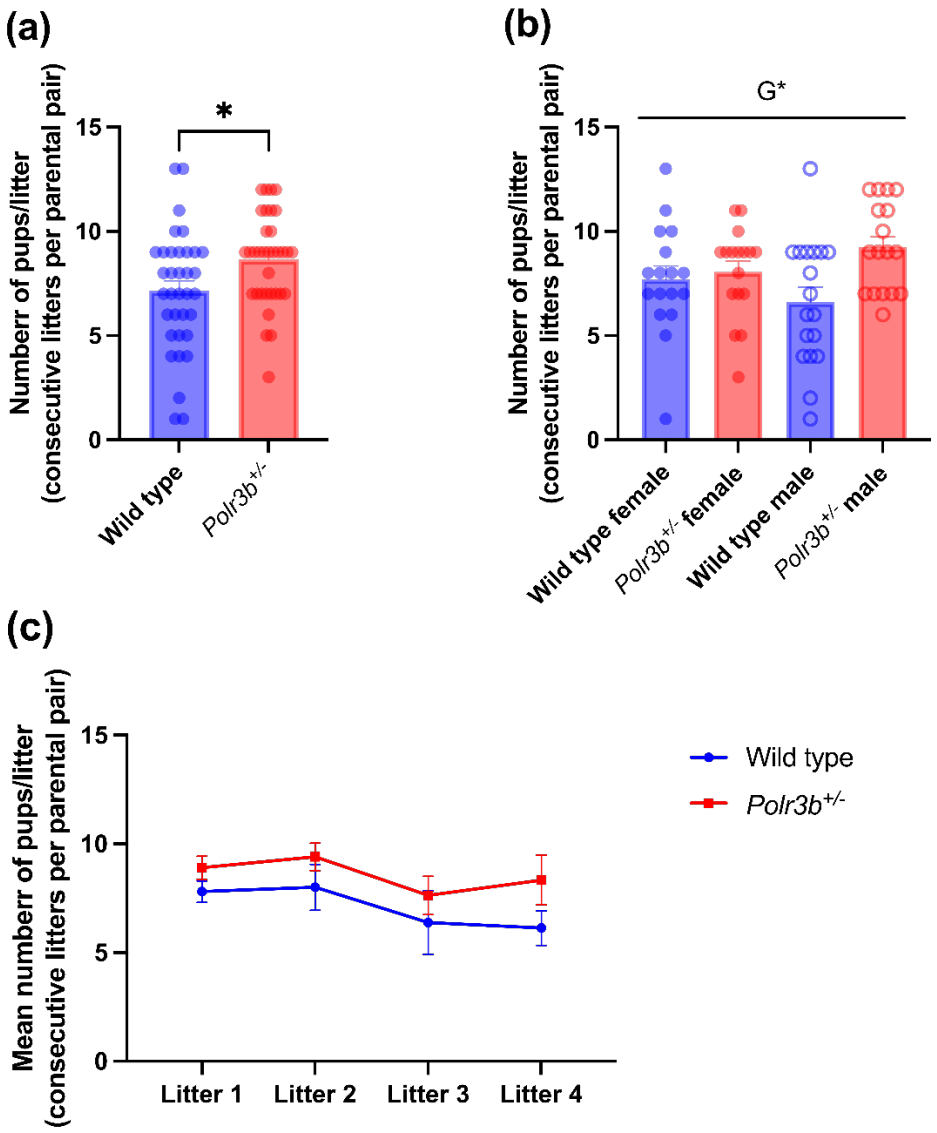

Figure 4-4 Litter size in WT and *Polr3b*$^{+/-}$ breeding pairs across four consecutive litters

*Litter size across all four consecutive litters at birth of WT and Polr3b$^{+/-}$ breeding pairs (blue and red, respectively) (a), and separated by all four reciprocal breeding combinations based on the sex and genotype of the breeding pairs (b). Histograms denote means ± SEM, with sample sizes indicated by individual points within a group. (c) Litter size across four consecutive litters (shown by Litter 1-4) in WT and Polr3b$^{+/-}$ breeding pairs; plot denotes means ± SEM, with n=8-10 for WT breeding pairs and n=6-10 for Polr3b$^{+/-}$ breeding pairs. Gaussian GLMM was used for statistical analysis. *=p<0.050, G*=Gaussian GLMM genotypic effect p<0.050.*

4.4.4 Male pups produced by *Polr3b*$^{+/-}$ parents had lower body weight at weaning

At weaning age (21 days), individual pups were weighed, and the average pup weight per litter was calculated across four consecutive litters derived from parents of two genotypes, *Polr3b*$^{+/-}$ and WT. A Gaussian GLMM was applied to assess whether pup weight was influenced by parental genotype. No significant difference in average pup weight was observed between *Polr3b*$^{+/-}$ and WT parents (*estimate=-0.298, t=-1.278, p=0.207*) (**Figure 4-5(a)**). Additionally, when the analysis was expanded to consider both genotype and sex of parent, no significant difference was found in average offspring weight between litters derived from *Polr3b*$^{+/-}$ versus WT females or males (genotype *F=1.646, p=0.205*; sex *F=1.001, p=0.321*; genotype* sex *F=1.355, p=0.249*) (**Figure 4-5(b)**).

To further investigate whether sex-specific differences in pup weight existed, female and male pups were analysed separately. A significant genotypic effect was detected among male pups: litters from *Polr3b*$^{+/-}$ breeding parents produced lighter male pups compared to those from WT controls (genotype *F=4.352, p=0.042*) (**Figure 4-6(b)**). Neither the sex of the parent not its interaction with genotype significantly affected male pup weight (sex *F=1.166, p=0.286*; genotype*sex *F=2.973, p=0.091*). In contrast, among female pups, the average weight at weaning was similar in litters born to *Polr3b*$^{+/-}$ and WT parents, regardless of parental sex and genotype (genotype *F=0.164, p=0.688*; sex *F=0.004, p=0.950*; genotype* sex *F=1.541, p=0.220*) (**Figure 4-6(a)**).

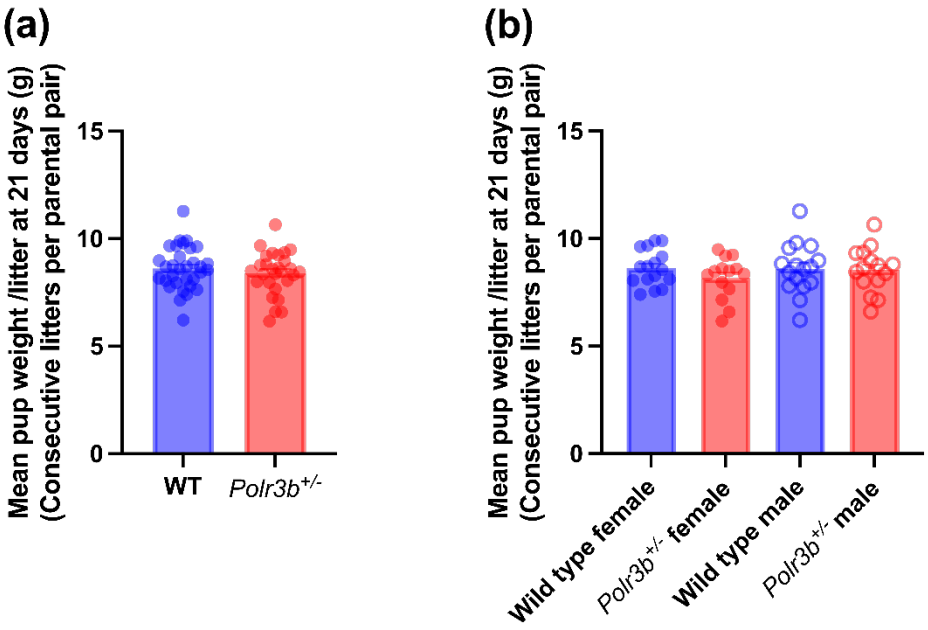

Figure 4-5 Average pup weight per litter at weaning in WT and *Polr3b*$^{+/-}$ breeding pairs across four consecutive litters

Average offspring weight per litter, collected across four consecutive litters at weaning (21 days post-birth), for WT and Polr3b$^{+/-}$ *breeding pairs (blue and red, respectively) (a), and separated by all four reciprocal breeding combinations based on the sex and genotype of the breeding parent (b). Histograms denote mean ± SEM, with sample sizes indicate by individual points within each group. Gaussian GLMM was used for statistical analysis.*

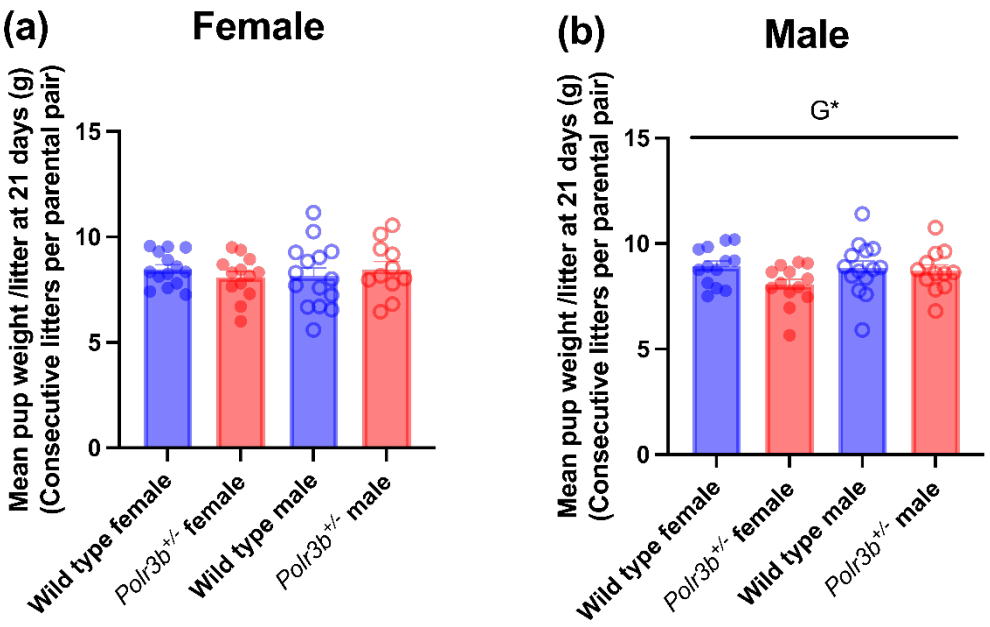

Figure 4-6 Average female and male pup weight per litter at weaning from WT and *Polr3b*$^{+/-}$ breeding pairs across four consecutive litters

Average female (a) or male (b) pup weight per litter, collected across four consecutive litters at weaning (21 days post-birth), for WT and Polr3b$^{+/-}$ (blue and red, respectively) of female and male breeding pairs. Histograms denote means ± SEM, with sample sizes indicate by individual points within each group. Gaussian GLMM was used for statistical analysis. G=Gaussian GLMM genotypic effect p<0.050.*

4.4.5 Pup weight declined across consecutive litters regardless of parental genotype

From the same Gaussian GLMM described above, a significant negative effect of litter number on average pup weight per litter was detected (*estimate=-0.403, t=-3.903, p=0.001*), indicating that pup weight consistently decreased across successive litters irrespective of parental genotype (**Figure 4-7**). This indicates a cumulative physiological cost of reproduction across successive litters.

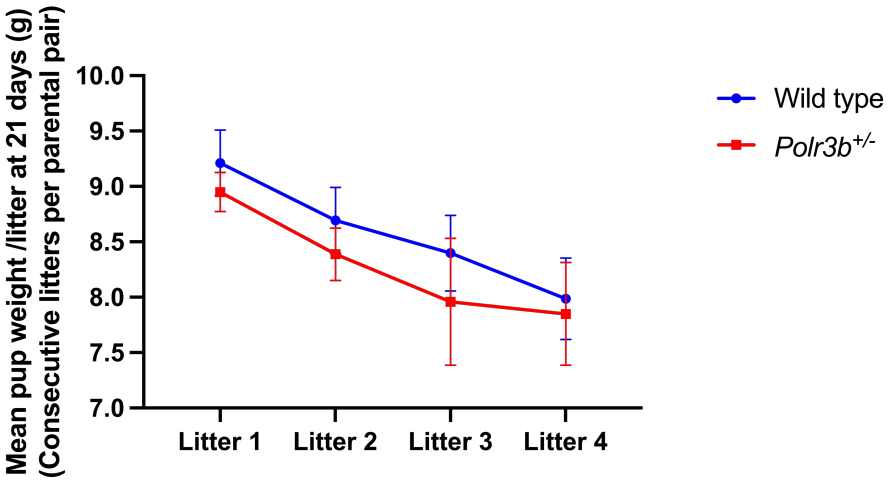

Figure 4-7 Average pup weight per litter across four consecutive litters in WT and *Polr3b*$^{+/-}$ breeding pairs

Average offspring weight per litter across four consecutive litters (shown by Litter 1-4) in WT and Polr3b$^{+/-}$ *breeding pairs. Plot denotes means ± SEM, with n=6-9 for WT breeding pairs and n=4-10 for Polr3b*$^{+/-}$ *breeding pairs. Gaussian GLMM was used for statistical analysis.*

4.4.6 Pups produced by *Polr3b*$^{+/-}$ parents exhibited higher pre-weaning mortality rates

To investigate whether the *Polr3b*$^{+/-}$ genotype influenced pre-weaning mortality, pups born to *Polr3b*$^{+/-}$ and WT breeding pairs were analysed across four consecutive litters. A binomial GLMM was used to model mortality (number of dead versus alive pups at 21 days postnatal) with parental genotype and litter number as fixed effects, and a random effect for breeding pair was included in the model to account for repeated litters from the same parents. A significant genotypic effect was detected ($X^2=4.691$, $p=0.030$), indicating litters from *Polr3b*$^{+/-}$ parents exhibited higher pre-weaning mortality rates compared to WT parents (**Figure 4-8(a)**).

To further analyse whether the effect of genotype varied with parental sex, mortality was compared between four reciprocal breeding groups. A binomial GLMM including sex, genotype, their interaction, and litter number was fitted. A significant genotypic effect was again observed ($X^2=3.876$, $p=0.049$), while neither the interaction between genotype and sex ($X^2=0.474$, $p=0.491$) nor the main effect of sex ($X^2=1.183$, $p=0.277$) was significant (**Figure 4-8(b)**). This effect was not dependent on whether the *Polr3b*$^{+/-}$ parent was female or male.

4.4.7 Pre-weaning mortality increased across consecutive litters regardless of parental genotype

Using the same Binomial GLMM described above, the effect of litter number on pre-weaning mortality was also assessed. Although the plotted mortality rates across litters did not display a strictly monotonic increase (**Figure 4-8(c)**), the model analysis again identified a significant effect of litter number ($X^2=12.542$, $p=0.001$) (**Figure 4-8(d)**), indicating an overall increase in pre-weaning mortality across successive litters. This pattern may reflect a cumulative physiological cost of reproduction, with increasing litter number exerting a progressively negative impact on offspring survival before weaning.

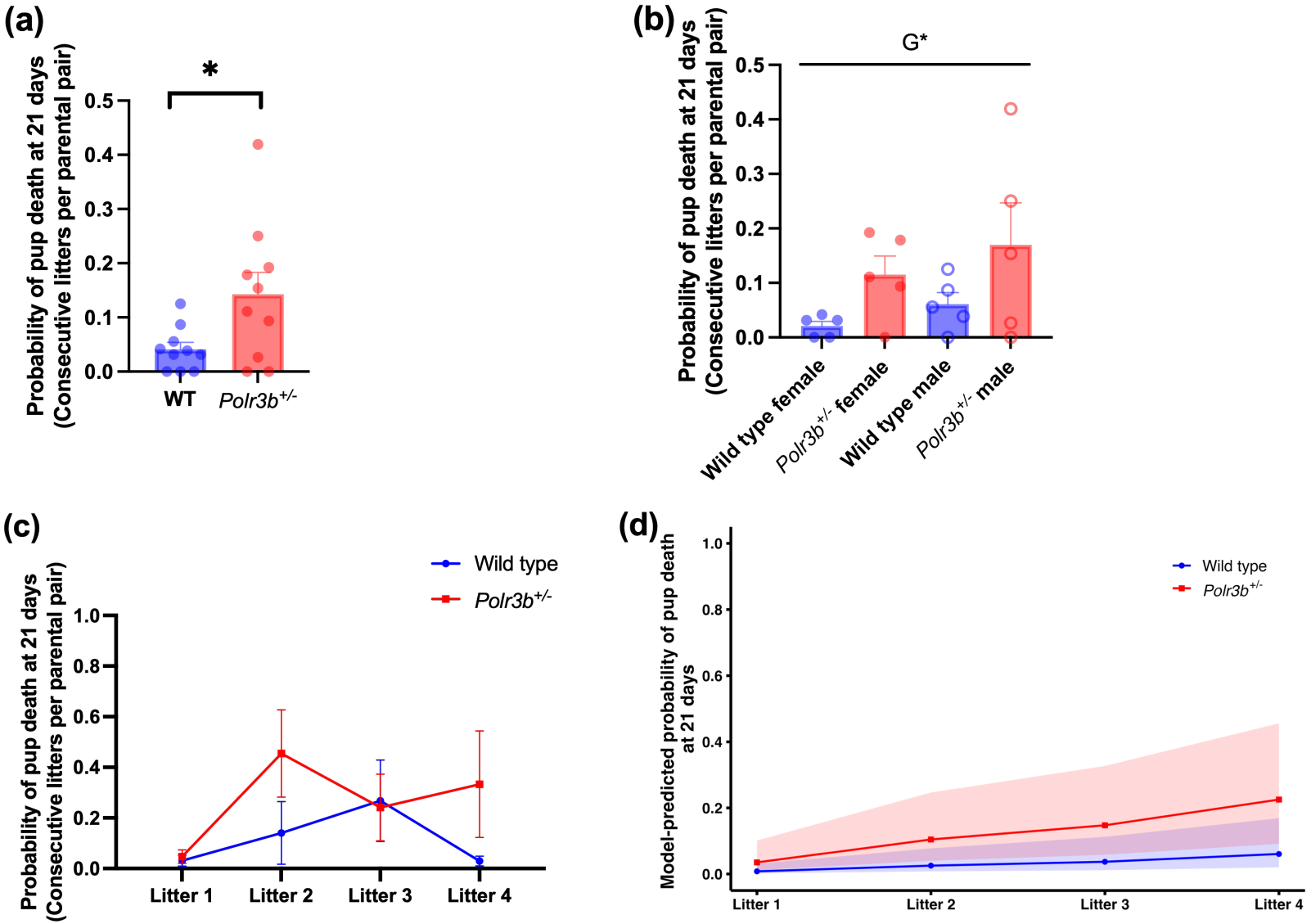
(a)
Probability of pup death at 21 days (Consecutive litters per parental pair)
0.5
0.4
0.3
0.2
0.1
0.0
*
WT
Polr3b+/-
(b)
Probability of pup death at 21 days (Consecutive litters per parental pair)
G*
0.5
0.4
0.3
0.2
0.1
0.0
Wild type female
Polr3b+/- female
Wild type male
Polr3b+/- male
(c)
Probability of pup death at 21 days (Consecutive litters per parental pair)
Wild type
Polr3b+/-
1.0
0.8
0.6
0.4
0.2
0.0
Litter 1
Litter 2
Litter 3
Litter 4
(d)
Model-predicted probability of pup death at 21 days
Wild type
Polr3b+/-
1.0
0.8
0.6
0.4
0.2
0.0
Litter 1
Litter 2
Litter 3
Litter 4

Figure 4-8 Pup mortality rate per litter across four consecutive litters in WT and *Polr3b*$^{+/-}$ breeding pairs

*Pup mortality rate per litter, collected across four consecutive litters at weaning (21 days post-birth), for WT and Polr3b$^{+/-}$ breeding pairs (blue and red, respectively) (a; plot denotes means ± SEM, with n=10 for each group), and separated by all four reciprocal breeding combinations based on the sex and genotype of the breeding parent (b; plot denotes means ± SEM, with n=5 for each group). (c) Pup mortality rate per litter across four consecutive litters (shown by Litter 1-4) in WT and Polr3b$^{+/-}$ breeding pairs, plot denotes means ± SEM, with n=8-10 for WT breeding pairs and n=6-10 for Polr3b$^{+/-}$ breeding pairs. (d) Predicted mortality rate, predicted values were obtained from the model, plot denotes means and shaded areas indicated the 95% confidence intervals around the predictions. Binomial GLMM was used for statistical analysis. *=p<0.050, G*=Binomial GLMM genotypic effect p<0.050.*

4.4.8 WT breeders produced male-biased litters, whereas *Polr3b*$^{+/-}$ breeders showed sex bias

Next, to assess whether deviations from expected genotype or sex ratios might contribute to the differences observed in litter size and pre-weaning survival, the distribution of pup genotypes and sexes was examined. As shown in **Figure 4-9(a)**, pups born to *Polr3b*$^{+/-}$ breeders exhibited no deviation from the expected Mendelian ratio (*p=0.218, 95%CI=[0.393, 0.524]*), indicating no genotypic bias. Analysis of sex ratios revealed a significant male bias in litters from WT breeding pairs (102 females v. 148 males; *p=0.004, 95%CI=[0.346, 0.472]*) (**Figure 4-9(b)**). In contrast, no sex ratio bias was detected in litters from *Polr3b*$^{+/-}$ breeders (*p=0.846, 95%CI=[0.443, 0.574]*) (**Figure 4-9(b)**). These findings indicate that the increased litter size and pre-weaning mortality observed in *Polr3b*$^{+/-}$ breeding pairs are not explained by deviations in Mendelian genotype ratios or sex-specific survival, as no significant biases were detected. This strengthens the idea that other mechanisms are driving the fecundity phenotypes.

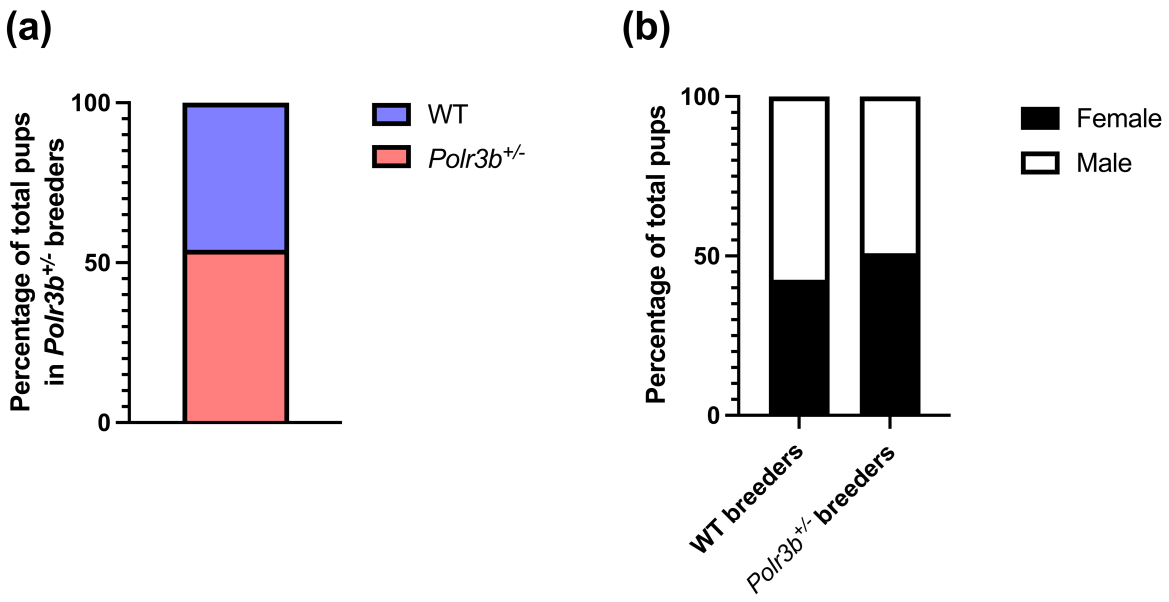

Figure 4-9 Genotype and sex distribution of offspring from WT and *Polr3b*$^{+/-}$ breeding pairs

Distribution of offspring genotypes (WT, blue; Polr3b$^{+/-}$, red) born from Polr3b$^{+/-}$ breeding pairs (a). Sex ratio of total offspring from WT and Polr3b$^{+/-}$ breeding pairs, coloured segments represent females (blue for WT, red for Polr3b$^{+/-}$), and white segments represent males (b). Sample size: n=250 pups from WT breeding pairs and n=238 pups from Polr3b$^{+/-}$ breeding pairs. Binomial test was used to assess deviations from the expected 1:1 ratio.

4.4.9 *Cyp19a1* expression was lower in *Polr3b*$^{+/-}$ ovaries

Key regulatory genes of reproductive hormone signalling, *Cyp19a1*, *Fshr*, and *Lhcgr*, were examined to investigate the reproductive phenotypes of larger litter size and higher pre-weaning mortality in *Polr3b*$^{+/-}$ breeders. **Figure 4-10(a)** revealed *Cyp19a1* in the *Polr3b*$^{+/-}$ ovaries showed lower expression compared to the WT genotype (*t=2.296, p=0.042*). No genotypic differences in the mRNA expression of *Cyp19a1* in testis (*t=0.543, p=0.596*), and no genotypic differences in the mRNA expression of *Fshr* (ovary *t=0.388, p=0.704*; testis *t=0.795, p=0.441*) and *Lhcgr* (ovary *t=0.332, p=0.745*; testis *t=1.200, p=0.253*) in the gonads of both female and male mice (**Figure 4-10**).

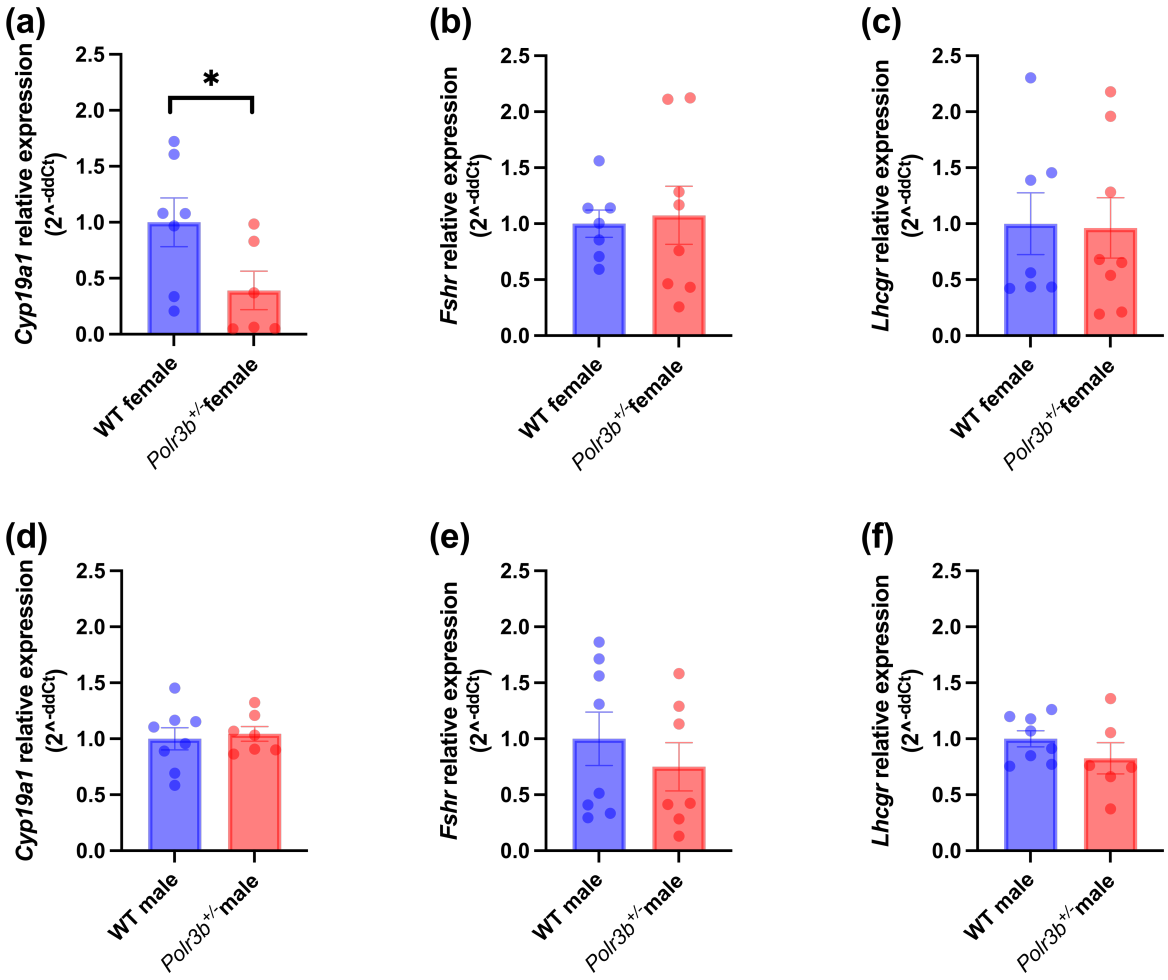

Figure 4-10 Expression of *Cyp19a1*, *Fshr*, *Lhcgr* in ovaries and testes of 3-month-old WT and *Polr3b*$^{+/-}$ mice

*Cyp19a1, Fshr, and Lhcgr mRNA expression in ovary (a-c) and testis (d-f) of 3-month-old female and male mice. Histograms denote mean ± SEM, with sample sizes indicate by individual points within each group. ROUT outlier tests were performed and two outliers were removed from (a) of Polr3b$^{+/-}$ group, one outlier was removed from (f) of Polr3b$^{+/-}$ group. An unpaired t-test was used to test for genotype differences. *=p<0.050.*

4.4.10 *Polr3b*$^{+/-}$ mice showed no differences in reproductive organ morphology compared to WT mice

To define whether there is a possible interplay of the morphological correlates of sex hormones in response to the Pol III heterozygous knockout, the external morphology of the gonads in parent mice was examined (**Figure 4-11**). No statistical differences were found among the external morphology of the ovaries and uterus in *Polr3b*$^{+/-}$ and WT of the male parental mice, same in the testes, *cauda epididymides*, *ductus deferentes* of the male *Polr3b*$^{+/-}$ and WT parental mice (**Table 4-S1**).

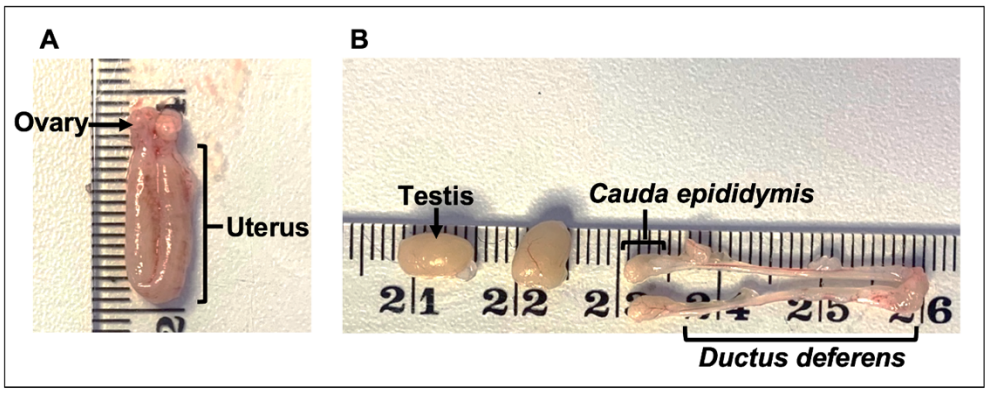

Figure 4-11 Representative photos of gonadal and associated reproductive organs

(A) Female reproductive organs, consisting of ovaries and uteri.

(B) male reproductive organs, consisting of testes, cauda epididymides, and ductus deferentes.

4.5 DISCUSSION

RNA Pol III supports the anabolic processes required for germ cell development, oocyte maturation, and early embryogenesis through its role in tRNA and 5S rRNA synthesis (Goodfellow & White, 2007; Moir & Willis, 2013; Ni & Buszczak, 2023; Willis & Moir, 2018). Studies in model organisms show that altering Pol III activity can influence reproductive output, including changes in brood size in *C. elegans* and reproductive impairment in ribosome-biogenesis mutants in *D. melanogaster* (Hammerquist & Curran, 2020; Khanna et al., 2014; Malik, Goncalves Silva, et al., 2024; Marygold et al., 2007). In mice, the loss of the Pol III repressor MAF1 leads to smaller litters and longer intervals between litters (Bonhoure et al., 2015), indicating that Pol III-related pathways can affect reproductive performance in mammals as well. Against this background, the present chapter examined how partial reduction of Pol III activity through *Polr3b* heterozygosity influences reproductive traits, focusing on measures of fecundity, fertility, and offspring development.

First of all, I found that *Polr3b* expression was significantly decreased in the testis but not the ovary in this study. The expression patterns of *Polr3b* are relatively high in both the ovary and testis (**Figure 4-12**). Given that these mice are heterozygous in *Polr3b* mutant, and in other chapters I have shown that *Polr3b* expression is not similar across tissues and sex differences also existed (*see chapters 3 and 5*). In line with this, *Polr3b* expression is not uniform across tissues or sexes, as shown in other chapters of this thesis. Borland et al. (2024) also reported sex- and tissue-specific phenotypes in *Polr3b*$^{+/-}$ mice, including divergent outcomes in bone, gut, and skin, while Watt et al. (2023) showing that Pol III-dependent transcripts and Pol III subunits vary across tissues and cell types, with altered Pol III transcription leading to distinct tissue-specific responses. All these may explain the inconsistent expression of *Polr3b* in the ovary and testis in the current chapter. Despite the testes of *Polr3b*$^{+/-}$ mice exhibiting reduced Polr3b expression, the paternal *Polr3b*$^{+/-}$ genotype did not significantly alter time to first litter or litter size when analysed by parental sex. However, this does not exclude paternal contributions to offspring growth or survival, since the present study did not assess sperm concentration, motility, morphology, viability or genomic integrity, or fertilisation capacity, all of which could influence fertilisation success, embryo development, or postnatal offspring

health (Kawai et al., 2006; Latham, 2025; Nakao et al., 2020). In addition, sperm-borne small tRNA-derived small RNAs (tsRNAs) have been linked to intergenerational transmission of acquired metabolic phenotypes, and sperm small RNA content can change during epididymal maturation (Chen et al., 2016; Sharma et al., 2016). Therefore, sperm functional and sperm small RNA/tsRNA profiling would be useful follow-up experiments to determine whether reduced testicular *Polr3b* expression is associated with altered paternal germline quality.

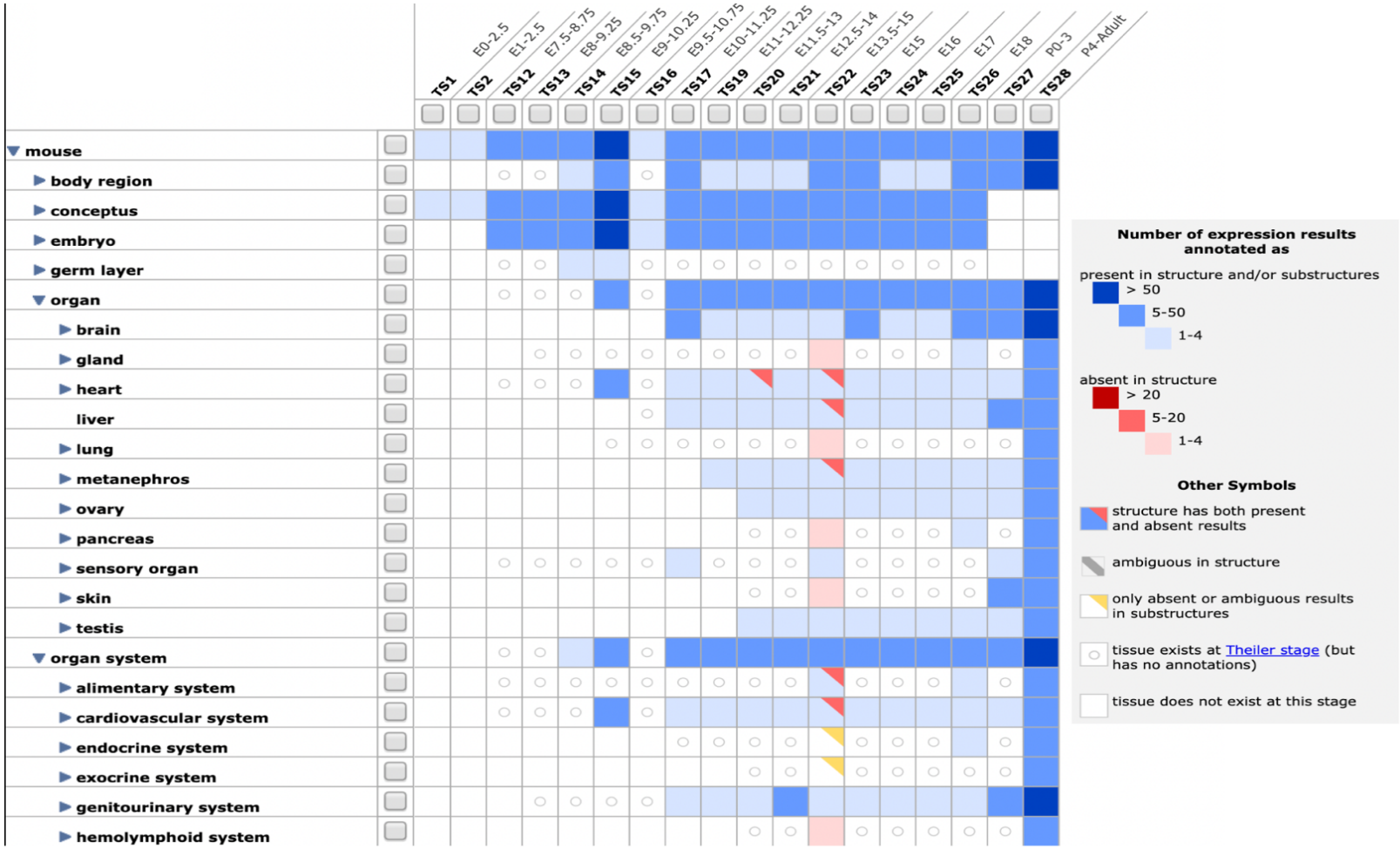

Figure 4-12 Expression of *Polr3b* across mouse organs. Figure obtained from Mouse Genome Informatics (https://www.informatics.jax.org/)

One of the most notable findings was that *Polr3b*$^{+/-}$ mice produced larger litters at birth with increased pre-weaning mortality. A similar pattern was observed in a study of *Maf1*$^{-/-}$ mice, which are expected to have increased Pol III transcription due to the loss of MAF1-mediated repression, and exhibited reduced litter sizes (Bonhoure et al., 2020). Together, these findings suggest that higher Pol III transcription may constrain reproductive output, whereas a partial reduction in Pol III activity, as in the present study, may enhance litter size at birth. By contrast, Filer et al. (2017) reported that reduction of Pol III activity in *Drosophila* via RNAi against the *C160* subunit (*Polr3a* homolog) did not affect egg production. However, egg number alone may not fully reflect reproductive output. Moreover, *Polr3a* and *Polr3b* encode distinct subunits, and mutations in different subunits are known to cause non-overlapping disease phenotypes (Yeganeh & Hernandez, 2020), suggesting that subunit-specific roles could underlie divergent reproductive phenotypes.

Furthermore, the present study demonstrated that reduced Pol III activity was associated with larger litter size at birth in *Polr3b*$^{+/-}$ breeders. However, larger litter size at birth does not always reflect greater reproductive success, as it does not account for offspring viability or postnatal investment such as milk production (Chahoud & Paumgartten, 2009; Stearns, 1992). Indeed, although *Polr3b*$^{+/-}$ breeders produced more pups overall (including stillborn pups), these litters also showed higher mortality before weaning and, in some litters, lower pup weight at weaning, particularly in later reproductive rounds. Despite this, the genotype distribution of pups from *Polr3b*$^{+/-}$ breeders and the sex ratio at weaning (postnatal day 21) did not deviate from the expected 1:1 ratio. Taken together, these patterns indicate that the reproductive traits observed in *Polr3b*$^{+/-}$ breeding pairs are unlikely to be explained by embryonic lethality linked to pup genotype or sex-specific differences in postnatal survival. However, the present design cannot fully distinguish whether the lower pup survival arose from prenatal or postnatal mechanisms. Prenatal contributors could include altered oocyte quality, sperm-derived effects, placental function, foetal growth, or the intrauterine hormonal environment (Denicol & Siqueira, 2023; Latham, 2025; Sferruzzi-Perri et al., 2023). In contrast, postnatal contributors could include maternal nursing behaviour, milk production, milk composition, thermoregulation, or increased competition between pups in larger

litters (Brajon et al., 2019; Fernandez et al., 2025; Morello et al., 2024; Nagasawa et al., 1989). This distinction is important because *Polr3b*$^{+/-}$ breeders produced larger litters at birth, and larger litters can increase competition for maternal resources after birth, thereby affecting both pup growth and survival (Chahoud & Paumgartten, 2009; Stearns, 1992). Therefore, the increased pre-weaning mortality observed here should be interpreted as a survival phenotype that may reflect combined prenatal and postnatal effects. Future studies could separate these mechanisms more directly. Cross-fostering pups between WT and *Polr3b*$^{+/-}$ dams would help determine whether pup survival is mainly driven by the prenatal environment of the birth mother or by postnatal maternal care. This approach has been used in mice to distinguish prenatal and postnatal maternal effects on offspring growth and maternal performance (Kurnianto et al., 1998; Young et al., 1965). Litter standardisation at birth would also be useful, as it would reduce variation in postnatal nutritional competition between litters and allow pup growth and mortality to be compared under more equal nursing demand (Chahoud & Paumgartten, 2009). In addition, monitoring of maternal behaviour and pup milk bands during the postnatal days could help identify whether pre-weaning pup loss is associated with impaired nursing or maternal care.

Polr3b$^{+/-}$ breeders were also found to have reduced male pup weight. Sex differences in early life vulnerability are well documented, with male offspring exhibiting higher rates of stillbirth, neonatal mortality, and reduced survival under adverse conditions such as maternal undernutrition or environmental stress (Alur, 2019). Moreover, there is consistent evidence that male foetuses are more sensitive to intrauterine stress and metabolic change (Geary et al., 2003; Ibanez et al., 2008; Mayhew et al., 2008; Stark et al., 2011). Therefore, it is possible that male offspring are more susceptible to long-term growth and metabolic disruption in response to early biosynthetic stress caused by Pol III reduction.

Reduced ovarian *Cyp19a1* was found in female *Polr3b*$^{+/-}$ mice. *Cyp19a1* encodes aromatase, the cytochrome P450 enzyme that converts androgens to oestrogens (Hussain & Gilloteaux, 2020). Lower expression of the *Cyp19a1* gene in ovaries can lead to a decrease in oestrogen production and an increase in androgen levels (Panghiyangani et al., 2020). RNA Pol III supports global protein synthesis

by generating short, non-coding RNAs necessary for ribosome function (Moir & Willis, 2013). Reducing Pol III leads to decreased protein synthesis (Filer et al., 2017), which may explain the deficiency in enzyme aromatase production in the *Polr3b*$^{+/-}$ ovaries. This, in turn, can lead to oestradiol reduction and adversely affect the oocyte quality and embryonic development (Cheng et al., 2022; Hussain & Gilloteaux, 2020; Luo et al., 2024).

The endocrine mechanism also remains unresolved because gene expression was measured at a single time point in non-breeding animals. Further hormonal profiling would be required to test whether the lower ovarian *Cyp19a1* expression is accompanied by altered circulating oestradiol, progesterone, LH, FSH, or prolactin, as these hormones fluctuate across the rodent oestrous cycle and regulate follicular development, ovulation, and luteal function (Goldman et al., 2007; Wall et al., 2023). Tracking the oestrous cycle by vaginal cytology before and during mating would also clarify whether *Polr3b*$^{+/-}$ females show altered cycle length, irregular cycling, or changes in the timing of ovulation (Cora et al., 2015; Goldman et al., 2007). These measurements would be able to better interpret the larger litter size and reduced pup survival phenotypes by linking reproductive outcome to endocrine state rather than gene expression alone.

A cause of reduced reproductive performance could be the size of the gonads and/or their associated reproductive organs. In mice, the size and the weight of the ovary, uterus and testis are impacted by hormones such as androgen and FSH, and in animals lacking androgen receptors or FSH-R leads to impaired fertility to various extents and/or leads to impaired folliculogenesis (Dierich et al., 1998; Hu et al., 2004; Yeh et al., 2002). In humans, a uterus with suboptimal size (either larger or smaller) is related to a lower pregnancy rate (Gao et al., 2019). In some other mammals, the size of the ovary and the quality of oocytes in the ovary are also found to be either positively or negatively associated with reproductive performance (Baez et al., 2016; Ireland et al., 2011). All these results indicated that gonads and their associated reproductive organs impact reproductive performance to various extents, and the underlying mechanisms are complex across species. The present study showed no difference in the size or weight of the ovary, uterus, testis, *Ductus deferens* or *Cauda epididymis* (male-associated reproductive organs that are responsible for sperm

concentration, maturation, motility and fertilising ability) (James et al., 2020), between the *Polr3b*$^{+/-}$ and the WT mice (**Table S4-1**). However, the sample size for these morphometric comparisons was limited. Notably, post hoc power analysis (**Table S4-2**) revealed that the study was underpowered to detect even large anatomical differences, with some traits showing large effect sizes but low statistical confidence. These findings should therefore be interpreted cautiously, and further studies with larger cohorts and making sure that tested animals are in the same oestrus cycling will be needed to accurately validate any potential morphological differences.

4.6 CONCLUSION

Mutations in the *Polr3b* allele, which partially reduce Pol III signalling, have resulted in varied effects on reproductive performance in mice. Specifically, the *Polr3b*$^{+/-}$ mice exhibited larger litter sizes at birth including stillborn, lower male pup bodyweight, higher pre-weaning mortality rates, and reduced *Cyp19a1* expression, these findings collectively indicating compromised reproductive success. These findings support a model in which Pol III-dependent biosynthetic capacity is essential not only for supporting reproduction but also for maintaining offspring viability. The sex-specific effects observed suggest that male offspring are particularly vulnerable to reduced parental biosynthetic capacity. These findings underscore the complex role of Pol III signalling in modulating reproductive performance in mice. Further work will be required to distinguish prenatal from postnatal contributors to pup survival, and to test whether endocrine signalling, maternal care, placental function, sperm function, or paternal sperm-borne small RNAs contribute to the phenotypes observed here.

4.7 Supplemental tables

Table S4-1 Morphometric parameters of gonads and associated reproductive organs in WT and *Polr3b*$^{+/-}$ parental mice

		WT		p-value, (t-value),	*Polr3b*$^{+/-}$	
		Min-max	Mean±SEM	n (WT, *Polr3b*$^{+/-}$)	Min-max	Mean±SEM
	Female age, days	241.00-259.00	250.75±3.75	n=4,4	212.00-253.00	236.25±8.88
	Female body weight, mg	32.50-38.30	34.70±1.25	0.815, (-0.244), n=4,4	30.50-46.60	35.65±3.69
Ovary	Weight, mg	14.00-32.00	22.25±4.55	0.334, (1.135), n=4,4	15.00-19.00	17.00±0.82
	Vertical length, mm	2.80-3.80	3.07±0.24	0.131, (1.746), n=4,4	2.00-3.00	2.45±0.26
	Horizontal length, mm	2.00-3.00	2.50±0.22	0.818, (0.240), n=4,4	2.00-2.90	2.42±0.22
Uterus	Weight, mg	100.00-157.00	135.67±17.95	0.980, (0.027), n=3,3	118.00-169.00	135.00±17.00
	Vertical length, mm	12.00-17.00	14.00±1.22	0.566, (0.607), n=4,4	9.0-15.5	12.88±1.39
	Horizontal length, mm	2.20-3.00	2.73±0.19	0.128, (-1.767), n=4,4	3.00-3.50	3.12±0.12
Ovary+uterus	Weight, mg	102.00-171.00	142.50±15.99	0.666, (-0.458), n=4,3	137.00-184.00	153.00±15.50
	Male age, days	184.00-246.00	223.00±11.41	n=5,5	184.00-246.00	227.00±11.82
	Male body weight, mg	25.10-35.70	31.64±1.93	0.368, (-0.963), n=5,4	30.30-37.70	34.20±1.72

Testis	Weight, mg	121.00-183.00	155.80±10.10	0.814, (-0.245), n=5,4	139.00-203.00	160.00±14.53
	Vertical length, mm	7.20-8.30	7.96±0.20	0.829, (0.224), n=5,4	7.20-8.80	7.88±0.35
	Horizontal length, mm	4.00-5.10	4.62±0.20	0.986, (-0.018), n=5,4	4.20-5.00	4.62±0.17
Ductus deferens	length, mm	22.00-22.00	22.0±0.00	0.157, (-2.219), n=2,3	23.00-27.00	24.67±1.20
Cauda epididymis	Vertical length, mm	3.00-3.50	3.25±0.25	0.402, (-0.915), n=2,5	3.00-5.00	3.86±0.39
	Horizontal length, mm	3.00-3.10	3.05±0.05	0.819, (-0.241), n=2,5	2.80-4.00	3.14±0.22
Ductus deferens +*Cauda epididymis*	Weight, mg	66.00-79.00	74.33±4.18	0.174, (-1.649), n=3,3	77.00-103.00	88.67±7.62

Table S4-2 Post hoc power analysis for morphometric parameters of gonads and reproductive organs

TRAIT	COHEN'S D	POWER
Ovary weight	0.80	0.16
Ovary vertical length	1.24	0.32
Ovary horizontal length	0.18	0.06
Uterus vertical length	0.43	0.08
Uterus horizontal length	1.23	0.31
Ovary + uterus weight	0.36	0.07
Testis weight	0.16	0.06
Testis vertical length	0.14	0.05
Testis horizontal length	0.00	0.05
Ductus deferens length	1.82	0.29
Cauda epididymis vertical	0.92	0.15
Cauda epididymis horizontal	0.26	0.06
Ductus deferens + CE weight	1.35	0.25

Effect sizes were estimated as Cohen's d from group means and SEM, and statistical power was calculated using two-sample t-tests with the actual group sizes for each trait. Despite several traits showing moderate to large effect sizes (e.g., ductus deferens length, d = 1.82), the small sample sizes resulted in low statistical power across all comparisons (range: 0.05-0.32)

Chapter 5: A retrospective study of idiopathic dermatitis during ageing in *Polr3b*$^{+/-}$ mice

5.1 INTRODUCTION

5.1.1 Idiopathic dermatitis

C57BL/6 mice are prone to age-related idiopathic dermatitis (ID), typically developing it between 10 and 16 months of age, with prevalence rates of 4% to 30%, depending on the demographics of the population examined (Alvarado et al., 2016; Kastenmayer et al., 2006; Neuhaus et al., 2012). ID is a spontaneous skin disorder with undetermined aetiology and poor treatment response, leading to a common cause of euthanasia in C57BL/6 mice (Alvarado et al., 2016; Andrews et al., 1994; Hampton et al., 2012; Williams-Fritze et al., 2011). While several treatments have been used to help treat ID, including nail trimming, maropitant citrate, ibuprofen, and vitamin E, none of these treatments are curative (Adams et al., 2016; Alvarado et al., 2016; Ezell et al., 2012; Lawson et al., 2005; Williams-Fritze et al., 2011). ID typically initially presents with intense pruritus and scratching, leading to excoriations that rapidly progress to deep ulcerative lesions. These lesions are most commonly located in the interscapular and dorsal cervical areas but may later on spread laterally and caudally to affect the head, ears, face, shoulders, and flanks (Andrews et al., 1994; Hampton et al., 2012; Kastenmayer et al., 2006; Lawson et al., 2005; Sundberg et al., 1994; Sundberg et al., 2011; Tynes, 2013). Specifically, mild ID is typically characterised by epidermal hyperplasia and ulceration, often accompanied by serocellular crusts with or without mild dermal inflammation, and granulation tissue formation observed during the wounding process (Gozalo et al., 2023; Kastenmayer et al., 2006; Williams-Fritze et al., 2011). As lesions progress, severe ID may involve bleeding, exposed musculature, and scar contracture due to dermal fibrosis replacing the normal dermis structure during the healing process (Gozalo et al., 2023; Kordestani, 2019).

The cause of ID is suspected to be multifaceted. Studies have shown that female mice are generally at higher risk of developing ID compared to males

(Kastenmayer et al., 2006; Sargent et al., 2015). Additionally, seasonal variation in ID has been reported, though findings remain inconsistent. Two studies observed a higher incidence in late spring and summer, while another reported an increased incidence in late autumn (De Biase et al., 2019; Kastenmayer et al., 2006; Sundberg et al., 1994). Regardless of the conflicting findings, the observed seasonality in the ID incidence may be due to annual fluctuations in humidity and temperature levels within specific vivariums. In addition, ageing, follicular dysplasia, high-fat diet, bacterial overgrowth, particularly *Staphylococcus xylosus*, and inflammatory events/induction), have all been linked to ID development (Andrews et al., 1994; Duarte-Vogel & Lawson, 2011; Hampton et al., 2015; Hampton et al., 2012; Kastenmayer et al., 2006; Krugner-Higby et al., 2012; Lawson et al., 2005; Neuhaus et al., 2012; Sundberg et al., 2011; Williams-Fritze et al., 2011; Won et al., 2002; Zhang et al., 2015). Moreover, within mice with clinical ID, systemic immune activation has been reported, including lymphadenopathy and splenomegaly (De Biase et al., 2019; Hampton et al., 2015; Kastenmayer et al., 2006). These immune responses are characterised by increased granulocytes (derived from innate immune system) and decreased B-cells (from adaptive immune system) in the spleen, along with histological evidence of extramedullary haematopoiesis, which reflecting increased inflammatory demand (Hampton et al., 2015).

The lesions of ID exhibit wound-like characteristics and undergo the normal wound healing process (Williams et al., 2012). The wound-healing process consists of four temporally overlapping phases: hemostasis (fibrin clot formation and platelet deposition), inflammation, proliferation (angiogenesis, fibrogenesis, and re-epithelialisation), and resolution (vessel regression and collagen remodelling (Gosain & DiPietro, 2004; Gubernatorova et al., 2020). In particular, the key steps of the wound healing process are regulated by extracellular matrix (ECM) and collagen deposition (Mathew-Steiner et al., 2021). In addition, several distinct progenitor populations, such as the hair follicle stem cells in the dermis, are found to give rise to epidermal cells that contribute to accelerating the skin regeneration (Takeo et al., 2015).

5.1.2 Histopathology of idiopathic dermatitis

Histologic examination of murine ID reveals varying levels of pathological skin changes. Mild lesions are characterised by superficial keratinocyte loss and minimal inflammation, while severe cases display extensive ulceration with coalescing pustules, pronounced edema, and significant inflammatory infiltration into the deeper epidermal and dermal layers (Sargent et al., 2015). In mild ID, skin lesions with adjacent hyperplastic epidermis are present, but as the ID progresses the underlying dermis becomes inflamed and is accompanied by inflammatory infiltrates comprising neutrophils, lymphocytes, macrophages, mast cells, and occasionally eosinophils (Andrews et al., 1994; De Biase et al., 2019; Gozalo et al., 2023).

Mast cells are of particular interest in ID due to their early recruitment and broad effector roles in cutaneous immunity. Increased mast cell numbers have been reported in early-stage lesions, often observed in a degranulating state prior to ulceration (De Biase et al., 2019; Gozalo et al., 2023). Upon activation, mast cells release histamine, chymase, carboxypeptidases, tryptase, and the pro-inflammatory cytokines TNF-α and IL-6 into surrounding tissues (Gozalo et al., 2023; Numata et al., 2022). These mediators contribute to keratinocyte activation and proliferation, immune cell recruitment, inflammation induction and suppression, as well as extracellular matrix degradation and remodelling (Ackermann & Harvima, 1998; Gozalo et al., 2023; Harvima & Nilsson, 2011). Histamine also promotes pruritus by depolarising sensory nerves and initiating the itch-scratch cycle that exacerbates lesion severity (Gozalo et al., 2023; Toyoshima & Okayama, 2022). While mast cell activation plays a constructive role in wound healing by promoting reepithelialisation and angiogenesis, inappropriate activation (as seen in urticaria, atopic dermatitis, and psoriasis) may perpetuate inflammation and tissue damage (Numata et al., 2022; Wulff & Wilgus, 2013). In addition to classical degranulation, mast cells can release cytokines and lipid mediators through degranulation-independent pathways, allowing persistent modulation of the local tissue microenvironment and potentially impeding repair (Numata et al., 2022; Wulff & Wilgus, 2013).

As ID progresses in severity, the areas of ulceration, dermal fibrosis, and the inflammatory infiltrate also increase, along with the appearance of epidermal

serocellular crusts (Andrews et al., 1994; Gozalo et al., 2023). Fibrosis then develops in response to chronic inflammation, varying from granulation tissue to advanced dermal scarring (Andrews et al., 1994; De Biase et al., 2019). It has also been reported that in the very early stage of ID, acute leukocytoclastic vasculitis may occur, which is characterised by intense perivascular neutrophilic infiltrates and thrombosis in dermal vessels; although it appears this feature becomes less prominent in the later chronic stage due to the transient nature of vasculitis (Andrews et al., 1994). Another study has also noted the presence of follicular abnormalities, including follicular dysplasia, in the affected areas, although this feature is not observed in all studies (De Biase et al., 2019; Gozalo et al., 2023; Sundberg et al., 2011). **Figure 5-1** shows representative changes in the mouse skin indicative of both mild and severe ID.

5.1.3 Inflammation in idiopathic dermatitis

Inflammation plays a central role in the pathophysiology of ID. Multiple studies have identified pro-inflammatory cytokines and immune signalling pathways that are elevated in association with the disease. IL-6 is one of the most prominent inflammatory cytokines and is widely implicated in many autoimmune and cutaneous inflammatory diseases (Choy et al., 2020; Gubernatorova et al., 2020; Neurath & Finotto, 2011; Tanaka et al., 2014; Yao et al., 2014). Elevated plasma levels of IL-6 and TNF-α have been reported in mice with ID, and increased mRNA expression of *Il6*, *Il1β*, and *Tnfα* has been observed in inflamed skin (De Biase et al., 2019; Hampton et al., 2015).

IL-6, IL-1β, and TNF-α are key effector cytokines of the innate immune system and are transcriptionally regulated by the NF-κB signalling pathway (Confalone et al., 2010). Activation of this pathway depends on multiple upstream regulators, including the paracaspase MALT1, which is essential for T-cell receptor-mediated NF-κB activation (Ruland et al., 2003; Schmitt et al., 2016). In addition to innate responses, adaptive immune cells also appear to contribute to the pathology of ID. De-Biase et al. (2019) reported increased dermal infiltration of T-helper 17 (Th17) cells in ID lesions (De Biase et al., 2019). Cytokines associated with Th17 polarisation, including *Il17α*, *Il22*, and *Il23α*, are

involved in neutrophil recruitment, keratinocyte activation, and sustained tissue inflammation (Weaver et al., 2013). IL-23α sustain and enhances Th-17 cells to produce IL-17α and IL-22, primarily impacting epithelial cells in tissues such as the gut, the lung, and the skin (Blaschitz & Raffatellu, 2010; Qu et al., 2013).

Chemokines that coordinate the migration and positioning of Th17 cells, such as the CCL20-CCR6 axis, are also implicated in this process (Getschman et al., 2017). Beyond immune cells, keratinocytes are active participants in inflammatory responses and are capable of producing a range of cytokines and chemokines (Gozalo et al., 2023). In addition to IL-1α, IL-1ß, and IL-6, murine keratinocytes also express IL-8 (mouse homolog of CXCL15), and can secrete chemokines including CCL20 to shape the local immune environment (Jiang et al., 2020).

5.1.4 RNA Polymerase III and idiopathic dermatitis

RNA Polymerase III (Pol III) is a pivotal evolutionarily conserved enzyme found in eukaryotic cells, and it mediates the production of non-coding RNAs whose transcriptions are known to fulfil housekeeping functions in cells and are critical for cell survival (Lata et al., 2021). Reduced Pol III signalling has been shown to promote longevity in yeast, *C. elegans*, and *D. melanogaster* (Filer et al., 2017; Malik, Goncalves Silva, et al., 2024). Borland et al. (2024) previously reported that neither female nor male C57BL/6N mice heterozygous for RNA Pol III (*Polr3b*$^{+/-}$) were long-lived relative to wild-type (WT) controls. However, this study observed that female *Polr3b*$^{+/-}$ mice exhibited a higher occurrence of ID compared to female WT mice, or male mice of either genotype (Borland et al., 2024). Furthermore, it is known that elevated levels of inflammation are commonly observed in the skin lesions with ID, which is akin to human conditions associated with inflammatory ulceration (Neuhaus et al., 2012; Sargent et al., 2015; Sundberg et al., 1994). A growing body of literature indicates that Pol III can elicit innate immune responses through multiple mechanisms. It can transcribe cytosolic viral DNA or host-derived non-coding RNAs, which activate or bind to RIG-I (Ablasser et al., 2009; Chiu et al., 2009; Y. Zhang et al., 2022; Zhao et al., 2018). This interaction triggers a cascade of events, ultimately activate

IFN-regulatory factors (IRFs) and NF-κB, leading to the transcription of type I/III interferons (IFN-I/III) and pro-inflammatory cytokines, respectively (Ablasser et al., 2009; Naesens et al., 2023). These together suggest an unappreciated role of Pol III in cutaneous health.

5.2 AIMS AND OBJECTIVES

Aims:

To further investigate the mechanisms underlying the higher incidence of idiopathic dermatitis in female *Polr3b*$^{+/-}$ mice, a retrospective study involving a life-analysis of female and male *Polr3b*$^{+/-}$ mice (51 and 52 mice, respectively) and female and male WT mice (53 and 50, respectively) was undertaken to identify and characterise ID disease trends, plasma IL-6, skin architecture, dermal mast cells, wound healing rate, dermal collagen content and inflammatory events in both *Polr3b*$^{+/-}$ and WT mice, across both sexes and two ages (14 and 20 months).

Objectives:

Objective 1: To determine the prevalence of idiopathic dermatitis, including the incidence of ID, age of onset of ID, seasonal pattern of ID, and splenomegaly incidence in female and male *Polr3b*$^{+/-}$ mice compared to wild-type mice.

Objective 2: To determine plasma IL-6 levels in female and male of *Polr3b*$^{+/-}$ and WT mice at 14 months (middle-aged) and 20 months (old age).

Objective 3: To evaluate the skin structure of female *Polr3b*$^{+/-}$ and WT mice at 14 months and 20 months. The assessment included epidermal, dermal, and adipose layer thickness, adipocyte count and size, number of cutaneous mast cells along with their degranulation ratio, and collagen content in the dermis.

Objective 4: To assess the wound healing rate of dermal fibroblasts *in vitro* for the female *Polr3b*$^{+/-}$ and WT mice by evaluating the fibroblast migration rate after wounding, as well as using a real-time cell assay technique (RTCA) to assess their cell performance.

Objective 5: To determine the skin expression of inflammatory makers in female *Polr3b*$^{+/-}$ and WT mice by RT-qPCR.

5.3 MATERIALS AND METHODS

5.3.1 Mouse model and husbandry

Polr3b wild-type (*Polr3b*$^{+/+}$) and heterozygous mutant (*Polr3b*$^{+/-}$) mice on a C57BL/6N background were used. Experimental animals were generated as previously described. Mice were housed under standard conditions with *ad libitum* access to water and standard mouse chow. All procedures were approved by the University of Glasgow Animal Welfare and Ethical Review Board and conducted under UK Home Office project licences. Full details are provided in **Chapter 2, section 2.1**.

5.3.2 Routine check, ante- and post-mortem evaluation

Routine welfare checks and monitoring procedures followed the protocols outlined in **Chapter 2** (**Section 2.2**). Briefly, monitoring was intensified for mice showing signs of pathology, including ID) (**Figure 5-1**), which was monitored daily. Mice with ID received standard treatment (green clay application and nail trimming) and were weighed and assessed until recovery or until human endpoints were met. Criteria for enhanced monitoring and euthanasia were as defined in **Chapter 2 and Appendix 2**. *Post-mortem* examinations were conducted for all mice that were euthanised or found dead.

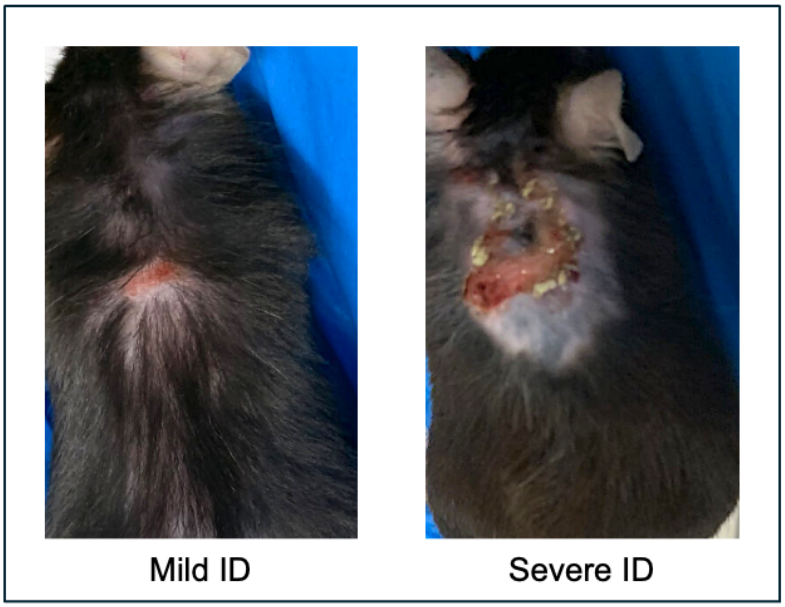

Figure 5-1 Mild ID and severe ID on the dorsal area of C57BL/6N mice

5.3.3 Pathology analysis of splenomegaly

Mice were examined for the presence of splenomegaly *post-mortem* (undertaken by Dr Gillian Borland, Prof Colin Selman, Dr Stephen E. Wilkie, or Zhe Wang). The total number of mice with and without splenomegaly was calculated for the *Polr3b*$^{+/-}$ female, WT female, *Polr3b*$^{+/-}$ male, and WT male groups, respectively. The number of ID-affected mice with and without splenomegaly was also assessed for each group to conduct a pathology analysis.

5.3.4 Plasma collection and processing

14- and 20-month-old mice were euthanised by Schedule 1 procedures, and the blood was collected immediately following cervical dislocation. Blood was allowed to drain into the collection tubes, and plasma was separated by centrifugation at 2,000 x g for 10 minutes at 4°C. Plasma samples were aliquoted and stored at -70°C until analysis, and all samples were thawed only once prior to assay.

5.3.5 Quantification of plasma IL-6

Plasma IL-6 concentrations were measured using a solid-phase sandwich ELISA (Mouse IL-6 DuoSet, R&D Systems; DY406) following the manufacturer's protocol. Briefly, microplates were coated with capture antibody, blocked, and incubated with 100 µL plasma samples or recombinant IL-6 standards. After washing, biotinylated detection antibody and streptavidin-HRP were applied sequentially, and colour development was achieved using TMB substrate. The reaction was stopped with acid stop solution and the absorbance was read at 540 nm with wavelength correction at 540/570 nm using a standard microplate reader. IL-6 concentrations were derived from a 4-parameter logistic (4-PL) standard curve covering the assay range of 15.6-1,000 pg/mL. Standards and plasma samples were assayed in duplicate.

5.3.6 Skin tissue collection and processing for histology

Full-thickness skin samples were collected *post-mortem* from the dorsal neck region immediately following euthanasia. Prior to dissection, overlying hair was removed using electric clippers to expose the skin surface. A rectangular section of dorsal skin (approximately 2 cm x 1 cm) was then excised and placed flat into a plastic histology tissue cassette, epidermis side up. Samples were immediately

submerged in 10% (v/v) neutral buffered formalin (NBF) and fixed at room temperature for 24-48 hours. Following fixation, the cassettes were transferred into 70% (v/v) ethanol and submitted to the Histology Research Service (HRS) at the University of Glasgow for embedding and staining.

Detailed procedures in the Haematoxylin & Eosin, Toluidine blue and Masson's trichrome staining are provided in **Chapter 2, Section 2.7.**

5.3.7 Histological analysis of skin sections using Haematoxylin and Eosin staining

The following parameters were measured in H&E using ImageScope v12.4.3.5008 (Leica Biosystems, retrieved from https://www.aperio.com): epidermal thickness, dermal thickness, adipose layer thickness, and adipocyte count. For each sample, three serial slides were analysed. Measurements were taken from three non-overlapping regions per slide, with ten measurements per region for each skin layer.

5.3.8 Histopathological analysis of mast cells using Toluidine blue staining

The following parameters were measured in Toluidine blue using ImageScope v12.4.3.5008 (Leica Biosystems, retrieved from https://www.aperio.com): mast cell total count and degranulated mast cell count. Each section contains three serial slides and each slide was measured three times.

5.3.9 Histopathological analysis of dermal collagen using Masson's trichrome staining

The following parameters were measured using ImageJ2 2.14.0/1.54f (Schindelin et al., 2012) in Masson's trichrome: Collagen content in dermal area. Each

sample has three serial slides, and each slide was measured three times to improve accuracy.

5.3.10 Cell culture for dermal fibroblasts

Primary dermal fibroblasts were isolated from ear tissue of 5-month-old female WT and *Polr3b*$^{+/-}$ mice and cultured under standard conditions. Cells were passaged and cryopreserved prior to downstream applications. Full details are provided in **Chapter 2, section 2.4.**

5.3.11 Wound healing assay

The scratch-wound assay is a two-dimensional (2D) in-vitro technique to assess cell migration. Prior to the experiment, the base of a sterile 12-well cell culture plate (Corning, ME, USA) was marked with 3 equal-distance parallel lines on each row of the wells. The cells were then seeded into the plate at 100,000 cells/well density in complete culture medium (10% FBS) and placed in an incubator (37°C, 5% CO_2). After cells were grown to confluence, a 20 µl pipette tip was used to scratch the cell surface to disrupt the cell confluent monolayer for the wound healing assay (**Figure 5-2**). The wells were then washed with DPBS and incubated in fresh culture medium. Zero-hour (0 h) photos were then taken at the areas as indicated for each well using a microscope (EVOS XL Core). Cells were then placed back into the incubator for twenty-four hours. After twenty-four hours, the plate was placed on the same microscope, and photos were taken at the same areas for each well (**all these experiments were undertaken by Ms Jackie Thomson)**. The images were then analysed using an open-source software Fiji (ImageJ2, version 2.14.0/1.54f; (Schindelin et al., 2012). The percentage of the wound area covered by cells after twenty-four hours was measured.

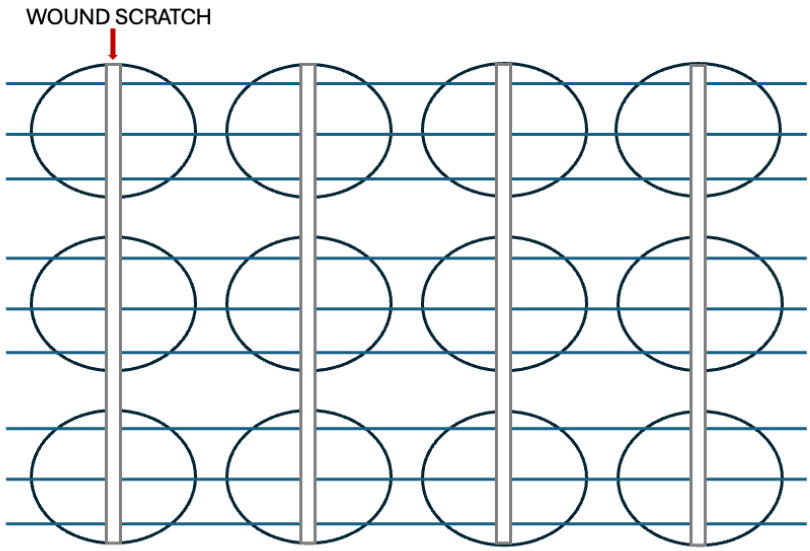

Figure 5-2 Scratch-wound assay

Nine parallel lines were drawn on the back of a 12-well plate using a marker pen. After the cells have just grown to confluence, a pipette tip was used to scratch the cells across the centre of the well to create a straight "wound" with equal width.

5.3.12 Real-Time Cell Analysis (RTCA) for wound healing assay

Wound healing was performed in E-Plate 96 (ACEA Biosciences, Inc., USA), a 96-well plate fused with gold micro-electrodes that can detect the presence of adherent cells. Cell growth was recorded with the xCELLigence® W380 RTCA Real-Time Cell Analyser (ACEA Biosciences, Inc., USA). Following seeding, the plate was placed in the RTCA instrument in the incubator (37°C, 5% CO_2) to measure cell proliferation. After the cells had grown to confluence, a sterile needle was used to scratch the cell's surface of each well to disrupt the cell confluent monolayer for the wound healing assay. The plate was then returned to the RTCA instrument in the incubator. A parameter termed cell index (including cell attachment and proliferation) was used to quantify cell health and status based on the detected cell-electrode impedance, and it was recorded every 15 minutes during a three-day period. RTCA cell analysis software (ACEA Biosciences, Inc., USA) was used to analyse the cell index, and the cell index had to be normalised to the scratch point for comparison. **(all these experiments were undertaken by Ms Jackie Thomson and Dr Gillian Borland**).

5.3.13 Skin tissue collection and processing for RT-qPCR

Full-thickness dorsal skin samples (approximately 2 cm x 1 cm) were collected from 14-month-old female WT and *Polr3b*$^{+/-}$ mice immediately following Schedule 1 killing. Hair was removed from the dorsal surface by shaving prior to dissection. Skin tissues were placed into sterile cryotubes, snap-frozen in liquid nitrogen, and stored at -70°C until RNA extraction for RT-qPCR analysis.

5.3.14 Reverse Transcriptase quantitative-PCR (RT-qPCR)

RNA extraction

Total RNA was extracted from both full-thickness dorsal skin tissue and cultured dermal fibroblasts using a RNeasy Mini Kit (Qiagen, Manchester, UK), following the manufacturer's protocols for animal tissues and cultured cells, respectively. For skin tissues, 20-30 mg of frozen sample was homogenised in Buffer RLT using a 20-gauge needle fitted to an RNase-free syringe. Homogenates were mixed with 70% ethanol and processed using spin columns. For dermal fibroblasts, cells were re-grown from cryopreserved vials and harvested at passage 3 by trypsinisation. The cell pellet was resuspended in Buffer RLT and processed following the vacuum/spin protocol for animal cells.

In both cases, on-column DNase digestion was performed using the RNase-Free DNase Set (Qiagen, Manchester, UK), as described in Appendix D of the RNeasy Mini Handbook, to remove genomic DNA contamination. After washing steps with RW1 and RPE buffers, RNA was eluted in RNase-free H_2O. RNA concentration and purity were assessed using a NanoDrop® Spectrophotometer ND-1000 (ThermoFisher, Wilmington, DE, USA).

cDNA synthesis and RT-qPCR

Total RNA extracted from liver tissue was reverse-transcribed to cDNA, followed by quantitative PRC (RT-qPCR) to assess gene expression. Detailed procedures for cDNA synthesis, qPCR reaction setup, and data analysis are described in **Chapter 2, Section 2.5.2**. Briefly, total RNA was reverse transcribed using M-MLV Reverse Transcriptase (ThermoFisher, Inchinnan, UK) and gene expression was quantified using SYBR Green-based RT-qPCR on an Applied Biosystems 7500 Fast Real-Time PCR System. Expression values were calculated using the $2^{\wedge DDCt}$ method, normalised to the geometric mean of stable reference gene sets *B2m, Hmbs, Ywhaz, and Ppia* (**Table 4-1**). Primer sequences are shown in **Table 4-2**.

Table 5-1 Housekeeping gene validation summary

Tissue / Cell Type	Housekeeping Gene(s) Used	Validation Method	Specific note
Female Skin	*B2m, Hmbs, Ppia, Ywhaz*	No significant difference in Ct between WT and *Polr3b*$^{+/-}$ (t-test)	For *Il1α, Cxcl15, Col1a1, Col3a1,* and *Il22*, *B2m* and *Ppia* retained based on expression stability across samples; For *Il17α, Il23α, Il6, and Ccl20*, and *Malt1*, *B2m*, *Hmbs*, and *Ywhaz* retained based on expression stability across samples.
Female Dermal Fibroblasts	*B2m, Hmbs*	No significant difference in Ct between WT and *Polr3b*$^{+/-}$ (t-test)	Ct values were stable across all samples, no genotype bias.

Table 5-2 Primer sequences used in PCR and RT-qPCR experiments

Gene	Forward primer	Reverse primer
B2m	5'-CATGGCTCGCTCGGTGAC-3'	5'-CAGTTCAGTATGTTCGGCTTCC-3'
Hmbs	5'-ATGAGGGTGATTCGAGTGGG-3'	5'-TTGTCTCCCGTGGTGGACATA-3'
Ppia	5'-GGCAAATGCTGGACCAAAC-3'	5'-CATTCCTGGACCCAAAACG-3'
Ywhaz	5'-GAAAAGTTCTTGATCCCCAATGC-3'	5'-TGTGACTGGTCCACAATTCCTT-3'
Ccl20	5'-GGTACTGCTGGCTCACCTCT-3'	5'-TGTACGAGGGGCAACAGTCG-3'
Col1a1	5'-AGGCGAACAAGGTGACAGAGG-3'	5'-GGAGAACCAGGAGAACCAGGAG-3'
Col3a1	5'-TCCAGGTCCTCCAGGTTCTCC -3'	5'-ATGTGGTCCAACTGGTCCTCT-3'
Ccl20	5'-GGTACTGCTGGCTCACCTCT -3'	5'-TGTACGAGAGGCAACAGTCG-3'
Cxcl15	5'-TCCTGCTGGCTGTCCTTAACC-3'	5'-TTCCTGAATACACAGACATCGTAGC-3'
Il6	5'-CTGCAAGAGACTTCCATCCAG-3'	5'- AGTGGTATAGACAGGTCTGTTGG-3'
Il1α	5'-CTGAAGAAGAGACGGCTGAGTTTC-3'	5'-TCTGGTAGGTGTAAGGTGCTGATC-3'
Il1B	5'- GAAATGCCACCTTTTGACAGTG-3'	5'- TGGATGCTCTCATCAGGACAG-3'
Tnfα	5'-GTCCCCAAAGGGATGAGAAGT-3'	5'-TTTGCTACGACGTGGGCTAC-3'
Malt1	5'-GACTGTGACTTCAGCACAGCC-3'	5'-CTGGGTTATAGCTGTAGATGTCAC-3'
Il17α	5'-TCCAGGGAGAGCTTCATCTGTGTC-3'	5'-TTGGACACGCTGAGCTTTGAGG-3'
Il22	5'-GTGCGATCTCTGATGGCTGTC-3'	5'-AGGGCAATGAGAAGCAGGCA-3'
Il23α	5'-TCCAGTGTGAAGATGGTTGTGAC-3'	5'-TTGCAAGCAGAACTGGCTGTTG-3'

Abbreviations: *B2m: Beta-2 microglobulin; Hmbs: Hydroxymethylbilane synthase; Ppia: Peptidylprolyl isomerase A; Ywhaz: Tyrosine 3-monooxygenase/tryptophan 5-monooxygenase activation protein zeta polypeptide; Ccl20: C-C Motif Chemokine Ligand 20; Cxcl15: C-X-C motif chemokine ligand 15; Il6: Interleukin 6; Il1α: Interleukin 1 Alpha; Il1B: Interleukin 1 Beta; Tnfα: Tumour Necrosis Factor alpha; Malt1: Mucosa-Associated Lymphoid Tissue Lymphoma Translocation gene 1; Il17α: Interleukin 17 Alpha; Il22: Interleukin 22; Il23α: Interleukin 23 Alpha*

5.3.15 Statistics and data analysis

All data analyses were performed using Prism 9.3.1 (GraphPad Software, LLC., 2021), SPSS 29.0.2.0 (20) (Armonk, NY: IBM Corp), and R 4.1.3 (GUI 1.77 Big Sur ARM build, ©R Foundation for Statistical Computing, 2021). Data were first analysed by the ROUT outlier test with Q set to 1%, and after that, all data were tested for normality. Any removed outliers are noted in the figure legends. The specific statistical tests are noted in the figure legends. For assessing the equality of variance, datasets with groups of the equal variances (p-value of F-test>0.050) used a normal unpaired t-test; datasets with groups of unequal variances (p-value of F-test <0.050) used an unpaired t-test with Welch's correction.

In the case of 2-way ANOVA, the approach examined genotype (*Polr3b*$^{+/-}$, wild-type), sex (female, male) or age (14 months, 20 months) as main (fixed) factors, also testing interaction effects. In all cases where non-significant interaction effects (*p>0.05*) were identified, these were subsequently removed, and the analysis was rerun with main effects to obtain the best-fit model. effects and differences were considered significant if the p-value <0.05, where * denotes a p-value of <0.050, ** denotes a p-value of <0.010, and *** denotes a p-value of <0.001. Any significant main or interaction effects are noted in the figures.

5.4 RESULTS

5.4.1 *Polr3b* expression is down-regulated in the skin of *Polr3b*$^{+/-}$ mice

To verify the heterozygous knock-out of *Polr3b* in *Polr3b*$^{+/-}$ mice, *Polr3b* expression levels were measured in female skin samples. As shown in **Figure 5-3**, the mRNA expression of *Polr3b* was significantly (*t=4.119, p<0.001*) reduced in *Polr3b*$^{+/-}$ females relative to WT females.

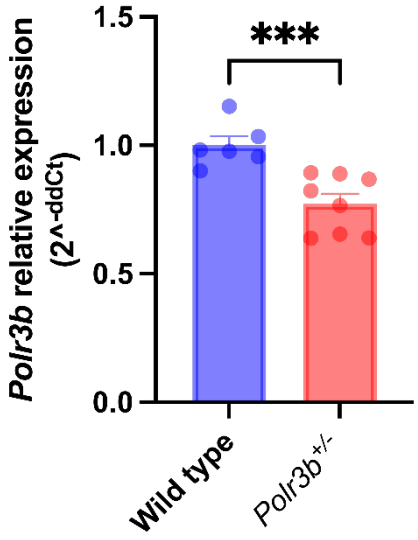

Figure 5-3 *Polr3b* mRNA expression in the skin of 14-month-old female WT and *Polr3b*$^{+/-}$ mice

*Histograms present mean ± SEM, with sample sizes indicate by individual points within a group. Two outliers were identified and removed from WT group. An unpaired t-test was used to test for genotype difference. ***=p<0.001.*

5.4.2 Increased incidence and greater severity of ID in *Polr3b*$^{+/-}$ female mice

The number of mice that developed ID was determined in both females and males *Polr3b*$^{+/-}$ and WT mice. The chi-square test showed female *Polr3b*$^{+/-}$ mice had a significantly higher risk of ID compared to the WT females (*RR=1.559, 95% CI [1.040-2.392], p=0.031*), with no significant difference observed in male mice (*RR=2.043, 95% CI [1.000-4.300], p=0.050*) (**Figure 5-4 (a)**). Although the p-value in males was marginal and did not meet the conventional threshold for significance, the effect size (*RR=2.043*) and confidence interval (*95% CI [1.000-4.300]*) suggest a possible trend towards increased ID risk that the study may have been underpowered to resolve.

Figure 5-4 (b) further showed that in *Polr3b*$^{+/-}$ female mice, there was a pronounced increase in the percentage of mice humanely euthanised because of ID compared to WT females (*RR=3.118, 95% CI [1.509-6.691], p=0.001*), with again no difference observed in male mice*(RR=0.964, 96% CI [0.276-3.375], p>0.999*). Consequently, these findings show that *Polr3b*$^{+/-}$ females were not only more prone to developing ID but that the ID they developed was significantly more severe.

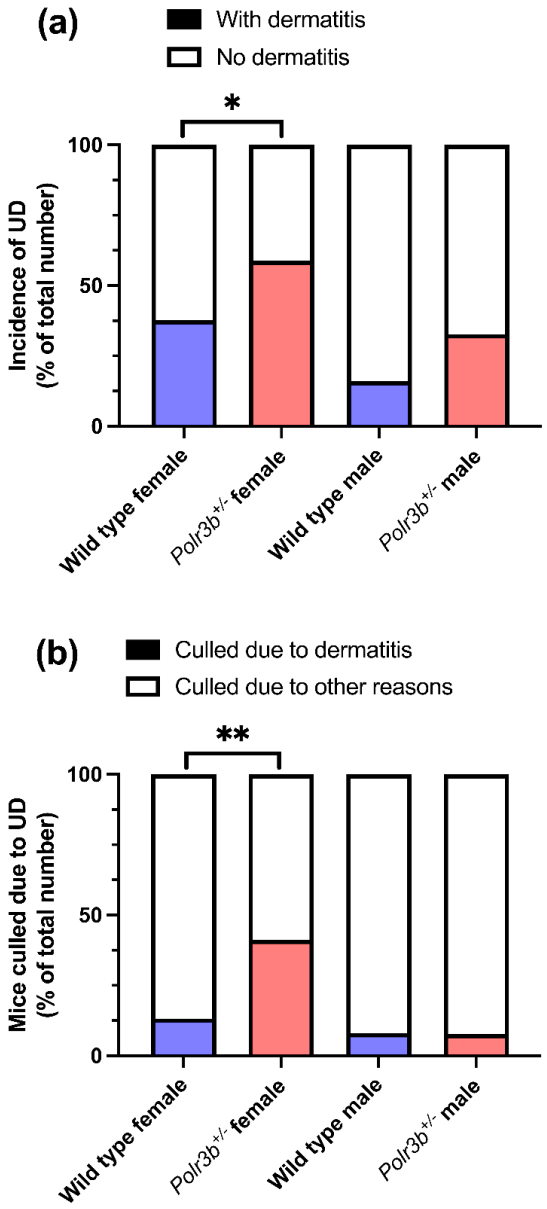

Figure 5-4 Incidence and culling rates due to idiopathic dermatitis in female and male WT and *Polr3b*$^{+/-}$ mice

Incidence of idiopathic dermatitis (a) and percentage of mice culled due to idiopathic dermatitis out of the total number of mice (b) in WT and Polr3b$^{+/-}$ *(blue and red, respectively) female and male mice. n=53 for WT females, n=51 for Polr3b*$^{+/-}$ *females, n=50 for WT males, and n=52 for Polr3b*$^{+/-}$ *males. A chi-square test was used for statistical analysis, except that a two-tailed Fisher's exact test was used in the male group of (b), as this data has an expected frequency of <5. *=p<0.050, **=p<0.010.*

5.4.3 The incidence of idiopathic dermatitis increased with age and female mice were more prone to develop the disease at a younger age

The age of the first clinical manifestation of ID was recorded for each mouse suffering from ID. As shown in **Figures 5-5 (a) and (b)**, the proportion of mice developing ID increased with age in both sexes.

To assess whether the age of ID onset differed by sex or genotype, a two-way ANOVA was performed. **Figure 5-6** revealed that sex had a significant influence on the age of onset (*F=6.057, p=0.016*), with female mice developing ID earlier than males. There was no significant main effect of genotype (*F=3.402, p=0.069*), nor was there a significant interaction between sex and genotype (*F=0.538, p=0.466*). These results suggest that the age of first ID onset is influenced by sex, but effect is consistent across genotypes.

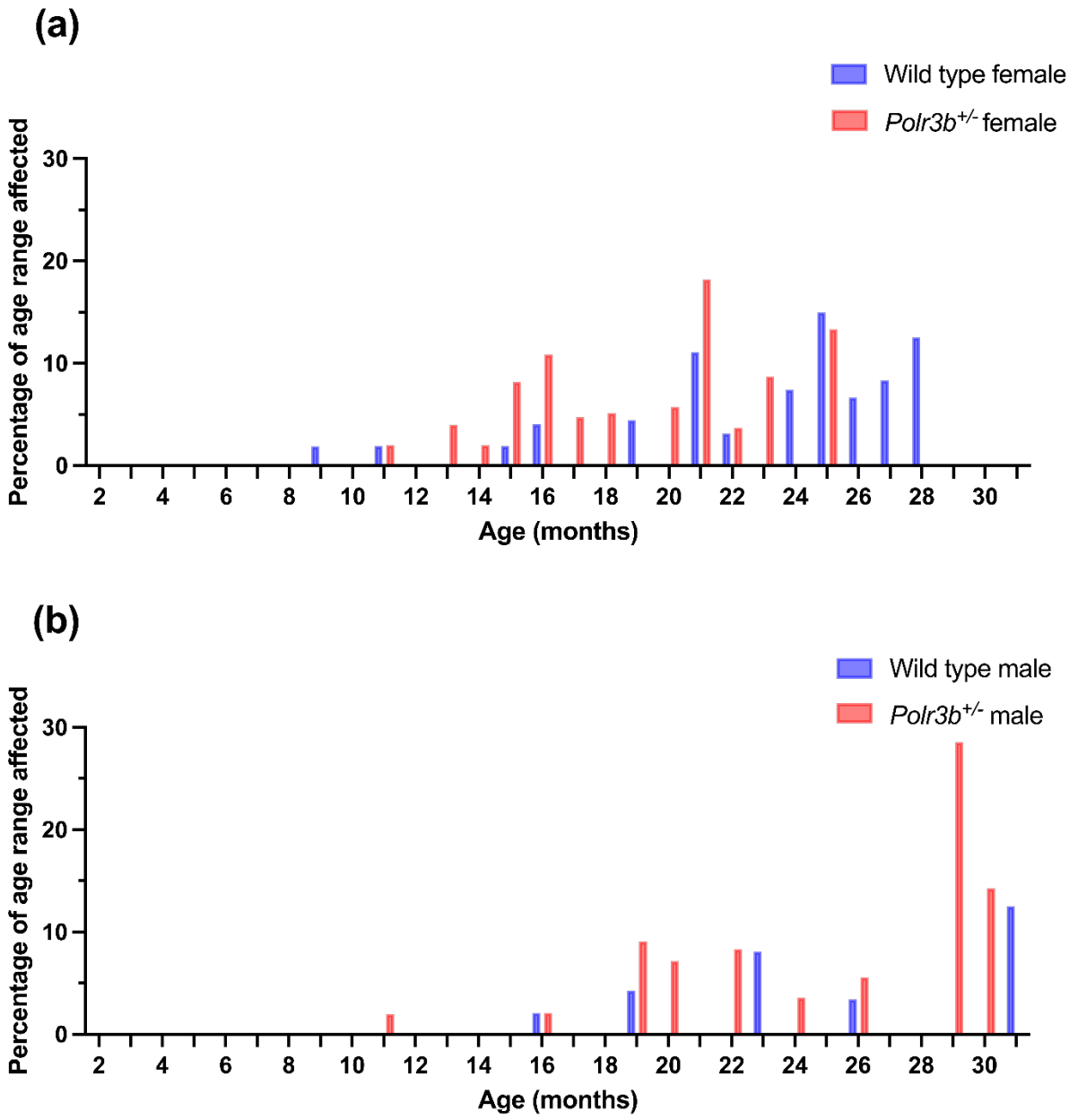

Figure 5-5 Age distribution of first clinical signs of idiopathic dermatitis in female and male WT and *Polr3b*$^{+/-}$ mice

Age in months of first clinical manifestation of idiopathic dermatitis in female (a) and male (b) mice, expressed as a percentage of the total population (per sex and genotype) for that age.

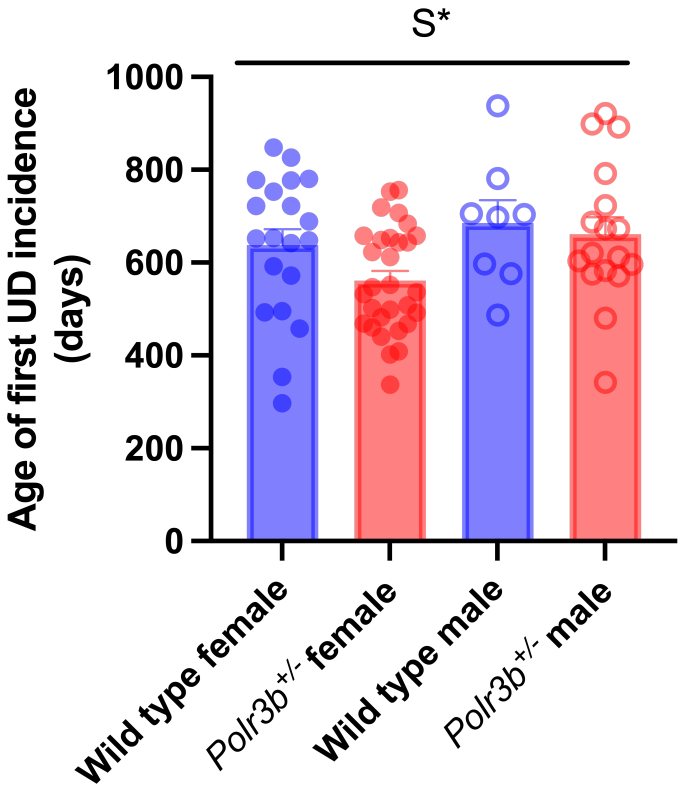

Figure 5-6 Age at first clinical presentation of idiopathic dermatitis in female and male WT and *Polr3b*$^{+/-}$ mice

Age of first clinical manifestation of idiopathic dermatitis in WT and Polr3b$^{+/-}$ *(blue and red, respectively) female and male mice. Plot denotes means ± SEM, with n=20 for WT females, n=30 for Polr3b*$^{+/-}$ *females, n=8 for WT males, and n=17 for Polr3b*$^{+/-}$ *males. A two-way ANOVA was used for sex and genotype effects (both main and interaction effects). S*=sex effect p<0.050.*

5.4.4 Monthly incidence of idiopathic dermatitis in mice

To examine whether the incidence of ID displayed seasonal variation, the date of onset of the first ID was assessed in each mouse over a 21-month period. When data from both genotypes were considered together, a mild but repeated increase in incidence was observed during spring to summer in both 2021 and 2022. This reflects a seasonal trend. In contrast, a sharply defined peak observed in November 2021. This peak was not observed in any other month within the study period and therefore appears episodic rather than seasonal, although recurrence outside the observation window cannot be excluded (**Figure 5-7 (a)**).

In male group, no recurring seasonal pattern was detected. Instead, a distinct episodic increase in incidence was observed in July-August 2022, specific to the *Polr3b*$^{+/-}$ group. Two additional, minor episodic increases were noted in autumn and winter of 2021, but these events were also not repeated within the observed timeframe. Collectively, these changes in male group are episodic fluctuations, though recurrence outside the observation window cannot be excluded (**Figure 5-7 (b)**).

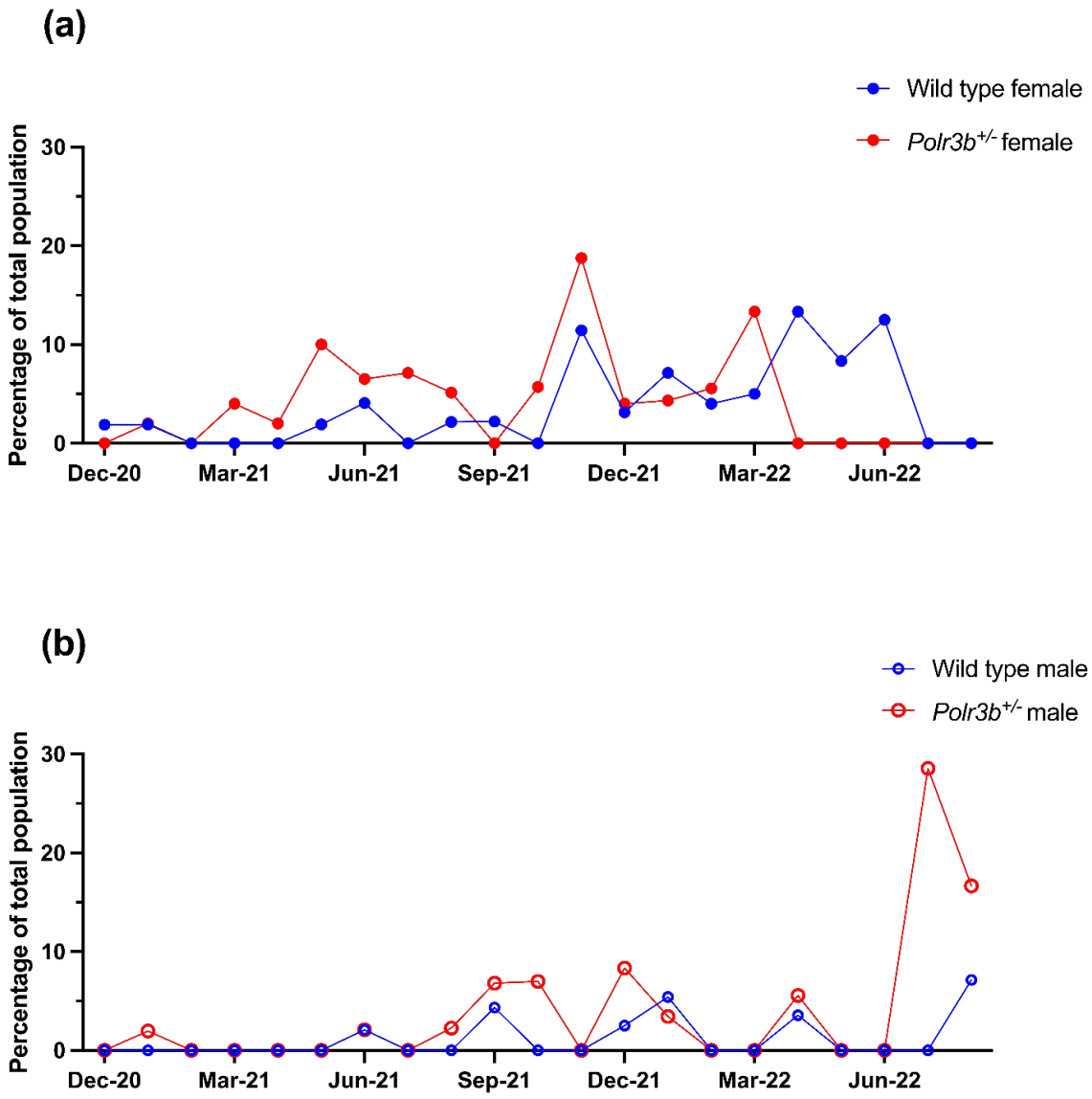

Figure 5-7 Monthly incidence rates of idiopathic dermatitis in female and male WT and *Polr3b*$^{+/-}$ mice

Monthly incidence of idiopathic dermatitis in female (a) and male (b) mice, expressed as a percentage of the total population (per sex and genotype) present during that month.

5.4.5 Splenomegaly was more prevalent in *Polr3b*$^{+/-}$ female mice with idiopathic dermatitis

To determine whether splenomegaly was more prevalent in mice with ID, Exact Binomial Tests (one-sample proportion tests) were conducted against a null expectation of 50%. A significantly greater proportion of *Polr3b*$^{+/-}$ females with ID exhibited splenomegaly compared to this expected value (*95% CI [0.651-0.956], p=0.001*). A significant result was also observed in WT females (*95% CI [0.501-0.932], p=0.049*), though the proportion was lower. The highest overall prevalence was seen in *Polr3b*$^{+/-}$ females (84.615%; **Figure 5-8(a)**), suggesting that female mice with ID are more likely to develop splenomegaly, especially in those that are *Polr3b*$^{+/-}$. In contrast, the proportion of splenomegaly did not differ significantly from 50% in either male group (*Polr3b*$^{+/-}$ males: *95% CI [0.234-0.833], p=1.000*; WT males: *95% CI [0.122-0.738], p=0.754*; **Figure 5-8(a)**).

To further evaluate the relationship between splenomegaly and disease severity, the same analysis was applied to mice euthanised due to severe ID. *Polr3b*$^{+/-}$ females again showed a significantly higher-than-expected incidence of splenomegaly relative to 50% (*95% CI [0.637-0.970], p=0.001*; **Figure 5-8 (b)**). No significant deviation from 50% was observed in the remaining groups (WT females: *p=0.146, 95% CI [0.428, 0.945]*; *Polr3b*$^{+/-}$ males: *95% CI [0.284-0.995], p=0.375;* WT males: *95% CI [0.006-0.806], p=0.625*).

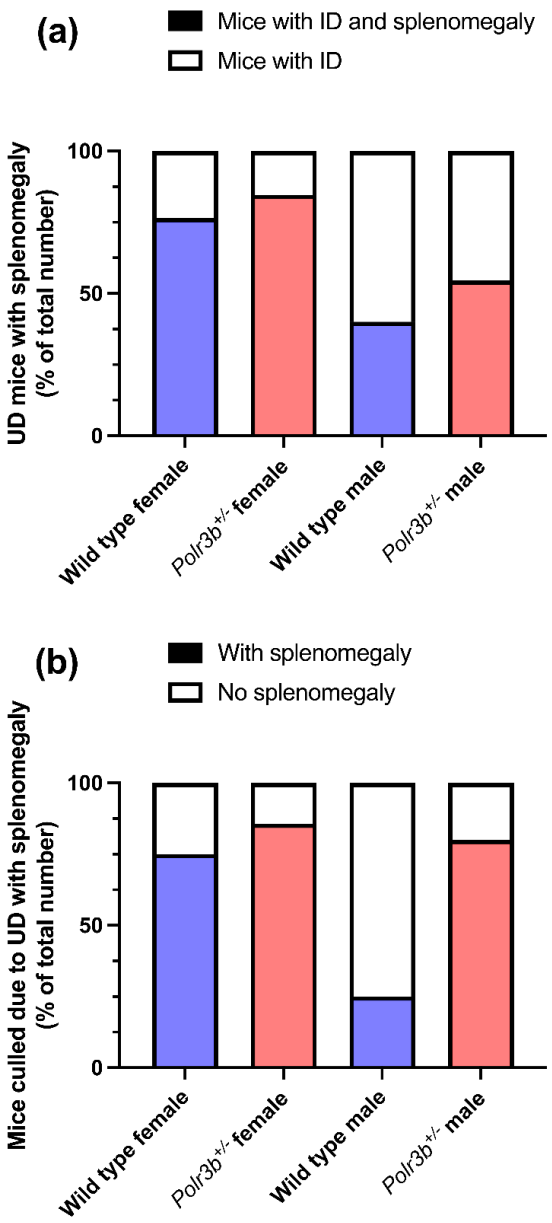

Figure 5-8 Co-occurrence of idiopathic dermatitis and splenomegaly in WT and *Polr3b*$^{+/-}$ female and male mice

Percentage of mice with idiopathic dermatitis and splenomegaly (a) and percentage of mice culled due to idiopathic dermatitis that has splenomegaly (b) in Polr3b$^{+/-}$ (blue and red, respectively) female and male mice; with n=17 for WT females, n=26 for Polr3b$^{+/-}$ females, n=10 for WT males, and n=11 for Polr3b$^{+/-}$ males in (a), and n=12 for WT females, n=21 for Polr3b$^{+/-}$ females, n=4 for WT males, and n=5 for Polr3b$^{+/-}$ males in (b). Exact binomial test was used for statistical analysis.

5.4.6 *Polr3b*$^{+/-}$ mice at 20 months exhibited elevated plasma IL-6

Plasma IL-6 levels were analysed in both 14- and 20-month-old mice across genotype and sex groups. Due to skewed distributions, IL-6 values were log-transformed prior to analysis using two-way ANOVA.

In 14-month-old mice, a significant sex effect was observed (*F=4.559, p=0.044*), with higher IL-6 levels in males compared to females (**Figure 5-9(a)**). No significant genotype effect was detected (*F=0.245, p=0.626*). In contrast, at 20-months of age, a significant genotype effect was observed (*F=6.260, p=0.0175*), with *Polr3b*$^{+/-}$ mice displaying higher plasma IL-6 levels than their WT counterparts (**Figure 5-9 (b)**). No significant difference by sex was found at this age (*F=0.001, p=0.9725*).

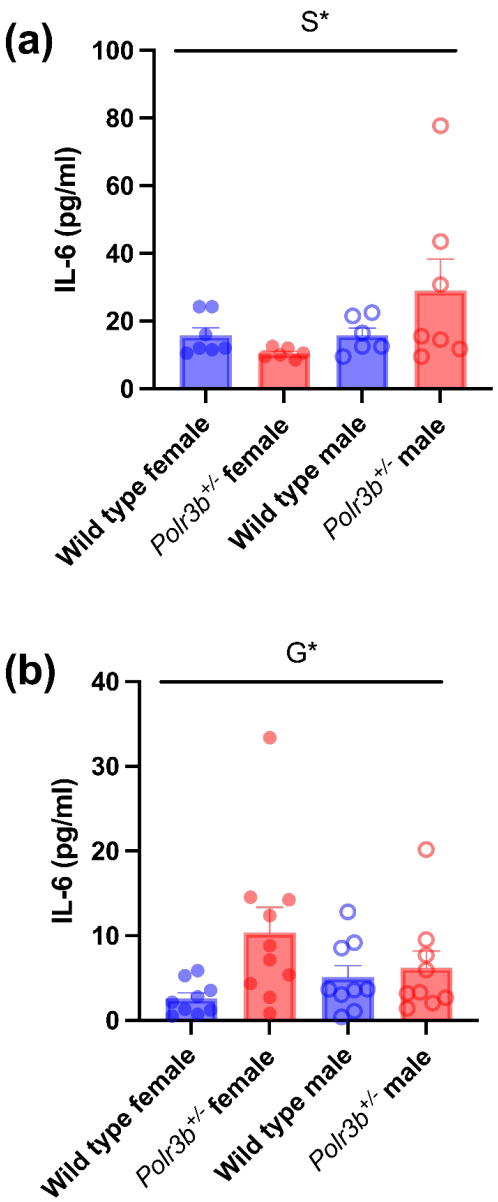

Figure 5-9 Plasma IL-6 levels in 14- and 20-month-old WT and *Polr3b*$^{+/-}$ female and male mice

Plasma IL-6 in 14-month-old (a) and 20-month-old (b) of WT and Polr3b$^{+/-}$ *(blue and red, respectively) female and male mice. Histograms denote means ± SEM, with sample sizes indicated by individual points within a group. An outlier was identified and removed from WT females, two outliers were removed from Polr3b*$^{+/-}$ *females in (a), and one outlier was removed from both the WT females and Polr3b*$^{+/-}$ *males in (b). Two-way ANOVA was used to test for sex and genotype effects (both main and interaction effects). S*=sex effect p<0.050, G*=genotypic effect p<0.050 (**Experiment was undertaken by Ms Jackie Thomson**).*

5.4.7 No effect of genotype or age on epidermal or dermal thickness in female mice at 14- and 20-months of age

Histological analysis of skin sections from 14- and 20-month-old female mice was performed to assess epidermal, dermal and adipose layer thickness. H&E staining revealed no significant effect of genotype or age on epidermal thickness (genotype *F=0.077, p=0.784*; age *F=2.955, p=0.098*) or dermal thickness (genotype *F=0.652, p=0.427*; age *F=0.061, p=0.807*) in female mice (**Figure 5-10**).

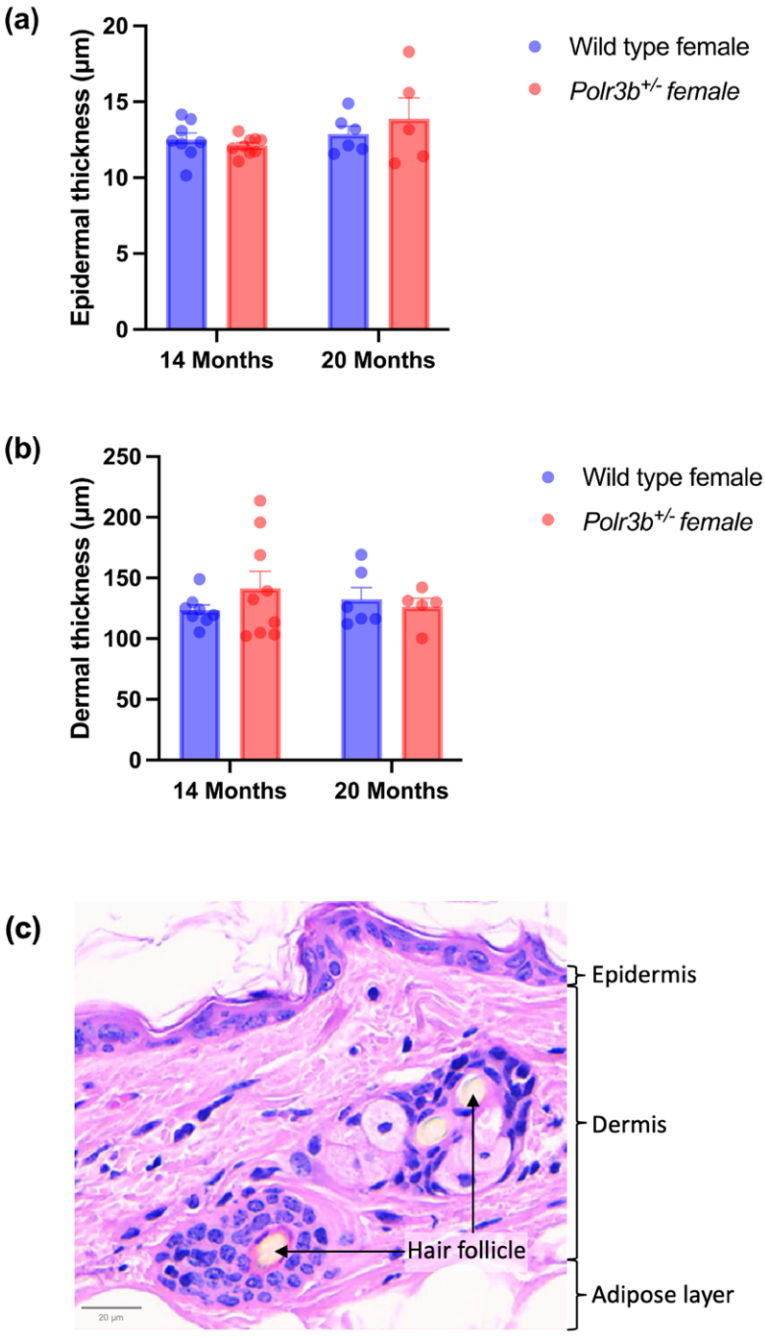

Figure 5-10 Histological analysis of epidermal and dermal thickness in WT and *Polr3b*$^{+/-}$ female mice at 14 and 20 months of age

Histology analysis of epidermal (a) and dermal (b) thickness in 14-month-old and 20-month-old WT and Polr3b$^{+/-}$ *(blue and red, respectively) female mice. Histograms denote means ± SEM, with sample sizes indicated by individual points within a group. Two-way ANOVAs were used to test for age and genotype effects (both main and interaction effects). Representative H&E staining image illustrating the epidermis, dermis, hair follicle, and adipose layer in the skin section of the female mice (c). Scale bar: 20 µm.*

5.4.8 20-month-old female mice had more adipocytes in the skin than the 14-month-old female mice

The skin adipose layer in 14- and 20-month-old female mice was also examined. No differences in adipose layer thickness were found between genotype at either age (*F=1.371, p=0.253*), nor was there an effect of age (*F=0.544, p=0.467*; **Figure 5-11 (a)**). These findings indicate that the higher incidence and more severe ID observed in the female *Polr3b*$^{+/-}$ mice does not appear to be linked to the adipose layer thickness.

Cell counts in the adipose layer were also assessed. Similar to adipose thickness, no genotypic differences were found at either age (*F=1.401, p=0.248*), and no interaction effect between genotype and age was observed for adipocyte number (*F=0.531, p=0.473*). However, an age difference was observed, with older female mice having smaller adipocytes per field of view compared to the younger group (*F=12.597, p=0.002*; **Figure 5-11 (b)** and **(d)**).

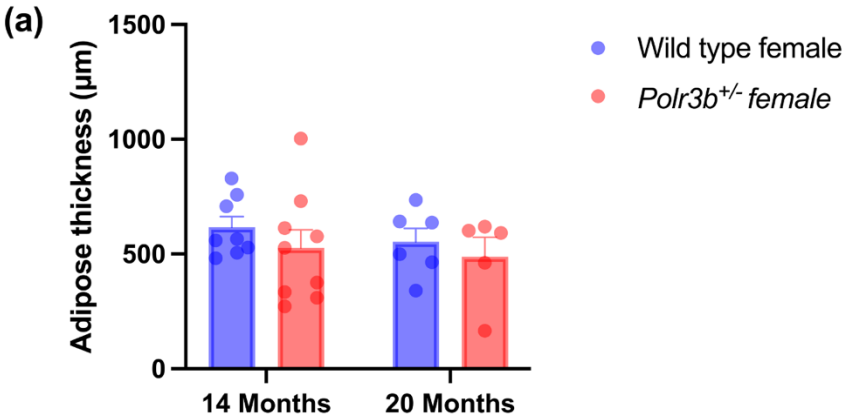
(a)
Adipose thickness (µm)
1500
1000
500
0
14 Months
20 Months
Wild type female
Polr3b+/- female

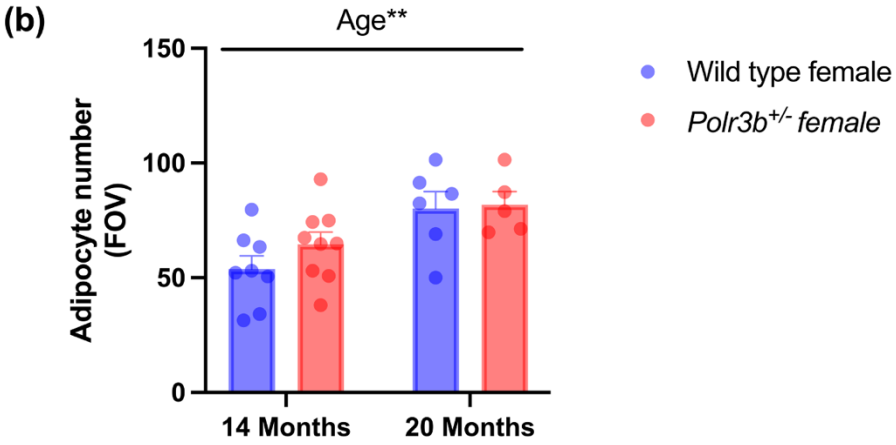
(b)
Age**
Adipocyte number (FOV)
150
100
50
0
14 Months
20 Months
Wild type female
Polr3b+/- female

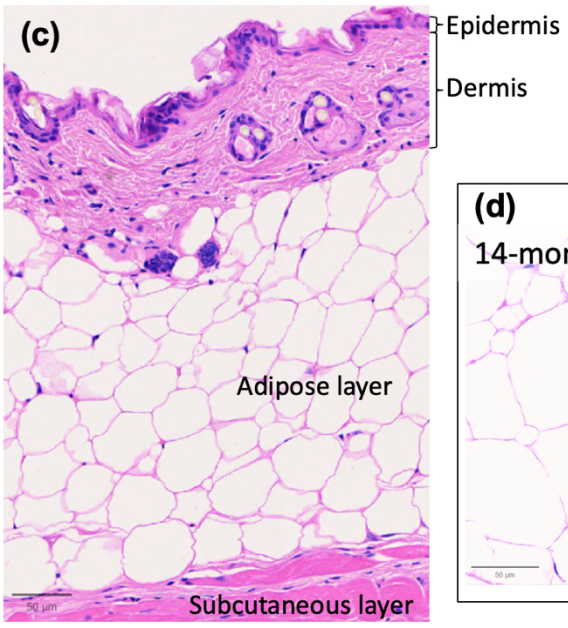
(c)
Epidermis
Dermis
Adipose layer
Subcutaneous layer

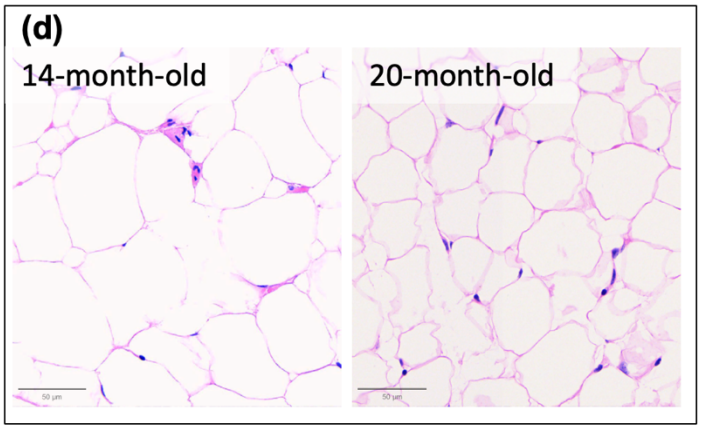
(d)
14-month-old
20-month-old

Figure 5-11 Histological assessment of adipose layer thickness and adipocyte counts in WT and *Polr3b*$^{+/-}$ female mice at 14 and 20 months of age

Histology analysis of adipose layer (a) and adipose counts (b) in the 14-month-old and 20-month-old WT and Polr3b$^{+/-}$ *(blue and red, respectively) female mice. Histograms denoted means ± SEM, with sample sizes indicate by individual points within a group. Two-way ANOVAs were used to test for age and genotype effects (both main and interaction effects). Representative H&E staining images illustrating the epidermis and dermis, adipose layer, and subcutaneous layer in the skin section of the female mice (c), as well as the adipocytes in the 14-month-old and 20-month-old WT female mice (d). Scale bar: 50 μm. Age**=age effect p<0.010.*

5.4.9 No genotypic differences in mast cell count in female mice

In murine skin, mast cells are primarily located near the junction of the dermis and the adipose layer (subcutaneous junction). To further investigate the incidence of ID in *Polr3b*$^{+/-}$ female mice, skin sections from both *Polr3b*$^{+/-}$ and WT female mice, at 14- and 20- months of age were stained with toluidine blue. The total number of mast cells per field of view was then counted. **Figure 5-12** shows that there were no significant effects of genotype or age on the number of mast cells found in the dermis (genotype *F=0.001, p=0.998; age F=0.001, p=0.977*) or adipose layer (genotype *F=0.981, p=0.332; age F=0.003, p=0.960*). Suggesting that the higher incidence and more severe ID observed in *Polr3b*$^{+/-}$ female mice was not associated in this study with differences in the total number of mast cells.

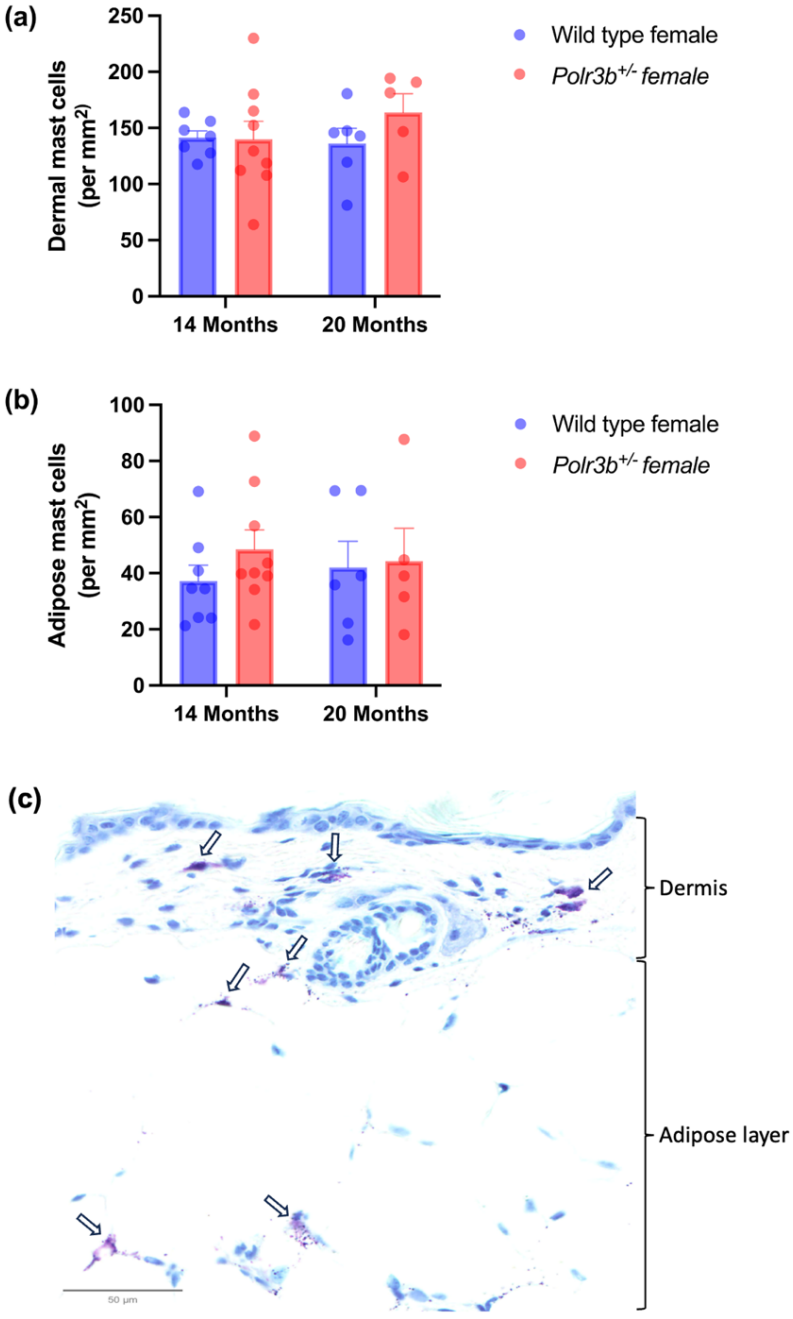

Figure 5-12 Quantification of dermal and adipose tissue mast cells in WT and *Polr3b*$^{+/-}$ female mice at 14 and 20 months of age

Histopathology analysis of the mast cell counts of the 14-month-old and 20-month-old WT and Polr3b$^{+/-}$ *(blue and red, respectively) mice in dermis (a) and adipose layer (b). Histograms present means ± SEM, with sample sizes indicate by individual points within a group. One outlier was identified and removed from WT female in (a). Two-way ANOVAs were used to test for age and genotype effects (both main and interaction effects). Representative Toluidine blue staining image illustrating the mast cells (denoted by arrows) in the dermis and adipose layer (c) in the skin section of the female mice. Scale bar: 50 µm.*

5.4.10 Dermal mast cell degranulation was reduced in *Polr3b*$^{+/-}$ females

Mast cell degranulation was quantified in skin sections from 14- and 20-month-old female mice using Toluidine blue staining. This method allows visualisation of residual granules following degranulation (**Figure 5-13 (c)**).

In the dermis, a significant main effect of genotype was detected (*F=10.744, p=0.003*), with *Polr3b*$^{+/-}$ female mice exhibiting a lower percentage of degranulated mast cells compared to WT controls at both ages (**Figure 5-13 (a)**). No significant effect of age (*F=1.804, p=0.191*) or genotype x age interaction (*F=0.791, p=0.383*) was observed. These findings suggest reduced dermal mast cell activation in *Polr3b*$^{+/-}$ females.

In contrast, far fewer mast cells were present in the adipose layer (**Figure 5-12**), with no genotypic nor age effects detected on the percentage of degranulated mast cells (genotype *F=1.447, p=0.240*; age *F=0.801, p=0.379*) (**Figure 5-13 (b)**).

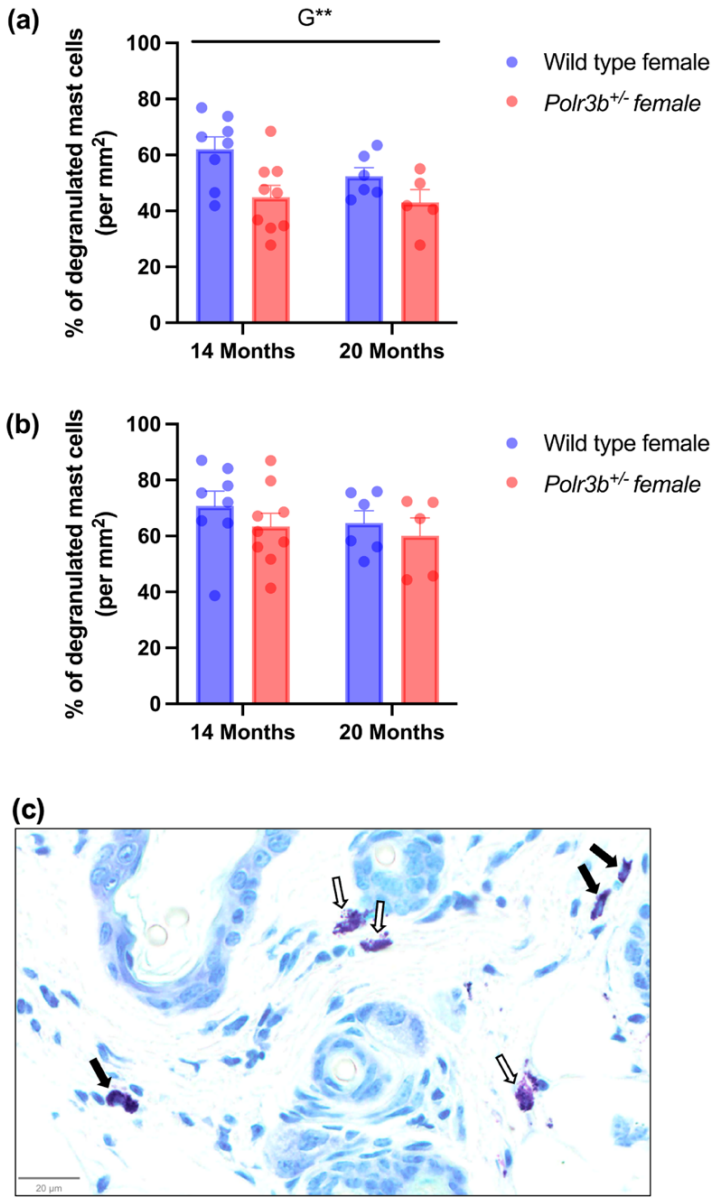

Figure 5-13 Proportion of degranulated mast cells in dermal and adipose tissue of WT and *Polr3b*$^{+/-}$ female at 14 and 20 months of age

*Histopathology analysis of the ratio of the skin degranulated mast cells, expressed as a percentage of the total mast cells of the 14-month-old and 20-month-old WT and Polr3b$^{+/-}$ (blue and red, respectively) female mice in the dermis (a) and adipose layer (b). Histograms present means ± SEM, with sample sizes indicate by individual points within a group. Two-way ANOVAs were used to test for age and genotype effects (both main and interaction effects). Representative Toluidine blue staining image illustrating the degranulated (white arrows) and intact (black arrows) mast cells in the dermis area of the skin section of the female mice (c). Scale bar: 20µm. G**=genotypic effect p<0.010.*

5.4.11 No difference in the wound-healing rates in dermal fibroblasts derived from 5-month-old *Polr3b*$^{+/-}$ and WT female mice

Scratch wound assay was performed to compare the wound-healing rate of the fibroblasts derived from female *Polr3b*$^{+/-}$ and WT mice. The analysis revealed no significant genotypic differences (*F=17.84, p=0.634*) (**Figure 5-14**).

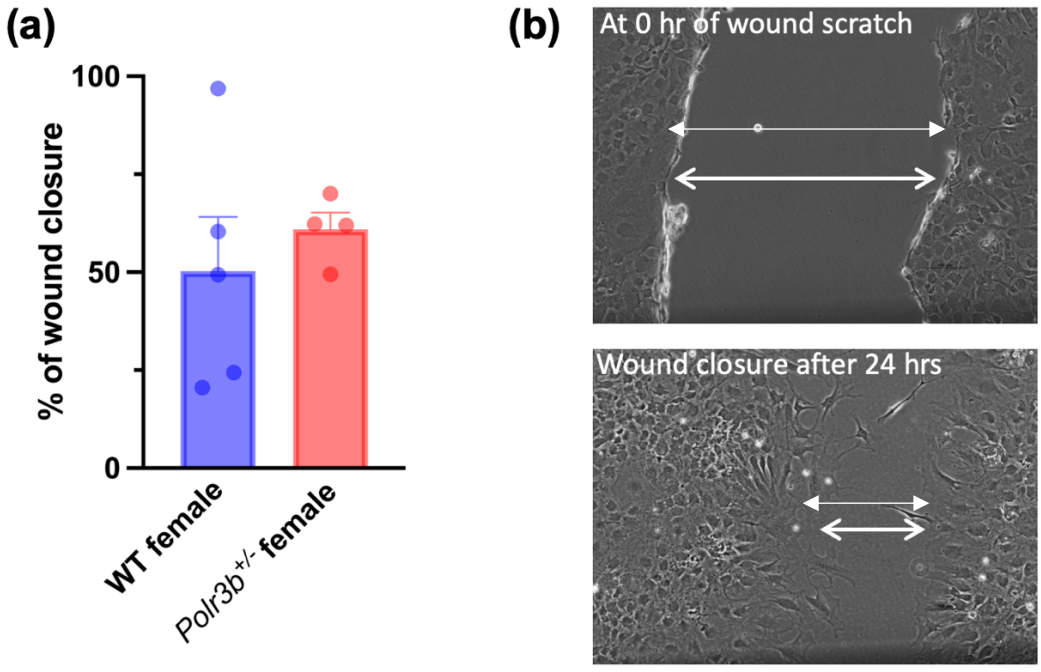

Figure 5-14 Wound healing capacity of dermal fibroblasts isolated from WT and *Polr3b*$^{+/-}$ female mice

*The wound healing rate of female isolated dermal fibroblasts, expressed as the percentage of the area covered by cells that have migrated 24 hours post-wounding (a). Histograms denote mean ± SEM, with sample sizes indicated by individual points within a group. A two-tailed Welch's t-test was used to test for genotype difference. Representative images (b) illustrate the experiment (**experiment was undertaken by Ms Jackie Thomson**), and the gap defines the areas lacking cells (wound area, ImageJ). Arrows indicate the width of the wound gap.*

5.4.12 No genotypic difference in the cell index was observed during wound healing in female fibroblasts

Real-time cell analysis (RTCA) was used to further assess fibroblast behaviour during wound healing. The cell index is a composite parameter derived from impedance-based sensing, reflecting dynamic changes in cell adhesion, proliferation, and morphology in real time (Wang et al., 2023). A higher cell index indicated more proliferative or migratory cells.

Dermal fibroblasts isolated from female *Polr3b*$^{+/-}$ and WT mice were assessed using the xCELLigence RTCA system. No significant difference in cell index was observed between the two genotypes (*t=1.210, p=0.254*), indicating no differences in cell behaviour during the wound healing assay (**Figure 5-15**).

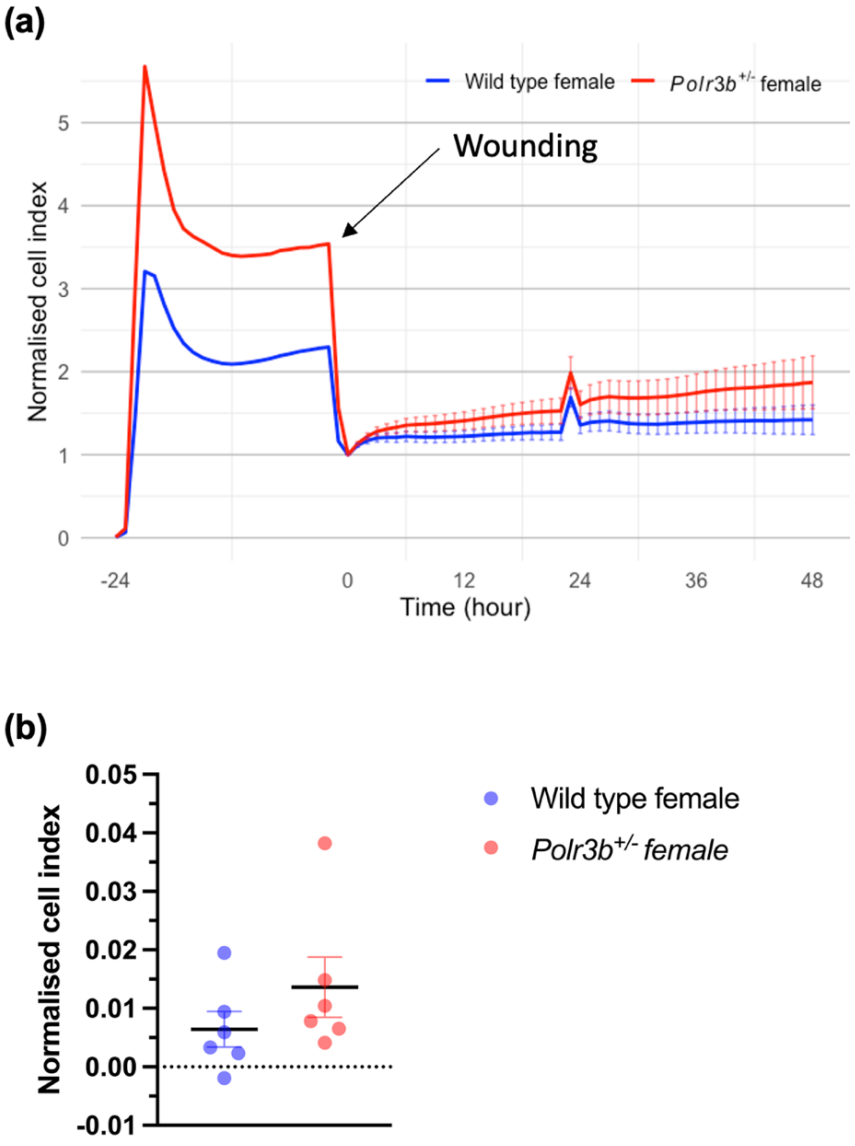

Figure 5-15 Real-time cell analysis of wound healing in dermal fibroblasts from 5-month-old WT and *Polr3b*$^{+/-}$ female mice

Real-time cell analysis (RTCA) assay of a wound healing assay on 5-month-old WT and Polr3b$^{+/-}$ *female fibroblasts (**experiment was undertaken by Dr Gillian Borland and Ms Jackie Thomson**), expressed as the normalised cell index, which starts from 0 at the time the fibroblast monolayer was scratched to 48 hr post-scratching. Both graphs present mean ± SEM (n=6). Graph (a) showed the slope of the normalised cell index for both female WT and Polr3b*$^{+/-}$ *fibroblasts over the period from 24hr before the scratch to 48hr after the scratch. Graph (b) shows the plot with sample sizes indicated by individual points within a group. A two-tailed unpaired t-test was used to test for genotype difference.*

5.4.13 Greater dermal collagen content in *Polr3b*$^{+/-}$ female mice

Dermal collagen content was quantified using Masson's trichrome staining in skin sections from 14- and 2-month-old female mice. Across both age groups, *Polr3b*$^{+/-}$ females exhibited significantly higher dermal collagen content compared to WT controls (genotype *F=16.179, p=0.001; age F=2.240, p=0.148; genotype*age interaction F=0.399, p=0.534*) (**Figure 5-16(a)**). Collagen content was expressed as the percentage of dermal area occupied by collagen relative to total dermal tissue area, as segmented in **Figure 5-16(b-c)**. Specifically, collagen occupied 56% of dermal area in 14-month-old *Polr3b*$^{+/-}$ mice, compared to 42% in age-matched WT female mice; at 20 months, collagen content was 47% in *Polr3b*$^{+/-}$ mice and 39% in WT females.

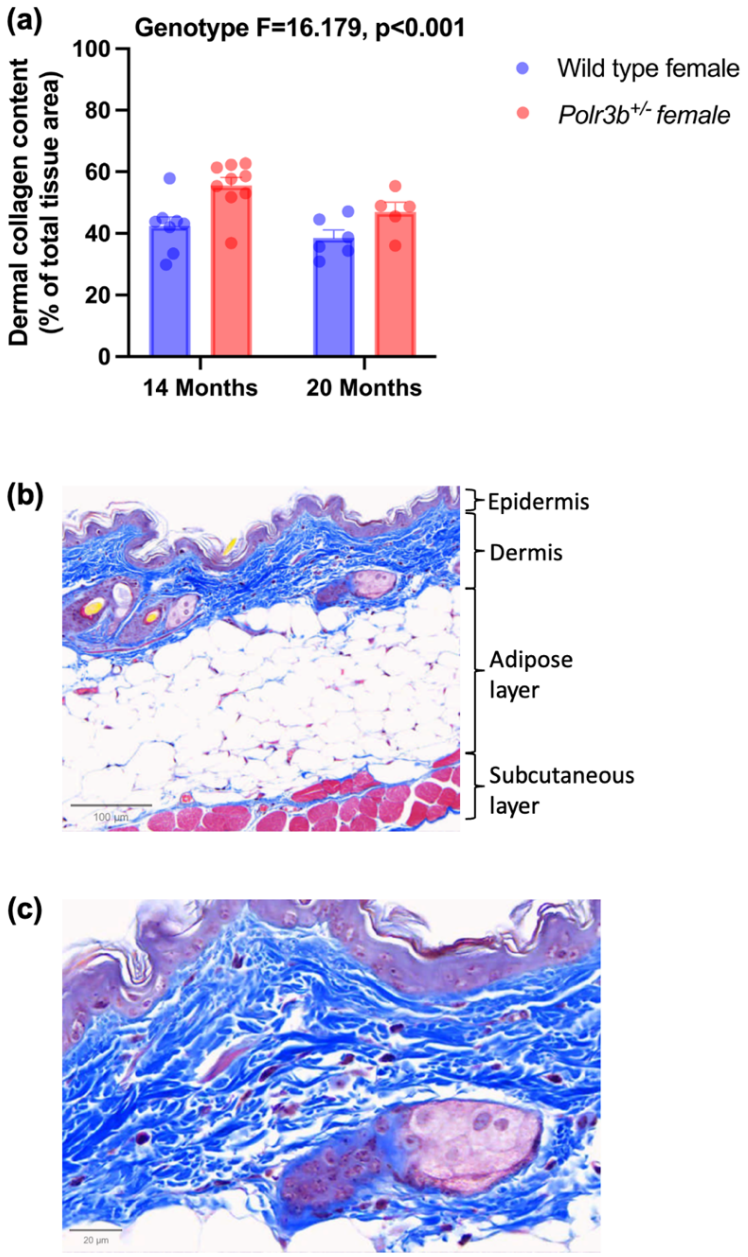

Figure 5-16 Dermal collagen content in WT and *Polr3b*$^{+/-}$ female mice at 14 and 20 months of age

Histopathology analysis of the dermal collagen content, expressed as the percentage of total dermal tissue area, in the 14- and 20-month-old WT and Polr3b$^{+/-}$ (blue and red, respectively) female mice (a). Histograms present means ± SEM, with sample sizes indicate by individual points within a group. A two-way ANOVA was used to test for age and genotype effects (both main and interaction effects). Representative Masson's trichrome staining images illustrate the location of collagen is in the dermis (b), and the areas with blue are the collagen fibres (c). Scale bar of (b): 100 µm; Scale bar of (c): 20 µm.

5.4.14 No genotype differences in expression of *Col1a1*, *Col3a1*, and *Col1a1/Col3a1* ratio in skin of 14-month-old female mice

To examine whether expression levels of *Col1a1* (which encodes the major component of type I collagen) and *Col3a1* (encodes the major component of type III collagen) were altered in the skin of *Polr3b*$^{+/-}$ relative to WT mice, levels were assessed by RT-PCR. Expression of *Col1a1* and *Col3a1* did not differ significantly in the skin of *Polr3b*$^{+/-}$ and WT females at 14 months of age (*Col1a1 t=0.840, p=0.417; Col1a1 t=1.151, p=0.272*) (**Figure 5-17 (a-b)**). Furthermore, no difference was observed in the ratio of *Cola1a/Col3a1* between the *Polr3b*$^{+/-}$ and WT at 14 months (*F=0.377, p=0.713*).

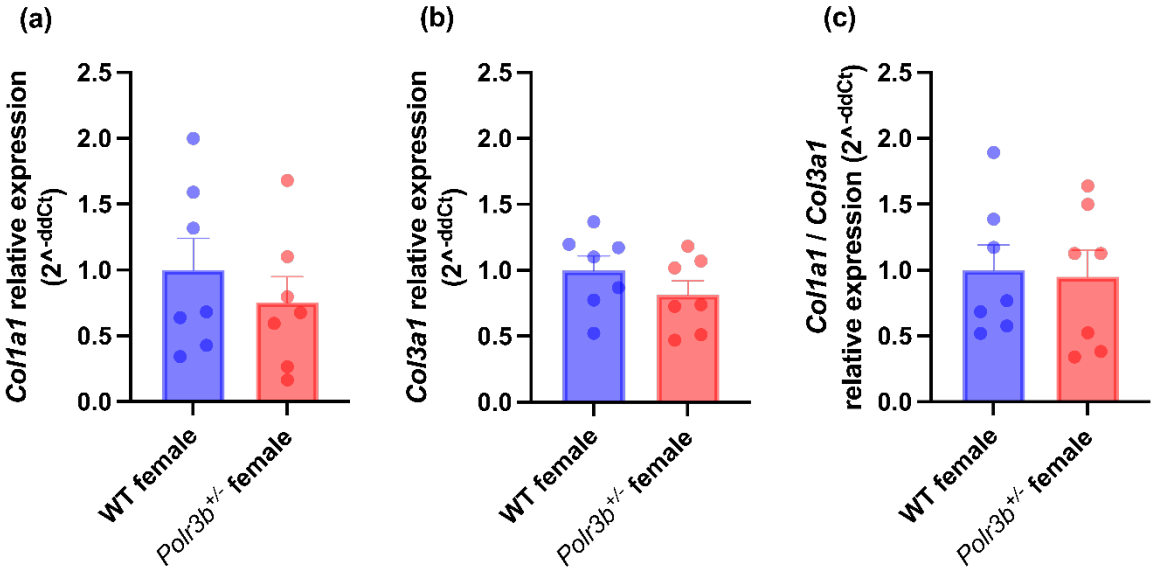

Figure 5-17 Expression of collagen-related genes *Col1a1* and *Col3a1* in the skin of 14-month-old WT and *Polr3b*$^{+/-}$ female mice

Skin collagen coding genes Col1a1 (a), Col3a1 (b), and Col1a1/Col3a1 (c) mRNA expression in 14-month-old WT and Polr3b$^{+/-}$ *(blue and red, respectively) female mice. Histograms present mean ± SEM, with sample sizes indicated by individual points within a group. Unpaired t-tests were used to test for genotype differences. All comparisons non-significant.*

5.4.15 No genotype differences in the expression of *Il6*, *Tnfα*, *Il1α*, *Il1β*, and *Malt1* in skin of 14-month-old female mice

Expression of *Il6*, *Tnfα*, *Il1α*, *Il1β* and *Malt1* was assessed in skin from female *Polr3b*$^{+/-}$ and WT mice. The expression of *Il-6 (t=0.573, p=0.579); Tnfα (t=0.406, p=0.691); Il1α (t=0.308, p=0.764); Il1β (t=0.393, p=0.701*) and *Malt1 (t=2.295, p=0.053)* were unaffected by genotype (**Figure 5-18**).

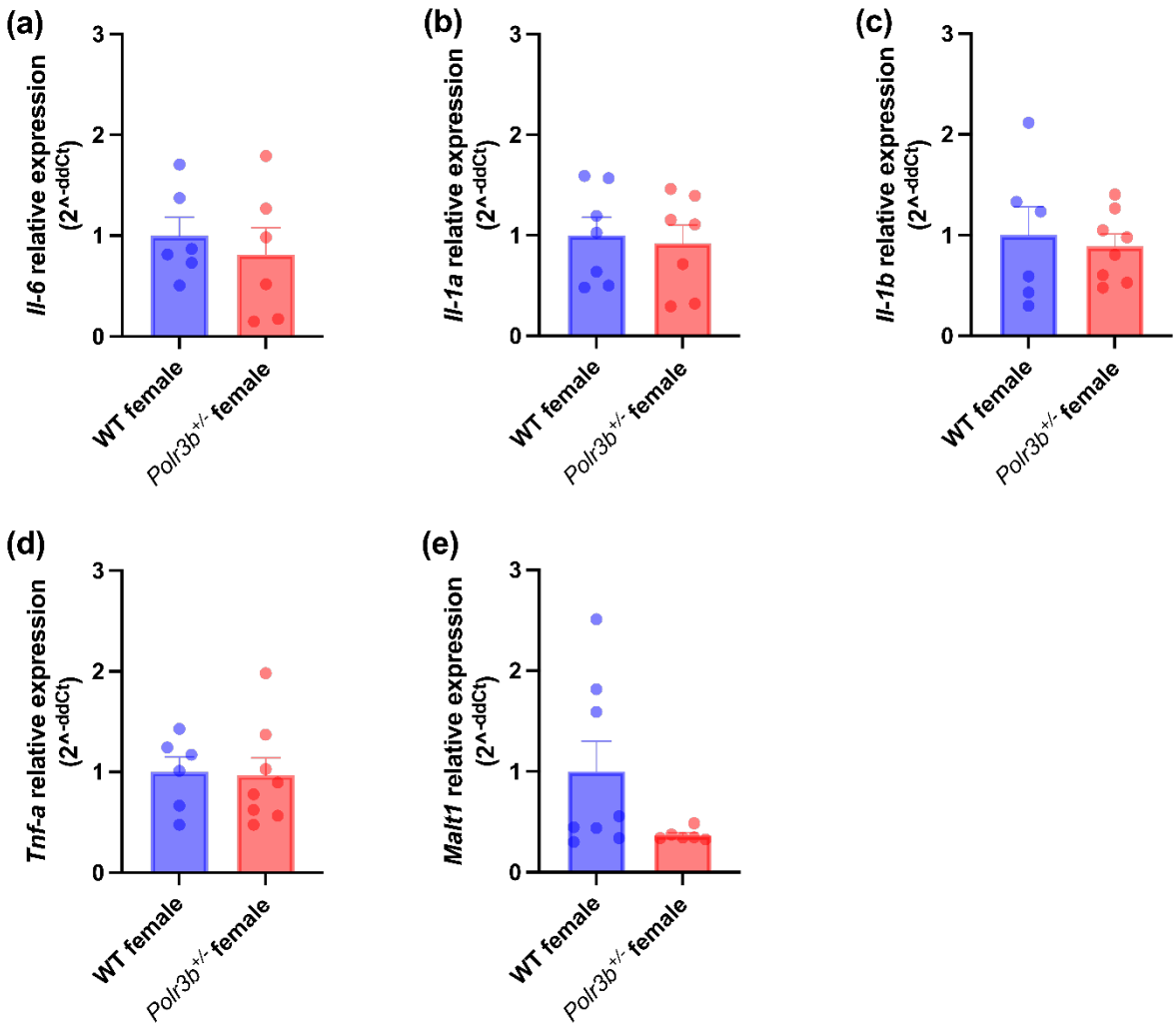

Figure 5-18 Inflammatory cytokine and *Malt1* gene expression in the skin of 14-month-old WT and *Polr3b*$^{+/-}$ female mice

Il6, Tnfα, Il1α, Il1B and Malt1 mRNA expression in the skin of 14-month-old female mice. Histograms present mean ± SEM, with sample sizes indicated by individual points within a group. Outliers were identified and two were each removed from WT and Polr3b$^{+/-}$ female groups in (a), WT females in (c), and Polr3b$^{+/-}$ females in (e). Unpaired t-tests were used to test for genotype differences.

5.4.16 No genotypic differences in the expression of *Il17α*, *Il22*, and *Il23α* in the skin of 14-month-old female mice

IL-17α, IL-22, and IL-23α are T-helper 17-related cytokines. **Figure 5-19** revealed no genotypic differences in the mRNA expression of *Il17α* (*t=0.120, p=0.906*), *Il22* (*t=0.554, p=0.591*), and *Il23α* (*t=0.816, p=0.429*) in the skin of 14-month-old female mice.

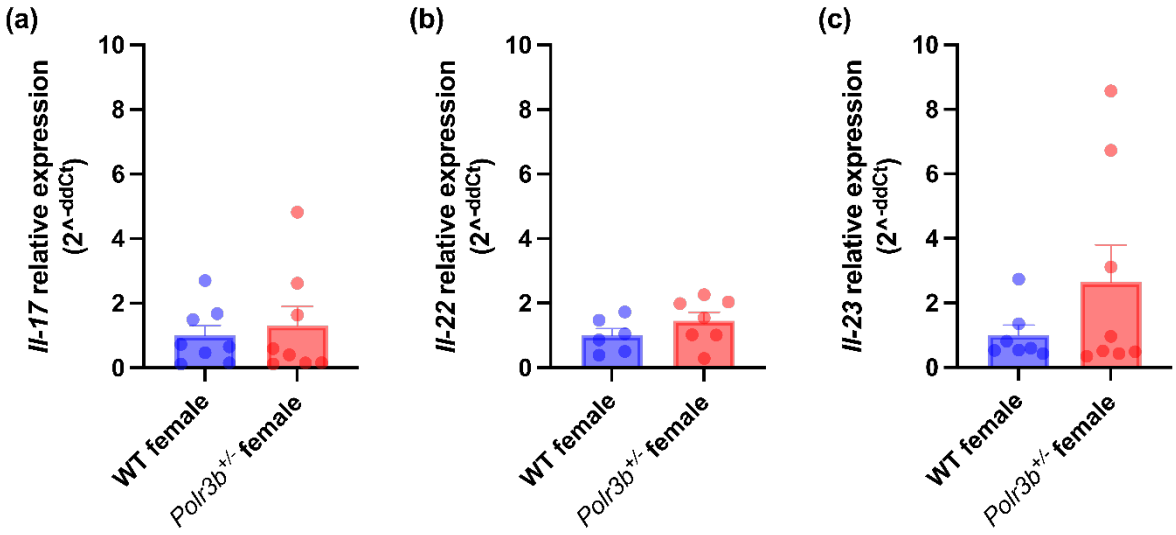

Figure 5-19 Expression of Th17-related genes *Il17α*, *Il-22*, and *Il23α* in the skin of 14-month-old WT and *Polr3b*$^{+/-}$ female mice

Il17α, Il22, and Il23α mRNA expression in skin of 14-month-old female mice. Histograms present mean ± SEM, with sample sizes indicated by individual points within a group. Outliers were identified, and one was each removed from WT female in (b) and (c). Unpaired t-tests were used to test for genotype differences.

5.4.17 *Ccl20* and *Cxcl15* expression was significantly upregulated in skin of 14-month-old *Polr3b*$^{+/-}$ females

CCL20 and CXCL15, were also examined as they facilitate the recruitment of immune cells including Th17 cells and are expressed in keratinocytes, respectively, so crucial to cutaneous health. **Figure 5-20** revealed increased *Ccl20* and *Cxcl15* mRNA expression in skin of *Polr3b*$^{+/-}$ females (*Ccl20 t=3.024, p=0.012; Cxcl15 t=2.477, p=0.033*).

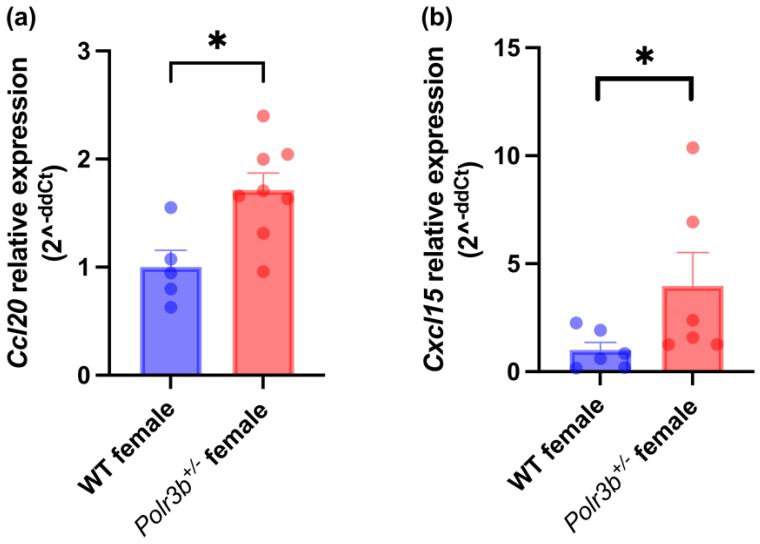

Figure 5-20 Expression of chemokine genes Ccl20 and Cxcl15 in the skin of 14-month-old WT and *Polr3b*$^{+/-}$ female mice

*Ccl20 and Cxcl15 mRNA expression in 14-month-old female mice. Histograms present mean ± SEM, with sample sizes indicated by individual points within a group. Outliers were identified, three were removed from WT female in (a) and one was removed from WT female in (b). Unpaired t-tests were used to test for genotype differences. *=p<0.050.*

5.4.18 No genotype differences in *Cramp* or *Il15* expression in isolated dermal fibroblasts from 5-month-old female mice

Cramp and *Il15* were also examined as they are crucial to skin barrier defence and immune cell recruitment, respectively. No genotypic differences were observed in *Cramp* and *Il15* mRNA expression (*Cramp t=0.832, p=0.438; Il15 t=0.405, p=0.698*) (**Figure 5-21**).

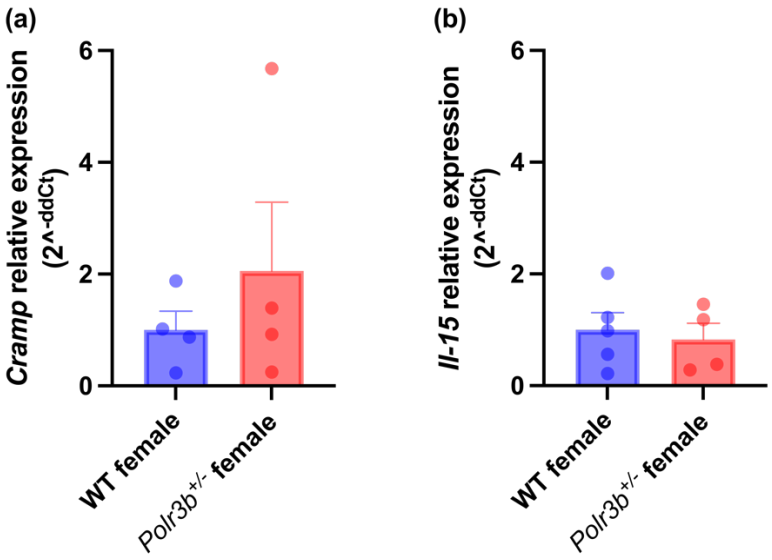

Figure 5-21 Expression of *Cramp* and *Il15* in dermal fibroblasts from 5-month-old WT and *Polr3b*$^{+/-}$ female mice

Cramp and Il15 mRNA expression in 5-month-old female fibroblasts. Histograms present mean ± SEM, with sample sizes indicated by individual points within a group. One outlier was identified and removed from the WT female in (a). Unpaired t-tests were used to test for genotype differences. All comparisons are non-significant.

5.5 DISCUSSION

Murine ID occurs spontaneously and sporadically in C57BL/6, including in the substrain C57BL/6N mice (Sargent et al., 2015). While its exact cause remains unclear, multiple contributing factors have been reported, including sex, season, ageing, follicular dysplasia, high-fat diet, bacteriological factors, and inflammation (Andrews et al., 1994; De Biase et al., 2019; Duarte-Vogel & Lawson, 2011; Hampton et al., 2015; Hampton et al., 2012; Kastenmayer et al., 2006; Krugner-Higby et al., 2012; Lawson et al., 2005; Neuhaus et al., 2012; Sargent et al., 2015; Sundberg et al., 1994; Sundberg et al., 2011; Williams-Fritze et al., 2011; Won et al., 2002; Zhang et al., 2015). RNA Pol III, a conserved enzyme in eukaryotic cells, is essential for various cellular processes and with its downregulation extending longevity from yeast to flies (Filer et al., 2017; Kulaberoglu et al., 2021). In contrast, our previous findings in *Polr3b*$^{+/-}$ mice revealed no lifespan extension (Borland et al., 2024). Instead, we observed a marked increase in ID incidence in *Polr3b*$^{+/-}$ female mice. This raises two key questions: why are females more affected, and how might reduced Pol III activity contribute to this susceptibility?

In this study, female mice not only showed a higher prevalence of ID but also developed lesions earlier than males, consistent with previous reports in C57BL/6 mice (Kastenmayer et al., 2006; Sargent et al., 2015). Additionally, splenomegaly was more frequent in *Polr3b*$^{+/-}$ mice, and this condition has been linked to systemic immune activation in ID-affected animals (De Biase et al., 2019; Hampton et al., 2015; Kastenmayer et al., 2006; Lawson et al., 2005). Histological and immunological analyses from earlier studies support the view that splenomegaly in ID reflects a systemic inflammatory response primarily mediated by the innate immune system (Hampton et al., 2015). Given that Pol III can activate innate immune pathways by transcribing cytosolic DNA or non-coding RNAs that stimulate RIG-I and NF-κB signalling, this suggests that *Polr3b*$^{+/-}$ mice may exist in a higher pro-inflammatory state, potentially predisposing them to ID (Ablasser et al., 2009; Chiu et al., 2009; Naesens et al., 2023). Although splenomegaly was assessed macroscopically in the current study, additional haematological analyses, including peripheral blood cell counts or flow cytometric immune profiling, were not performed. As this study was retrospective in design and primarily focused on skin-associated phenotypes

during ageing, blood collection suitable for comprehensive immunophenotyping was not consistently available across all animals. Previous studies of murine ID have reported splenomegaly alongside altered immune cell populations, including increased granulocytes, reduced splenic B-cell populations, and evidence of extramedullary haematopoiesis in affected mice (Hampton et al., 2015). Therefore, future studies incorporating haematological and immunophenotyping approaches would be valuable to determine whether the increased splenomegaly observed in *Polr3b*$^{+/-}$ female mice is accompanied by comparable systemic immune alterations.

When analysing the seasonal pattern of ID, ID incidence increased consistently in female mice during spring and summer, aligning with earlier findings (De Biase et al., 2019; Kastenmayer et al., 2006). In contrast, males displayed only episodic increases, which may be due to their later onset and lower overall incidence of ID within the same observational window. Although environmental conditions such as temperature and humidity were largely regulated, prior studies have documented subtle seasonal humidity shifts, with highest humidity found in the mid-summer in animal unit environment, which could contribute to seasonal susceptibility of ID in mice (Kastenmayer et al., 2006). In addition to seasonal environmental variation, alterations in skin microbial communities may also influence susceptibility to ID. Previous studies have isolated bacterial species *Staphylococcus xylosus* from ID lesions, suggesting that disruption of normal skin barrier integrity may permit bacterial overgrowth and amplification of local inflammation (Kastenmayer et al., 2006; Won et al., 2002). Since microbiome composition was not examined in the current study, it remains possible that host-microbe interactions may contribute to the increased susceptibility observed in *Polr3b*$^{+/-}$ female mice.

Given the established role of inflammation in ID pathogenesis, this study measured IL-6 levels to assess systemic and local inflammatory responses (Andrews et al., 1994; De Biase et al., 2019; Duarte-Vogel & Lawson, 2011; Williams-Fritze et al., 2011). Plasma IL-6 was elevated in *Polr3b*$^{+/-}$ mice at 20 months, indicating a chronic inflammatory environment. This systemic upregulation of IL-6 may exacerbate ID risk, as IL-6 contributes to both acute and chronic inflammation (Gabay, 2006; B. Gong et al., 2022). In contrast, *Il6* mRNA levels in the skin remained unchanged, likely because samples were

collected from asymptomatic mice without active lesions, unlike previous studies using ID-affected skin (De Biase et al., 2019). It is also worth noting that Pol III, when transcribed some non-coding host-derived RNAs, can activate RIG-I-dependent inflammation to regulate IFN-I/III and cytokine production (Choi et al., 2020; Naesens et al., 2023; Y. Zhang et al., 2022; Zhao et al., 2018). Dysregulation of the Pol III-RIG-I sensing axis with uncontrolled production of IFN-I and other cytokines (such as TNF-α and IL-6) has been associated with several inflammatory conditions (Naesens et al., 2023). Higher systemic IL-6 in the *Polr3b*$^{+/-}$ mice may, therefore, also be the result of the homeostatic imbalance of the Pol III-RIG-I sensing axis due to the dysregulation of Pol III signalling. In addition, INF-I has also been shown to be triggered by several bacteria, including *Streptococcus*, which had previously been isolated from the ID lesions (Adams et al., 2016). A potential explanation is that the impaired Pol III-RIG-I sensing axis may reduce the transcription of INF-I and lead to the failure to eliminate bacteria in the skin, ultimately leading to the development of ID.

Histological examination of dermal thickness and architecture revealed no major genotypic differences in skin structure among asymptomatic mice, which is consistent with the absence of active or prior ID (Andrews et al., 1994; De Biase et al., 2019; Sargent et al., 2015). Moreover, older mice exhibited smaller dermal adipocytes, despite unchanged adipose layer thickness, which may reflect a shift toward more insulin-sensitive adipocytes that produce higher levels of insulin-sensitising adipocytokines (Medina-Gomez et al., 2007). Smaller adipocytes may also reflect enhanced lipolytic activity, reduced uptake or circulating lipids, or reduced synthesis of triglyceride, as smaller adipocytes have been shown to differ in lipid turnover dynamics and respond more effectively to antilipolytic signalling, which may suggest impaired lipid storage and possible thermoregulatory deficits (Fang et al., 2015; McLaughlin et al., 2014; McLaughlin et al., 2007; Müller et al., 2011). The smaller subcutaneous adipocytes found in the aged mice of the current report may also suggest cell necrosis and impaired lipid depots, which may lead to lipid dysfunction as well as impaired thermoregulation of the skin for the aged mice (Stenkula & Erlanson-Albertsson, 2018; Yanina et al., 2012). Further experiments are needed to determine the exact mechanism causing the smaller adipocyte in older mice.

Despite previous reports of increased mast cell density and degranulation at ID sites, reduced mast cell degranulation was observed in *Polr3b*$^{+/-}$ females in the current study, despite unchanged total mast cell numbers (Andrews et al., 1994; De Biase et al., 2019; Gozalo et al., 2023). This may suggest that mast cell functional activation, rather than absolute mast cell abundance, is altered in *Polr3b*$^{+/-}$ mice. Mast cells can influence cutaneous inflammation and wound repair through the release of histamine, proteases, cytokines, and growth factors following degranulation (Ackermann & Harvima, 1998; Harvima & Nilsson, 2011). Reduced degranulation may therefore reflect an impaired or delayed early inflammatory response during tissue injury. Since mast cell degranulation contributes to early inflammatory responses during wound healing, including leukocyte recruitment and the release of mediators that influence keratinocytes, endothelial cells, and fibroblasts, reduced mast cell degranulation may therefore impair coordinated tissue repair and contribute to lesion chronicity or severity in ID (Wulff & Wilgus, 2013). However, because only asymptomatic skin samples were examined in the current study, it remains unclear whether mast cell behaviour differs further during active ID lesions.

Wound healing capacity was also examined using dermal fibroblast migration and cell index (via RTCA assay). Although no genotypic differences were detected in migration rate or cell index post-wounding, the small sample size may have limited the statistical power. Thus, larger sample sizes are probably needed. It should also be noted that the wound-healing assays performed in the current study were restricted to *in vitro* fibroblast-based systems, which primarily assess migratory and proliferative properties in isolation. *In vivo* wound-healing models, including murine full-thickness excisional wound assays, would allow additional investigation of processes that cannot be recapitulated *in vitro*, including inflammatory cell recruitment, angiogenesis, keratinocyte re-epithelialisation, extracellular matrix remodelling, and scar formation (Rhea & Dunnwald, 2020).

A consistent increase in dermal collagen content was also observed in *Polr3b*$^{+/-}$ females, which may signify fibrosis due to chronic low-grade inflammation. Excessive collagen deposition is associated with suboptimal wound healing, fibrosis, and impaired skin flexibility (El Ayadi et al., 2020; Jinnin, 2010; Wynn, 2008). Notably, *Ccl20* was significantly upregulated in the skin of *Polr3b*$^{+/-}$

female mice and has been shown to promote collagen synthesis (Bandow et al., 2023). Its elevation may therefore linked Pol III-dependent inflammation to cutaneous collagen synthesis (fibrosis-like changes), at least partially. Moreover, a study revealed that downregulation of CCL20 by blocking Cysteine-rich angiogenic inducer 61 (Cyr61/CCN1) is associated with skin inflammation amelioration in a psoriasis-like mouse model (Li et al., 2017); therefore, the upregulated *Ccl20* in the skin of *Polr3b*$^{+/-}$ female mice could further explain the more severe ID found in this genotype. Furthermore, *Cxcl15*, another inflammatory chemokine, was upregulated in female *Polr3b*$^{+/-}$ skin and may contribute to a pro-inflammatory microenvironment, although its specific role in fibrosis or ID remains to be defined. Interestingly, despite the increased dermal collagen accumulation observed histologically in *Polr3b*$^{+/-}$ females, no significant changes were detected in *Col1a1* or *Col3a1* mRNA expression in asymptomatic skin samples. This may indicate that collagen accumulation is regulated post-transcriptionally or reflects altered extracellular matrix turnover rather than increased collagen gene transcription alone. During chronic inflammatory or fibrotic processes, collagen accumulation may persist due to dysregulated extracellular matrix turnover, reduced matrix degradation, or impaired tissue remodelling (El Ayadi et al., 2020; Wynn, 2008). This may partially explain why increased dermal collagen content was detected histologically in *Polr3b*$^{+/-}$ skin despite unchanged *Col1a1* and *Col3a1* mRNA expression at the time of tissue collection. Since all molecular analyses were performed using clinically unaffected skin, it is also possible that transcriptional alterations occur primarily during active lesion development or wound repair phases rather than during quiescent periods. Further experiments using affected skin samples with active ID would be required to further investigate the disease mechanism.

While this retrospective study did not directly investigate tRNA dysfunction as the result of partial Pol III inhibition, recent reports have also revealed the importance of homeostasis in tRNA expression and their post-transcription histone modification in many inflammation conditions, including psoriasis, that exhibits several phenotypes similar to ID (Lin et al., 2022; Malik, Kulaberoglu, et al., 2024; Nestle et al., 2009). Moreover, changes in the tRNA pool or post-transcriptional histone modification which affect tRNA stability as the result of Pol III mutation have been found in many known Pol III-mutated diseases in

humans (Azmanov et al., 2016; Bento-Abreu et al., 2018; Choquet, Forget, et al., 2019). Therefore, it can also be postulated that there may be specific tRNA expression necessary for maintaining skin health.

5.6 CONCLUSION

The current study demonstrates that the female mice with reduced RNA Pol III (*Polr3b*$^{+/-}$) exhibited a higher incidence and greater severity of ID, together with an increased frequency of splenomegaly and elevated systemic plasma IL-6 levels. These findings suggest the presence of a heightened inflammatory state in *Polr3b*$^{+/-}$ female mice. Furthermore, with the rest of the examination focus on the female mice, females with *Polr3b*$^{+/-}$ genotype exhibited reduced dermal mast cell degranulation and increased dermal collagen accumulation, which may contribute to the increased severity of ID or chronicity of ID observed in this genotype. Increased expression of inflammatory chemokines *Ccl20* and *Cxcl15* in the skin of *Polr3b*$^{+/-}$ female mice further supports a role for altered cutaneous inflammatory signalling in disease susceptibility. Collectively, these findings suggest a novel role for Pol III in maintaining skin homeostasis. Several limitations should also be considered. Histological and molecular analyses were performed using clinically unaffected skin and therefore may not fully capture transcriptional or inflammatory alterations occurring during active lesion development. In addition, the current study did not include *in vivo* wound-healing experiments or detailed systemic immunophenotyping, which may help further clarify the mechanisms linking reduced Pol III signalling to impaired skin repair and inflammation. Since this study primarily focused on female mice, further work examining sex hormones, immune cell populations, and inflammatory responses in both sexes may help clarify the mechanisms underlying the observed sex dimorphism effect in ID susceptibility. Further investigation into whether disruptions in the tRNA pool, post-transcriptional histone modifications, or X-linked non-coding RNAs contribute to disease susceptibility in *Polr3b*$^{+/-}$ female mice may also provide further insight into disease mechanisms.

Chapter 6: The role of RNA Polymerase III in liver function

6.1 INTRODUCTION

6.1.1 Ageing in humans and mice: implications for liver function

Ageing is a biological process characterised by a gradual decline in physiological integrity, leading to reduced function and increased vulnerability to disease (Lopez-Otin et al., 2013). In mammals, including humans and rodents, systemic ageing involves several conserved molecular hallmarks, including genomic instability, telomere attrition, mitochondrial dysfunction, loss of proteostasis, altered intercellular communication, and cellular senescence (Lopez-Otin et al., 2013). These processes result in impaired tissue regeneration, elevated oxidative stress, and chronic low-grade inflammation, which contribute to the onset of multiple age-related diseases across organ systems (Franceschi et al., 2018; Lopez-Otin et al., 2013; Oh et al., 2014).

Comparative studies reveal that many features, including ageing-related genes, anatomy, organ function and architecture, are conserved between humans and mice, making rodents a useful model for investigating organ-specific ageing (Vanhooren & Libert, 2013). Among mammalian organs, the liver demonstrates a remarkable ability for regeneration. However, it is also vulnerable to age-related dysregulation of metabolic functions and nutrient-sensing pathways, which can cause cellular senescence and low-grade inflammation (Hunt et al., 2019). These changes induce phenotypic alterations in liver cells and structure, such as a decrease in the number of hepatocytes, enlarged and polyploid nuclei due to genomic instability, increased deposition of hepatic fibrosis, an increase in activated Kupffer cells that contribute to the inflammatory phenotype of old age, accompanied by higher expression of pro-inflammatory cytokines such as IL-6 and TNF-α (Hunt et al., 2019). These changes, combined with altered AMPK and TORC1 signalling, contribute to lipid accumulation, decreased detoxification and metabolic capacity, weaken hepatic function and increase its susceptibility

to the chronic liver diseases (Hunt et al., 2019; Marcondes-de-Castro et al., 2023).

Common chronic liver disorders associated with ageing include hepatic steatosis, non-alcoholic fatty liver disease (NAFLD), cholangiopathies, and cirrhosis (Georgieva et al., 2023). Among these, liver steatosis is characterised by the excessive deposition of triglyceride within hepatocytes (Portincasa et al., 2005). Histologically, this is recognised as the presence of intracellular lipid droplets, commonly referred to as fatty infiltration (**Figure 6-1**) (Portincasa et al., 2005). The liver contains epithelial cells lining the sinusoids and bile duct (cholangiocytes). In cholangiocytes, the junctional adhesion molecule A (JAM-A) stabilises epithelial tight junctions, protecting the biliary epithelium from bile acid leakage (Salas-Silva et al., 2021). Damage to this biliary epithelium contributes to cholangiopathies and biliary inflammation (Salas-Silva et al., 2021). Cirrhosis, on the other hand, is an end-stage of many liver diseases and is characterised by impaired liver function caused by fibrosis, the process of scar tissue formation due to liver injury (Georgieva et al., 2023). On the other hand, recent studies have shown that inhibition of mTOR-associated signalling alleviates hepatic inflammation in mouse models of liver cirrhosis, whereas hyperactivation of mTORC1 promotes hepatic lipid accumulation and contributes to the development of non-alcoholic fatty liver disease (NAFLD) (Marcondes-de-Castro et al., 2023; Z. Zhang et al., 2023). These findings collectively highlight the central role of mTOR in coordinating hepatic metabolism and immune regulation.

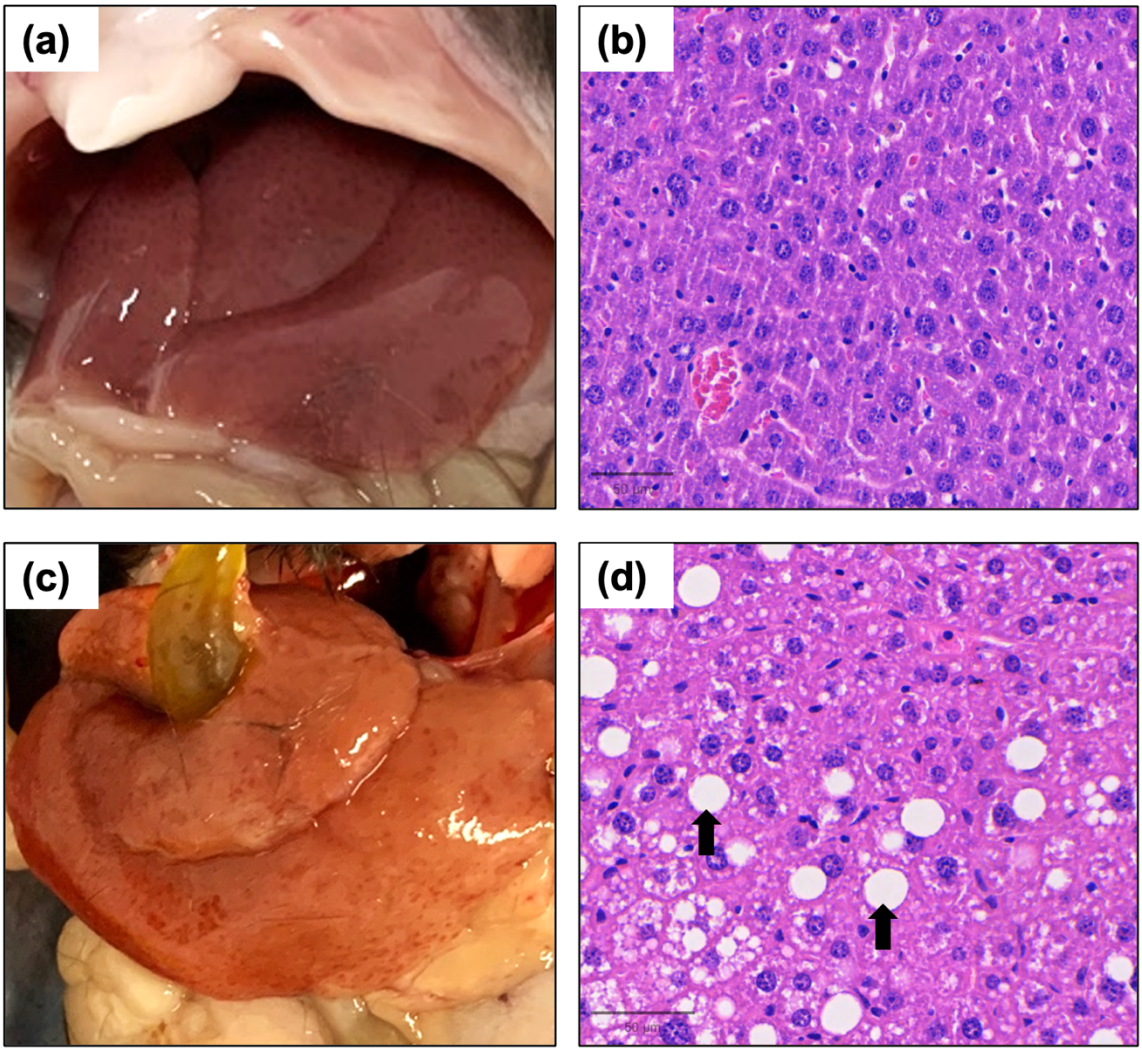

Figure 6-1 Representative diagram of liver steatosis

Gross anatomy of a normal mouse liver (a) and a liver with steatosis (c), showing that the fatty liver is increased in mass and has a yellowish appearance. Section of liver samples embedded in paraffin wax stained with H&E, showing no lipid droplets (b) and steatosis phenotype with many lipid droplets (d). Scale bar: 50 μm.

6.1.2 Role of RNA Polymerase III transcription in liver function

Pol III acts downstream of the TORC1 pathway in longevity (Filer et al., 2017; Malik, Goncalves Silva, et al., 2024). Pol III-dependent transcription is essential for cell proliferation and oncogenic transformation, primarily mediated through the TFIIIB complex, which integrates regulation by oncogenic and tumour suppressor proteins (Johnson & Johnson, 2008; Willis & Moir, 2018). Abnormal expression of TFIIIB subunits or Pol III-transcribed genes has been associated with hepatocellular carcinoma (HCC) and other liver pathologies. Specifically, Pol III transcription is upregulated in human liver cancer cell lines HepG2 and HuH7, and in mouse liver-derived lines AML-12 and TSCML, where Pol III promotes the proliferative activity of these cells by affecting the recruitment ability of its TFIIIB complex (Yi et al., 2017; C. Zhang et al., 2023). Additionally, a study using the liver cancer cell line HepG2 and primary mouse hepatocytes found that increased Pol III-dependent transcription correlates with the severity of fatty liver disease, that Pol III upregulation promotes steatosis and liver damage, and this is mediated by the TFIIIB complex under the activation of stress kinase JNK1 (Zhong et al., 2011). In a transgenic mouse model expressing the hepatitis C virus (HCV) NS5A protein on the C57BL/6 strain, animals developed severe fatty liver disease and hepatomegaly accompanied by elevated expression of Pol III genes (pre-tRNA^{Leu}, 5S rRNA) and TFIIIB components (TBP, Brf1) in both tumour and non-tumour liver tissues (Zhong et al., 2011). These findings collectively demonstrate that increases in the expression of TFIIIB components or enhanced TFIIIB recruitment resulted in overexpression of Pol III products, thereby contributing to hepatocellular proliferation and liver damage, ultimately promoting tumorigenesis.

Both DNA and RNA viruses, such as HCV, can cause progressive liver injury that leads to chronic inflammation, cirrhosis, and HCC (McGivern & Lemon, 2009). Both DNA and certain RNA viruses, including HCV, replicate more efficiently during the S phase of the cell cycle, although the underlying mechanisms that regulate this process differ between these virus classes (McGivern & Lemon, 2009). The cell cycle is tightly controlled by cyclin-dependent kinase inhibitors (CDKIs), notably p16 and p21, which act as key mediators of cellular senescence (Saul et al., 2023). In a normal cell cycle, the E2F transcription factor family promote cells entering S phase from G1 phase and perform DNA replication

(Wang et al., 2024). The upregulation of CDK inhibitors p16 and p21 repress E2F transcription factors and their target genes, arresting the cell cycle in G1 phase upon stress responses (Wang et al., 2024). On the other hand, HCV proteins NS3 and NS5A have been shown to repress p21 transcription by modulating p53 activity, thereby disrupting cell-cycle checkpoint control and promoting hepatocyte proliferation (McGivern & Lemon, 2009). Consequently, p16 and p21 serve as molecular markers of hepatocellular senescence, reflecting cell-cycle arrest and the accumulation of damaged hepatocytes during chronic liver damage (Saul et al., 2023).

Liver is a powerhouse of metabolic activity, and there is growing interest in the interplay between the host metabolism and the immune system. For instance, TORC1 has been shown to play an essential role in integrating environmental cues, including CD28, IL-2R, and amino acids, to regulate immune responses such as the Th1 and Th17 responses (Chang et al., 2013). Not only that, Pol III has also been shown to participate in immune regulation. In human cell lines, Pol III-transcribed host noncoding RNAs (e.g., 5S rRNA, tRNAs) can bind to cytoplasmic RIG-I-like receptors (RLR) to detect both DNA and RNA viruses, and trigger downstream immune signalling (Naesens et al., 2023). Upon activation, the RIG-I-MAVS pathway induces interferon regulatory factors (IRFs) and nuclear factor kappa-light-chain-enhancer of activated B cells (NF-κB), leading to the expression of type I interferons (IFN-I) and inflammatory cytokines/chemokines (e.g., IL-1, IL-6, TNF-α, Th-17 related cytokines), respectively (Liu et al., 2017; Naesens et al., 2023; T. Zhang et al., 2021).

Collectively, these findings highlight a complex role of Pol III transcription in liver physiology, spanning metabolic regulation, cell-cycle control, and innate immune activation, and suggest that disruption in Pol III transcription may contribute to both chronic liver disease progression and tumour development.

6.2 AIMS AND OBJECTIVES

Aims:

RNA Polymerase III functions downstream of the TORC1 signalling pathway to regulate cellular growth, metabolism, and immune responses through the transcription of non-coding RNAs essential for protein synthesis and stress adaptation. Dysregulation of Pol III activity has been implicated in metabolic imbalance, inflammation, and tumorigenesis, yet its role in maintaining liver structure and inflammatory homeostasis remains poorly defined

This chapter aims to determine how reduced Pol III activity caused by *Pol3b* heterozygosity affects hepatic morphology, lipid accumulation, hepatic fibrosis content, and molecular markers of inflammation and senescence, and whether these effects are influenced by sex.

Objectives:

Objective 1: To quantify liver-to-body weight ratios and assess the incidence of liver tumour in female and male *Polr3b*$^{+/-}$ and WT mice, to evaluate whether reduced Pol III activity alters overall liver phenotype or tumour susceptibility.

Objective 2: To characterise histological features of the liver in female and male *Polr3b*$^{+/-}$ and WT mice at 20 months. The assessments included hepatocyte nuclear morphology, polyploid, lipid droplet accumulation, hepatic collagen deposition, and hepatic inflammatory foci, using H&E and Masson's trichrome staining.

Objective 3: To quantify hepatic mRNA expression of cell-cycle regulators (*p16,* p21) and inflammatory cytokines (*Il1a*, *Il6*, *Tnfa*, *Il17a*, *Il22*, *Il23a*, *Ccl20*, *Jam-a)* by RT-qPCR, to assess molecular indicators of senescence, immune activation, and epithelial integrity in the liver of female and male *Polr3b*$^{+/-}$ and WT mice at 20 months.

6.3 METHODS

6.3.1 Mouse model and husbandry

Polr3b wild-type (*Polr3b*$^{+/+}$) and heterozygous mutant (*Polr3b*$^{+/-}$) mice, both on a C57BL/6N background were used. Experimental animals were generated as previously described. Mice were housed under standard conditions with *ad libitum* access to water and standard mouse chow. All procedures were approved by the University of Glasgow Animal Welfare and Ethical Review Board and conducted under UK Home Office project licences PDBDC7568, PP2141975, and personal licence I01541544. Full details are provided in **Chapter 2, Section 2.1**.

6.3.2 Pathology analysis of liver tumour

Mice from the lifespan cohort underwent *post-mortem* gross liver examination by Dr Gillian Borland, Prof Colin Selman, Dr Stephen E. Wilkie, or Zhe Wang. The total number of mice with or without suspected liver tumour was calculated for the *Polr3b*$^{+/-}$ female, WT female, *Polr3b*$^{+/-}$ male, and WT male groups. A lesion was classified as a suspected liver tumour (by gross examination only) if it was a discrete mass ≥3 mm in maximal diameter and showed ≥2 of the following features: (i) pallor or other discolouration relative to adjacent parenchyma, (ii) increased firmness on palpation, (iii) mottled/irregular surface or distortion of lobular architecture, or (iv) umbilication or necrosis present (**Figure 6-2)**.

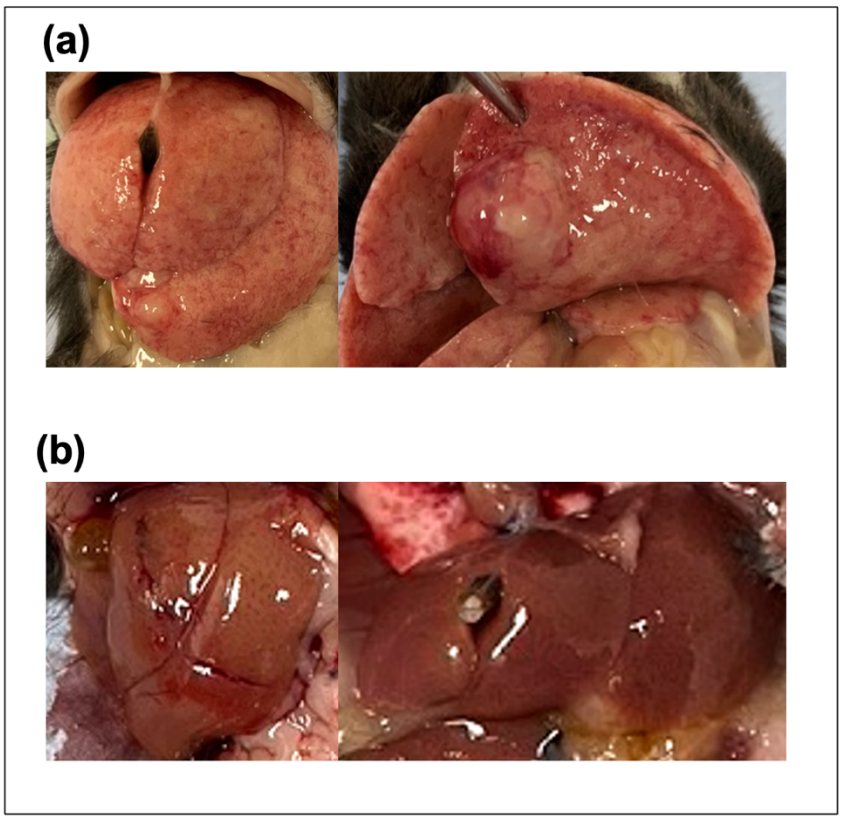

Figure 6-2 Spontaneous liver tumour in mice

Livers showing multiple discrete tumour nodules with a mottled surface (a), and normal livers with no discrete lesions (b).

6.3.3 Liver tissue collection and processing for histology

Representative liver lobes, including the left lateral and median lobes, were collected *post-mortem* from 20-month-old female and male WT and *Polr3b*$^{+/-}$ mice immediately following Schedule 1 killing. Full fixation, embedding, sectioning, H&E staining and Masson's trichrome staining procedures are described in **Chapter 2, Section 2.7.**

6.3.4 Histological analysis of liver sections using Haematoxylin and Eosin staining

The following parameters were analysed in H&E using QuPath (version 0.5.0) and ImageJ2 2.14.0/1.54f (Schindelin et al., 2012): Hepatocyte nucleus counts & size, polyploid hepatocyte count, hepatic lipid droplets counts & size, and

inflammatory foci count. For each sample, three non-overlapping fields were selected randomly at 15x magnification. Regions of interest were exported from QuPath as original-resolution TIFF files and analysed in ImageJ. Nuclei and lipid vacuoles were quantified following colour deconvolution to isolate haematoxylin or eosin channels, respectively. Thresholding and binary segmentation were applied to identify individual nuclei or fat droplets, followed by particle analysis using defined and consistent size (Nuclei (pixel^2): 500-Infinity; Fat droplets (μm^2): 50-infinity/1000) and circularity (Nuclei: 0.05-1.00; Fat droplets: 0.5-1.00) parameters to ensure all other artefact structures were excluded. For the inflammatory foci count, the number of inflammatory infiltrates was counted for the whole area of each sample.

6.3.5 Histopathological analysis of hepatic collagen using Masson's trichrome staining

The following parameters were analysed in Masson's trichrome using QuPath (version 0.5.0) and ImageJ2 2.14.0/1.54f (Schindelin et al., 2012): Collagen content in total liver tissue area. For each sample, three non-overlapping fields were selected randomly at 15x magnification. Regions of interest were exported from QuPath as original-resolution TIFF files and analysed in ImageJ. Colour deconvolution and thresholding were applied to isolate the Masson's trichrome colour channels and to identify the collagen area, respectively.

6.3.6 Liver tissue collection and processing for RT-qPCR

Liver lobes were collected from 20-month-old female and male WT and *Polr3b*$^{+/-}$ mice immediately following Schedule 1 killing. Liver tissues were placed into sterile cryotubes, snap-frozen in liquid nitrogen, and stored at -70°C until RNA extraction for RT-qPCR analysis.

6.3.7 Reverse Transcriptase quantitative-PCR (RT-qPCR)

RNA extraction

Total RNA was extracted from 20-30mg liver tissue using the RNeasy Mini Kit (Qiagen, Manchester, UK). RNA concentration and purity were assessed using a NanoDrop® Spectrophotometer ND-1000 (ThermoFisher, Wilmington, DE, USA). Full procedures are described in **Chapter 2, Section 2.5.1.**

cDNA synthesis and RT-qPCR

cDNA synthesis, qPCR setup and data analysis were performed as described in **Chapter 2, Section 2.5.2**. Briefly, total RNA was reverse transcribed using M-MLV Reverse Transcriptase (ThermoFisher, Carlsbad, CA, USA), and gene expression was quantified using SYBR Green-based RT-qPCR. Expression values were calculated using the $2^{-\Delta\Delta Ct}$ method and normalised to the geometric mean of stable reference gene sets *β-actin, Ywhaz, and Ppia*. Primer sequences are shown in **Table 6-1**.

Table 6-1 Primer sequences used in RT-qPCR experiments

Gene	Full gene name	Forward primer	Reverse primer
B-actin	*Actin beta*	5'-AGTGCATCTCCTTACGCGCT-3'	5'-TCCTGACCTCTCTGAGCTGTT-3'
Ppia	*Peptidylprolyl isomerase A*	5'-GGCAAATGCTGGACCAAAC-3'	5'-CATTCCTGGACCCAAAACG-3'
Ywhaz	*Tyrosine 3-monooxygenase/tryptophan 5-monooxygenase activation protein zeta polypeptide*	5'-GAAAAGTTCTTGATCCCCAATGC-3'	5'-TGTGACTGGTCCACAATTCCTT-3'
Polr3b	*RNA polymerase III polypeptide B*	5'-TTGGAGCCTCAGTTACCAGC-3'	5'-GAATCGACCCTGTTTCACGG-3'
P16	*Cyclin dependent kinase inhibitor 2A, transcript variant 2*	5'-TGTTGAGGCTAGAGAGGATCTTG-3'	5'-CGAATCTGCACCGTAGTTGAGC-3'
P21	*Cyclin dependent kinase inhibitor 1A, transcript variant 1*	5'-CCAGACATTCAGAGCCACAGG-3'	5'-CAACTGCTCACTGTCCACGG-3'
Il6	*Interleukin 6*	5'- CTGCAAGAGACTTCCATCCAG-3'	5'- AGTGGTATAGACAGGTCTGTTGG-3'
Il1α	*Interleukin 1α*	5'-CTGAAGAAGAGACGGCTGAGTTTC-3'	5'-TCTGGTAGGTGTAAGGTGCTGATC-3'
Il1B	*Interleukin 1 B*	5'- GAAATGCCACCTTTTGACAGTG-3'	5'- TGGATGCTCTCATCAGGACAG-3'
Tnfα	*Tumour necrosis factor*	5'-GTCCCCAAAGGGATGAGAAGT-3'	5'-TTTGCTACGACGTGGGCTAC-3'
Il10	*Interleukin 10*	5'-CAGAGCCACATGCTCCTAGA-3'	5'-TGTCCAGCTGGTCCTTTGTT-3'
Il17α	*Interleukin 17α*	5'-TCCAGGGAGAGCTTCATCTGTGTC-3'	5'-TTGGACACGCTGAGCTTTGAGG-3'
Il22	*Interleukin 22*	5'-GTGCGATCTCTGATGGCTGTC-3'	5'-AGGGCAATGAGAAGCAGGCA-3'

Il23α	*Interleukin 23α*	5’-TCCAGTGTGAAGATGGTTGTGAC-3’	5’-TTGCAAGCAGAACTGGCTGTTG-3’
Ccl20	*C-C Motif Chemokine Ligand 20*	5’-GGTACTGCTGGCTCACCTCT -3’	5’-TGTACGAGAGGCAACAGTCG-3’
Cxcl15	*C-X-C motif ligand 15*	5’-TCCTGCTGGCTGTCCTTAACC-3’	5’-TTCCTGAATACACAGACATCGTAGC-3’
Jam-a	*Junctional adhesion molecule-A*	5’-TCTCTTCACGTCTATGATCCTGG-3’	5’-TTTGATGGACTCGTTCTCGGG-3’

6.3.8 Statistics and data analysis

All analyses were performed using Prism 10.4.2 (GraphPad Software, LLC., 2025), SPSS Statistics 29.0.2.0 (IBM Corp., 2023), and RStudio 2025.09.0+387 (Posit Software, PBC., 2025) with R (version 4.5.1). Data were first analysed by ROUT outlier test with Q set to 1%, after that all data were tested for normality. Any removed outliers are noted in figure legends. The specific statistical tests are noted in figure legends.

For the normalised liver weight dataset (Genotype: *Polr3b*$^{+/-}$, wild-type; Sex: Female, Male; Age: 12 months, 20 months), a 3-way ANOVA was fitted within the general linear model in R (packages car, emmeans). The full factorial model examined genotype, sex, and age as fixed factors, also testing interaction effects. If the 3-way interaction was non-significant, it was removed and the model was refit with all 2-way interactions; if all 2-way interactions were non-significant, the final model included only main effects. Assumptions were checked via Q-Q plots and the Shapiro-Wilk test for residual normality, and Levene's test for homogeneity of variances across the 2x2x2 cells.

For the liver tumour incidence dataset, analyses were performed separately within each sex. For each 2x2 contingency table (genotype x tumour status), expected frequencies were calculated for each cell (each combination of genotype and tumour presence/absence). Chi-square tests were applied when at least 80% of the expected counts were ≥5; otherwise, Fisher's exact test was used.

In the case of 2-way ANOVA, the approach examined genotype (*Polr3b*$^{+/-}$, wild-type) and sex (female, male) as main (fixed) factors, also testing interaction effects. In all cases where non-significant interaction effects ($p>0.05$) were identified, these were subsequently removed, and the analysis was rerun with main effects to obtain the best-fit model. For the dataset that did not pass normality tests, data were analysed with a rank-based aligned two-way ANOVA (ART) (package ARTool, emmeans) to test the main and interaction effects.

For all analyses, effects and differences were considered significant if the p-value <0.05, where * denotes a p-value of <0.050, ** denotes a p-value of

<0.010, and *** denotes a p-value of <0.001. Any significant main or interaction effects are noted in the figures.

6.4 RESULTS

6.4.1 *Polr3b* expression was reduced in the liver of *Polr3b*$^{+/-}$ mice

To verify the heterozygous knock-out of *Polr3b* in *Polr3b*$^{+/-}$ mice, *Polr3b* expression levels were measured in the liver of 14-month-old mice. As shown in **Figure 6-3**, *Polr3b* expression was significantly reduced in *Polr3b*$^{+/-}$ mice compared with WT controls in both sexes (*F=5.823, p=0.024*). Meanwhile, no significant sex effect was found (*F=3.622, p=0.069*) (**Figure 6-3**).

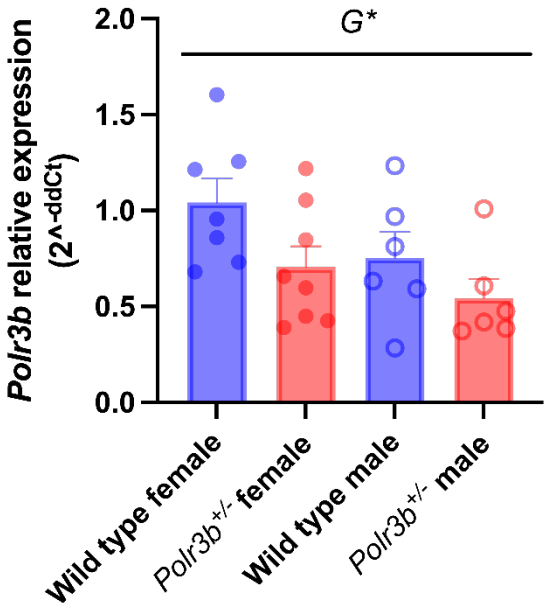

Figure 6-3 Expression of *Polr3b* in the liver of 14-month-old WT and *Polr3b*$^{+/-}$ mice

Polr3b mRNA expression in liver of 14-month-old female and male mice. Histograms present mean ± SEM, with sample sizes indicated by individual points within a group. A two-way ANOVA was used to test for genotype and sex effects (both main and interaction effects). G=genotypic effect p<0.050. (Experiment undertaken by Dr Gillian Borland, and the analysis was conducted by the author)*

6.4.2 Male mice had higher normalised liver weight than females

Liver weights of 12-month-old and 20-month-old female and male mice (both genotypes) were normalised to total body weight. Across both age groups, males exhibited a higher liver-to-body weight ratio than females (sex main effect *F=12.391, p=0.001*; female mean 3.42%, male mean 3.95%), and the male-female difference was larger at 20 months than at 12 months (Sex x Age interaction effect *F=5.428, p=0.024*; with 12 months: Female 3.50% v. Male 3.73%; 20 months: Female 3.34% v. Male 4.17%). No significant effects of age (*F=0.775, p=0.383*) or genotype (*F=0.168, p=0.684*) were detected. Interaction terms involving Genotype were not significant and are not reported further (**Figure 6-4**).

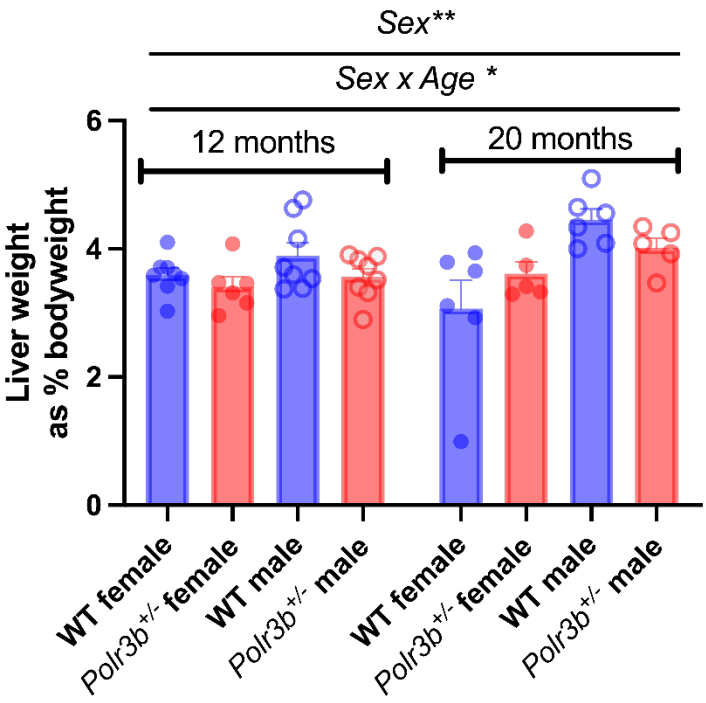

Figure 6-4 Liver-to-body weight ratio of female and male mice at 12 and 20 months

*Normalised liver weight as a percentage of body weight for 12-month-old and 20-month-old mice. Histograms denote means ± SEM, with sample sizes indicated by individual points within a group. Statistical analysis was performed using three-way ANOVA. Sex**=sex effect p<0.010, Sex x Age * =sex and age interaction effect p<0.050.*

6.4.3 No genotypic difference in liver tumour incidence

The number of mice that developed liver tumours was determined in both female and male *Polr3b*$^{+/-}$ and WT mice. No genotype-dependent differences in liver tumour incidence were detected in either sex (female *RR=1.333, 95% CI [0.350-5.123], p=0.999*; Male *RR=0.416, CI [0.145-1.164], p=0.099*) (**Figure 6-5**). This suggests that *Polr3b*$^{+/-}$ mice were not prone to develop liver tumours.

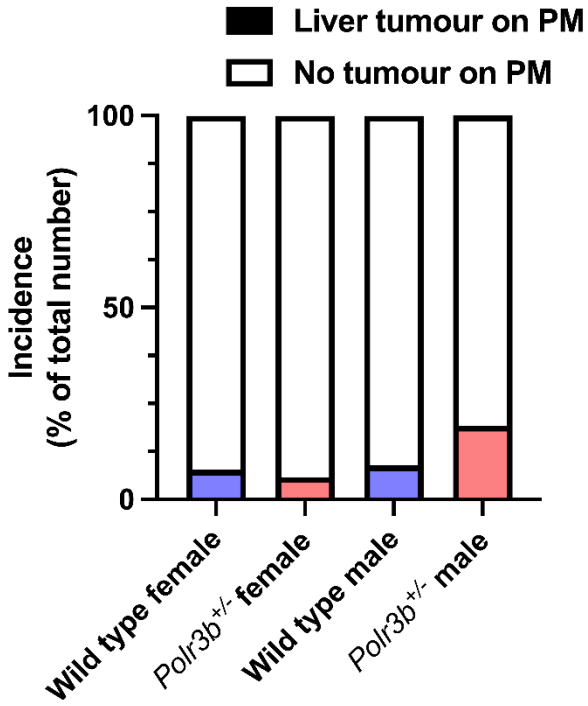

Figure 6-5 Incidence of liver tumour in female and male WT and *Polr3b*$^{+/-}$ mice

Incidence of liver tumour in WT and Polr3b$^{+/-}$ *(blue and red, respectively) female and male mice. n=50 for WT females, n=50 for Polr3b*$^{+/-}$ *females, n=50 for WT males, and n=52 for Polr3b*$^{+/-}$ *males. A Fisher's exact test and a chi-square test were used for statistical analysis in the female and male groups, respectively.*

6.4.4 No genotypic differences in hepatocyte nucleus count and nucleus size

To investigate the conditions of the hepatocyte nucleus, the liver sections from female and male *Polr3b*$^{+/-}$ and WT mice were stained with H&E. The total number of hepatocyte nuclei per field of view, as well as the size of the nucleus, were examined. **Figure 6-6** shows that neither hepatocyte nuclear count (genotype *F=1.205, p=0.286*; sex *F=2.858, p=0.107*) nor nuclear size (genotype *F=0.444, p=0.513*; sex *F=4.095, p=0.057*) differed by genotype or sex.

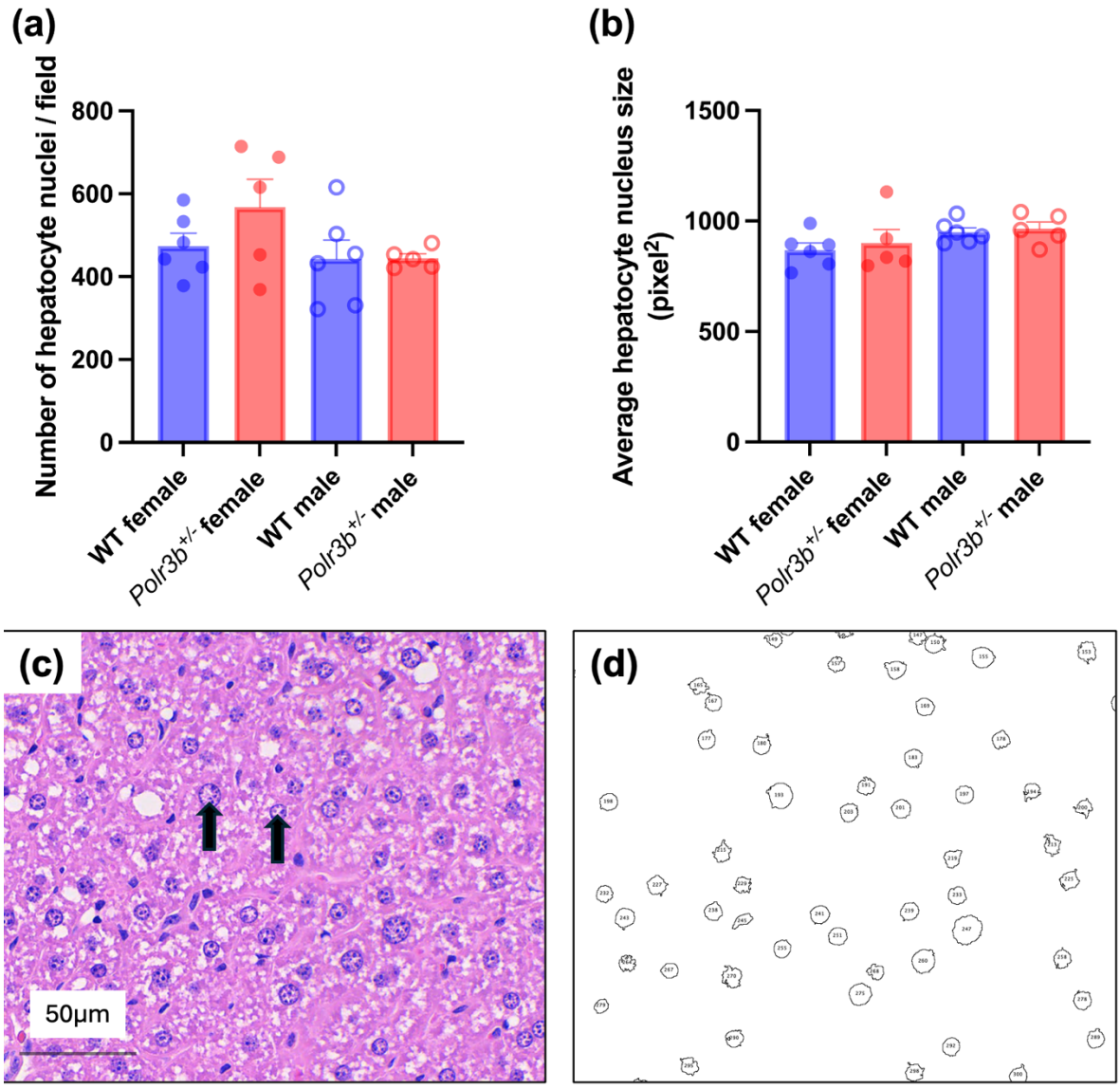

Figure 6-6 Quantification of hepatocyte nuclei in WT and *Polr3b*$^{+/-}$ mice at 20 months of age

Histopathology analysis of the hepatocyte nuclei counts (a) and nucleus size (b) of the 20-month-old WT and Polr3b$^{+/-}$ *(blue and red, respectively) mice. Histograms present means ± SEM, with sample sizes indicated by individual points within a group. Two-way ANOVAs were used to test for genotype and sex effects (both main and interaction effects). Representative H&E sections highlighting mouse hepatocyte nuclei (arrows) (c), and the counting overlay showing per-nucleus count labels used for quantification (d). Scale bar: 50 µm.*

6.4.5 No genotypic differences in polyploid hepatocyte count

To investigate whether *Polr3b*$^{+/-}$ mice show changes in the number of polyploid hepatocytes, hepatocytes with two or more nuclei were quantified in liver sections from 20-month-old female and male *Polr3b*$^{+/-}$ and WT mice under H&E staining. **Figure 6-7** indicated no genotype or sex effects were detected for multinucleated hepatocyte counts (genotype *F=0.011, p=0.919*; sex *F=2.143, p=0.160*), nor any difference in their ratio to the total nuclei (genotype *F=0.195, p=0.664*; sex *F=1.579, p=0.244*).

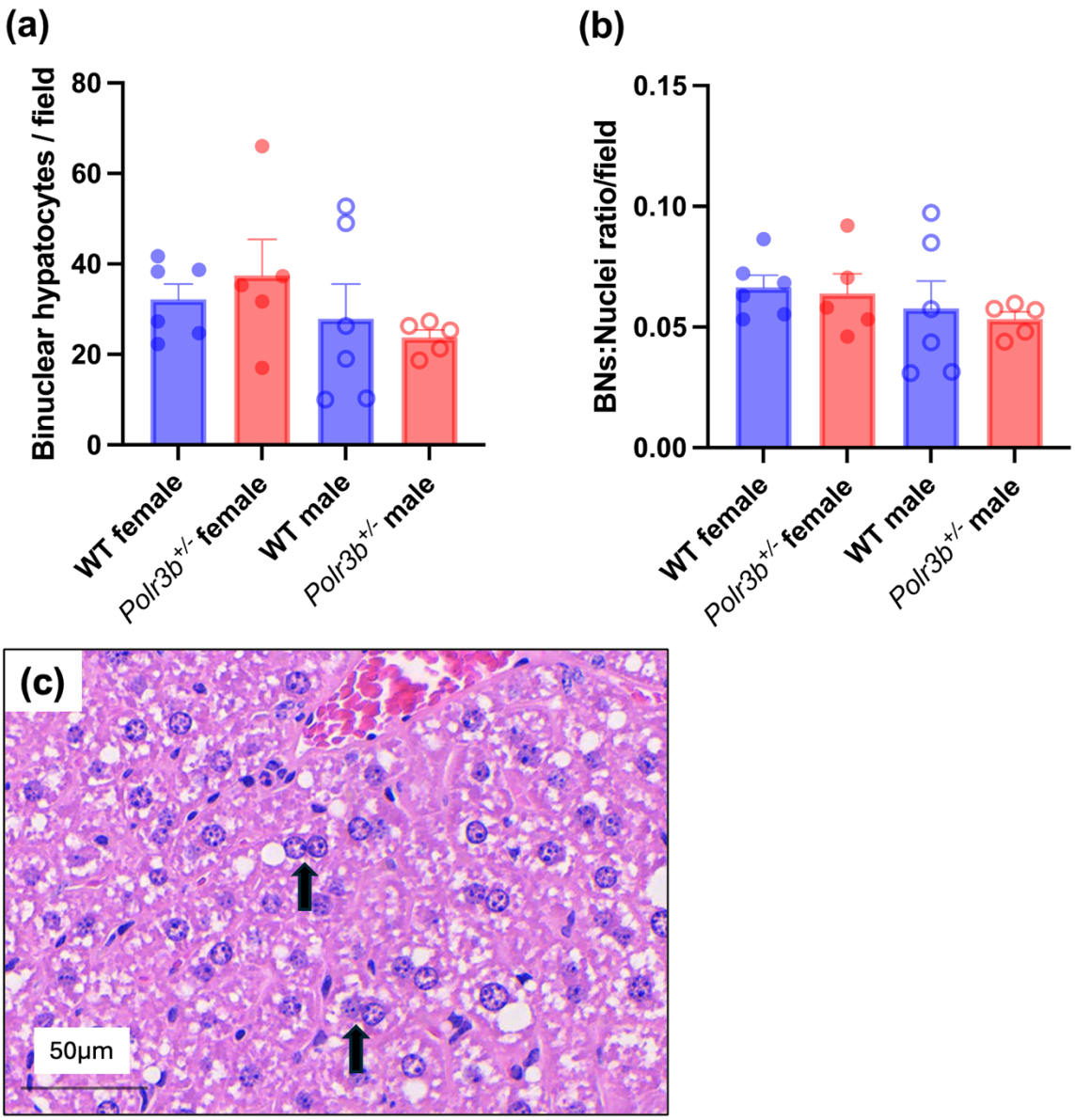

Figure 6-7 Quantification of hepatocyte multi-nuclei in WT and *Polr3b*$^{+/-}$ mice at 20 months of age

Histopathology analysis of the hepatocyte multi-nuclei counts (a) and the ratio of multi-nuclei hepatocytes to the total hepatocytes (b) of the 20-month-old WT and Polr3b$^{+/-}$ (blue and red, respectively) mice. Histograms present means ± SEM, with sample sizes indicated by individual points within a group. Two-way ANOVAs were used to test for genotype and sex effects (both main and interaction effects). Representative H&E section highlighting mouse hepatocyte multi-nuclei (arrows). Scale bar: 50 μm.

6.4.6 Male mice had larger hepatic lipid droplets than female mice

Hepatic lipid droplets were also quantified in 20-month-old mice. There was no genotypic or sex effect on the lipid droplet counts in the *Polr3b*$^{+/-}$ and WT mice (genotype *F=1.895, p=0.186*; sex *F=3.676, p=0.198*) (**Figure 6-8(a)**). Male mice exhibited larger hepatic lipid droplets than females (*F=4.742, p=0.043*), while no genotypic effect was found (*F=0.020, p=0.890*) (**Figure 6-8(b)**).

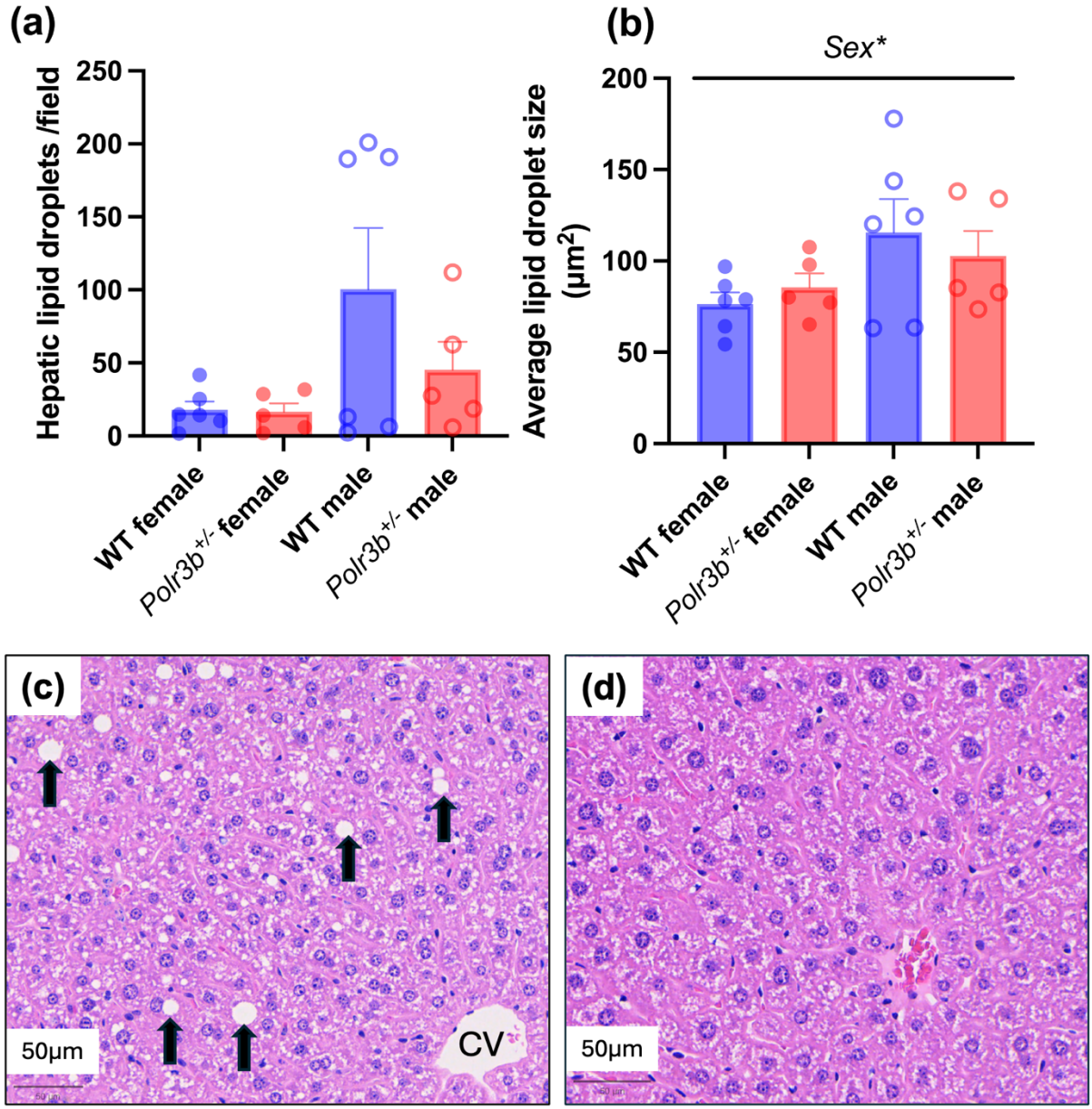

Figure 6-8 Quantification of hepatic lipid droplets in WT and *Polr3b*$^{+/-}$ mice at 20 months of age

Histopathology analysis of the hepatic lipid droplet counts (a) and lipid droplet size (b) of the 20-month-old WT and Polr3b$^{+/-}$ *(blue and red, respectively) mice. Histograms present means ± SEM, with sample sizes indicated by individual points within a group. Two-way ANOVA was used to test for genotype and sex effects (both main and interaction effects) for dataset (b), and an alternative nonparametric ART was used for dataset (a) due to the bimodality distribution in the WT male group. Representative H&E sections showing hepatic lipid droplets (arrows) (c), and no lipid droplets present (d). Scale bar: 50 μm. Sex*=sex effect p<0.050.*

6.4.7 No difference in the hepatic collagen content between *Polr3b*$^{+/-}$ and WT mice

To assess whether hepatic collagen content differed between genotypes, liver sections from 20-month-old *Polr3b*$^{+/-}$ and WT female and male mice were stained with Masson's trichrome and quantified. **Figure 6-9** shows that there was no genotypic (*F=3.323, p=0.*084) or sex effect (*F=0.402, p=0.*533) in the hepatic collagen content, as a percentage of the total liver tissue area.

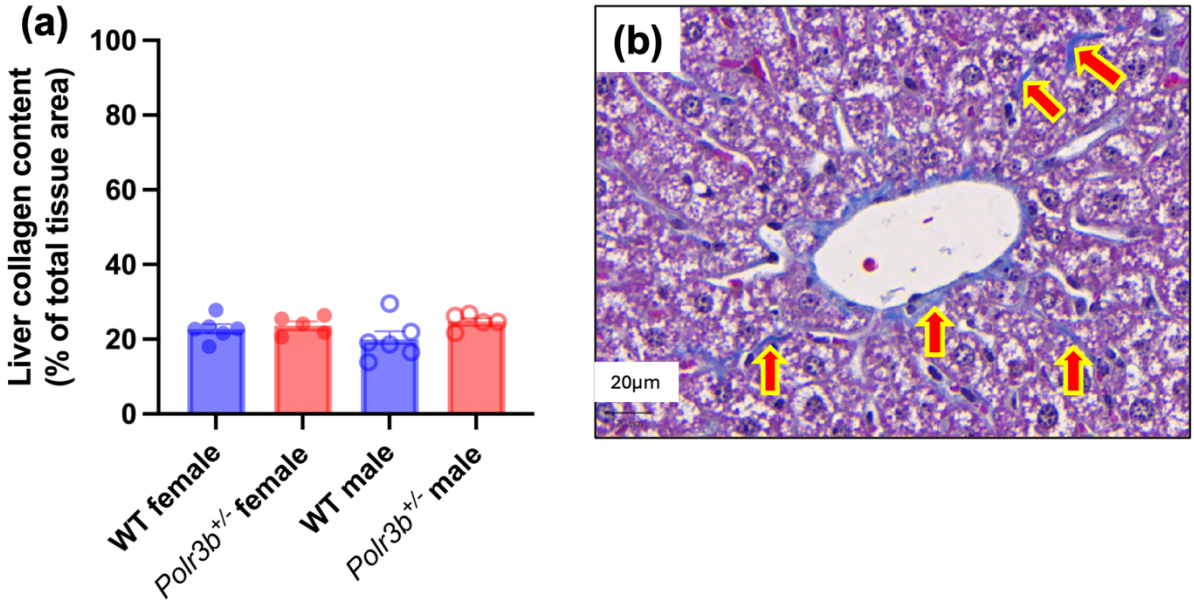

Figure 6-9 Hepatic collagen content in WT and *Polr3b*$^{+/-}$ mice at 20 months of age

Histopathology analysis of the hepatic collagen content, expressed as the percentage of total liver tissue area, in the 20-month-old WT and Polr3b$^{+/-}$ *(blue and red, respectively) mice (a). Histograms present means ± SEM, with sample sizes indicated by individual points within a group. A two-way ANOVA was used to test for genotype and sex effects (both main and interaction effects). Representative Masson's trichrome staining image illustrates the areas with blue are the collagen fibres (b). Scale bar 20 µm.*

6.4.8 No genotypic difference in hepatic inflammatory foci count in the liver section of *Polr3b*$^{+/-}$ and WT mice

To investigate whether a change in inflammatory activity is present in the liver of *Polr3b*$^{+/-}$ mice, the total count of hepatic inflammatory foci per section per mouse was examined. **Figure 6-10** shows that inflammatory foci counts did not differ by genotype (*F=2.004, p=0.*173) or sex *(F=0.246, p=0.*625).

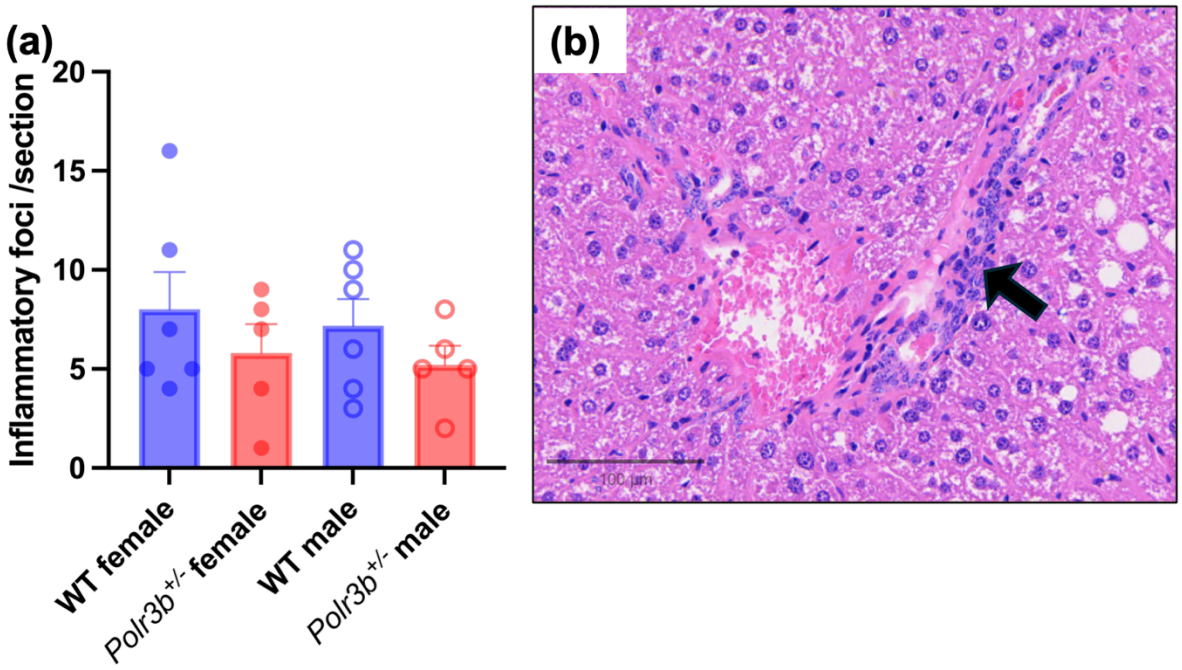

Figure 6-10 Quantification of hepatic inflammatory foci in WT and *Polr3b*$^{+/-}$ mice at 20 months of age

Histopathology analysis of the hepatic inflammatory foci counts of the 20-month-old WT and Polr3b$^{+/-}$ *(blue and red, respectively) mice (a). Histograms present means ± SEM, with sample sizes indicated by individual points within a group. Two-way ANOVA was used to test for genotype and sex effects (both main and interaction effects). Representative H&E section showing a cluster of inflammatory cells in the liver of a mouse (b). Scale bar: 100 µm.*

6.4.9 *Il1α* expression was downregulated in liver of 20-month-old *Polr3b*$^{+/-}$ males

To further assess inflammatory signalling in *Polr3b*$^{+/-}$ liver tissue, the expression of the pro-inflammatory cytokines *Il6, Il1α, Il1β, Tnfα* and anti-inflammatory cytokine *Il10* were quantified in female and male *Polr3b*$^{+/-}$ and WT liver tissue. **Figure 6-11 (b)** revealed no genotype-dependent difference in *Il1α* expression in the liver of *Polr3b*$^{+/-}$ and WT female mice, but a decrease was found in the *Polr3b*$^{+/-}$ males *(Female t=0.067, p=0.948; Male t=3.410, p=0.005)* (**Figure 6-12 (b)**). Expression of *Il6 (Female t=0.160,p=0.877; Male t=1.749, p=0.104), Il1β (Female t=0.114,p=0.911; Male t=0.599, p=0.559), Tnfα (Female t=0.406, p=0.691; Male t=1.022, p=0.324)* and *Il10 (Female t=0.056, p=0.956; Male t=0.969, p=0.349)* were unaffected by genotype in both sexes (**Figure 6-11** and **6-12**).

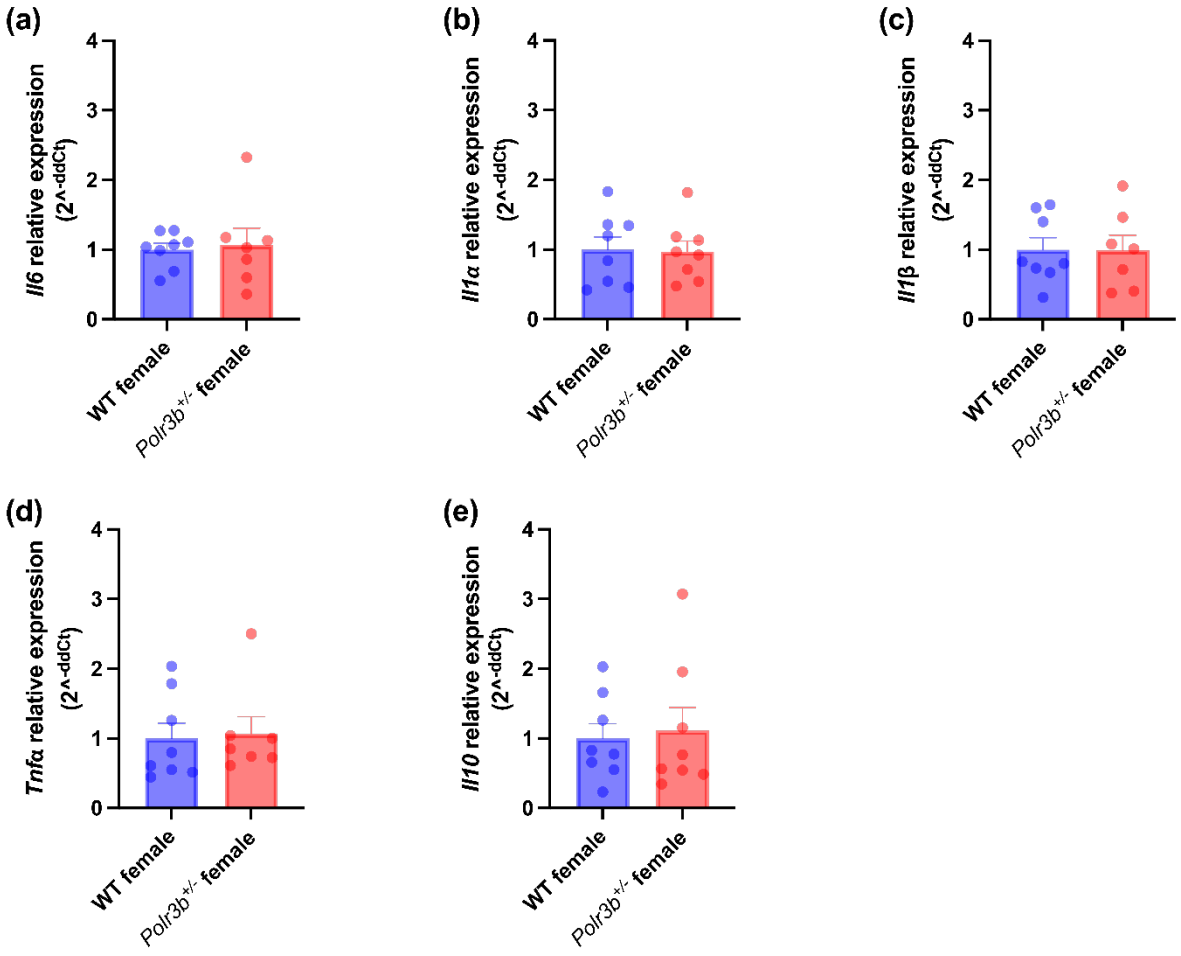

Figure 6-11 Inflammatory cytokine gene expression in the liver of 20-month-old WT and *Polr3b*$^{+/-}$ female mice

Il6, Il1α, Il1B, Tnfα, and Il10 mRNA expression relative to B-Actin, Ywhaz or Ppia expression in liver of 20-month-old female mice. Histograms present mean ± SEM, with sample sizes indicated by individual points within a group. An outlier was identified and removed from Polr3b$^{+/-}$ *in (a). Unpaired t-tests were used to test for genotype differences, except for the dataset in (a) used Welch's t-test because of the unequal SD.*

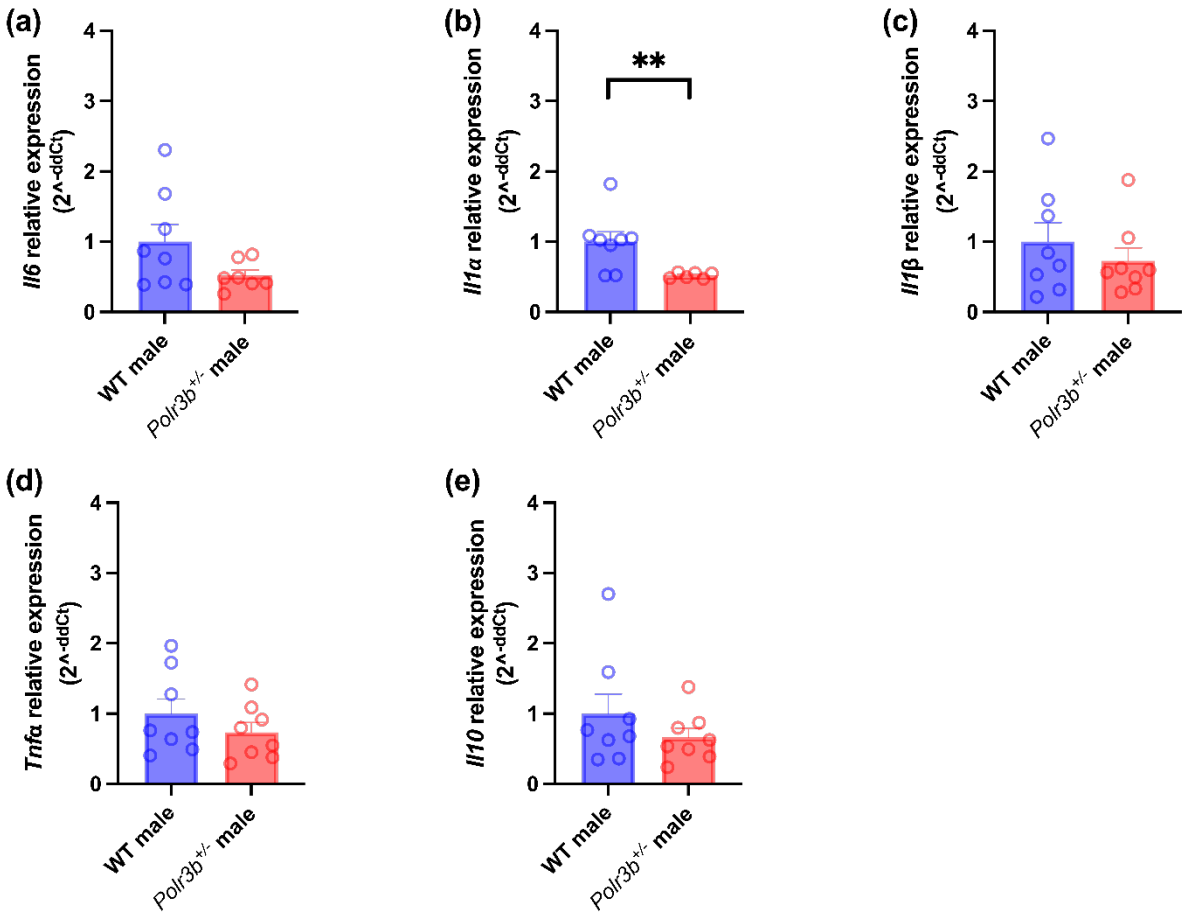

Figure 6-12 Inflammatory cytokine gene expression in the liver of 20-month-old WT and *Polr3b*$^{+/-}$ male mice

Il6, Il1α, Il1B, Tnfα, and Il10 mRNA expression relative to B-Actin, Ywhaz or Ppia expression in liver of 20-month-old male mice. Histograms present mean ± SEM, with sample sizes indicated by individual points within a group. Outliers were identified, one was removed from Polr3b$^{+/-}$ *in (a), and two were removed from Polr3b*$^{+/-}$ *in (b). Unpaired t-tests were used to test for genotype differences. **=p<0.010.*

6.4.10 *Il17α* expression was upregulated in liver of 20-month-old *Polr3b*$^{+/-}$ males

No genotype-dependent difference was observed in females (*t=0.242, p=0.812*) (**Figure 6-13 (a)**), whereas *Il17α* expression was increased in the liver of *Polr3b*$^{+/-}$ males (*t=2.258, p=0.043*) (**Figure 6-13 (d)**). Moreover, no genotypic differences were detected in the expression of *Il-22* (Female *t=0.686, p=0.504*; Male *t=1.322, p=0.216*) and *Il23α* (Female *t=1.680, p=0.115*; Male *t=0.048, p=0.963*) in the liver of 20-month-old female and male mice (**Figure 6-13**).

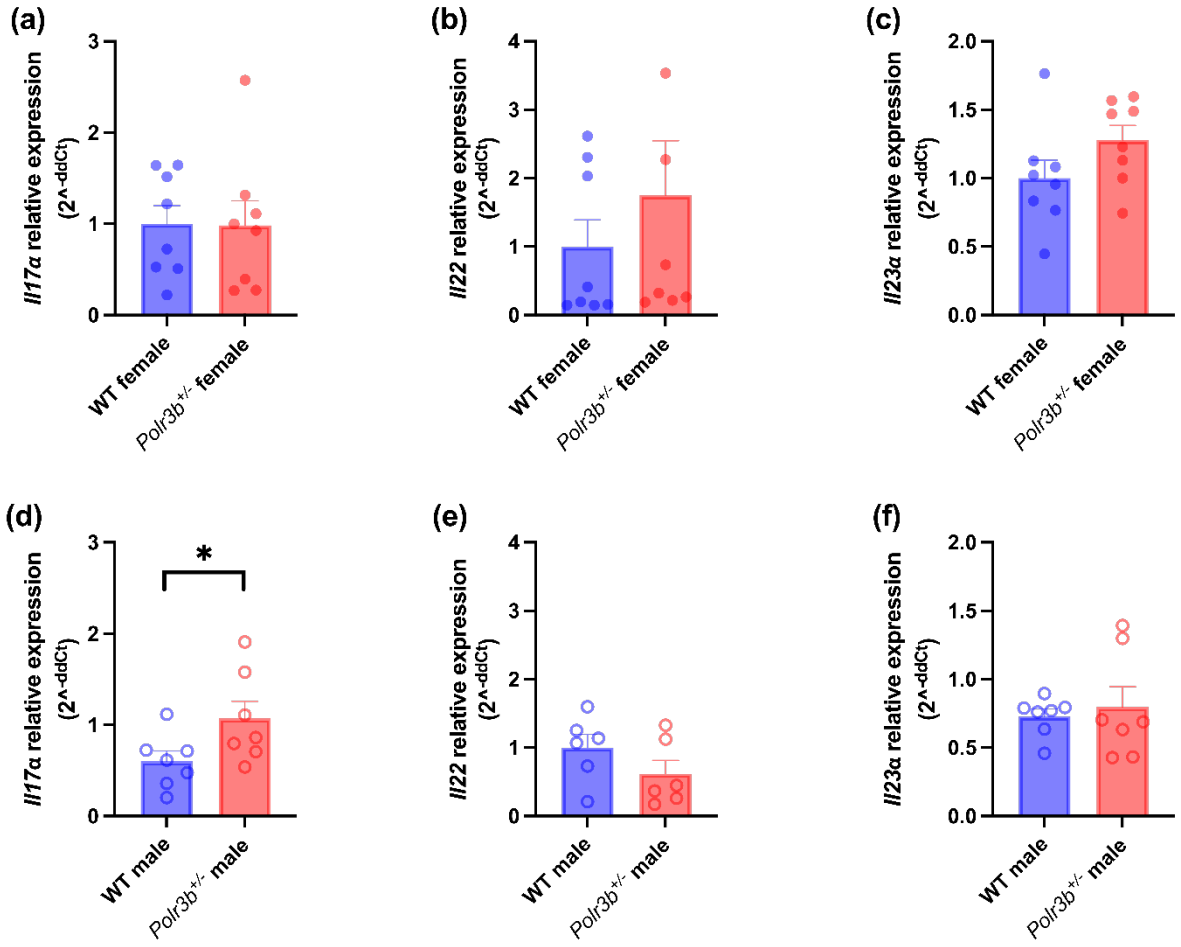

Figure 6-13 Expression of Th17-related genes *Il17α*, *Il22*, and *Il23α* in the liver of 20-month-old WT and *Polr3b*$^{+/-}$ mice

*Il17α, Il22, Il23α mRNA expression relative to β-Actin and Ywhaz expression in liver of 20-month-old female (a-c) and male (d-e) mice. Histograms present mean ± SEM, with sample sizes indicated by individual points within a group. Outliers were identified and one was each removed from WT in (d) and (f), two were each removed from WT and Polr3b$^{+/-}$ groups in (e). Unpaired t-tests were used to test for genotype differences. *=p<0.050.*

6.4.11 No genotypic differences in the expression of *Ccl20*, *Cxcl15*, and *Jam-a* in the liver of 20-month-old mice

Ccl20, *Cxcl15*, and *Jam-a* were also examined due to their involvement in hepatic inflammation and liver injury. No genotypic differences were observed in *Ccl20* (Female *t=0.586, p=0.568*; Male *t=0.191, p=0.851*), *Cxcl15* (Female *t=0.205, p=0.840*; Male *t=0.559, p=0.592*), and *Jam-a* (Female *t=0.253, p=0.804*; Male *t=0.051, p=0.960*) expression in either sex at 20 months of age (**Figure 6-14**).

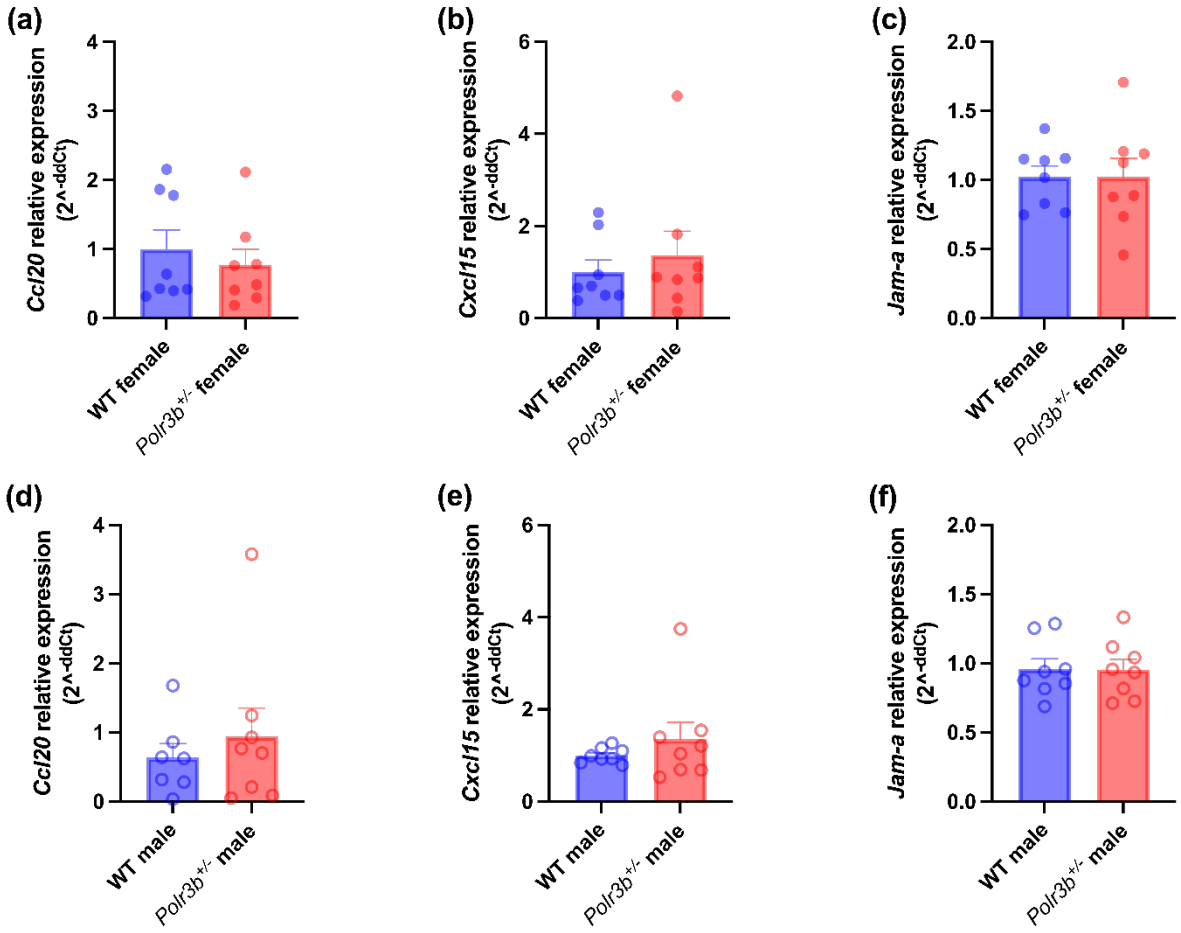

Figure 6-14 Expression of *Ccl20, Cxcl15, Jam-a* in the liver of 20-month-old WT and *Polr3b*$^{+/-}$ mice

Ccl20, Cxcl15, Jam-a mRNA expression relative to B-Actin and Ywhaz expression in liver of 20-month-old female (a-c) and male (d-f) mice. Histograms present mean ± SEM, with sample sizes indicated by individual points within a group. One outlier was identified and was removed from WT in (d). Unpaired t-tests were used to test for genotype differences except for dataset in (e) used Welch's t test due to the unequal SD.

6.4.12 No genotypic differences in the expression of *p16* and *p21* in the liver of 20-month-old mice

P16 and P21 are the key signalling molecules in replicative senescence, and the expression of these markers can indicate ageing-related conditions and hepatic tissue dysfunction. **Figure 6-15** demonstrated that expression of *p16* (Female *t=0.609, p=0.553*; Male *t=0.540, p=0.598*) and *p21* (Female *t=0.572, p=0.577*; Male *t=0.052, p=0.960*) did not differ significantly in the liver of *Polr3b*$^{+/-}$ and WT mice at 20 months of age.

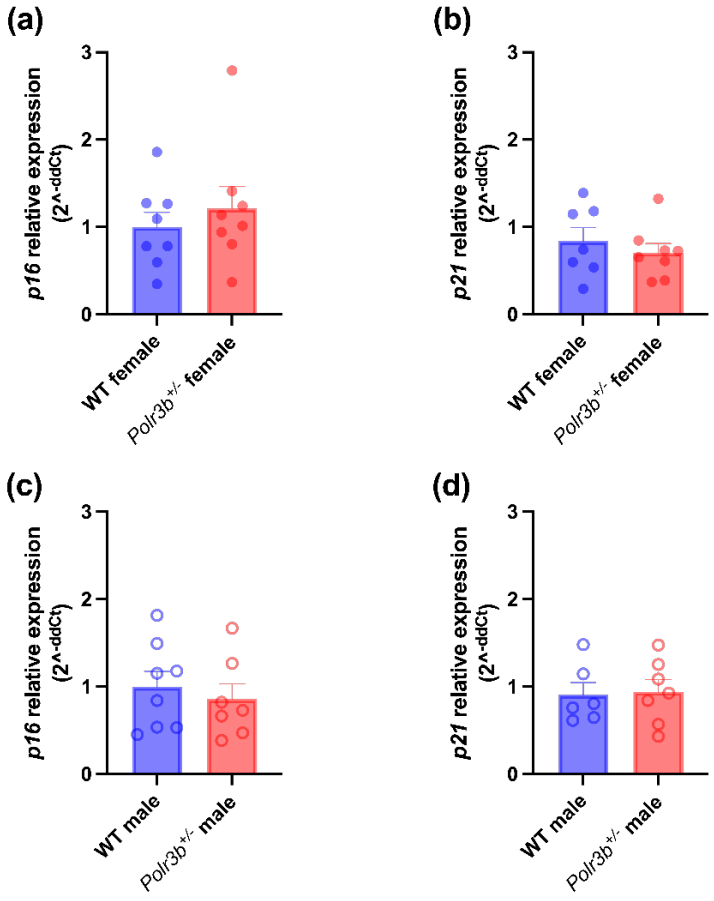

Figure 6-15 Expression of *p16* and *p21* in the liver of 20-month-old WT and *Polr3b*$^{+/-}$ mice

P16 and *p21 mRNA expression relative to ß-Actin and Ywhaz expression in liver of 20-month-old female (a-b) and male (c-d) mice. Histograms present mean ± SEM, with sample sizes indicated by individual points within a group. Unpaired t-tests were used to test for genotype differences.*

6.5 DISCUSSION

RNA polymerase III transcribes small non-coding RNAs, including 5S rRNA and tRNAs, which are essential for protein synthesis and cellular metabolism. The liver functions as a major metabolic organ, coordinating carbohydrate, lipid, and protein homeostasis (Mohallem et al., 2025). Elevated Pol III activity has been associated with hepatocellular carcinoma and transformed cells, supporting the high demand for protein synthesis and cell growth in the aberrant proliferating cells (Lei et al., 2017; Willis & Moir, 2018). Moreover, loss of the Pol III repressor MAF1 confers resistance to obesity and non-alcoholic fatty liver disease, likely due to enhanced turnover of futile tRNA cycle and metabolic adaptation (Bonhoure et al., 2015). Together, these findings highlight the central role of Pol III signalling in hepatic metabolism and disease progression.

The catalytic subunit POLR3b, together with POLR3a, forms the active centre of Pol III (Saitsu et al., 2011). In this chapter, the effects of *Polr3b* heterozygosity (*Polr3b*$^{+/-}$) were investigated in mice to determine how partial Pol III reduction influences the liver functions at the morphological, histological and molecular levels. Mice show a low spontaneous incidence of hepatocellular carcinoma (HCC). One study reported a 23.8% spontaneous HCC occurrence in males and 4.5% in females, typically developing around 13 months of age and the incidence is higher in male mice (Tamano et al., 1988). The current study supports the higher incidence of HCC in the C57BL/6N background mice, with the occurrence of HCC being 6.7% in females and 14.1% in males. The differences in the reported incidence of spontaneous HCC in males between the present study and the previous report may reflect differences in neoplasm diagnoses, as HCC in the current study was not confirmed histologically. Moreover, no genotypic differences were found in the normalised liver weight (% body weight) or in the incidence of HCC between *Polr3b*$^{+/-}$ and WT mice upon *post-mortem*. The liver-to-body weight ratio is an important health indicator. A healthy mouse generally has a liver-to-body weight ratio of 3-5% (Pritchard & Apte, 2015). The current results demonstrated that both the *Polr3b*$^{+/-}$ and WT mice at both 12 and 20 months of age were within this range. The mechanisms regulating liver-to-body mass ratio are not yet fully understood; however, factors such as a high-fat diet (HFD) and ageing have been shown to influence this ratio (Lessard-Beaudoin et al., 2015; J. Zhang et al., 2021). The current study also showed a higher liver-to-

body weight ratio in male mice at both 12 and 20 months of age, with the difference being more pronounced at 20 months. Moreover, a study showed that liver weight in male mice was more affected by HFD, with a higher liver weight observed only in males under HFD, whereas female liver weights remained unaffected (J. Zhang et al., 2021). Histological assessment further revealed larger hepatic lipid droplets in males compared with females. Together, these findings suggest that male livers may be more susceptible to lipid accumulation and less resistant to obesity-related metabolic stress. However, the relatively mild liver phenotype observed between genotypes in the present study differs from previous reports linking Pol III dysregulation with hepatic steatosis, hepatocellular carcinoma and metabolic dysfunction (Bonhoure et al., 2015; Lei et al., 2017; Palian et al., 2014; Zhong et al., 2011). Importantly, many of these studies examined liver phenotypes under conditions of enhanced metabolic or transcriptional stress. Bonhoure et al. (2015) demonstrated that *Maf1* knockout mice were resistant to obesity and hepatic steatosis following high-fat diet feeding, indicating that Pol III-associated metabolic phenotypes become more apparent under dietary challenge (Bonhoure et al., 2015; Bonhoure et al., 2020). Similarly, Palian et al. (2014) showed that Maf1 participates in PTEN/PI3K/AKT-dependent regulation of hepatic lipogenesis under high-carbohydrate dietary conditions. In addition, studies investigating TFIIIB signalling have largely focused on pathological activation of Pol III transcription. Zhong et al. (2011) demonstrated that alcohol exposure increased TFIIIB components including TBP and Brf1, leading to enhanced Pol III-dependent transcription in liver-derived cells, while Lei et al. (2017) reported abnormal expression of TFIIIB subunits and Pol III genes in hepatocellular carcinoma. Compared with these metabolically stressed or disease-associated models, the aged chow-fed *Polr3b*$^{+/-}$ mice examined in the present study displayed relatively limited hepatic pathology, suggesting that partial reduction of Pol III activity may be insufficient to disrupt liver homeostasis under baseline physiological conditions.

At the molecular level, the cell cycle inhibitors p16 and p21, which act as key markers of cellular senescence, were examined. These CDK inhibitors maintain cell-cycle arrest in the G1 phase in response to various cellular stresses such as DNA damage, metabolic imbalance, ribosomal stress, or oncogenic activation (Gorgoulis et al., 2019). In the present study, hepatic *p16* and *p21* expression

remained unchanged between *Polr3b*$^{+/-}$ and wild-type groups. Considering Pol III's established role in supporting cell cycle and proliferation, reduced Pol III activity might have been expected to suppress proliferation or induce cellular stress response (Moir & Willis, 2013). Moreover, in the liver, the accumulation of p16+ and p21+ senescent hepatocytes during ageing is linked to hepatocellular stress as well as activated inflammatory and fibrotic signalling pathways (Saul et al., 2023; B. Wang et al., 2024). The unchanged expression of hepatic *p16* and *p21,* as well as the unchanged hepatic fibrosis in the histology samples between *Polr3b*$^{+/-}$ and wild-type mice might suggest that heterozygous *Polr3b* loss does not compromise hepatocellular stress and cell-cycle control. However, since p16 and p21 reflect only the cell-intrinsic component of senescence, further evaluation of the activity of the enzyme senescence-associated ß-galactosidase (SA- ß-gal) for detecting the lysosomal changes, and the evaluation of the senescence-associated secretory phenotype (SASP), which is secreted by the senescent cells and the components include a wide range of interleukins, cytokines, chemokines, growth factors, proteases, exosomes, and leukotrienes, would be necessary to determine whether Pol III reduction affects cellular senescence, secretory and inflammatory responses in the liver (Gorgoulis et al., 2019; Saul et al., 2023).

Pol III also contributes to innate immune defence against various pathogens (Ablasser et al., 2009; Chiu et al., 2009). Upon sensing cytosolic AT-rich DNA of viral or bacterial origin, Pol III can transcribe this DNA into 5'-triphosphorylated RNA intermediates, which are recognised by RIG-I and activate the RIG-I-MAVS signalling pathway (Chiu et al., 2009; Naesens et al., 2023). This leads to activation of IRF and NF-κB signalling, resulting in the production of IFN-I and pro-inflammatory cytokines (Naesens et al., 2023). In this study, sex-specific differences were observed in the expression of two pro-inflammatory cytokines, with lower *Il1α* and higher *Il17α* expression detected in male *Polr3b*$^{+/-}$ livers; while pro-inflammatory cytokines *Il6, Il1B, Tnfα, Il22, Il23α, Cxcl15* (homologue of human *IL-8*) and anti-inflammatory cytokine *Il10* showed no genotypic differences in expression levels compared to WT mice. Similarly, expression of the Th-17-related chemokine *Ccl20* and *Jam-a*, the latter encoding a tight junction protein in cholangiocytes, remained unchanged. All these findings suggest that partial Pol III reduction does not induce widespread hepatic

inflammation under chow-fed conditions. Instead, the findings may reflect subtle alterations in immune signalling pathways that are more detectable at the transcriptional level than at the structural level. Sexual dimorphism in hepatic metabolism and inflammatory regulation may also contribute to these male-specific effects, as male mice are generally more susceptible to hepatic lipid accumulation and inflammatory liver injury than females, particularly under the effect of lower oestrogen in males (Della Torre, 2020; Lonardo et al., 2019). Oestrogen signalling has also been reported to influence T-cell and regulatory T-cell (Treg) populations in the liver, while regulatory T cells can exhibit plasticity toward IL-17A-producing phenotypes under inflammatory conditions (Li & Boussiotis, 2013; Lonardo et al., 2019). Although Treg populations were not assessed in the present study, altered immune-cell regulation may contribute to the sex-specific cytokine changes observed in male *Polr3b*$^{+/-}$ mice. However, despite changes in certain cytokine expression in male *Polr3b*$^{+/-}$ mice, no corresponding increase in collagen deposition or inflammatory infiltrates was detected histologically, suggesting that the magnitude of inflammatory signalling change was insufficient to drive overt fibrosis or liver injury at 20 months of age. It should be noted that the mice were culled at 20 months of age, when the majority of the cohort remained healthy (72.49% of females alive, 85.08% of males alive; Borland et al., 2024). The relatively healthy physiological state of the animals at 20 months may explain the subtle inflammatory changes observed. Mice at 24 months or older, where less than half of the animals in the cohort were alive, may be worth assessing to possibly reveal more pronounced hepatic effects of Polr3b heterozygosity.

In relation to the reduced *Il1α* expression observed in male *Polr3b*$^{+/-}$ mice, IL-1α promotes neutrophil recruitment to the inflammation site and, within the liver, its pro-inflammatory effect contributes to liver damage (Lee et al., 2011; de Menezes et al., 2019). Upon activation, neutrophils release neutrophil serine proteases (NSPs), which further amplify pro-inflammatory cytokines and promote hepatic steatosis (Mirea et al., 2018). Therefore, the decreased *Il1α* expression observed in *Polr3b*$^{+/-}$ mice may indicate a potential role of Pol III activity in regulating inflammatory pathways linked to steatosis development. Consistent with this, Bonhoure *et al.* (2015) reported that mice lacking Pol III repressor MAF1 were resistant to obesity and hepatic steatosis. Collectively, these findings

may point toward a potential role of Pol III in hepatic steatosis formation, potentially through modulation of IL1-α-driven neutrophil activation and inflammatory signalling. However, no difference in steatosis was observed in the liver histology of *Polr3b*$^{+/-}$ mice. Future studies incorporating metabolic challenge paradigms, such as high-fat diet feeding, may help determine whether reduced Pol III activity modifies susceptibility to hepatic steatosis.

mTOR activation can promote Th17 cell proliferation (Chang et al., 2013). Upon activation, IL-23 sustains Th17 cells and enhances their production of IL-17 and IL-22, leading to the chemokine-mediated recruitment of neutrophils and strengthening of the epithelial barrier function (Chang et al., 2013; Valeri & Raffatellu, 2016). Although IL-22 primarily acts on epithelial barriers in mucosal tissues, this cytokine is also active in the liver, where hepatocytes and cholangiocytes maintain epithelial features during infection and chronic inflammation (Huang et al., 2016; Rutz et al., 2013; Valeri & Raffatellu, 2016). Unchanged expressions of *Il22* and *Jam-a* in the liver of *Polr3b*$^{+/-}$ mice suggest that Pol III activity does not substantially affect hepatic epithelial barrier integrity and cholangiocyte function (Rutz et al., 2013; Salas-Silva et al., 2021). On the other hand, IL-17A, the predominant isoform of IL-17, is a tumour-promoting cytokine that amplifies hepatic inflammation through activation of Kupffer cells and other hepatic immune populations (Ma et al., 2020). Not only that, but the IL-17 receptor (IL-17R) also activates hepatic stellate cells to produce collagen type I and cause liver fibrosis (Ma et al., 2016). This raises the possibility that upregulated *Il17*α in the liver of *Polr3b*$^{+/-}$ mice may lead to a higher potential for hepatic fibrosis. However, Masson's trichrome staining revealed no significant differences in collagen deposition between genotypes, suggesting that the partial Pol III loss in this *Polr3b*$^{+/-}$ mouse model is insufficient to induce structural fibrosis, even in the presence of pro-inflammatory cytokine elevation.

A further limitation of this study is that whole-liver tissue was used for gene expression analysis. The liver contains hepatocytes, Kupffer cells, hepatic stellate cells, endothelial cells, cholangiocytes and infiltrating immune cells, each of which may respond differently to changes in Pol III activity (Liu et al., 2024). Therefore, a cell-type-specific phenotype may be diluted when analysed

at the whole-tissue level. Cell-type-specific approaches would be particularly useful in future studies. For example, hepatocyte-specific Pol III reduction could clarify whether Pol III directly regulates lipid handling, protein synthesis demand and hepatocyte stress responses. Kupffer cell- or myeloid-specific approaches could determine whether the changes in *Il1α* and *Il17α* reflect altered immune-cell activation (Weston et al., 2019; Zhao et al., 2025). Stellate cell-specific models would help establish whether Pol III contributes to fibrotic signalling and collagen deposition (Kamm & McCommis, 2022).

6.6 CONCLUSION

The findings demonstrate that heterozygous loss of Polr3b does not alter gross hepatic morphology, hepatocyte phenotype, lipid accumulation, fibrosis, or senescence marker expression p16 and p21 under chow-fed conditions, although modest sex-specific inflammatory changes were detected in male mice. Despite altered *Il1α* and *Il17α* expression, no corresponding histological evidence of fibrosis or inflammatory loci change was detected, indicating that the degree of Pol III reduction achieved in the heterozygous model is insufficient to substantially disrupt liver homeostasis under baseline physiological conditions. These findings contrast with previous studies linking Pol III, MAF1 and TFIIIB dysregulation to hepatic steatosis, metabolic dysfunction and liver pathology under metabolically stressed or disease-associated conditions, indicating that additional metabolic or inflammatory challenge may be required to reveal a stronger hepatic phenotype. Future studies using high-fat diet paradigms, advanced ageing cohorts, and cell-type-specific Pol III knockdown models will be important to clarify how Pol III activity contributes to hepatic metabolic regulation, inflammatory signalling and regenerative pathways. Moreover, the histological assessments were performed without blinding to genotype or sex, which may introduce potential observer bias. Although quantitative measurements reduce subjectivity, the absence of blinding in this study should still be considered a methodological limitation.

Chapter 7: General discussion

7.1 RNA Polymerase III as a regulator of translational capacity and tissue adaptation

RNA Polymerase III (Pol III) is a highly conserved, 17-subunit enzyme responsible for transcribing short non-coding RNAs (including tRNAs and 5S rRNA) that are essential for protein synthesis (Moir & Willis, 2013; Willis & Moir, 2018). Recent cryo-EM studies of human Pol III have further resolved the structural organisation of the 17-subunit complex, including the catalytic core formed by POLR3a and POLR3b and the arrangement of subunits involved in transcription initiation, elongation and termination (Girbig et al., 2021; Ramsay et al., 2020). Pol III activity is tightly regulated by nutrient-sensing pathways TORC1 through the Pol III repressor MAF1 (Moir & Willis, 2013). A reduction in Pol III activity has been shown to extend lifespan in lower organisms from yeast to flies (Filer et al., 2017; Malik, Goncalves Silva, et al., 2024). Notably, Filer et al. (2017) also demonstrated that this longevity effect in invertebrates is accompanied by preserved gut health, reduced protein synthesis, and increased tolerance to proteostatic stress, which are considered hallmarks of an improved healthspan. In mammals, *Polr3b*$^{+/-}$ mice did not show an increased lifespan (**Figure 7-1**), but they displayed health improvements, including enhanced bone health, preserved gut integrity, and increased tolerance to proteostatic stress during ageing that varied by sex and/or organ (Borland et al., 2024; Malik, Kulaberoglu, et al., 2024). The present study aimed to investigate how a partial reduction in Pol III activity, achieved through *Polr3b* heterozygosity (*Polr3b*$^{+/-}$), affects molecular, physiological, and reproductive functions in mice. Specifically, it examined how *Polr3b* heterozygosity influences (1) molecular markers related to Pol III activity, (2) cutaneous maintenance, (3) skin physiology, and (4) liver structure and inflammatory signalling.

Collectively, the findings presented in this thesis suggest that partial reduction of Pol III function in mammals produces complex and context-dependent physiological effects rather than a uniform suppression of tissue function. The tissue-specific vulnerability to altered Pol III activity reflects differences in translational demand as well as context-dependent regulation of Pol III

transcription (Watt et al., 2023). Furthermore, although changes were detected across metabolic, reproductive, and ageing-related phenotypes, the overall effects observed under baseline conditions were relatively modest. This is consistent with the broader physiological robustness of mammalian systems, in which partial genetic perturbations may be tolerated while preserving core tissue function (El-Brolosy & Stainier, 2017; Nijhout et al., 2019). In the current model, residual *Polr3b* expression from the intact allele may have been sufficient to maintain physiological function under basal conditions. Together, these findings support the idea that, in higher vertebrates including mammals, Pol III function extends beyond maintaining basal translational capacity and may contribute to tissue-specific physiological adaptation.

To understand the physiological consequences of altered Pol III activity within complex hierarchy biology system, Pol III can be viewed as an important interface linking nutrient sensing pathways with translational homeostasis. Under nutrient-replete conditions, mTORC1 signalling suppresses MAF1-mediated repression of Pol III, thereby promoting transcription of tRNAs and other small untranslated RNAs required for efficient protein synthesis. Conversely, nutrient limitation or TOR inhibition activates MAF1 and reduces Pol III transcriptional output (Moir & Willis, 2013; Turowski & Tollervey, 2016). Because translational regulation is closely integrated with proteostatic maintenance and cellular stress adaptation, even subtle alterations in Pol III activity may differentially affect tissues with high anabolic demand, elevated regenerative turnover, or increased sensitivity to proteotoxic stress (Morimoto, 2020; Su & Dai, 2017; Watt et al., 2023). In this context, altered Pol III function not only influence translational capacity, but also downstream processes including protein quality control, autophagic turnover, stress signalling, and inflammatory responses (Su & Dai, 2017; Willis & Moir, 2018). Therefore, the findings presented here are consistent with the possibility that a partial loss-of-function in Pol III reduction as a result of the global heterozygous loss of *Polr3b* alters the regulation or adaptability of translational capacity rather than inducing major global suppression of protein synthesis. Although substantial reductions in puromycin incorporation were not consistently observed across tissues, selective alterations in tissue integrity, inflammatory signalling and reproductive phenotypes suggest that some physiological systems such as liver, brain, reproductive and cutaneous systems that exhibit increased cellular demand, higher regenerative turnover,

proteostatic burden or complex endocrine regulation, may be more sensitive to subtle changes in translational regulation.

7.2 Pharmacological modulation of TOR-Pol III signalling

The close relationship between mTOR signalling and Pol III-dependent transcription also raises potential pharmacological implications. Inhibition of mTOR signalling by compounds such as rapamycin suppresses anabolic processes including ribosome biogenesis and protein synthesis, partly through MAF1-mediated repression of Pol III transcription (Michels et al., 2010). Since elevated mTOR and Pol III activity are closely associated with increased biosynthetic demand and cellular proliferation, modulation of the TOR-MAF1-Pol III axis has also attracted interest in cancer biology and age-associated disease research.

In addition to indirect modulation through mTOR inhibition, direct pharmacological targeting of Pol III has also been explored experimentally. The small-molecule compound ML-60218 was identified as an inhibitor of Pol III transcription and has primarily been used in mechanistic studies investigating Pol III function (Wu et al., 2003). More recent transcription-targeting compounds such as BMH-21, which primarily inhibits Pol I activity but can also affect Pol III-associated transcription to a lesser extent, further highlight growing interest in therapeutic modulation of RNA polymerase-dependent biosynthetic pathways in highly proliferative cells (Jacobs & Schneider, 2024).

However, the findings from the present study together with previous mammalian models suggest that the physiological consequences of altered Pol III activity are highly context dependent. Despite global heterozygous reduction of *Polr3b*, the phenotypic effects observed in the present study differed substantially between tissues and sexes, with relatively modest hepatic changes but increased susceptibility to ageing-associated skin pathology in females. These findings suggest that therapeutic modulation of the TOR-MAF1-Pol III axis in mammals may produce complex tissue-specific effects beyond simple suppression of anabolic activity, particularly in tissues with high biosynthetic, regenerative or inflammatory demand.

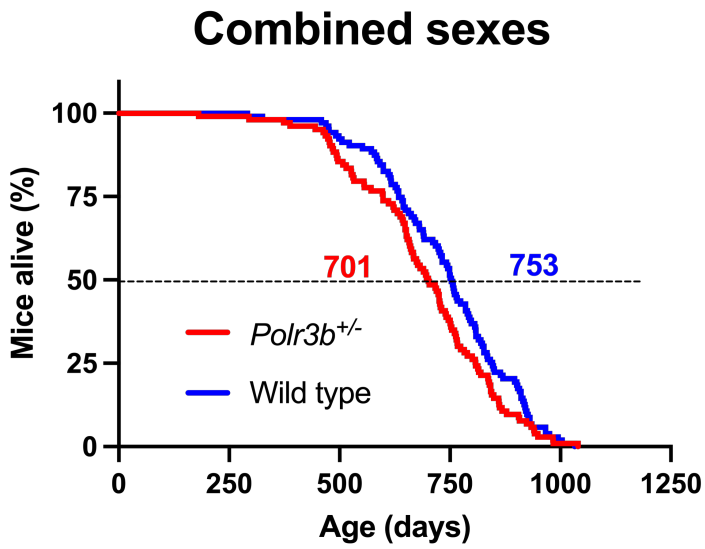

Figure 7-1 Kaplan-Meier survival curves for combined female and male WT and *Polr3b*$^{+/-}$ mice (combined sexes)

Survival curves comparing WT and Polr3b$^{+/-}$ *mice of both sexes combined. No significant difference in survival was observed (Log-rank* X^2*=3.084, p=0.079; n=103 per genotype). Figure reproduced from Borland et al. (2024) with permission from the authors.*

7.3 Summary of key findings from each chapter

In **Chapter 3**, I examined how global heterozygous knockout of *Polr3b* (*Polr3b*$^{+/-}$) affects Pol III-related cascade kinases and protein synthesis in 4-month-old female and male mice. I expected that *Polr3b* expression and protein synthesis would be down given that Pol III is involved in protein synthesis (Willis & Moir, 2018). To test these, I measured the mRNA expression and protein levels of the core Pol III subunits (*Polr3b* and *Polr3a*), the Pol III repressor *Maf1*, the TORC1 activity (assessed by S6 phosphorylation), and the protein synthesis across multiple tissues of liver, brain, skeletal muscle, and primary dermal fibroblasts, from female and male *Polr3b*$^{+/-}$ and WT mice. The major finding of this chapter was that *Polr3b*$^{+/-}$ exerts variable tissue- and sex-specific effects (**Figure 7-2**). In males, *Polr3b* mRNA expression was significantly decreased in the liver and brain, whereas females showed no reduction in transcript levels in any tissue but skin (result from chapter 6). At the protein level, the pattern was reversed: female *Polr3b*$^{+/-}$ mice displayed a pronounced reduction in POLR3b protein in the liver, while no difference was observed in males. Expression of the partner catalytic subunit *Polr3a* remained unchanged across all tissues and sexes. This suggests that there is no compensatory transcriptional or translational regulation of Polr3a in response to partial loss of *Polr3b*.

Changes in the Pol III repressor *Maf1* were similarly variable across sexes and tissues. An increase in *Maf1* mRNA expression was observed in the male liver, whereas *Maf1* transcript levels remained unchanged in the brain and skeletal muscle of males. Additionally, no alterations were seen in any tested tissues in females. At the protein level, however, the MAF1 protein level was reduced in dermal fibroblasts from both sexes, suggesting the possible interaction of Pol III signalling and MAF1. The mTORC1 activity, as measured by the ratio of phosphorylated to total S6, remained unchanged in all tissues. Despite stable mTORC1 activity, *Polr3b*$^{+/-}$ female mice exhibited evidence of reduced proteostatic capacity, as brain tissue from female *Polr3b*$^{+/-}$ mice showed significantly lower rates of puromycin incorporation, reflecting reduced protein synthesis. Taken together, these data reveal that the consequences of *Por3b* heterozygosity in this *Polr3b*$^{+/-}$ mouse model are tissue- and sex- dependent. It might be because Pol III transcripts and Pol III subunits are expressed differently across tissues and cell types (Watt et al., 2023). A more robust and tissue-

targeted knockout strategy would be required to achieve a more consistent reduction in Pol III activity.

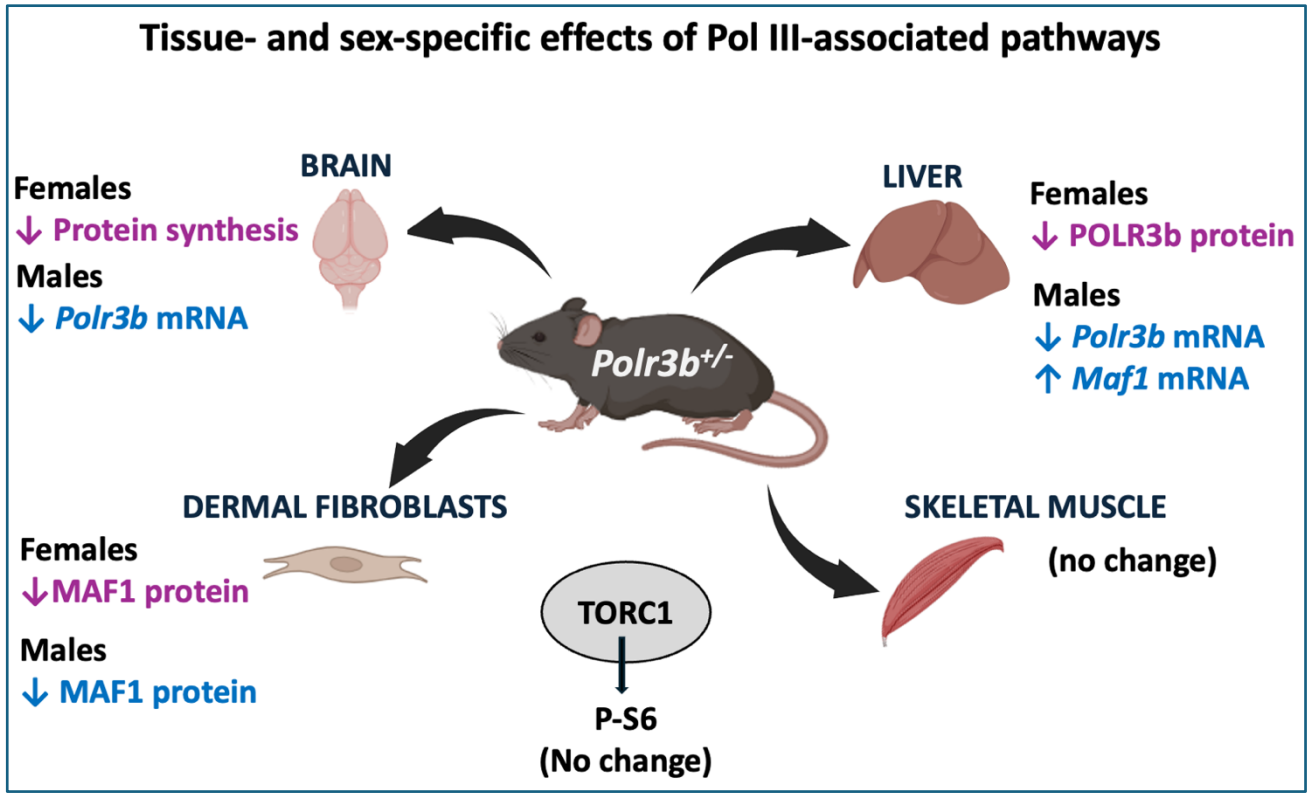

Figure 7-2 Summary of tissue- and sex-specific effects

Schematic diagram summarising the major findings from Chapter 3. Polr3b$^{+/-}$ resulted in tissue- and sex-specific outcomes across tissues. In the liver, changes in Polr3b and Maf1 expression as well as POLR3b protein level were detected; In the brain, changes in Polr3b expression and protein synthesis were detected; In dermal fibroblasts, changes in MAF1 protein level were detected. No changes in terms of Polr3b, Porl3a, Maf1 expressions and POLR3b protein level were observed in the skeletal muscles.

In **Chapter 4**, I investigated the impact of reduced Pol III on reproductive performance, including fertility, litter outcomes, and offspring development. Given the central role of Pol III in synthesising small non-coding RNAs necessary for protein synthesis and growth (Willis & Moir, 2018) (**Figure 7-3**), I hypothesised that a reduction in Pol III might impair reproductive capacity or alter offspring development.

The results demonstrated that *Polr3b* expression was reduced in the testis but not in the ovary of *Polr3b*$^{+/-}$ mice, indicating tissue-specific variations in *Polr3b* expression. This finding is consistent with the other chapters' results (Chapters 3 and 5) that Polr3b expression is not uniform across tissues or sexes in this mouse model. Watt et al. (2023) highlighted that expression of Pol III subunit and their downstream transcripts vary across tissue types, often resulting in distinct phenotypic outcomes when Pol III activity is perturbed globally. To assess reproductive performance, I used a reciprocal breeding strategy in which *Polr3b*$^{+/-}$ and WT mice were crossed in both parental orientations (see **Chapter 4 Figure 4-1**). Each pair was continuously housed and allowed to produce up to four litters. I found that the interval from mating to the first litter was unaffected. However, *Polr3b*$^{+/-}$ mice produced larger litters than WT controls across all four litters. This increase in litter size occurred irrespective of whether the *Polr3b*$^{+/-}$ parent was female or male, indicating that this effect was not limited to a specific parental sex. Interestingly, studies using *Maf1*$^{-/-}$ mice, which lack the key repressor of Pol III, reported reduced litter sizes (Bonhoure et al., 2015; Bonhoure et al., 2020), suggesting that Pol III may play an important role in controlling litter size in mice.

Examination of offspring growth revealed that male pups were significantly lighter at weaning when either parent carried the *Polr3b*$^{+/-}$ genotype, whether from *Polr3b*$^{+/-}$ females crossed with the C57BL/6N males or *Polr3b*$^{+/-}$ males crossed with C57BL/6N females. In contrast, female pups were unaffected. This sex-specific outcome may indicate sex-specific vulnerability to early-life metabolic constraints or maternal resource allocation (Alur, 2019; Stark et al., 2011), that male pups might be more susceptible to growth and metabolic disruption in response to biosynthetic stress caused by Pol III reduction. In addition, pups born to *Polr3b*$^{+/-}$ breeders showed higher pre-weaning mortality. Importantly, these reproductive effects could not be explained by altered pup

genotypes or skewed sex ratios, as both followed the expected 1:1 ratio. This further suggests that the reproductive phenotypes observed in *Polr3b*$^{+/-}$ breeders are unlikely to be explained by pup genotype or sex-specific survival effects, but rather by parental genotype effects and potentially sex-specific differences in offspring vulnerability.

At the molecular level, reduced *Cyp19a1* (aromatase) expression was detected in the ovaries of *Polr3b*$^{+/-}$ females. Given the central role of aromatase in converting androgens to oestrogens, this reduction may lead to decreased oestradiol synthesis, which is critical for follicular development, oocyte maturation, and overall female fertility (Cheng et al., 2022; Hussain & Gilloteaux, 2020; Luo et al., 2024). Further study should test the level of oestrogens in ovaries and plasma to critically confirm this finding.

The findings from **Chapter 4** also revealed that *Polr3b*$^{+/-}$ breeders exhibited a reproductive profile marked by increased litter size at birth, but this was accompanied by elevated pre-weaning mortality and reduced male pup weight. While the increased number of pups per litter at birth may reflect enhanced early reproductive output, the concurrent rise in neonatal losses and sex-specific growth impairments points to an underlying cost in offspring quality (Chahoud & Paumgartten, 2009; Stearns, 1992). Notably, the lower body weight was restricted to male pups, consistent with prior evidence that male offspring are more vulnerable to intrauterine stress and metabolic disruption (Alur, 2019; Geary et al., 2003; Ibanez et al., 2008; Mayhew et al., 2008; Stark et al., 2011). These findings align with life-history theory, which predicts that when biosynthetic capacity is constrained (as would be expected under reduced Pol III activity), organisms may prioritise reproductive output at the expense of individual offspring investment (Chahoud & Paumgartten, 2009; Stearns, 1992). The partial reduction in Pol III activity, therefore, appears to shift the reproductive strategy of *Polr3b*$^{+/-}$ mice toward higher quantity at birth but lower-quality offspring. Collectively, Chapter 4 results provide evidence that Pol III signalling contributes to the regulation of reproductive capacity and offspring viability.

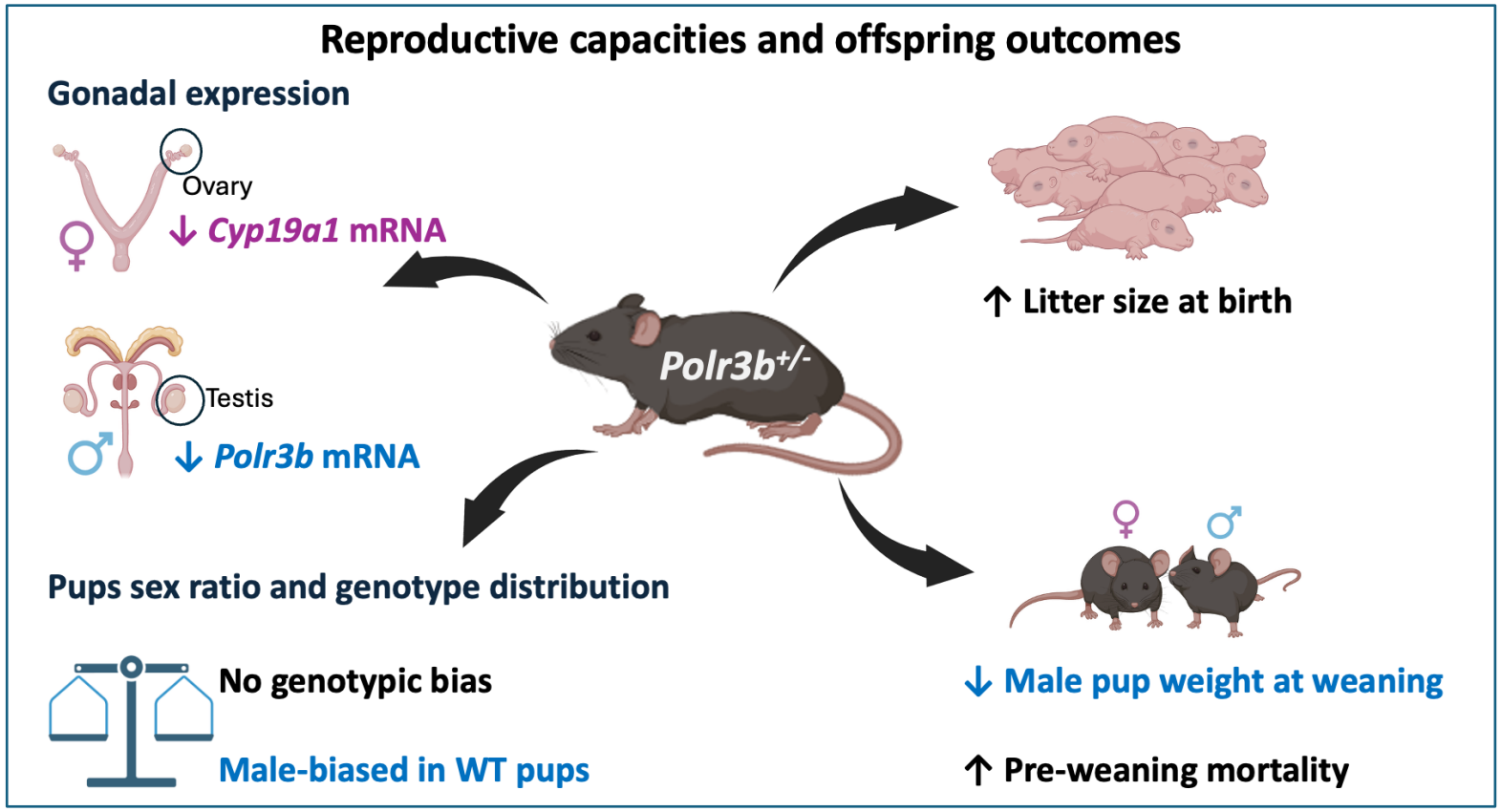

Figure 7-3 Reproductive capacities and offspring outcomes of *Polr3b*$^{-/+}$ mice

Graphical summary of the reproductive findings presented in Chapter 4. In summary, Polr3b$^{+/-}$ breeders of both sexes produced larger litters at birth compared with their WT controls. However, these litters exhibited higher pre-weaning mortality and reduced male pup weight at weaning. At the molecular level, testicular Polr3b expression was reduced, and ovarian Cyp19a1 expression was also lower in Polr3b$^{+/-}$ mice.

In **Chapter 5**, I investigated how reduced Pol III affects skin health and age-associated changes. Borland et al. (2024) had previously observed that *Polr3b*$^{+/-}$ females showed a greater incidence of idiopathic dermatitis (ID) (**Figure 7-4**). I therefore examined how reduced Pol III activity in influences skin integrity, inflammatory status, and age-related changes in female mice (**Figure 7-5**). Firstly, I found that *Polr3b* mRNA expression was significantly reduced in the skin of *Polr3b*$^{+/-}$ females, confirming Pol III reduction. This reduction was associated with a markedly higher incidence and earlier onset of ID, particularly in females, accompanied by increased disease severity and a greater proportion of animals requiring euthanasia due to the dermatitis. These clinical outcomes coincided with elevated systemic inflammation, evidenced by higher plasma IL-6 levels and more frequent splenomegaly in affected females, suggesting a higher inflammatory state. Despite these pathological findings, the overall skin architecture remained unaffected relatively to WT females, with no genotypic differences in epidermal or dermal thickness at both 14 and 20 months of age. However, *Polr3b*$^{+/-}$ females showed fewer degranulating dermal mast cells, suggesting reduced local immune activation and insufficient wound repair (Wulff & Wilgus, 2013; Younan et al., 2011), *Polr3b*$^{+/-}$ females also showed a significant increase in dermal collagen content. Excessive collagen deposition is known to impair wound healing and skin flexibility, and is commonly associated with fibrotic responses (El Ayadi et al., 2020; Jinnin, 2010; Wynn, 2008). Furthermore, elevated expression of chemokines *Ccl20* and *Cxcl15* in the skin suggests dysregulated inflammatory signalling that may promote inflammation and collagen synthesis (Bandow et al., 2023; Li et al., 2017).

Collectively, these findings suggest that reduced Pol III activity compromises cutaneous resilience through dysregulated immune signalling and altered extracellular matrix composition. In *Polr3b*$^{+/-}$ females, this was reflected by increased dermal collagen deposition and reduced mast cell degranulation, both of which may impair wound healing and exacerbate inflammatory skin pathology. These mice also showed elevated systemic IL-6 and local upregulation of *Ccl20* and *Cxcl15*, indicating a pro-inflammatory state. Notably, *Ccl20* has been reported to promote collagen synthesis (Bandow et al., 2023), suggesting that its increased expression in *Polr3b*$^{+/-}$ skin may contribute to fibrosis-like changes. In addition, suppression of *Ccl20* expression has been associated with reduced skin

inflammation in mouse models of psoriasis (Li et al., 2017), further implicating this chemokine in dermal pathology. Together, these observations support a model in which Pol III deficiency enhances inflammatory state and tissue remodelling, predisposing female mice to more severe ID. This female bias in ID susceptibility aligns with prior reports (Kastenmayer et al., 2006; Sargent et al., 2015), and may reflect sex-specific immune responses, although hormonal contributions remain to be explored. Moreover, dysregulation of the Pol III-associated immune-sensing Pol III-RIG-I pathways can also lead to immune diseases and cancer, further illustrating the role of Pol III in immune regulation (Naesens et al., 2023). These findings build on the role of Pol III in immune regulation and skin homeostasis, and highlight the need for further studies investigating the cutaneous health under the influences of sex hormones and immune signalling under the conditions of reduced Pol III activity.

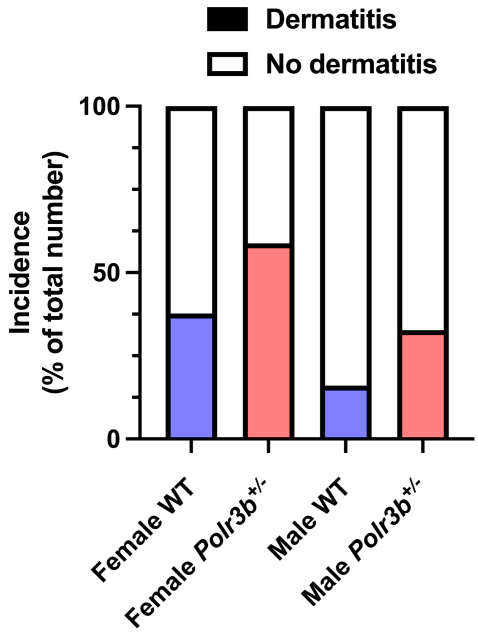

Figure 7-4 Percentage of mice (of total number) presenting with idiopathic dermatitis.

The chi-square test showed that Polr3b$^{+/-}$ female mice had a significantly higher risk of idiopathic dermatitis compared to the WT females (RR=1.559, 95% CI [1.040-2.392], P=0.031). Figure reproduced from Borland et al. (2024) with permission from the authors.

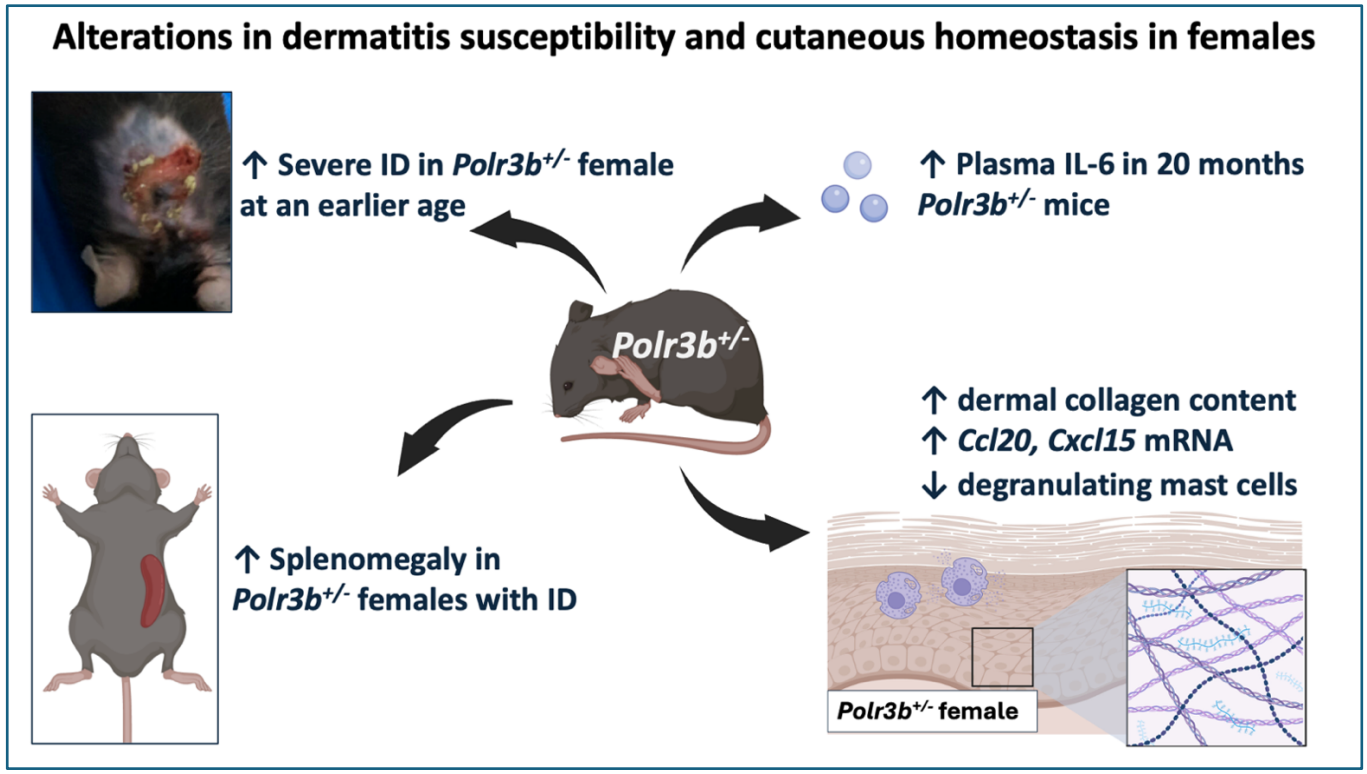

Figure 7-5 Alterations in idiopathic dermatitis susceptibility and cutaneous homeostasis in *Polr3b*$^{+/-}$ female mice

Graphical summary of the skin-related findings presented in Chapter 5. Polr3b$^{+/-}$ female mice exhibited a higher incidence, earlier onset, and greater severity of ID compared with WT females. This increased susceptibility was accompanied by systemic inflammation, reflected by elevated plasma IL-6 and increased splenomegaly in affected mice. Polr3b$^{+/-}$ females also showed reduced mast cell degranulation, greater dermal collagen accumulation, and upregulated inflammatory chemokines Ccl20 and Cxcl15, suggesting low-grade immune dysregulation and fibrosis-like remodelling.

In **Chapter 6**, I examined whether reduced Pol III activity affects liver structure, inflammatory balance, and age-related molecular markers in 20-month-old *Polr3b*$^{+/-}$ mice of both sexes, given the liver's central role in protein homeostasis and metabolic regulation. I assessed histological, molecular, and morphological measures to evaluate hepatic consequences of *Polr3b* heterozygosity. The main findings were that *Polr3b* mRNA expression was significantly reduced in the liver of *Polr3b*$^{+/-}$ mice of both sexes, confirming effective Pol III reduction in the liver of the *Polr3b*$^{+/-}$ mice. There were no genotypic differences in liver weight (as a percentage of total body weight), hepatocyte morphology, polyploidy, or liver tumour incidence. Additionally, the liver-to-body weight ratio in both *Polr3b*$^{+/-}$ and WT mice fell within the expected 3-5% range for healthy livers (Pritchard & Apte, 2015). All these findings suggest that overall liver function, tissue architecture, and regenerative capacity were preserved in *Polr3b*$^{+/-}$ mice. Males consistently showed larger hepatic lipid droplets than females, indicating sex-related differences in lipid metabolism independent of genotype. At the molecular level, *Polr3b*$^{+/-}$ males had reduced *Il1α* and increased *Il17α* mRNA expression, while other cytokines (*Il6, Il1β, Tnfα, Il22, Il23α, Il10*), chemokines (*Ccl20, Cxcl15*), and senescence markers (*p16, p21*) remained unchanged across sexes and genotypes. No genotypic differences in hepatic collagen deposition or inflammatory foci were observed, and no structural or histopathological abnormalities were detected in the liver. Together, these findings suggest that partial Pol III reduction in *Polr3b*$^{+/-}$ mice does not overtly impair hepatic integrity, inflammatory balance, or fibrosis.

The sex-specific increase in *Il1α* and *Il17α* expression observed in *Polr3b*$^{+/-}$ males suggests sexually dimorphic immune modulation in the liver. This pattern is consistent with broader tissue- and sex-dependent phenotypes previously observed in *Polr3b*$^{+/-}$ mice, including increased bone mass, greater susceptibility to idiopathic dermatitis, and impaired gut barrier function in *Polr3b*$^{+/-}$ females, as well as improved intestinal integrity in *Polr3b*$^{+/-}$ males (Borland et al., 2024). Such divergent phenotypes are consistent with the previous findings of variation in *Polr3b* mRNA and protein levels across tissues and between sexes (Chapter 3-6), which likely contributes to the heterogeneity observed in the physiological outcomes. Notably, because POLR3b is only one of the two essential catalytic subunits of Pol III, partial loss of POLR3b alone may not be insufficient to

substantially diminish overall Pol III activity. In contrast, targeted suppression of the other core subunit, POLR3a, has been shown to extend lifespan and improve healthspan in invertebrate models of *C. elegans* and *D. melanogaster* (Filer et al., 2017; Malik, Goncalves Silva, et al., 2024). This suggests that future mouse models directly targeting POLR3a, or employing conditional knockdowns, may yield a more robust reduction in Pol III activity, leading to more consistent and pronounced physiological effects.

Finally, the prior study showed that dermal fibroblasts from *Polr3b*$^{+/-}$ mice showed improved tolerance to proteostatic stress under experimental challenge (Malik, Kulaberoglu, et al., 2024). However, the mice in the present study were maintained under standard, non-stressful laboratory conditions, which may have masked phenotypes that would only emerge in metabolically challenged environments. Indeed, Bonhoure et al. (2015) reported that *Maf1*$^{-/-}$ mice exhibiting enhanced Pol III activity on a chow diet showed limited hepatic differences, while a high-fat diet revealed clear metabolic phenotypes such as obesity resistance against hepatic steatosis. Therefore, future studies using tissue-specific Pol III knockdowns and introducing metabolic stressors such as HFD may be required to unmask latent Pol III-linked phenotypes, particularly those involving stress responses or metabolic resilience.

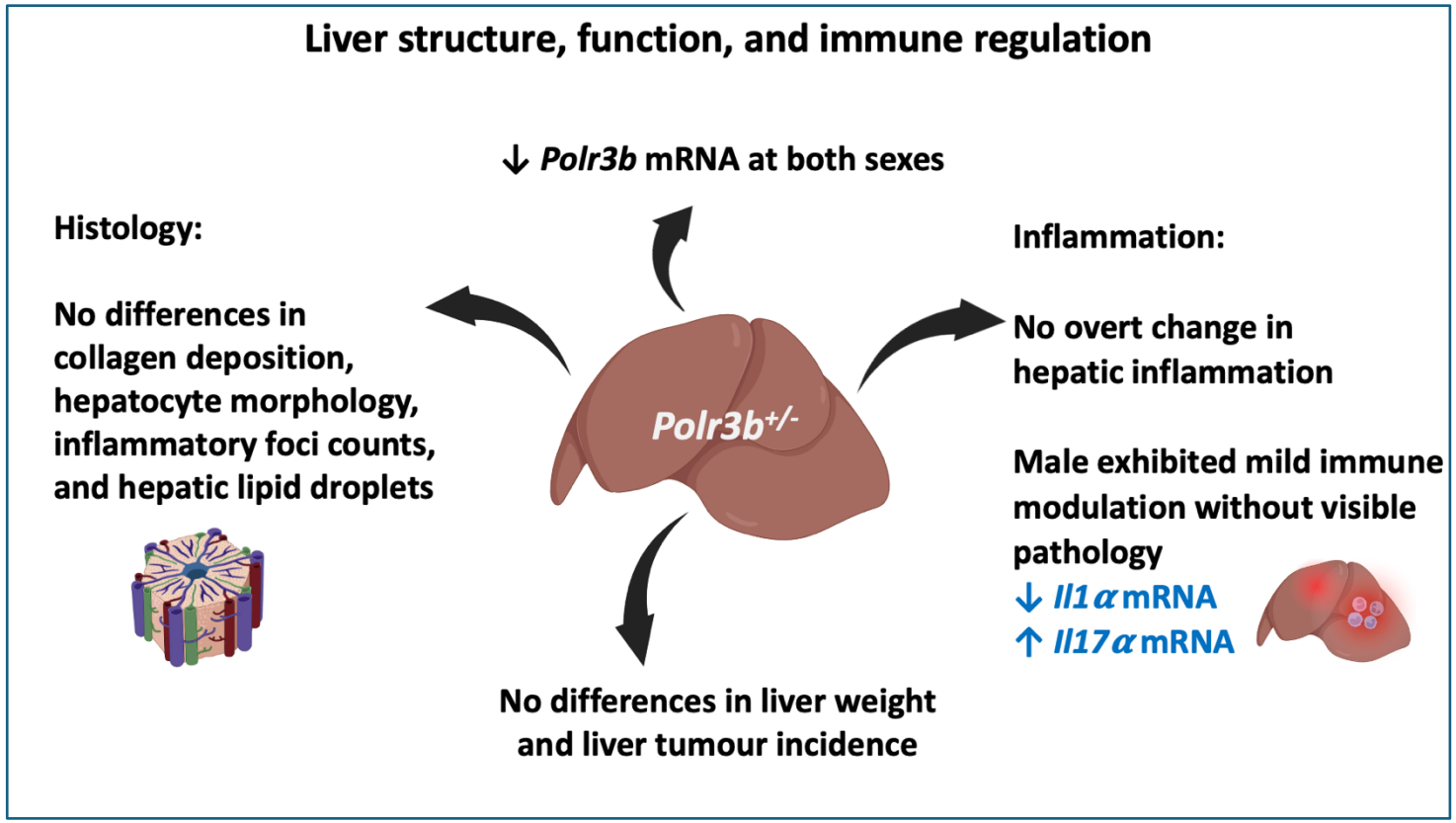

Figure 7-6 Hepatic function, structure, and immune balance in *Polr3b*$^{+/-}$ mice

Graphical summary of the findings presented in Chapter 6. Despite reduced Polr3b expression confirming partial Pol III knockout in the liver. No morphological alterations were observed between Polr3b$^{+/-}$ *and WT mice of both sexes. Liver weight, hepatocyte size, nuclear morphology, polyploidy, and collagen deposition remained unchanged, indicating preserved hepatic architecture. At the molecular level, Polr3b*$^{+/-}$ *males showed reduced Il1α and increased Il17α expression.*

7.4 Mechanisms underlying tissue- and sex-specific responses to Pol III reduction

The selective nature of the phenotypes observed across tissues suggests that the physiological consequences of global heterozygous loss of *Polr3b* are likely influenced by differences in tissue-specific translational demand and regenerative capacity. Tissues characterised by rapid cellular turnover or high biosynthetic activity may be more sensitive to altered Pol III regulation due to increased reliance on efficient tRNA synthesis and translational coordination.

In the liver, only relatively modest phenotypic alterations were observed despite detectable changes in inflammatory markers and sex-dependent differences in protein expression. This may be due to the substantial metabolic adaptability and regenerative capacity of hepatic tissue, which could buffer moderate reductions in Pol III function under baseline conditions (Hunt et al., 2019; Michalopoulos, 2017). In contrast, the increased prevalence of ageing-associated skin lesions observed in female *Polr3b*$^{+/-}$ mice may indicate greater sensitivity of highly regenerative epithelial tissues to altered translational regulation, particularly in the context of ageing-associated proteostatic decline, inflammatory signalling and extracellular matrix remodelling processes (Eckhart et al., 2019). Skin tissue may be particularly sensitive to subtle alterations in translational homeostasis due to its high cellular turnover and dependence on tightly coordinated mTOR-responsive repair and inflammatory pathways (Wang et al., 2022).

Reproductive tissues may similarly display selective sensitivity to partial Pol III reduction due to the substantial translational demands associated with gametogenesis, endocrine regulation and early developmental support. In the present study, reduced testicular *Polr3b* expression, altered ovarian *Cyp19a1* expression, increased litter size and higher pre-weaning mortality together suggest that moderate disruption of Pol III activity may influence reproductive homeostasis without causing overt gonadal pathology. Spermatogenesis and ovarian function both rely heavily on coordinated translational control and RNA regulatory pathways, particularly during germ cell maturation and hormonally responsive stages of reproduction (Mercer et al., 2021; Stocco, 2008). It is therefore possible that reproductive tissues are more sensitive to subtle

alterations in Pol III-dependent RNA synthesis, which may contribute to the changes in offspring viability and sex-dependent phenotypes observed in this study.

Apart from the tissue variability, another recurring feature of this thesis is that the effects of *Polr3b* haploinsufficiency were not the same in females and males. This was observed at several levels, including the mismatch between *Polr3b* mRNA and POLR3b protein levels, male-specific hepatic cytokine changes, increased ageing-associated skin lesions in females, reduced ovarian *Cyp19a1* expression, and reduced male pup weight. These findings suggest that the physiological consequences of global heterozygous *Polr3b* loss are modified not only by tissue type but also by sex-dependent regulatory mechanisms.

One possible explanation for these divergent responses is that Pol III reduction interacts with sexually dimorphic regulation of protein homeostasis and nutrient-responsive signalling pathways. In the present study, reductions in *Polr3b* mRNA and POLR3b protein were not consistently matched across tissues and sexes, suggesting that post-transcriptional regulation and protein turnover contribute substantially to the phenotypes. This is consistent with previous evidence showing that mRNA abundance does not always directly predict protein levels due to variation in translation efficiency, protein turnover and degradation dynamics (Liu et al., 2016).

Sex hormones may further modify these responses through interactions with nutrient-sensing pathways. Oestrogen signalling interacts closely with insulin-PI3K-Akt-mTOR signalling and contributes to the regulation of protein turnover, mitochondrial metabolism and metabolic homeostasis (Tao & Cheng, 2023). Previous studies have also shown that rapamycin treatment produces sex-specific effects on protein synthesis and proteostatic regulation in mouse tissues (Wolff et al., 2021). Together, these findings suggest that female and male tissues may not regulate translational demand and proteostatic maintenance in the same way under conditions of altered mTOR-Pol III signalling.

This may help explain the sex-dependent phenotypes observed in the present study. Male *Polr3b*$^{+/-}$ mice exhibited altered hepatic expression of *Il1α* and *Il17α* despite the absence of overt liver pathology, whereas female *Polr3b*$^{+/-}$ mice

showed greater susceptibility to age-associated skin lesions. Sexual dimorphism in hepatic metabolism and inflammatory regulation is well established, with males generally showing greater susceptibility to inflammatory and metabolic liver dysfunction, partly due to lower oestrogen-mediated protection (Della Torre, 2020; Lonardo et al., 2019). Oestrogen signalling and sex hormone fluctuations in female animals additionally contribute to the regulation of skin homeostasis, wound repair and inflammatory responses, including hypersensitivity-related processes (Chen et al., 2008; Thornton, 2002). Given the close interaction between endocrine signalling, mTOR-associated metabolic pathways and protein turnover, sex-dependent endocrine regulation may influence how tissues adapt to reductions in Pol III-dependent translational capacity during ageing. Collectively, these findings suggest that the physiological consequences of altered Pol III activity are strongly influenced by tissue context, sex and metabolic state. Similar context-dependent effects have also been reported in previous invertebrate and mammalian models of altered Pol III signalling.

7.5 Comparison with previous models of altered Pol III signalling

The relatively modest and tissue-dependent phenotypes observed in the present study differ from several invertebrate models in which reduced Pol III activity promoted substantial lifespan extension and improved late-life physiology. Previous studies in *D. melanogaster* and *C. elegans* demonstrated that partial reduction of Pol III activity can extend lifespan when induced during adulthood (Filer et al., 2017; Malik, Goncalves Silva, et al., 2024). These studies further showed that Pol III function interacts closely with TOR signalling, particularly during post-developmental stages when anabolic growth requirements decline. Since Pol III synthesises tRNAs and 5S rRNA required for protein translation, reduced Pol III activity is thought to lower translational and biosynthetic demand downstream of TORC1 signalling. In flies, gut-specific Pol III inhibition improved intestinal dysfunction (Filer et al., 2017), while in *C. elegans*, adult-specific *rpc-1* knockdown improved late-life motility and muscle mitochondrial organisation (Malik, Goncalves Silva, et al., 2024). However, the physiological effects of partial Pol III reduction in mammals appear more variable and tissue dependent

than those observed in invertebrate systems. Borland et al. (2024) that using the same *Polr3b*$^{+/-}$ mouse model as the present study, reported both beneficial and detrimental ageing-associated phenotypes depending on tissue and sex. Male *Polr3b*$^{+/-}$ mice displayed preserved gut barrier integrity, whereas females showed increased intestinal permeability and susceptibility to ID. Similarly, the present study identified relatively subtle but tissue- and sex-specific alterations, including increased incidence and greater severity of skin lesions in female mice, modest hepatic inflammatory changes in males. These findings suggest that reduction of Pol III activity in mammals does not uniformly improve ageing-related phenotypes, but instead alters tissue homeostasis in a sex-dependent manner.

Several factors may contribute to the differences between mammalian and invertebrate responses to reduced Pol III activity. Unlike many invertebrate studies in which Pol III inhibition was induced during adulthood or targeted to specific tissues, the *Polr3b*$^{+/-}$ model represents lifelong constitutive heterozygous reduction of Pol III function across all tissues. Despite this global reduction, the physiological effects observed in both the present study and Borland et al. (2024) were highly tissue- and sex-dependent, suggesting compensatory buffering capacity in mammalian systems (Nijhout et al., 2019). This may reflect differences in translational demand, regenerative turnover and stress responsiveness between tissues. In addition, mammalian endocrine, metabolic and immune regulatory networks are considerably more complex than those of invertebrate systems and may modify how tissues adapt to altered Pol III-dependent translational activity during ageing.

Comparison with *Maf1* knockout mice further highlights the complexity of mTOR-Maf1-Pol III biology in mammals. MAF1 functions as a conserved repressor of Pol III transcription downstream of mTOR signalling (Willis & Moir, 2018). Unlike *Polr3b* haploinsufficiency, however, *Maf1* deficiency increases Pol III transcriptional activity (Bonhoure et al., 2020). Despite these opposing effects on Pol III regulation, *Maf1*$^{-/-}$ mice exhibited several beneficial metabolic phenotypes, including resistance to diet-induced obesity and hepatic steatosis together with female lifespan extension (Bonhoure et al., 2015; Bonhoure et al., 2020). Importantly, MAF1 has regulatory functions beyond Pol III repression alone. In mammalian cells, MAF1 can influence transcriptional regulation

through all three nuclear RNA polymerases and additionally contributes to metabolic regulation, including lipid metabolic pathways (Johnson et al., 2007; Palian et al., 2014). The diverse phenotypes observed between *Maf1*$^{-/-}$ and *Polr3b*$^{+/-}$ mouse models therefore suggest that the physiological consequences of altered Pol III signalling in mammals are shaped by broader metabolic and regulatory interactions that are likely more complex than those described in invertebrate models.

Importantly, many mammalian studies showed significant changes in phenotypes have examined animals under dietary or pathological stress conditions. For example, *Maf1* knockout mice displayed resistance to obesity and fatty liver following high-fat diet feeding, whereas the present study primarily examined aged chow-fed mice under baseline physiological conditions. It is therefore possible that partial reduction of Pol III activity exerts stronger effects during metabolic, inflammatory or regenerative challenge than under unstressed ageing conditions alone.

7.6 Conclusion

Overall, the findings from this thesis show that partial reduction in Pol III activity through loss-of-function in *Polr3b* heterozygosity produces subtle, tissue- and sex-dependent effects, rather than broad or systemic disruption. Although lifespan was not extended, and liver and skin structure remained largely preserved, several tissue-specific and sex-dependent phenotypes were observed. These included altered protein synthesis and *Maf1* expression in liver and brain, increased litter size at birth accompanied by higher pre-weaning mortality and reduced male pup weight, elevated susceptibility to idiopathic dermatitis in females, and mild inflammatory changes in the liver. These results support a modulatory role for Pol III in regulating protein synthesis, reproductive function, and immune homeostasis, with outcomes depending on both tissue context and sex.

7.7 Limitations and future directions

Several limitations should be considered when interpreting the findings of this thesis. First, the present study did not directly quantify Pol III transcriptional activity. Instead, conclusions regarding altered Pol III function were based on measurements of Polr3b expression, POLR3b protein abundance, and protein synthesis measurements. However, these measures do not directly assess real-time Pol III transcriptional output. Future studies should therefore incorporate more direct approaches to quantify Pol III activity, including pre-tRNA analysis, tRNA-seq or Pol III chromatin occupancy assays (Alla & Cairns, 2014; Bonhoure et al., 2020; Padhiar et al., 2024). Pre-tRNA analysis may be particularly informative because pre-tRNAs represent newly synthesised Pol III transcripts and more closely reflect ongoing transcriptional activity (Turowski & Tollervey, 2016).

Second, protein synthesis in the present study was assessed using puromycin incorporation, which provides an estimate of bulk translational activity but does not identify transcript-specific translational changes. This is important because partial reduction of Pol III activity may alter translation efficiency without necessarily causing a global reduction in protein synthesis. Future studies could therefore incorporate approaches such as ribosome profiling, polysome profiling or stable isotope labelling to determine whether *Polr3b*$^{+/-}$ tissues exhibit selective translational alterations in metabolic, inflammatory or stress-response pathways (Goodman & Hornberger, 2013; Ingolia et al., 2009; Rodriguez-Martinez & Young-Baird, 2025). Future work should also examine MAF1 regulation at the level of phosphorylation and subcellular localisation. In the present study, total MAF1 abundance was assessed; however, MAF1 activity is primarily regulated by mTORC1-dependent phosphorylation, which controls its nuclear localisation and repression of Pol III transcription (Michels et al., 2010; Shor et al., 2010). Assessment of phospho-MAF1 and nuclear localisation would therefore provide a more direct mechanistic link between nutrient signalling and Pol III regulation.

Third, the *Polr3b*$^{+/-}$ mouse model used in this thesis represents a global constitutive heterozygous reduction of Pol III function. While this model is useful for assessing the systemic consequences of partial Pol III reduction, it cannot

determine whether the observed phenotypes arise from direct tissue-specific effects or from systemic adaptations, and the phenotypes would not be clearly identified due to the systemic adaptations or under the baseline conditions. Future studies using tissue-specific knockouts or targeting the POLR3a subunit, as well as incorporating dietary or physiological stressors such as high-fat feeding or ageing beyond 20 months, may help uncover latent effects of reduced Pol III signalling. In terms of the tissue- or cell-type-specific approaches, neural-lineage Cre models including Nestin-Cre, or Olig2-Cre could be useful for investigating cell-type-specific responses in neural progenitors and oligodendrocyte-lineage cells, particularly given the established involvement of Pol III subunits in hypomyelinating leukodystrophy models (Matsuoka et al., 2005; Sclafani et al., 2006; Watt et al., 2023; K. Zhang et al., 2022). Moreover, since the present study identified subtle changes in skin pathology and reproductive biology, and previous MAF1 studies found alterations in liver metabolism, therefore the tissue-specific knock-out targeting skin, reproductive organs, and liver tissues would be also considered for future studies (Bonhoure et al., 2015; Bonhoure et al., 2020).

Additional physiological challenge paradigms may also help clarify the functional consequences of reduced Pol III activity. High-fat diet feeding, fasting refeeding paradigms, *in vivo* wound-healing assays, stress or inflammatory challenge could determine whether Pol III reduction alters tissue adaptation to increased metabolic, inflammatory or regenerative demand. This may be particularly relevant because several metabolic phenotypes associated with altered Pol III or MAF1 signalling become more pronounce under dietary stress conditions (Bonhoure et al., 2015; Palian et al., 2014).

Given the recurrent sex-specific findings identified throughout this thesis, endocrine profiling should also be considered in future work. Measurement of circulating oestradiol, testosterone, gonadotrophins, insulin and other metabolic hormones may help determine whether sex-dependent phenotypes are influenced by endocrine modulation. This may be particularly relevant for understanding the increased susceptibility to ageing-associated skin pathology observed in female *Polr3b*$^{+/-}$ mice.

Finally, the reproductive and skin phenotype identified in this thesis would benefit from more target molecular characterisation. Although paternal *Polr3b*$^{+/-}$ genotype did not significantly affect time to first litter or litter size, the reduced testicular *Polr3b* expression along with reduced male pup weight raises the possibility that sperm quality or sperm-borne RNA content may be altered. Sperm functional analysis together with small RNA or tRNA-derived small RNA (tsRNA) profiling may therefore help determine whether Pol III reduction influences paternal germline quality or offspring physiology (Chen et al., 2016; Sharma et al., 2016). In addition, transcriptomic approaches including lesion transcriptomics, spatial transcriptomics or single-cell RNA-sequencing could help define the molecular pathways underlying the increased ID phenotype observed in female *Polr3b*$^{+/-}$ mice, particularly with respect to inflammatory signalling, keratinocyte responses and extracellular matrix remodelling (Rodriques et al., 2019; Ståhl et al., 2016).

Appendix 1: Scripts of the statistical analyses

https://github.com/nnzwang0707/PhD-thesis-codes_ZW-2025

Appendix 2: Selman Lab Scoring/Endpoints

A typical median mouse life-span of C57Bl/6J mice is about 750-800 days when maintained on an ad libitum chow diet, while long-lived dietary restricted and genetic mutant mice have been shown to live as long as 1250 days, with a median lifespan around 900-950 days. Progeroid models, by definition, will have much reduced lifespans typically of several weeks or months. As mice age they will start to develop well established characteristics typical of ageing. It is often difficult to distinguish between age-related changes ('normal' ageing or senescence) from pathology as they both present as impairment. Since ageing/lifespan studies will mean that mice will experience normal ageing but also will be susceptible to diseases of old age, they will be monitored closely to ensure our pre-determined humane end-points are always applied; i.e. that clinical signs of ill health are identified and an informed decision is taken, including euthanasia if appropriate. Often aged mice die suddenly from natural causes with no overt signs of disease present prior to death or any obvious causes of death identified at post-mortem. Typically, most aged mice will experience one (or more) of these adverse effects from ~700 days of age (example C57BL/6J) but the likely incidence and age of onset is highly genotype and sex dependent.

Age-related characteristics observed in mice

1. Body weight will increase initially and peaks in middle age (15-18 months for wild-type mice) but as mice age their bodyweight will start to drop. In our published studies for an individual mouse a weight loss of ~30% occurring gradually over an 18 month period (i.e. ~1g/month) from their mid-life peak body mass as they age would be regarded as within normal limits for C57BL/6J mice. Our monitoring protocols are therefore aimed at managing acute weight loss that may indicate underlying disease rather than weight loss reflective of the ageing process.

2. Aged mice have reduced activity, may be less alert and may exhibit abnormal gait, e.g. circling, head tilt and an unstable, shuffling gait.

3. Changes in body condition

4. Hunched appearance

5. Scoliosis

6. Cataracts may form and general clouding and dry eyes indicative of infection

7. Greying and loss of fur, dirty, dull or unkempt coat, piloerection, dehydration, skin thickening

8. Dermatitis (ulcerative) may develop on the skin, particularly inter-scapular.

9. Teeth may break or become overgrown, malocclusion

10. Lumps and swellings may form under the skin or internally, and may represent tumours

11. Rectal prolapses are common in C57BL/6J mice during ageing.

12. Enlarged seminal vesicles are common in aged male mice.

As our mice age we will seek advice from the NACWO and NVS where appropriate, to determine whether an animal is experiencing adverse pathological effects rather than simply displaying the characteristics of old age. However, at all times will be guided by our pre- determined humane end-points.

How will you monitor for, control, and limit any of these adverse effects?

A number of parameters (e.g. food intake (either by a continuous recording device or from the food missing from the hopper), faeces production, body weight, grip strength) may be measured by non-regulated methods at regular periods throughout the protocol.

Gradual body weight loss, cataract formation, greying and loss of fur and some reduction in activity and change in body habitus would be regarded as anticipated features of ‘normal’ ageing. Age-related features such as tooth overgrowth and rectal prolapses which may have welfare issues will be monitored and addressed in the appropriate way (e.g. tooth clipping, easy access to soft/palatable diet, fluids, extra

nesting material or a change in bedding material, heat or prolapse treatment) in consultation with NVS who will also help determine the number of times that these interventions can be repeated on the same individual before humane end-points are addressed.

Cages containing animals over 12 months of age should be clearly marked as ‘Aged animals’.

Records of measurement will be made available in the same room as the animals, in either an electronic format or as paper copies.

When measurement or clinical observations on any individual starts to deviate from the normal (age, treatment and sex-matched) then this should be brought to the attention of the PPL holder and the NACWO, and both body weight and body condition scored more frequently, e.g. daily. The NACWO may also contact the NVS at this time.

Progeroid models will be scored more frequently, e.g. daily, for both body weight and body condition from weaning onwards if approaching the limits of ‘healthy’ ageing (strain- dependent).

Cages containing progeroid models should be clearly marked as ‘Progeroid animals’ at all times.

Wherever possible a necropsy will be undertaken and any pathology or abnormalities noted.

If any animal exhibits unexpected adverse effects with welfare impact this then should be brought to the attention of the NACWO, who may contact the NVS. The NVS may also be contacted directly if appropriate, e.g. the NVS is in the unit or the situation is urgent. Any adverse effects will be reported by the PPL as a SC18 to Home Office and if the animals are alive and there is scientific justification for keeping alive in face of said adverse effect then a 'keeping alive ' request must urgently be made.

What are the humane endpoints for this step?

Typically our aged colonies (typically >12 months of age) are checked daily for potential deterioration of individual animals, with body weight and body condition

checked weekly. Progeroid models will be typically scored more frequently, e.g. daily for both body weight and body condition from weaning onwards if approaching the limits of 'healthy' ageing (strain- dependent). We will utilise our humane end-points and limits of severity for these models in line with our other ageing mice but these humane endpoints will be initiated much earlier in life (strain and genotype dependent).

We have generated a pre-determined humane end-point protocol for our ageing colonies using established protocols and criteria (a scoring system (0-5) based on general physical appearance, respiratory rate/breathing characteristics, spontaneous activity including gait, body weight, body condition) that we have in put in place to monitor and assess our ageing colonies, in order to help identify any adverse effects in our ageing mouse colonies that may impact on welfare. These protocols will be undertaken alongside our general colony monitoring of individuals.

Our specific humane endpoints are based on the following 5 parameters:

1. General physical appearance (e.g. coat/skin condition, general demeanour, presence of overt infection, lumps or growths)

2. Respiratory rate/breathing characteristics

3. Spontaneous activity including gait

4. Body weight

5. Body condition

Each of these criteria will graded as described below and appropriate action taken. Each element within our humane end-point protocol is attributed a score to assist in tracking animal health condition. All scores are used as a guide/monitoring tool and not viewed in isolation, in that the animal health condition is consequently a composite of these different parameters.

A. General physical appearance: observe coat/skin condition, general demeanour, lumps or growths, cataracts

SCORE:

0. Normal

1. Slightly abnormal- coat colour dull, coat slightly dirty or slightly unkempt, lack of grooming or over grooming,

2. Evidence of a small a discrete area of dermatitis, piloerection, abnormal behaviour (e.g. subdued or solitary behaviour), alopecia, pelage depigmentation, cataracts, rectal prolapse.

4. Evidence of a lump or growth, coat clearly dirty or pronounced piloerection, evidence of dehydration, or the presence of extensive dermatitis, alopecia or skin thickening that is not interfering with normal behaviour or function, and when body weight and body composition is unaffected. Discuss with the NAWCO and NVS regarding appropriate treatments.

5. If lump or growth interferes with normal movement, or leads to a consistent or rapid weight loss, a consistent or rapid reduction in body condition score, or where there is evidence of ulceration or other features outlined in the NCRN guidelines, or when extensive dermatitis or rectal prolapse interferes with behaviour or normal function and/or does not respond to treatment then humanely kill by schedule 1.

B. Respiratory rate/breathing characteristic:

SCORE:

0. Normal

3. Abdominal breathing

5. Gasping/rapid breathing then humanely kill by schedule 1.

C. Spontaneous activity including gait: Ability to move around cage, general gait

SCORE:

0. Normal

1. Slightly impaired movement- minor changes in activity level

3. Moderately impaired- obvious mobility problems, less mobile or less alert

4. Moves to stimulus but not spontaneously

5. Huddled, not moving following stimulation or if individual shows a failure to weight bear on a hind limb/s which impairs their ability to feed or drink then humanely kill by schedule 1

D. Body weight: as compared to an individual's own long-term body weight profile or where appropriate comparison with littermates of the same sex and genotype and experimental manipulation

SCORE:

0. Weight normal

2. 10% weight loss over a 2 week period. Weight and general appearance (e.g. coat condition, gait, breathing, posture, behaviour) will be monitored and teeth will be checked. The animal will also be body condition scored (BCS) - see below.

3. 10-15% weight loss over a 2 week period. Weight and general appearance (as above) will be monitored, teeth will be checked and interventions provided relevant to condition (e.g. easy access to soft/palatable diet, fluids, extra nesting material, access to heat).

5. 10-20% weight loss over a 2 week period and the mouse is unresponsive to treatment/intervention as described above over a period not exceeding 5 days then above then humanely kill by schedule 1.

5. If weight loss exceeds 20% of that individual's weigh in the preceding 2 weeks then humanely kill by schedule 1.

This parameter is primarily aimed at identifying acute weight loss that may indicate underlying health issues, as opposed to typical, relatively long-term reductions in body weight seen in mice beyond middle age or those under dietary restriction.

E. Body Condition (to evaluate the body condition of animals that show normal body weight but may have declining health due to organ enlargement, internal tumours or cachexia for example).

SCORE:

0. BC3-4

0. BC5 if mouse on high fat diet

0. BCS2-3 if mouse on dietary restriction

3. BC2 or if BC5 and mouse on chow diet. Monitor and score on at least daily basis: if infection or pain, consider appropriate treatment as advised by NVS. If no change in BCS within 7 days then then humanely kill by schedule 1.

If individual pathology score or combined pathology score for more than one pathology score equals or exceeds a score of 5 then we will humanely kill by schedule 1. Mice with idiopathic dermatitis that is unresponsive to treatment, or which affects normal mouse behaviour and function will be humanely killed. Mice showing abnormal gait and posture will be brought to the attention of NACWO/NVS. If they show failure to weight bear on a hind limb/s which impairs their ability to feed or drink freely they will be humanely killed. Mice with a lump or growth that interferes with normal movement or behaviour, or leads to a consistent or rapid weight loss, a consistent or rapid reduction in body condition score, or where the is evidence of ulceration or other features outlined in the Guidelines for the Welfare and Use of Animals in Cancer Research Guidelines (Workman et al. 2010) will be humanely killed. Mice showing gasping/rapid breathing will be humanely killed. If a mouse has lost 15-20% in body weight within a 7 day period and is unresponsive to treatment/intervention, or if body weight loss greater than 20% of that individual's weight over the previous 2 weeks it will be humanely killed.

If any animal exhibits unexpected adverse effects with welfare impact this then should be brought to the attention of the NACWO, who may contact the NVS. The NVS may also be contacted directly if appropriate, e.g. the NVS is in the unit or the

situation is urgent. Any adverse effects will be reported by the PPL as a SC18 to Home Office and if the animals are alive and there is scientific justification for keeping alive in face of said adverse effect then a 'keeping alive ' request must urgently be made.

Wherever possible a necropsy will be undertaken and any pathology or abnormalities noted. This information will be sent to the NACWO and NVS and noted in a workbook situated in same room as the animals.

Appendix 3: Published work

Polr3b heterozygosity in mice induces both beneficial and deleterious effects on health during ageing with no effect on lifespan

Gillian Borland[1], Stephen E. Wilkie[1,4], Jackie Thomson[1], Zhe Wang[1], Jennifer M.A. Tullet[3], Nazif Alic[2] and Colin Selman[1,*]

[1]School of Biodiversity, One Health and Veterinary Medicine, University of Glasgow, Glasgow, United Kingdom.

[2]Department of Genetics Evolution and Environment, Institute of Healthy Ageing, University College London, London, United Kingdom.

[3]Faculty of Natural Sciences, University of Kent, Canterbury, United Kingdom.

[4]Current address: Division of Molecular Metabolism, Department of Medical Biochemistry and Biophysics, Karolinska Institutet, 171 65, Sweden

Running title: RNA polymerase III and mammalian lifespan.

Corresponding authors: *Colin Selman, colin.selman@glasgow.ac.uk

The genetic pathways that modulate ageing in multicellular organisms are typically conserved across wide evolutionary distances. Recently RNA polymerase III (Pol III) was shown to promote ageing in yeast, *C. elegans* and *D. melanogaster.* In this study we investigated the role of Pol III in mammalian ageing using C57BL/6N mice heterozygous for Pol III (*Polr3b*$^{+/-}$). We identified sexually dimorphic, organ-specific beneficial as well as detrimental effects of the *Polr3b*$^{+/-}$ mutation on health. Female *Polr3b*$^{+/-}$ mice displayed improved bone health during ageing, but their ability to maintain an effective gut barrier function was compromised and they were susceptible to idiopathic dermatitis. In contrast, male *Polr3b*$^{+/-}$ mice were lighter than wild-type (WT) males and had a significantly improved gut barrier function in old age. Several metabolic parameters were affected by both age and sex, but no genotype differences were detected. Neither male nor female *Polr3b*$^{+/-}$ mice were long-lived compared to WT controls. Overall, we find no evidence that a reduced Pol III activity extends mouse lifespan but we do find some potential organ- and sex-specific benefits for old-age health.

The ageing process is associated with a profound decline in physiological function and increased prevalence in multiple pathologies (Figueira et al., 2016). It is well established that lifespan can be extended through dietary, pharmacological, and genetic means (Fontana & Partridge, 2015; Gems & Partridge, 2013; Mannick & Lamming, 2023), with several of these interventions also delaying and/or reducing age-related pathology (Selman & Withers, 2011). RNA polymerase III (Pol III) is one of three nuclear RNA polymerases found in eukaryotes. It transcribes a number of short non-coding RNAs (e.g. tRNAs, snRNAs, 5S rRNA (Kulaberoglu et al., 2021)), and is estimated to account for ~15% of total cellular transcription (Moir & Willis, 2013). Pol III inhibition extends lifespan in yeast, *C. elegans* and *D. melanogaster*, acting through the intestine/intestinal stem cells to achieve this in worms and flies respectively (Filer et al., 2017). Inhibition also preserves age-related health in flies and acts downstream of mTORC1 (Filer et al., 2017).

In mammals, Pol III consists of 17 subunits, of which Polr3a and Polr3b are the largest and form the catalytic subunit of the polymerase (Choquet, Pinard, et al., 2019; Kulaberoglu et al., 2021). Given that Pol III can modulate lifespan in invertebrate models and that this phenotype appears not to be subunit-specific in flies (Filer et al., 2017), we examined longevity and aspects of age-related health in mice heterozygous for *Polr3b* (*Polr3b*$^{+/-}$) which encodes the second largest catalytic subunit of Pol III (Fig. S1A-B); homozygous loss of *Polr3b* causes embryonic lethality (see Methods). Mice bred with expected Mendelian frequencies (Fig. 1A) and hepatic expression of *Polr3b* was reduced in both female and male *Polr3b*$^{+/-}$ mice (Fig. 1B; Hepatic POLR3b protein levels were also reduced in female, but not male, mice) Fig. S2A-B)). Performing extensive phenotyping at different ages, we observed both beneficial and detrimental, sexually dimorphic, organ-specific effects of the heterozygous *Polr3b* mutation on health. Akin to humans, mice exhibit age-related bone loss (Jilka, 2013) and this loss can be assessed by microCT (Selman et al., 2009). Female *Polr3b*$^{+/-}$ mice showed increased trabecular bone relative to wild-type (WT) females particularly evident at mid-life (Fig. 1C-E, Fig. S3), similar to our previously findings in long-lived IIS and mTOR mutants (Selman et al., 2008; Selman et al., 2009), indicating that reduced Pol III activity may help maintain bone health during ageing in female mice. No phenotypic differences in bone characteristics were observed in males (Fig S4A-C).

With age, the barrier function of the mouse gut becomes compromised, and this leakiness can be observed as an increase in faecal albumin (Wang et al., 2021).

In contrast to the preserved gut barrier function observed in older flies with attenuated Pol III activity (Filer et al., 2017), female *Polr3b*$^{+/-}$ mice showed increased gut permeability compared to age-matched WT controls (Fig. 1F). These females were also susceptible to idiopathic dermatitis (ID) (Fig. 1G). On the other hand, *Polr3b*$^{+/-}$males were lighter (Fig. 1H) and their gut barrier function was preserved in old age (Fig. 1F), relative to wild-type controls. For several other metabolic phenotypes (Fig. S4D-I) and for grip strength (Fig. S4J), no genotypic differences were detected at any age in either sex, although several significant age and sex effects were seen.

We evaluated lifespan in female and male C57BL/6N wild-type mice compared to *Polr3b*$^{+/-}$ mice. Combined data of both sexes (Fig. 2A) showed no significant effect of genotype on median or maximum lifespan (oldest 10% of cohort, Fig. S5A: Table S1). Similarly, when each sex was analysed separately neither female nor male *Polr3b*$^{+/-}$ mice were long-lived (Fig. 2B and 2C; Fig. S5B-C: Table S1). Male WT mice lived significantly longer than female WT mice (X^2 = 10.420, p=0.001), with a similar sex-specific trend seen in *Polr3b*$^{+/-}$ mice (X^2 = 3.810, p=0.051). Median lifespan of our C57BL/6N WT mice was shorter than our previously published data for C57BL/6J mice (Selman et al., 2008; Selman et al., 2009). C57BL/6J and 6N mice differ in a range of metabolic parameters (Selman & Swindell, 2018), but there is a current dearth of published lifespan data for C57BL/6N mice. However, our lifespans compare favourably with published lifespans for this strain (Reid et al., 2023; Tang et al., 2021). No genotype difference in cancer incidence upon post-mortem was identified in our ageing cohorts (Fig. 2D). Note that censoring female mice euthanised for ID did not alter the lifespan outcome (Fig. S5D; X^2 = 0.001, p=0.970).

Overall, we observed an indication of organ- and sex-specific benefits for old-age health achieved by a partial loss-of-function in Pol III with no effect on lifespan. In support, pathogenic conditions associated with Pol III appear to show pronounced tissue-specific responses following perturbation in Pol III transcription (Watt et al., 2023). The difference to the net beneficial effect on invertebrate lifespan may result from a more complex physiological role of Pol III in mammals. For example, Pol III plays a critical noncanonical role in viral and bacterial DNA sensing within the innate immune response (Chiu et al., 2009). It is possible that the appropriate response to bacterial and viral challenge at the skin surface is impaired in female *Polr3b*$^{+/-}$ mice causing ID. Our mice were heterozygous for *Polr3b*, and at the level of both protein

and gene expression the reduction in *Polr3b* observed was variable both within and between sexes. It is possible that a more substantial reduction in Polr3b expression in specific cell types is required to obtain a longevity phenotype. Still, the observation of some beneficial effects, for example on bone health in females, suggests that cell-type specific attenuation of Pol III function may have positive effect on aspects of mammalian ageing, as indicated by a recent analysis of human genetic data (Javidnia et al., 2022).

AUTHOR CONTRIBUTIONS

NA, JMAT and CS conceived the study and obtained the funding. GB, SEW, JT, ZW and CS performed the experiments. GB and CS analysed the data. GB, NA, JMAT and CS wrote the manuscript with contributions from all authors.

ACKNOWLEDGEMENTS

We are grateful to the Biological Services Staff for animal care and husbandry and to Professor Maggie Harnett (all Univ. Glasgow). We thank Debbie Wilkinson (Univ. Aberdeen) for the bone microCT analysis. This work was funded by the Biotechnology and Biological Sciences Research Council (BBSRC) grant BB/S014357/1 to CS, JMAT and NA. SEW was funded through a Medical Research Council Doctoral Training Program to CS (Reference MR/N013166/1). The mouse line C57BL/6N-Polr3b<em7(IMPC)Tcp>/Tcp was made as part of the NorCOMM2 project funded by Genome Canada and the Ontario Genomics Institute (OGI-051) at the Toronto Centre for Phenogenomics and obtained through the Canadian Mouse Mutant Repository.

CONFLICT OF INTEREST STATEMENT

The authors declare no conflicts of interest.

FIGURE LEGENDS

Figure 1: (A) Mendelian frequencies of mice born from heterozygous x wild-type (WT) parents. (B) Hepatic *Polr3b* expression in 14-month-old mice. (C) Percentage bone volume, (D) Trabecular separation, (E) Trabecular number in female mouse femurs at 14 and 20 months. (F) Faecal albumin levels in female and male mice at 22 months. (G) Percentage of mice (of total number) presenting with idiopathic dermatitis. (H) Body mass (mean±SEM) across the life-course in female and male WT and *Polr3b*$^{+/-}$ mice. Histograms denote mean±SEM, with sample sizes indicated by individual points within a group. For Fig. 1B-F, a 2-way ANOVA was used to test for age/sex and genotype effects (both main and interaction effects). Only significant main and/or interaction effects are reported within the figures.

Figure 2: (A) Kaplan-Meier survival curves for combined female and male wild-type (WT) and *Polr3b*$^{+/-}$ mice (Log-rank X^2=3.084, p=0.079, n=103 for WT, n=103 for *Polr3b*$^{+/-}$). Survival curves for female (B; Log-rank X^2=1.040, p=0.308, n=53 for WT, n=51 for *Polr3b*$^{+/-}$) and male (C; Log-rank X^2=2.355, p=0.125, n=50 for WT, n=52 for *Polr3b*$^{+/-}$) mice. Numbers denote median lifespan (days). (D) Percentage of mice presenting post-mortem with macroscopic tumours.

REFERENCES

Ablasser, A., Bauernfeind, F., Hartmann, G., Latz, E., Fitzgerald, K. A., & Hornung, V. (2009). RIG-I-dependent sensing of poly(dA:dT) through the induction of an RNA polymerase III-transcribed RNA intermediate. *Nat Immunol*, *10*(10), 1065-1072. https://doi.org/10.1038/ni.1779

Ackermann, L., & Harvima, I. T. (1998). Mast cells of psoriatic and atopic dermatitis skin are positive for TNF-α and their degranulation is associated with expression of ICAM-1 in the epidermis. *Archives of Dermatological Research*, *290*(7), 353-359. https://doi.org/10.1007/s004030050317

Adams, S. C., Garner, J. P., Felt, S. A., Geronimo, J. T., & Chu, D. K. (2016). A "Pedi" Cures All: Toenail Trimming and the Treatment of Ulcerative Dermatitis in Mice. *PLoS One*, *11*(1), e0144871. https://doi.org/10.1371/journal.pone.0144871

Ajayi, A. F., Oyovwi, M. O., Olatinwo, G., & Phillips, A. O. (2024). Unfolding the complexity of epigenetics in male reproductive aging: a review of therapeutic implications. *Mol Biol Rep*, *51*(1), 881. https://doi.org/10.1007/s11033-024-09823-9

Alla, R. K., & Cairns, B. R. (2014). RNA polymerase III transcriptomes in human embryonic stem cells and induced pluripotent stem cells, and relationships with pluripotency transcription factors. *PLoS One*, *9*(1), e85648. https://doi.org/10.1371/journal.pone.0085648

Alur, P. (2019). Sex Differences in Nutrition, Growth, and Metabolism in Preterm Infants. *Front Pediatr*, *7*, 22. https://doi.org/10.3389/fped.2019.00022

Alvarado, C. G., Franklin, C. L., & Dixon, L. W. (2016). Retrospective Evaluation of Nail Trimming as a Conservative Treatment for Ulcerative Dermatitis in Laboratory Mice. *J Am Assoc Lab Anim Sci*, *55*(4), 462-466.

Andrews, A. G., Dysko, R. C., Spilman, S. C., Kunkel, R. G., Bummer, D. W., & Johnson, K. J. (1994). Immune Complex Vasculitis with Secondary Ulcerative Dermatitis in Aged C57BL/6NNia Mice. *Vet Pathol*, *31*(3), 293-300.

Antell, D. E., & Taczanowski, E. M. (1999). How Environment and Lifestyle Choices Influence the Aging Process. *Annals of Plastic Surgery*, *43*(6), 585-588. https://journals.lww.com/annalsplasticsurgery/fulltext/1999/12000/how_environment_and_lifestyle_choices_influence.1.aspx

Aravinthan, A., Challis, B., Shannon, N., Hoare, M., Heaney, J., & Alexander, G. J. M. (2015). Selective insulin resistance in hepatocyte senescence. *Exp Cell Res*, *331*(1), 38-45. https://doi.org/10.1016/j.yexcr.2014.09.025

Azmanov, D. N., Siira, S. J., Chamova, T., Kaprelyan, A., Guergueltcheva, V., Shearwood, A. M. J., Liu, G., Morar, B., Rackham, O., Bynevelt, M., Grudkova, M., Kamenov, Z., Svechtarov, V., Tournev, I., Kalaydjieva, L., & Filipovska, A. (2016). Transcriptome-wide effects of a POLR3A gene mutation in patients with an unusual phenotype of striatal involvement. *Human Molecular Genetics*, *25*(19), 4302-4314. https://doi.org/10.1093/hmg/ddw263

Baez, G. M., Barletta, R. V., Guenther, J. N., Gaska, J. M., & Wiltbank, M. C. (2016). Effect of uterine size on fertility of lactating dairy cows. *Theriogenology*, *85*(8), 1357-1366. https://doi.org/10.1016/j.theriogenology.2015.04.022

Baiocchi, L., Glaser, S., Francis, H., Kennedy, L., Felli, E., Alpini, G., & Gracia-Sancho, J. (2021). Impact of Aging on Liver Cells and Liver Disease: Focus on the Biliary and Vascular Compartments. *Hepatol Commun*, *5*(7), 1125-1137. https://doi.org/10.1002/hep4.1725

Balough, J. L., Dipali, S. S., Velez, K., Kumar, T. R., & Duncan, F. E. (2024). Hallmarks of female reproductive aging in physiologic aging mice. *Nature Aging*, *4*(12), 1711-1730. https://doi.org/10.1038/s43587-024-00769-y

Bandow, K., Smith, A., Watkins, T., Shenk, S., Gerami-Naini, B., & Garlick, J. A. (2023). CC chemokine ligand 20 (CCL20) positively regulates collagen type I production in 3D skin equivalent tissues. *Exp Dermatol*, *32*(4), 379-391. https://doi.org/10.1111/exd.14712

Baratta, J. L., Ngo, A., Lopez, B., Kasabwalla, N., Longmuir, K. J., & Robertson, R. T. (2009). Cellular organization of normal mouse liver: a histological, quantitative immunocytochemical, and fine structural analysis. *Histochem Cell Biol*, *131*(6), 713-726. https://doi.org/10.1007/s00418-009-0577-1

Barcena, C., Mayoral, P., & Quiros, P. M. (2018). Mitohormesis, an Antiaging Paradigm. *Int Rev Cell Mol Biol*, *340*, 35-77. https://doi.org/10.1016/bs.ircmb.2018.05.002

Bartke, A. (2000). Delayed aging in Ames dwarf mice. Relationships to endocrine function and body size. *Results Probl Cell Differ*, *29*, 181-202. https://doi.org/10.1007/978-3-540-48003-7_10

Barton, C., Sturge, G., & Harker, R. (2024). *The UK's changing population*. House of Commons Library. https://commonslibrary.parliament.uk/the-uks-changing-population/

Bates, D., Mächler, M., Bolker, B., & Walker, S. (2015). Fitting Linear Mixed-Effects Models Using lme4. *Journal of Statistical Software*, *67*(1), 1 - 48. https://doi.org/10.18637/jss.v067.i01

Battaglioni, S., Benjamin, D., Walchli, M., Maier, T., & Hall, M. N. (2022). mTOR substrate phosphorylation in growth control. *Cell*, *185*(11), 1814-1836. https://doi.org/10.1016/j.cell.2022.04.013

Beauregard-Lacroix, E., Salian, S., Kim, H., Ehresmann, S., D'Amours, G., Gauthier, J., Saillour, V., Bernard, G., Mitchell, G. A., Soucy, J. F., Michaud, J. L., & Campeau, P. M. (2020). A variant of neonatal progeroid syndrome, or Wiedemann-Rautenstrauch syndrome, is associated with a nonsense variant in POLR3GL. *Eur J Hum Genet*, *28*(4), 461-468. https://doi.org/10.1038/s41431-019-0539-6

Bento-Abreu, A., Jager, G., Swinnen, B., Rué, L., Hendrickx, S., Jones, A., Staats, K. A., Taes, I., Eykens, C., Nonneman, A., Nuyts, R., Timmers, M., Silva, L., Chariot, A., Nguyen, L., Ravits, J., Lemmens, R., Cabooter, D., Van Den Bosch, L.,…et al. (2018). Elongator subunit 3 (ELP3) modifies ALS through tRNA modification. *Human Molecular Genetics*, *27*(7), 1276-1289. https://doi.org/10.1093/hmg/ddy043

Bernard, G., Chouery, E., Putorti, M. L., Tetreault, M., Takanohashi, A., Carosso, G., Clement, I., Boespflug-Tanguy, O., Rodriguez, D., Delague, V., Abou Ghoch, J., Jalkh, N., Dorboz, I., Fribourg, S., Teichmann, M., Megarbane, A., Schiffmann, R., Vanderver, A., & Brais, B. (2011). Mutations of POLR3A encoding a catalytic subunit of RNA polymerase Pol III cause a recessive hypomyelinating leukodystrophy. *Am J Hum Genet*, *89*(3), 415-423. https://doi.org/10.1016/j.ajhg.2011.07.014

Berndtson, W. E., Judd, J. E., & Castro, A. C. S. (1997). Inherent Variability Among Measures of Fertility of Rats and Its Implications in the Design of Mating Trials. *Journal of Andrology*, *18*(6), 717-724. https://doi.org/https://doi.org/10.1002/j.1939-4640.1997.tb02449.x

Bjedov, I., Toivonen, J. M., Kerr, F., Slack, C., Jacobson, J., Foley, A., & Partridge, L. (2010). Mechanisms of life span extension by rapamycin in the fruit fly Drosophila melanogaster. *Cell Metab*, *11*(1), 35-46. https://doi.org/10.1016/j.cmet.2009.11.010

Blackburn, E. H., Greider, C. W., & Szostak, J. W. (2006). Telomeres and telomerase: the path from maize, Tetrahymena and yeast to human cancer and aging. *Nature Medicine*, *12*(10), 1133-1138. https://doi.org/10.1038/nm1006-1133

Blagosklonny, M. V. (2006). Aging and immortality: quasi-programmed senescence and its pharmacologic inhibition. *Cell Cycle*, *5*(18), 2087-2102. https://doi.org/10.4161/cc.5.18.3288

Blaschitz, C., & Raffatellu, M. (2010). Th17 Cytokines and the Gut Mucosal Barrier. *Journal of Clinical Immunology*, *30*(2), 196-203. https://doi.org/10.1007/s10875-010-9368-7

Blasco, M. A. (2007). Telomere length, stem cells and aging. *Nature Chemical Biology*, *3*(10), 640-649. https://doi.org/10.1038/nchembio.2007.38

Blasimme, A. (2021). The plasticity of ageing and the rediscovery of ground-state prevention. *History and Philosophy of the Life Sciences*, *43*(2), 67. https://doi.org/10.1007/s40656-021-00414-6

Blondet, N. M., Messner, D. J., Kowdley, K. V., & Murray, K. F. (2018). Chapter 43 - Mechanisms of Hepatocyte Detoxification. In H. M. Said (Ed.), *Physiology of the Gastrointestinal Tract (Sixth Edition)* (pp. 981-1001). Academic Press. https://doi.org/https://doi.org/10.1016/B978-0-12-809954-4.00043-8

Boguta, M. (2013). Maf1, a general negative regulator of RNA polymerase III in yeast. *Biochim Biophys Acta*, *1829*(3-4), 376-384. https://doi.org/10.1016/j.bbagrm.2012.11.004

Bonawitz, N. D., Chatenay-Lapointe, M., Pan, Y., & Shadel, G. S. (2007). Reduced TOR signaling extends chronological life span via increased respiration and upregulation of mitochondrial gene expression. *Cell Metab*, *5*(4), 265-277. https://doi.org/10.1016/j.cmet.2007.02.009

Bonhoure, N., Byrnes, A., Moir, R. D., Hodroj, W., Preitner, F., Praz, V., Marcelin, G., Chua, S. C., Jr., Martinez-Lopez, N., Singh, R., Moullan, N., Auwerx, J., Willemin, G., Shah, H., Hartil, K., Vaitheesvaran, B., Kurland, I., Hernandez, N., & Willis, I. M. (2015). Loss of the RNA polymerase III repressor MAF1 confers obesity resistance. *Genes Dev*, *29*(9), 934-947. https://doi.org/10.1101/gad.258350.115

Bonhoure, N., Praz, V., Moir, R. D., Willemin, G., Mange, F., Moret, C., Willis, I. M., & Hernandez, N. (2020). MAF1 is a chronic repressor of RNA polymerase III transcription in the mouse. *Sci Rep*, *10*(1), 11956. https://doi.org/10.1038/s41598-020-68665-0

Borland, G., Wilkie, S. E., Thomson, J., Wang, Z., Tullet, J. M. A., Alic, N., & Selman, C. (2024). Polr3b heterozygosity in mice induces both beneficial and deleterious effects on health during ageing with no effect on lifespan. *Aging Cell*, *23*(5), e14141. https://doi.org/10.1111/acel.14141

Boulon, S., Pradet-Balade, B., Verheggen, C., Molle, D., Boireau, S., Georgieva, M., Azzag, K., Robert, M. C., Ahmad, Y., Neel, H., Lamond, A. I., & Bertrand, E. (2010). HSP90 and its R2TP/Prefoldin-like cochaperone are involved in the cytoplasmic assembly of RNA polymerase II. *Mol Cell*, *39*(6), 912-924. https://doi.org/10.1016/j.molcel.2010.08.023

Boyer, J. L. (2013). Bile formation and secretion. *Compr Physiol*, *3*(3), 1035-1078. https://doi.org/10.1002/cphy.c120027

Brajon, S., Munhoz Morello, G., Teixeira, M. S., Hultgren, J., Gilbert, C., & Olsson, I. A. S. (2019). Social environment as a cause of litter loss in laboratory

mouse: A behavioural study. *Applied Animal Behaviour Science*, *218*, 104827. https://doi.org/https://doi.org/10.1016/j.applanim.2019.06.008
Broekmans, F. J., Soules, M. R., & Fauser, B. C. (2009). Ovarian aging: mechanisms and clinical consequences. *Endocr Rev*, *30*(5), 465-493. https://doi.org/10.1210/er.2009-0006
Brow, D. A., & Guthrie, C. (1990). Transcription of a yeast U6 snRNA gene requires a polymerase III promoter element in a novel position. *Genes Dev*, *4*(8), 1345-1356. https://doi.org/10.1101/gad.4.8.1345
Brown, E. J., Albers, M. W., Shin, T. B., Ichikawa, K., Keith, C. T., Lane, W. S., & Schreiber, S. L. (1994). A mammalian protein targeted by G1-arresting rapamycin-receptor complex. *Nature*, *369*(6483), 756-758. https://doi.org/10.1038/369756a0
Brown-Borg, H. M., Borg, K. E., Meliska, C. J., & Bartke, A. (1996). Dwarf mice and the ageing process. *Nature*, *384*(6604), 33. https://doi.org/10.1038/384033a0
Bustamante-Barrientos, F. A., Luque-Campos, N., Araya, M. J., Lara-Barba, E., de Solminihac, J., Pradenas, C., Molina, L., Herrera-Luna, Y., Utreras-Mendoza, Y., Elizondo-Vega, R., Vega-Letter, A. M., & Luz-Crawford, P. (2023). Mitochondrial dysfunction in neurodegenerative disorders: Potential therapeutic application of mitochondrial transfer to central nervous system-residing cells. *J Transl Med*, *21*(1), 613. https://doi.org/10.1186/s12967-023-04493-w
Cafferkey, R., Young, P. R., McLaughlin, M. M., Bergsma, D. J., Koltin, Y., Sathe, G. M., Faucette, L., Eng, W. K., Johnson, R. K., & Livi, G. P. (1993). Dominant missense mutations in a novel yeast protein related to mammalian phosphatidylinositol 3-kinase and VPS34 abrogate rapamycin cytotoxicity. *Mol Cell Biol*, *13*(10), 6012-6023. https://doi.org/10.1128/mcb.13.10.6012-6023.1993
Campisi, J., & d'Adda di Fagagna, F. (2007). Cellular senescence: when bad things happen to good cells. *Nat Rev Mol Cell Biol*, *8*(9), 729-740. https://doi.org/10.1038/nrm2233
Castilho, R. M., Squarize, C. H., Chodosh, L. A., Williams, B. O., & Gutkind, J. S. (2009). mTOR mediates Wnt-induced epidermal stem cell exhaustion and aging. *Cell Stem Cell*, *5*(3), 279-289. https://doi.org/10.1016/j.stem.2009.06.017
Castillo-Quan, J. I., Tain, L. S., Kinghorn, K. J., Li, L., Gronke, S., Hinze, Y., Blackwell, T. K., Bjedov, I., & Partridge, L. (2019). A triple drug combination targeting components of the nutrient-sensing network maximizes longevity. *Proc Natl Acad Sci U S A*, *116*(42), 20817-20819. https://doi.org/10.1073/pnas.1913212116
Cavlar, T., Ablasser, A., & Hornung, V. (2012). Induction of type I IFNs by intracellular DNA-sensing pathways. *Immunol Cell Biol*, *90*(5), 474-482. https://doi.org/10.1038/icb.2012.11
Chahoud, I., & Paumgartten, F. J. (2009). Influence of litter size on the postnatal growth of rat pups: is there a rationale for litter-size standardization in toxicity studies? *Environ Res*, *109*(8), 1021-1027. https://doi.org/10.1016/j.envres.2009.07.015
Chamani, I. J., & Keefe, D. L. (2019). Epigenetics and Female Reproductive Aging. *Front Endocrinol (Lausanne)*, *10*, 473. https://doi.org/10.3389/fendo.2019.00473
Chang, J., Burkett, P. R., Borges, C. M., Kuchroo, V. K., Turka, L. A., & Chang, C. H. (2013). MyD88 is essential to sustain mTOR activation necessary to promote T helper 17 cell proliferation by linking IL-1 and IL-23 signaling.

Proc Natl Acad Sci U S A, *110*(6), 2270-2275. https://doi.org/10.1073/pnas.1206048110

Chen, Q., Yan, M., Cao, Z., Li, X., Zhang, Y., Shi, J., Feng, G. H., Peng, H., Zhang, X., Zhang, Y., Qian, J., Duan, E., Zhai, Q., & Zhou, Q. (2016). Sperm tsRNAs contribute to intergenerational inheritance of an acquired metabolic disorder. *Science*, *351*(6271), 397-400. https://doi.org/10.1126/science.aad7977

Chen, W., Mempel, M., Schober, W., Behrendt, H., & Ring, J. (2008). Gender difference, sex hormones, and immediate type hypersensitivity reactions. *Allergy*, *63*(11), 1418-1427. https://doi.org/10.1111/j.1398-9995.2008.01880.x

Cheng, J., Yang, S., Ma, H., Liang, Y., & Zhao, J. (2022). Estradiol (E (2)) Reduction Adversely Affect the Embryo Quality and Clinical Outcomes of In Vitro Fertilization and Embryo transfer (IVF-ET). *J Healthc Eng*, *2022*, 2473876. https://doi.org/10.1155/2022/2473876

Cheng, Y.-W., Liu, J., & Finkel, T. (2023). Mitohormesis. *Cell Metabolism*, *35*(11), 1872-1886. https://doi.org/10.1016/j.cmet.2023.10.011

Chiu, Y. H., Macmillan, J. B., & Chen, Z. J. (2009). RNA polymerase III detects cytosolic DNA and induces type I interferons through the RIG-I pathway. *Cell*, *138*(3), 576-591. https://doi.org/10.1016/j.cell.2009.06.015

Choi, J., & Smitz, J. (2014). Luteinizing hormone and human chorionic gonadotropin: origins of difference. *Mol Cell Endocrinol*, *383*(1-2), 203-213. https://doi.org/10.1016/j.mce.2013.12.009

Choi, J. H., Burke, J. M., Szymanik, K. H., Nepal, U., Battenhouse, A., Lau, J. T., Stark, A., Lam, V., & Sullivan, C. S. (2020). DUSP11-mediated control of 5′-triphosphate RNA regulates RIG-I sensitivity. *Genes & Development*, *34*(23–24), 1697-1712. https://doi.org/10.1101/gad.340604.120

Choquet, K., Forget, D., Meloche, E., Dicaire, M. J., Bernard, G., Vanderver, A., Schiffmann, R., Fabian, M. R., Teichmann, M., Coulombe, B., Brais, B., & Kleinman, C. L. (2019). Leukodystrophy-associated POLR3A mutations down-regulate the RNA polymerase III transcript and important regulatory RNA BC200. *Journal of Biological Chemistry*, *294*(18), 7445-7459. https://doi.org/10.1074/jbc.RA118.006271

Choquet, K., Pinard, M., Yang, S., Moir, R. D., Poitras, C., Dicaire, M. J., Sgarioto, N., Lariviere, R., Kleinman, C. L., Willis, I. M., Gauthier, M. S., Coulombe, B., & Brais, B. (2019). The leukodystrophy mutation Polr3b R103H causes homozygote mouse embryonic lethality and impairs RNA polymerase III biogenesis. *Mol Brain*, *12*(1), 59. https://doi.org/10.1186/s13041-019-0479-7

Chowdhury, T., & Kohler, J. R. (2015). Ribosomal protein S6 phosphorylation is controlled by TOR and modulated by PKA in Candida albicans. *Mol Microbiol*, *98*(2), 384-402. https://doi.org/10.1111/mmi.13130

Choy, E. H., De Benedetti, F., Takeuchi, T., Hashizume, M., John, M. R., & Kishimoto, T. (2020). Translating IL-6 biology into effective treatments. *Nature Reviews Rheumatology*, *16*(6), 335-345. https://doi.org/10.1038/s41584-020-0419-z

Clancy, D. J., Gems, D., Harshman, L. G., Oldham, S., Stocker, H., Hafen, E., Leevers, S. J., & Partridge, L. (2001). Extension of life-span by loss of CHICO, a Drosophila insulin receptor substrate protein. *Science*, *292*(5514), 104-106. https://doi.org/10.1126/science.1057991

Cohen, P. (2002). The origins of protein phosphorylation. *Nat Cell Biol*, *4*(5), E127-130. https://doi.org/10.1038/ncb0502-e127

Confalone, E., D'Alessio, G., & Furia, A. (2010). IL-6 Induction by TNFα and IL-1β in an Osteoblast-Like Cell Line. *International Journal of Biomedical Science : IJBS*, *6*(2), 135-140.

Conti, M., Hsieh, M., Zamah, A. M., & Oh, J. S. (2012). Novel signaling mechanisms in the ovary during oocyte maturation and ovulation. *Mol Cell Endocrinol*, *356*(1-2), 65-73. https://doi.org/10.1016/j.mce.2011.11.002

Cooper, G. M. (2000). Protein Folding and Processing. In *The Cell: A Molecular Approach.* (2nd edition ed.). Sinauer Associates.

Cora, M. C., Kooistra, L., & Travlos, G. (2015). Vaginal Cytology of the Laboratory Rat and Mouse: Review and Criteria for the Staging of the Estrous Cycle Using Stained Vaginal Smears. *Toxicologic Pathology*, *43*(6), 776-793. https://doi.org/10.1177/0192623315570339

Dai, Q., Qing, X., Jiang, W., Wang, S., Liu, S., Liu, X., Huang, F., & Zhao, H. (2024). Aging aggravates liver fibrosis through downregulated hepatocyte SIRT1-induced liver sinusoidal endothelial cell dysfunction. *Hepatol Commun*, *8*(1). https://doi.org/10.1097/HC9.0000000000000350

Danilovich, N., & Sairam, M. R. (2002). Haploinsufficiency of the follicle-stimulating hormone receptor accelerates oocyte loss inducing early reproductive senescence and biological aging in mice. *Biol Reprod*, *67*(2), 361-369. https://doi.org/10.1095/biolreprod67.2.361

Daoud, H., Tetreault, M., Gibson, W., Guerrero, K., Cohen, A., Gburek-Augustat, J., Synofzik, M., Brais, B., Stevens, C. A., Sanchez-Carpintero, R., Goizet, C., Naidu, S., Vanderver, A., & Bernard, G. (2013). Mutations in POLR3A and POLR3B are a major cause of hypomyelinating leukodystrophies with or without dental abnormalities and/or hypogonadotropic hypogonadism. *J Med Genet*, *50*(3), 194-197. https://doi.org/10.1136/jmedgenet-2012-101357

Dauwerse, J. G., Dixon, J., Seland, S., Ruivenkamp, C. A. L., van Haeringen, A., Hoefsloot, L. H., Peters, D. J. M., Boers, A. C.-d., Daumer-Haas, C., Maiwald, R., Zweier, C., Kerr, B., Cobo, A. M., Toral, J. F., Hoogeboom, A. J. M., Lohmann, D. R., Hehr, U., Dixon, M. J., Breuning, M. H., & Wieczorek, D. (2011). Mutations in genes encoding subunits of RNA polymerases I and III cause Treacher Collins syndrome. *Nature Genetics*, *43*(1), 20-22. https://doi.org/10.1038/ng.724

David, M. R., & Jennifer, L. (2021). Skin collagen through the lifestages: importance for skin health and beauty. *Plastic and Aesthetic Research*, *8*, 2. https://doi.org/10.20517/2347-9264.2020.153

Davis, M., Stroud, C., & Institute of Medicine (U.S.). Forum on Neuroscience and Nervous System Disorders. (2013). *Neurodegeneration : exploring commonalities across diseases : workshop summary*. National Academies Press. National Academies Press http://www.nap.edu/catalog.php?record_id=18341

De Biase, D., Esposito, F., De Martino, M., Pirozzi, C., Luciano, A., Palma, G., Raso, G. M., Iovane, V., Marzocco, S., Fusco, A., & Paciello, O. (2019). Characterization of inflammatory infiltrate of ulcerative dermatitis in C57BL/6NCrl-Tg(HMGA1P6)1Pg mice. *Lab Anim*, *53*(5), 447-458. https://doi.org/10.1177/0023677218815718

de Magalhães, J. P. (2025). An overview of contemporary theories of ageing. *Nature Cell Biology*, *27*(7), 1074-1082. https://doi.org/10.1038/s41556-025-01698-7

de Magalhaes, J. P., & Church, G. M. (2005). Genomes optimize reproduction: aging as a consequence of the developmental program. *Physiology (Bethesda)*, *20*, 252-259. https://doi.org/10.1152/physiol.00010.2005

Della Torre, S. (2020). Non-alcoholic Fatty Liver Disease as a Canonical Example of Metabolic Inflammatory-Based Liver Disease Showing a Sex-Specific Prevalence: Relevance of Estrogen Signaling. *Front Endocrinol (Lausanne)*, *11*, 572490. https://doi.org/10.3389/fendo.2020.572490

Denicol, A. C., & Siqueira, L. G. B. (2023). Maternal contributions to pregnancy success: from gamete quality to uterine environment. *Anim Reprod*, *20*(2), e20230085. https://doi.org/10.1590/1984-3143-AR2023-0085

Dibble, C. C., & Cantley, L. C. (2015). Regulation of mTORC1 by PI3K signaling. *Trends Cell Biol*, *25*(9), 545-555. https://doi.org/10.1016/j.tcb.2015.06.002

Dieci, G., Fiorino, G., Castelnuovo, M., Teichmann, M., & Pagano, A. (2007). The expanding RNA polymerase III transcriptome. *Trends Genet*, *23*(12), 614-622. https://doi.org/10.1016/j.tig.2007.09.001

Dierich, A., Sairam, M. R., Monaco, L., Fimia, G. M., Gansmuller, A., LeMeur, M., & Sassone-Corsi, P. (1998). Impairing follicle-stimulating hormone (FSH) signaling in vivo: targeted disruption of the FSH receptor leads to aberrant gametogenesis and hormonal imbalance. *Proc Natl Acad Sci U S A*, *95*(23), 13612-13617. https://doi.org/10.1073/pnas.95.23.13612

Dorboz, I., Dumay-Odelot, H., Boussaid, K., Bouyacoub, Y., Barreau, P., Samaan, S., Jmel, H., Eymard-Pierre, E., Cances, C., Bar, C., Poulat, A. L., Rousselle, C., Renaldo, F., Elmaleh-Berges, M., Teichmann, M., & Boespflug-Tanguy, O. (2018). Mutation in POLR3K causes hypomyelinating leukodystrophy and abnormal ribosomal RNA regulation. *Neurol Genet*, *4*(6), e289. https://doi.org/10.1212/NXG.0000000000000289

Dorschner, R. A., Pestonjamasp, V. K., Tamakuwala, S., Ohtake, T., Rudisill, J., Nizet, V., Agerberth, B., Gudmundsson, G. H., & Gallo, R. L. (2001). Cutaneous injury induces the release of cathelicidin anti-microbial peptides active against group A Streptococcus. *J Invest Dermatol*, *117*(1), 91-97. https://doi.org/10.1046/j.1523-1747.2001.01340.x

Driskell, R. R., Lichtenberger, B. M., Hoste, E., Kretzschmar, K., Simons, B. D., Charalambous, M., Ferron, S. R., Herault, Y., Pavlovic, G., Ferguson-Smith, A. C., & Watt, F. M. (2013). Distinct fibroblast lineages determine dermal architecture in skin development and repair. *Nature*, *504*(7479), 277-281. https://doi.org/10.1038/nature12783

Duarte-Vogel, S. M., & Lawson, G. W. (2011). Association between hair-induced oronasal inflammation and ulcerative dermatitis in C57BL/6 mice. *Comparative Medicine*, *61*(1), 13-19. https://www.ncbi.nlm.nih.gov/pubmed/21819677

Eckhart, L., Tschachler, E., & Gruber, F. (2019). Autophagic Control of Skin Aging. *Front Cell Dev Biol*, *7*, 143. https://doi.org/10.3389/fcell.2019.00143

Eicher, E. M., & Beamer, W. G. (1976). Inherited ateliotic dwarfism in mice. Characteristics of the mutation, little, on chromosome 6. *J Hered*, *67*(2), 87-91. https://doi.org/10.1093/oxfordjournals.jhered.a108682

Eisenberg, T., Knauer, H., Schauer, A., Buttner, S., Ruckenstuhl, C., Carmona-Gutierrez, D., Ring, J., Schroeder, S., Magnes, C., Antonacci, L., Fussi, H., Deszcz, L., Hartl, R., Schraml, E., Criollo, A., Megalou, E., Weiskopf, D., Laun, P., Heeren, G.,…Madeo, F. (2009). Induction of autophagy by spermidine promotes longevity. *Nat Cell Biol*, *11*(11), 1305-1314. https://doi.org/10.1038/ncb1975

El Ayadi, A., Jay, J. W., & Prasai, A. (2020). Current Approaches Targeting the Wound Healing Phases to Attenuate Fibrosis and Scarring. *Int J Mol Sci*, *21*(3). https://doi.org/10.3390/ijms21031105

El-Brolosy, M. A., & Stainier, D. Y. R. (2017). Genetic compensation: A phenomenon in search of mechanisms. *PLoS Genet*, *13*(7), e1006780. https://doi.org/10.1371/journal.pgen.1006780

Eschenlauer, J. B., Kaiser, M. W., Gerlach, V. L., & Brow, D. A. (1993). Architecture of a yeast U6 RNA gene promoter. *Mol Cell Biol*, *13*(5), 3015-3026. https://doi.org/10.1128/mcb.13.5.3015-3026.1993

Ezell, P. C., Papa, L., & Lawson, G. W. (2012). Palatability and Treatment Efficacy of Various Ibuprofen Formulations in C57BL/6 Mice with Ulcerative Dermatitis. *Journal of the American Association for Laboratory Animal Science, 51(5)*.

Fabbri, L. M., & Rabe, K. F. (2007). From COPD to chronic systemic inflammatory syndrome? *The Lancet*, *370*(9589), 797-799. https://doi.org/10.1016/S0140-6736(07)61383-X

Fang, L., Guo, F., Zhou, L., Stahl, R., & Grams, J. (2015). The cell size and distribution of adipocytes from subcutaneous and visceral fat is associated with type 2 diabetes mellitus in humans. *Adipocyte*, *4*(4), 273-279. https://doi.org/10.1080/21623945.2015.1034920

Fernandez, Y., Rodel, H. G., Feron, C., Reyes-Meza, V., Hudson, R., & Bautista, A. (2025). Individual differences in the development of thermoregulation among littermates of the domestic rabbit. *J Therm Biol*, *131*, 104189. https://doi.org/10.1016/j.jtherbio.2025.104189

Figueira, I., Fernandes, A., Mladenovic Djordjevic, A., Lopez-Contreras, A., Henriques, C. M., Selman, C., Ferreiro, E., Gonos, E. S., Trejo, J. L., Misra, J., Rasmussen, L. J., Xapelli, S., Ellam, T., & Bellantuono, I. (2016). Interventions for age-related diseases: Shifting the paradigm. *Mech Ageing Dev*, *160*, 69-92. https://doi.org/10.1016/j.mad.2016.09.009

Filer, D., Thompson, M. A., Takhaveev, V., Dobson, A. J., Kotronaki, I., Green, J. W. M., Heinemann, M., Tullet, J. M. A., & Alic, N. (2017). RNA polymerase III limits longevity downstream of TORC1. *Nature*, *552*(7684), 263-267. https://doi.org/10.1038/nature25007

Finch, C. E., & Kirkwood, T. (2000). *Chance, Development, and Aging*. Oxford University Press. https://doi.org/10.1023/A:1026536128119

https://link.springer.com/article/10.1023/A:1026536128119

Flurkey, K., Papaconstantinou, J., Miller, R. A., & Harrison, D. E. (2001). Lifespan extension and delayed immune and collagen aging in mutant mice with defects in growth hormone production. *Proc Natl Acad Sci U S A*, *98*(12), 6736-6741. https://doi.org/10.1073/pnas.111158898

Fontana, L., & Partridge, L. (2015). Promoting health and longevity through diet: from model organisms to humans. *Cell*, *161*(1), 106-118. https://doi.org/10.1016/j.cell.2015.02.020

Fontana, L., Partridge, L., & Longo, V. D. (2010). Extending healthy life span--from yeast to humans. *Science*, *328*(5976), 321-326. https://doi.org/10.1126/science.1172539

Franceschi, C., Garagnani, P., Parini, P., Giuliani, C., & Santoro, A. (2018). Inflammaging: a new immune-metabolic viewpoint for age-related diseases. *Nat Rev Endocrinol*, *14*(10), 576-590. https://doi.org/10.1038/s41574-018-0059-4

Gabay, C. (2006). Interleukin-6 and chronic inflammation. *Arthritis Research & Therapy*, *8*(Suppl 2), S3. https://doi.org/10.1186/ar1917

Gao, H., Liu, D. E., Li, Y., Tang, J., Hu, S., Wu, X., Tian, Z., & Tan, H. (2019). Uterine size and volume are associated with a higher clinical pregnancy rate in patients undergoing assisted reproduction technology: A longitudinal

study (A STROBE-compliant article). *Medicine (Baltimore)*, *98*(8), e14366. https://doi.org/10.1097/MD.0000000000014366
Geary, M. P., Pringle, P. J., Rodeck, C. H., Kingdom, J. C., & Hindmarsh, P. C. (2003). Sexual dimorphism in the growth hormone and insulin-like growth factor axis at birth. *J Clin Endocrinol Metab*, *88*(8), 3708-3714. https://doi.org/10.1210/jc.2002-022006
Gebhardt, R. (1992). Metabolic zonation of the liver: regulation and implications for liver function. *Pharmacol Ther*, *53*(3), 275-354. https://doi.org/10.1016/0163-7258(92)90055-5
Gems, D. (2022). The hyperfunction theory: An emerging paradigm for the biology of aging. *Ageing Res Rev*, *74*, 101557. https://doi.org/10.1016/j.arr.2021.101557
Gems, D., & Partridge, L. (2013). Genetics of longevity in model organisms: debates and paradigm shifts. *Annu Rev Physiol*, *75*, 621-644. https://doi.org/10.1146/annurev-physiol-030212-183712
Georgieva, M., Xenodochidis, C., & Krasteva, N. (2023). Old age as a risk factor for liver diseases: Modern therapeutic approaches. *Exp Gerontol*, *184*, 112334. https://doi.org/10.1016/j.exger.2023.112334
Getschman, A. E., Imai, Y., Larsen, O., Peterson, F. C., Wu, X., Rosenkilde, M. M., Hwang, S. T., & Volkman, B. F. (2017). Protein engineering of the chemokine CCL20 prevents psoriasiform dermatitis in an IL-23-dependent murine model. *Proceedings of the National Academy of Sciences of the United States of America*, *114*(47), 12460-12465. https://doi.org/10.1073/pnas.1704958114
Ghasemi, A., & Zahediasl, S. (2012). Normality tests for statistical analysis: a guide for non-statisticians. *Int J Endocrinol Metab*, *10*(2), 486-489. https://doi.org/10.5812/ijem.3505
Girbig, M., Misiaszek, A. D., Vorlander, M. K., Lafita, A., Grotsch, H., Baudin, F., Bateman, A., & Muller, C. W. (2021). Cryo-EM structures of human RNA polymerase III in its unbound and transcribing states. *Nat Struct Mol Biol*, *28*(2), 210-219. https://doi.org/10.1038/s41594-020-00555-5
Gkioni, L., Nespital, T., Baghdadi, M., Monzo, C., Bali, J., Nassr, T., Cremer, A. L., Beyer, A., Deelen, J., Backes, H., Gronke, S., & Partridge, L. (2025). The geroprotectors trametinib and rapamycin combine additively to extend mouse healthspan and lifespan. *Nat Aging*, *5*(7), 1249-1265. https://doi.org/10.1038/s43587-025-00876-4
Goldman, J. M., Murr, A. S., & Cooper, R. L. (2007). The rodent estrous cycle: characterization of vaginal cytology and its utility in toxicological studies. *Birth Defects Research Part B: Developmental and Reproductive Toxicology*, *80*(2), 84-97. https://doi.org/https://doi.org/10.1002/bdrb.20106
Gong, B., Huang, L., He, Y., Xie, W., Yin, Y., Shi, Y., Xiao, J., Zhong, L., Zhang, Y., Jiang, Z., Hao, F., Zhou, Y., Li, H., Jiang, L., Yang, X., Song, X., Kang, Y., Tuo, L., Huang, Y.,…et al. (2022). A genetic variant in IL-6 lowering its expression is protective for critical patients with COVID-19. *Signal Transduction and Targeted Therapy*, *7*(1), 112. https://doi.org/10.1038/s41392-022-00923-1
Gong, J., Tu, W., Liu, J., & Tian, D. (2022). Hepatocytes: A key role in liver inflammation. *Front Immunol*, *13*, 1083780. https://doi.org/10.3389/fimmu.2022.1083780
González, A., & Hall, M. N. (2017). Nutrient sensing and TOR signaling in yeast and mammals. *The EMBO Journal*, *36*(4), 397-408. https://doi.org/10.15252/embj.201696010

Goodfellow, S. J., Graham, E. L., Kantidakis, T., Marshall, L., Coppins, B. A., Oficjalska-Pham, D., Gerard, M., Lefebvre, O., & White, R. J. (2008). Regulation of RNA polymerase III transcription by Maf1 in mammalian cells. *J Mol Biol*, *378*(3), 481-491. https://doi.org/10.1016/j.jmb.2008.02.060

Goodfellow, S. J., & White, R. J. (2007). Regulation of RNA polymerase III transcription during mammalian cell growth. *Cell Cycle*, *6*(19), 2323-2326. https://doi.org/10.4161/cc.6.19.4767

Goodman, C. A., & Hornberger, T. A. (2013). Measuring Protein Synthesis With SUnSET: A Valid Alternative to Traditional Techniques? *Exercise and Sport Sciences Reviews*, *41*(2). https://journals.lww.com/acsm-essr/fulltext/2013/04000/measuring_protein_synthesis_with_sunset__a_valid.7.aspx

Gorgoulis, V., Adams, P. D., Alimonti, A., Bennett, D. C., Bischof, O., Bishop, C., Campisi, J., Collado, M., Evangelou, K., Ferbeyre, G., Gil, J., Hara, E., Krizhanovsky, V., Jurk, D., Maier, A. B., Narita, M., Niedernhofer, L., Passos, J. F., Robbins, P. D.,…Demaria, M. (2019). Cellular Senescence: Defining a Path Forward. *Cell*, *179*(4), 813-827. https://doi.org/10.1016/j.cell.2019.10.005

Gosain, A., & DiPietro, L. A. (2004). Aging and wound healing. *World J Surg*, *28*(3), 321-326. https://doi.org/10.1007/s00268-003-7397-6

Gozalo, A. S., Zerfas, P. M., Qin, J., Alves, D. A., Akkaya, M., Pena, M. Y., & Elkins, W. R. (2023). Contributions of Diet and Age to Ulcerative Dermatitis in Female C57BL/6J Mice. *Comp Med*, *73*(2), 109-119. https://doi.org/10.30802/AALAS-CM-22-000096

Gubernatorova, E. O., Gorshkova, E. A., Polinova, A. I., & Drutskaya, M. S. (2020). IL-6: Relevance for immunopathology of SARS-CoV-2. *Cytokine Growth Factor Rev*, *53*, 13-24. https://doi.org/10.1016/j.cytogfr.2020.05.009

Guillen, C., & Benito, M. (2018). mTORC1 Overactivation as a Key Aging Factor in the Progression to Type 2 Diabetes Mellitus. *Front Endocrinol (Lausanne)*, *9*, 621. https://doi.org/10.3389/fendo.2018.00621

Guo, J., Huang, X., Dou, L., Yan, M., Shen, T., Tang, W., & Li, J. (2022). Aging and aging-related diseases: from molecular mechanisms to interventions and treatments. *Signal Transduction and Targeted Therapy*, *7*(1), 391. https://doi.org/10.1038/s41392-022-01251-0

Guo, Z., & Yu, Q. (2019). Role of mTOR Signaling in Female Reproduction. *Front Endocrinol (Lausanne)*, *10*, 692. https://doi.org/10.3389/fendo.2019.00692

Haigis, M. C., & Yankner, B. A. (2010). The aging stress response. *Mol Cell*, *40*(2), 333-344. https://doi.org/10.1016/j.molcel.2010.10.002

Hammerquist, A. M., & Curran, S. P. (2020). Roles for the RNA polymerase III regulator MAFR-1 in regulating sperm quality in Caenorhabditis elegans. *Sci Rep*, *10*(1), 19367. https://doi.org/10.1038/s41598-020-76423-5

Hammes, S. R., & Levin, E. R. (2019). Impact of estrogens in males and androgens in females. *J Clin Invest*, *129*(5), 1818-1826. https://doi.org/10.1172/JCI125755

Hampton, A. L., Aslam, M. N., Naik, M. K., Bergin, I. L., Allen, R. M., Craig, R. A., Kunkel, S. L., Veerapaneni, I., Paruchuri, T., Patterson, K. A., Rothman, E. D., Hish, G. A., Varani, J., & Rush, H. G. (2015). Ulcerative Dermatitis in C57BL/6NCrl Mice on a Low-Fat or High-Fat Diet With or Without a Mineralized Red-Algae Supplement. *Journal of the American Association for Laboratory Animal Science : JAALAS*, *54*(5), 487-496.

Hampton, A. L., Hish, G. A., Aslam, M. N., Rothman, E. D., Bergin, I. L., Patterson, K. A., Naik, M., Paruchuri, T., Varani, J., & Rush, H. G. (2012). Progression of ulcerative dermatitis lesions in C57BL/6Crl mice and the development of

a scoring system for dermatitis lesions. *Journal of the American Association for Laboratory Animal Science : JAALAS*, *51*(5), 586-593. https://pmc.ncbi.nlm.nih.gov/articles/PMC3447447/

Handelsman, D. J., Walters, K. A., & Ly, L. P. (2020). Simplified Method to Measure Mouse Fertility. *Endocrinology*, *161*(8). https://doi.org/10.1210/endocr/bqaa114

Harrison, D. E., Strong, R., Sharp, Z. D., Nelson, J. F., Astle, C. M., Flurkey, K., Nadon, N. L., Wilkinson, J. E., Frenkel, K., Carter, C. S., Pahor, M., Javors, M. A., Fernandez, E., & Miller, R. A. (2009). Rapamycin fed late in life extends lifespan in genetically heterogeneous mice. *Nature*, *460*(7253), 392-395. https://doi.org/10.1038/nature08221

Hartig, F. (2024, 2024-10-17). *DHARMa: residual diagnostics for hierarchical (multi-level/mixed) regression models*. CRAN R Project. https://cran.r-project.org/web/packages/DHARMa/vignettes/DHARMa.html

Harvima, I., & Nilsson, G. (2011). Mast cells as regulators of skin inflammation and immunity. *Acta Dermato Venereologica*, *91*(6), 644-650. https://doi.org/10.2340/00015555-1197

Hipp, M. S., Kasturi, P., & Hartl, F. U. (2019). The proteostasis network and its decline in ageing. *Nature Reviews Molecular Cell Biology*, *20*(7), 421-435. https://doi.org/10.1038/s41580-019-0101-y

Hoeijmakers, J. H. (2009). DNA damage, aging, and cancer. *N Engl J Med*, *361*(15), 1475-1485. https://doi.org/10.1056/NEJMra0804615

Hofmann, J. W., Zhao, X., De Cecco, M., Peterson, A. L., Pagliaroli, L., Manivannan, J., Hubbard, G. B., Ikeno, Y., Zhang, Y., Feng, B., Li, X., Serre, T., Qi, W., Van Remmen, H., Miller, R. A., Bath, K. G., de Cabo, R., Xu, H., Neretti, N., & Sedivy, J. M. (2015). Reduced expression of MYC increases longevity and enhances healthspan. *Cell*, *160*(3), 477-488. https://doi.org/10.1016/j.cell.2014.12.016

Holliday, R. (1989). Food, reproduction and longevity: is the extended lifespan of calorie-restricted animals an evolutionary adaptation? *Bioessays*, *10*(4), 125-127. https://doi.org/10.1002/bies.950100408

Holtze, S., Gorshkova, E., Braude, S., Cellerino, A., Dammann, P., Hildebrandt, T. B., Hoeflich, A., Hoffmann, S., Koch, P., Terzibasi Tozzini, E., Skulachev, M., Skulachev, V. P., & Sahm, A. (2021). Alternative Animal Models of Aging Research. *Front Mol Biosci*, *8*, 660959. https://doi.org/10.3389/fmolb.2021.660959

Holzenberger, M., Dupont, J., Ducos, B., Leneuve, P., Geloen, A., Even, P. C., Cervera, P., & Le Bouc, Y. (2003). IGF-1 receptor regulates lifespan and resistance to oxidative stress in mice. *Nature*, *421*(6919), 182-187. https://doi.org/10.1038/nature01298

Hornung, V., & Latz, E. (2010). Intracellular DNA recognition. *Nature Reviews Immunology*, *10*(2), 123-130. https://doi.org/10.1038/nri2690

Horstman, A. M., Dillon, E. L., Urban, R. J., & Sheffield-Moore, M. (2012). The role of androgens and estrogens on healthy aging and longevity. *J Gerontol A Biol Sci Med Sci*, *67*(11), 1140-1152. https://doi.org/10.1093/gerona/gls068

Hu, C., Yang, J., Qi, Z., Wu, H., Wang, B., Zou, F., Mei, H., Liu, J., Wang, W., & Liu, Q. (2022). Heat shock proteins: Biological functions, pathological roles, and therapeutic opportunities. *MedComm (2020)*, *3*(3), e161. https://doi.org/10.1002/mco2.161

Hu, Y. C., Wang, P. H., Yeh, S., Wang, R. S., Xie, C., Xu, Q., Zhou, X., Chao, H. T., Tsai, M. Y., & Chang, C. (2004). Subfertility and defective folliculogenesis in female mice lacking androgen receptor. *Proc Natl Acad Sci U S A*, *101*(31), 11209-11214. https://doi.org/10.1073/pnas.0404372101

Huang, Q., Chu, S., Yin, X., Yu, X., Kang, C., Li, X., & Qiu, Y. (2016). Interleukin-17A-Induced Epithelial-Mesenchymal Transition of Human Intrahepatic Biliary Epithelial Cells: Implications for Primary Biliary Cirrhosis. *Tohoku J Exp Med*, *240*(4), 269-275. https://doi.org/10.1620/tjem.240.269

Hudson, R., & Trillmich, F. (2008). Sibling competition and cooperation in mammals: challenges, developments and prospects. *Behavioral Ecology and Sociobiology*, *62*(3), 299-307. https://doi.org/10.1007/s00265-007-0417-z

Hunt, N. J., Kang, S. W. S., Lockwood, G. P., Le Couteur, D. G., & Cogger, V. C. (2019). Hallmarks of Aging in the Liver. *Comput Struct Biotechnol J*, *17*, 1151-1161. https://doi.org/10.1016/j.csbj.2019.07.021

Hunzicker-Dunn, M., & Maizels, E. T. (2006). FSH signaling pathways in immature granulosa cells that regulate target gene expression: branching out from protein kinase A. *Cell Signal*, *18*(9), 1351-1359. https://doi.org/10.1016/j.cellsig.2006.02.011

Hussain, A., & Gilloteaux, J. (2020). The human testes: Estrogen and ageing outlooks. *Translational Research in Anatomy*, *20*, 100073. https://doi.org/https://doi.org/10.1016/j.tria.2020.100073

Hwang, K. A., Yi, B. R., & Choi, K. C. (2011). Molecular mechanisms and in vivo mouse models of skin aging associated with dermal matrix alterations. *Lab Anim Res*, *27*(1), 1-8. https://doi.org/10.5625/lar.2011.27.1.1

Ibanez, L., Sebastiani, G., Lopez-Bermejo, A., Diaz, M., Gomez-Roig, M. D., & de Zegher, F. (2008). Gender specificity of body adiposity and circulating adiponectin, visfatin, insulin, and insulin growth factor-I at term birth: relation to prenatal growth. *J Clin Endocrinol Metab*, *93*(7), 2774-2778. https://doi.org/10.1210/jc.2008-0526

Ingolia, N. T., Ghaemmaghami, S., Newman, J. R., & Weissman, J. S. (2009). Genome-wide analysis in vivo of translation with nucleotide resolution using ribosome profiling. *Science*, *324*(5924), 218-223. https://doi.org/10.1126/science.1168978

Ireland, J. J., Smith, G. W., Scheetz, D., Jimenez-Krassel, F., Folger, J. K., Ireland, J. L., Mossa, F., Lonergan, P., & Evans, A. C. (2011). Does size matter in females? An overview of the impact of the high variation in the ovarian reserve on ovarian function and fertility, utility of anti-Mullerian hormone as a diagnostic marker for fertility and causes of variation in the ovarian reserve in cattle. *Reprod Fertil Dev*, *23*(1), 1-14. https://doi.org/10.1071/RD10226

Jacob, T., Annusver, K., Czarnewski, P., Dalessandri, T., Kalk, C., Levra Levron, C., Campama Sanz, N., Kastriti, M. E., Mikkola, M. L., Rendl, M., Lichtenberger, B. M., Donati, G., Bjorklund, A. K., & Kasper, M. (2023). Molecular and spatial landmarks of early mouse skin development. *Dev Cell*, *58*(20), 2140-2162 e2145. https://doi.org/10.1016/j.devcel.2023.07.015

Jacobs, R. Q., & Schneider, D. A. (2024). Transcription elongation mechanisms of RNA polymerases I, II, and III and their therapeutic implications. *J Biol Chem*, *300*(3), 105737. https://doi.org/10.1016/j.jbc.2024.105737

James, E. R., Carrell, D. T., Aston, K. I., Jenkins, T. G., Yeste, M., & Salas-Huetos, A. (2020). The Role of the Epididymis and the Contribution of Epididymosomes to Mammalian Reproduction. *Int J Mol Sci*, *21*(15). https://doi.org/10.3390/ijms21155377

Jarrous, N. (2017). Roles of RNase P and Its Subunits. *Trends Genet*, *33*(9), 594-603. https://doi.org/10.1016/j.tig.2017.06.006

Jaskelioff, M., Muller, F. L., Paik, J. H., Thomas, E., Jiang, S., Adams, A. C., Sahin, E., Kost-Alimova, M., Protopopov, A., Cadinanos, J., Horner, J. W., Maratos-

Flier, E., & Depinho, R. A. (2011). Telomerase reactivation reverses tissue degeneration in aged telomerase-deficient mice. *Nature*, *469*(7328), 102-106. https://doi.org/10.1038/nature09603

Javidnia, S., Cranwell, S., Mueller, S. H., Selman, C., Tullet, J. M. A., Kuchenbaecker, K., & Alic, N. (2022). Mendelian randomization analyses implicate biogenesis of translation machinery in human aging. *Genome Res*, *32*(2), 258-265. https://doi.org/10.1101/gr.275636.121

Jiang, Y., Tsoi, L. C., Billi, A. C., Ward, N. L., Harms, P. W., Zeng, C., Maverakis, E., Kahlenberg, J. M., & Gudjonsson, J. E. (2020). Cytokinocytes: the diverse contribution of keratinocytes to immune responses in skin. *JCI Insight*, *5*(20). https://doi.org/10.1172/jci.insight.142067

Jilka, R. L. (2013). The relevance of mouse models for investigating age-related bone loss in humans. *J Gerontol A Biol Sci Med Sci*, *68*(10), 1209-1217. https://doi.org/10.1093/gerona/glt046

Jinnin, M. (2010). Mechanisms of skin fibrosis in systemic sclerosis. *J Dermatol*, *37*(1), 11-25. https://doi.org/10.1111/j.1346-8138.2009.00738.x

Johnson, D. L., & Johnson, S. A. (2008). Cell biology. RNA metabolism and oncogenesis. *Science*, *320*(5875), 461-462. https://doi.org/10.1126/science.1158680

Johnson, S. S., Zhang, C., Fromm, J., Willis, I. M., & Johnson, D. L. (2007). Mammalian Maf1 Is a Negative Regulator of Transcription by All Three Nuclear RNA Polymerases. *Molecular Cell*, *26*(3), 367-379. https://doi.org/10.1016/j.molcel.2007.03.021

Jurgensen, H. J., van Putten, S., Norregaard, K. S., Bugge, T. H., Engelholm, L. H., Behrendt, N., & Madsen, D. H. (2020). Cellular uptake of collagens and implications for immune cell regulation in disease. *Cell Mol Life Sci*, *77*(16), 3161-3176. https://doi.org/10.1007/s00018-020-03481-3

Kaeberlein, M., Powers, R. W., 3rd, Steffen, K. K., Westman, E. A., Hu, D., Dang, N., Kerr, E. O., Kirkland, K. T., Fields, S., & Kennedy, B. K. (2005). Regulation of yeast replicative life span by TOR and Sch9 in response to nutrients. *Science*, *310*(5751), 1193-1196. https://doi.org/10.1126/science.1115535

Kalluri, R., & Zeisberg, M. (2006). Fibroblasts in cancer. *Nat Rev Cancer*, *6*(5), 392-401. https://doi.org/10.1038/nrc1877

Kalra, A., Yetiskul, E., Wehrle, C. J., & Tuma, F. (2023). Physiology, Liver. In *StatPearls* (Updated 2023 May 1 ed.). StatPearls Publishing. https://www.ncbi.nlm.nih.gov/books/NBK535438/

Kamm, D. R., & McCommis, K. S. (2022). Hepatic stellate cells in physiology and pathology. *J Physiol*, *600*(8), 1825-1837. https://doi.org/10.1113/jp281061

Kapahi, P., Zid, B. M., Harper, T., Koslover, D., Sapin, V., & Benzer, S. (2004). Regulation of Lifespan in Drosophila by Modulation of Genes in the TOR Signaling Pathway. *Current Biology*, *14*(10), 885-890. https://doi.org/10.1016/j.cub.2004.03.059

Kastenmayer, R. J., Fain, M. A., & Perdue, K. A. (2006). A retrospective study of idiopathic ulcerative dermatitis in mice with a C57BL/6 background. *J Am Assoc Lab Anim Sci*, *45*(6), 8-12. https://www.ncbi.nlm.nih.gov/pubmed/17089984

https://docserver.ingentaconnect.com/deliver/connect/aalas/15596109/v45n6/s1.pdf?expires=1688733561&id=0000&titleid=72010024&checksum=59F393BCCE0A36A867DA3EC629315552&host=https://www.ingentaconnect.com

Kawai, Y., Hata, T., Suzuki, O., & Matsuda, J. (2006). The relationship between sperm morphology and in vitro fertilization ability in mice. *J Reprod Dev*, *52*(4), 561-568. https://doi.org/10.1262/jrd.18023

Kenyon, C. (2005). The Plasticity of Aging: Insights from Long-Lived Mutants. *Cell*, *120*(4), 449-460. https://doi.org/10.1016/j.cell.2005.02.002
Khan, A. H., Zou, Z., Xiang, Y., Chen, S., & Tian, X. L. (2019). Conserved signaling pathways genetically associated with longevity across the species. *Biochim Biophys Acta Mol Basis Dis*, *1865*(7), 1745-1755. https://doi.org/10.1016/j.bbadis.2018.09.001
Khanna, A., Johnson, D. L., & Curran, S. P. (2014). Physiological roles for mafr-1 in reproduction and lipid homeostasis. *Cell Rep*, *9*(6), 2180-2191. https://doi.org/10.1016/j.celrep.2014.11.035
Kieckhaefer, J., Lukovac, S., Ye, D. Z., Lee, D., Beetler, D. J., Pack, M., & Kaestner, K. H. (2016). The RNA polymerase III subunit Polr3b is required for the maintenance of small intestinal crypts in mice. *Cell Mol Gastroenterol Hepatol*, *2*(6), 783-795. https://doi.org/10.1016/j.jcmgh.2016.08.003
Kirkwood, T. B. (1977). Evolution of ageing. *Nature*, *270*(5635), 301-304. https://doi.org/10.1038/270301a0
Klass, M. R. (1983). A method for the isolation of longevity mutants in the nematode Caenorhabditis elegans and initial results. *Mech Ageing Dev*, *22*(3-4), 279-286. https://doi.org/10.1016/0047-6374(83)90082-9
Klover, P. J., & Mooney, R. A. (2004). Hepatocytes: critical for glucose homeostasis. *Int J Biochem Cell Biol*, *36*(5), 753-758. https://doi.org/10.1016/j.biocel.2003.10.002
Knecht, D., Środoń, S., & Duziński, K. (2015). The impact of season, parity and breed on selected reproductive performance parameters of sows. *Arch. Anim. Breed.*, *58*(1), 49-56. https://doi.org/10.5194/aab-58-49-2015
Kordestani, S. S. (2019). Wound Healing Process. In *In Atlas of Wound Healing (pp. 11–22). Elsevier*. https://doi.org/10.1016/B978-0-323-67968-8.00003-3
Kounig, B., Riester, J., & Markl, H. (1988). Maternal care in house mice (Mus musculus): II. The energy cost of lactation as a function of litter size. *Journal of Zoology*, *216*(2), 195-210. https://doi.org/https://doi.org/10.1111/j.1469-7998.1988.tb02425.x
Krishnan, V., Chow, M. Z., Wang, Z., Zhang, L., Liu, B., Liu, X., & Zhou, Z. (2011). Histone H4 lysine 16 hypoacetylation is associated with defective DNA repair and premature senescence in Zmpste24-deficient mice. *Proc Natl Acad Sci U S A*, *108*(30), 12325-12330. https://doi.org/10.1073/pnas.1102789108
Kruglikov, I. L., & Scherer, P. E. (2016). Skin aging: are adipocytes the next target? *Aging (Albany NY)*, *8*(7), 1457-1469. https://doi.org/10.18632/aging.100999
Kruglikov, I. L., Zhang, Z., & Scherer, P. E. (2022). Skin aging: Dermal adipocytes metabolically reprogram dermal fibroblasts. *Bioessays*, *44*(1), e2100207. https://doi.org/10.1002/bies.202100207
Krugner-Higby, L., Brown, R., Rassette, M., Behr, M., Okwumabua, O., Cook, M., Bell, C., Flowers, M. T., Ntambi, J., & Gendron, A. (2012). Ulcerative dermatitis in C57BL/6 mice lacking stearoyl CoA desaturase 1. *Comp Med*, *62*(4), 257-263. https://www.ncbi.nlm.nih.gov/pubmed/23043777

https://www.ncbi.nlm.nih.gov/pmc/articles/PMC3415366/pdf/cm2012000257.pdf
Kulaberoglu, Y., Malik, Y., Borland, G., Selman, C., Alic, N., & Tullet, J. M. A. (2021). RNA Polymerase III, Ageing and Longevity. *Front Genet*, *12*, 705122. https://doi.org/10.3389/fgene.2021.705122
Kurnianto, E., Shinjo, A., & Suga, D. (1998). Prenatal and postnatal maternal effects on body weight in cross-fostering experiment on two subspecies of mice. *Exp Anim*, *47*(2), 97-103. https://doi.org/10.1538/expanim.47.97

Kurosu, H., Yamamoto, M., Clark, J. D., Pastor, J. V., Nandi, A., Gurnani, P., McGuinness, O. P., Chikuda, H., Yamaguchi, M., Kawaguchi, H., Shimomura, I., Takayama, Y., Herz, J., Kahn, C. R., Rosenblatt, K. P., & Kuro-o, M. (2005). Suppression of aging in mice by the hormone Klotho. *Science*, *309*(5742), 1829-1833. https://doi.org/10.1126/science.1112766

Kuznetsova, A., Brockhoff, P. B., & Christensen, R. H. B. (2017). lmerTest Package: Tests in Linear Mixed Effects Models. *Journal of Statistical Software*, *82*(13), 1 - 26. https://doi.org/10.18637/jss.v082.i13

Labib, P. L., Goodchild, G., & Pereira, S. P. (2019). Molecular Pathogenesis of Cholangiocarcinoma. *BMC Cancer*, *19*(1), 185. https://doi.org/10.1186/s12885-019-5391-0

Lambert, R. (2007). Breeding strategies for maintaining colonies of laboratory mice: A Jackson Laboratory resource manual. *Jackson Laboratories www. jax. org/jaxmice doi*, *10*.

Lamming, D. W., Ye, L., Sabatini, D. M., & Baur, J. A. (2013). Rapalogs and mTOR inhibitors as anti-aging therapeutics. *J Clin Invest*, *123*(3), 980-989. https://doi.org/10.1172/JCI64099

Laplante, M., & Sabatini, David M. (2012). mTOR Signaling in Growth Control and Disease. *Cell*, *149*(2), 274-293. https://doi.org/10.1016/j.cell.2012.03.017

Lata, E., Choquet, K., Sagliocco, F., Brais, B., Bernard, G., & Teichmann, M. (2021). RNA Polymerase III Subunit Mutations in Genetic Diseases. *Front Mol Biosci*, *8*, 696438. https://doi.org/10.3389/fmolb.2021.696438

Latham, K. E. (2025). Paternal Effects in Mammalian Reproduction: Functional, Environmental, and Clinical Relevance of Sperm Components in Early Embryos and Beyond. *Mol Reprod Dev*, *92*(3), e70020. https://doi.org/10.1002/mrd.70020

Laurie, E. M. O., & Goodrich, E. S. (1946). The reproduction of the house-mouse (Mus musculus) living in different environments. *Proceedings of the Royal Society of London. Series B - Biological Sciences*, *133*(872), 248-281. https://doi.org/doi:10.1098/rspb.1946.0012

Lawson, G. W., Sato, A., Fairbanks, L. A., & Lawson, P. T. (2005). Vitamin E as a treatment for ulcerative dermatitis in C57BL/6 mice and strains with a C57BL/6 background. *Contemporary Topics in Laboratory Animal Science*, *44*(3), 18-21.

Ledda-Columbano, G. M., Pibiri, M., Cossu, C., Molotzu, F., Locker, J., & Columbano, A. (2004). Aging does not reduce the hepatocyte proliferative response of mice to the primary mitogen TCPOBOP. *Hepatology*, *40*(4), 981-988. https://doi.org/10.1002/hep.20403

Lee, S. H., & Sacks, D. L. (2024). Resilience of dermis resident macrophages to inflammatory challenges. *Exp Mol Med*, *56*(10), 2105-2112. https://doi.org/10.1038/s12276-024-01313-z

Lei, J., Chen, S., & Zhong, S. (2017). Abnormal expression of TFIIIB subunits and RNA Pol III genes is associated with hepatocellular carcinoma. *Liver Res*, *1*(2), 112-120. https://doi.org/10.1016/j.livres.2017.08.005

Lesniewska, E., & Boguta, M. (2017). Novel layers of RNA polymerase III control affecting tRNA gene transcription in eukaryotes. *Open Biol*, *7*(2). https://doi.org/10.1098/rsob.170001

Lessard-Beaudoin, M., Laroche, M., Demers, M. J., Grenier, G., & Graham, R. K. (2015). Characterization of age-associated changes in peripheral organ and brain region weights in C57BL/6 mice. *Exp Gerontol*, *63*, 27-34. https://doi.org/10.1016/j.exger.2015.01.003

Lewis, S. E. M., Goldspink, D. F., Phillips, J. G., Merry, B. J., & Holehan, A. M. (1985). The effects of aging and chronic dietary restriction on whole body

growth and protein turnover in the rat. *Experimental Gerontology*, *20*(5), 253-263. https://doi.org/https://doi.org/10.1016/0531-5565(85)90050-6
Li, H., Li, H., Huo, R., Wu, P., Shen, Z., Xu, H., Shen, B., & Li, N. (2017). Cyr61/CCN1 induces CCL20 production by keratinocyte via activating p38 and JNK/AP-1 pathway in psoriasis. *J Dermatol Sci*, *88*(1), 46-56. https://doi.org/10.1016/j.jdermsci.2017.05.018
Li, L., & Boussiotis, V. A. (2013). The role of IL-17-producing Foxp3+ CD4+ T cells in inflammatory bowel disease and colon cancer. *Clinical Immunology*, *148*(2), 246-253. https://doi.org/https://doi.org/10.1016/j.clim.2013.05.003
Li, Y., Moir, R. D., Sethy-Coraci, I. K., Warner, J. R., & Willis, I. M. (2000). Repression of ribosome and tRNA synthesis in secretion-defective cells is signaled by a novel branch of the cell integrity pathway. *Mol Cell Biol*, *20*(11), 3843-3851. https://doi.org/10.1128/MCB.20.11.3843-3851.2000
Lin, Y., Qiu, T., Wei, G., Que, Y., Wang, W., Kong, Y., Xie, T., & Chen, X. (2022). Role of Histone Post-Translational Modifications in Inflammatory Diseases. *Frontiers in Immunology*, *13*, 852272. https://doi.org/10.3389/fimmu.2022.852272
Liu, G. Y., & Sabatini, D. M. (2020). mTOR at the nexus of nutrition, growth, ageing and disease. *Nat Rev Mol Cell Biol*, *21*(4), 183-203. https://doi.org/10.1038/s41580-019-0199-y
Liu, S., Cheng, C., Zhu, L., Zhao, T., Wang, Z., Yi, X., Yan, F., Wang, X., Li, C., Cui, T., & Yang, B. (2024). Liver organoids: updates on generation strategies and biomedical applications. *Stem Cell Research & Therapy*, *15*(1), 244. https://doi.org/10.1186/s13287-024-03865-3
Liu, T., Zhang, L., Joo, D., & Sun, S. C. (2017). NF-kappaB signaling in inflammation. *Signal Transduct Target Ther*, *2*, 17023-. https://doi.org/10.1038/sigtrans.2017.23
Liu, Y., Beyer, A., & Aebersold, R. (2016). On the Dependency of Cellular Protein Levels on mRNA Abundance. *Cell*, *165*(3), 535-550. https://doi.org/10.1016/j.cell.2016.03.014
Liu, Y., Masternak, M. M., Schneider, A., & Zhi, X. (2022). Dwarf mice as models for reproductive ageing research. *Reprod Biomed Online*, *44*(1), 5-13. https://doi.org/10.1016/j.rbmo.2021.09.016
Lonardo, A., Nascimbeni, F., Ballestri, S., Fairweather, D., Win, S., Than, T. A., Abdelmalek, M. F., & Suzuki, A. (2019). Sex Differences in Nonalcoholic Fatty Liver Disease: State of the Art and Identification of Research Gaps. *Hepatology*, *70*(4), 1457-1469. https://doi.org/10.1002/hep.30626
Lopez-Garcia, B., Lee, P. H., Yamasaki, K., & Gallo, R. L. (2005). Anti-fungal activity of cathelicidins and their potential role in Candida albicans skin infection. *J Invest Dermatol*, *125*(1), 108-115. https://doi.org/10.1111/j.0022-202X.2005.23713.x
Lopez-Otin, C., Blasco, M. A., Partridge, L., Serrano, M., & Kroemer, G. (2013). The hallmarks of aging. *Cell*, *153*(6), 1194-1217. https://doi.org/10.1016/j.cell.2013.05.039
Lovell, C. R., Smolenski, K. A., Duance, V. C., Light, N. D., Young, S., & Dyson, M. (1987). Type I and III collagen content and fibre distribution in normal human skin during ageing. *Br J Dermatol*, *117*(4), 419-428. https://doi.org/10.1111/j.1365-2133.1987.tb04921.x
Luo, X., Zhang, D., Zheng, J., Liu, H., Sun, L., Guo, H., Wang, L., & Cui, S. (2024). Casein kinase 1alpha mediates estradiol secretion via CYP19A1 expression in mouse ovarian granulosa cells. *BMC Biol*, *22*(1), 176. https://doi.org/10.1186/s12915-024-01957-3

Ma, H. Y., Xu, J., Liu, X., Zhu, Y., Gao, B., Karin, M., Tsukamoto, H., Jeste, D. V., Grant, I., Roberts, A. J., Contet, C., Geoffroy, C., Zheng, B., Brenner, D., & Kisseleva, T. (2016). The role of IL-17 signaling in regulation of the liver-brain axis and intestinal permeability in Alcoholic Liver Disease. *Curr Pathobiol Rep*, *4*(1), 27-35. https://doi.org/10.1007/s40139-016-0097-3

Ma, H. Y., Yamamoto, G., Xu, J., Liu, X., Karin, D., Kim, J. Y., Alexandrov, L. B., Koyama, Y., Nishio, T., Benner, C., Heinz, S., Rosenthal, S. B., Liang, S., Sun, M., Karin, G., Zhao, P., Brodt, P., McKillop, I. H., Quehenberger, O.,…Kisseleva, T. (2020). IL-17 signaling in steatotic hepatocytes and macrophages promotes hepatocellular carcinoma in alcohol-related liver disease. *J Hepatol*, *72*(5), 946-959. https://doi.org/10.1016/j.jhep.2019.12.016

Magnuson, B., Ekim, B., & Fingar, D. C. (2012). Regulation and function of ribosomal protein S6 kinase (S6K) within mTOR signalling networks. *Biochem J*, *441*(1), 1-21. https://doi.org/10.1042/BJ20110892

Malik, Y., Goncalves Silva, I., Diazgranados, R. R., Selman, C., Alic, N., & Tullet, J. M. (2024). Timing of TORC1 inhibition dictates Pol III involvement in Caenorhabditis elegans longevity. *Life Sci Alliance*, *7*(7). https://doi.org/10.26508/lsa.202402735

Malik, Y., Kulaberoglu, Y., Anver, S., Javidnia, S., Borland, G., Rivera, R., Cranwell, S., Medelbekova, D., Svermova, T., Thomson, J., Broughton, S., von der Haar, T., Selman, C., Tullet, J. M. A., & Alic, N. (2024). Disruption of tRNA biogenesis enhances proteostatic resilience, improves later-life health, and promotes longevity. *PLoS Biol*, *22*(10), e3002853. https://doi.org/10.1371/journal.pbio.3002853

Mann, O. N., Kong, C. S., Lucas, E. S., Brosens, J. J., Hanyaloglu, A. C., & Brighton, P. J. (2022). Expression and function of the luteinizing hormone choriogonadotropin receptor in human endometrial stromal cells. *Sci Rep*, *12*(1), 8624. https://doi.org/10.1038/s41598-022-12495-9

Mannick, J. B., & Lamming, D. W. (2023). Targeting the biology of aging with mTOR inhibitors. *Nat Aging*, *3*(6), 642-660. https://doi.org/10.1038/s43587-023-00416-y

Marcondes-de-Castro, I. A., Reis-Barbosa, P. H., Marinho, T. S., Aguila, M. B., & Mandarim-de-Lacerda, C. A. (2023). AMPK/mTOR pathway significance in healthy liver and non-alcoholic fatty liver disease and its progression. *J Gastroenterol Hepatol*, *38*(11), 1868-1876. https://doi.org/10.1111/jgh.16272

Marshall, L., Rideout, E. J., & Grewal, S. S. (2012). Nutrient/TOR-dependent regulation of RNA polymerase III controls tissue and organismal growth in Drosophila. *EMBO J*, *31*(8), 1916-1930. https://doi.org/10.1038/emboj.2012.33

Marshall, L., & White, R. J. (2008). Non-coding RNA production by RNA polymerase III is implicated in cancer. *Nat Rev Cancer*, *8*(12), 911-914. https://doi.org/10.1038/nrc2539

Marygold, S. J., Roote, J., Reuter, G., Lambertsson, A., Ashburner, M., Millburn, G. H., Harrison, P. M., Yu, Z., Kenmochi, N., Kaufman, T. C., Leevers, S. J., & Cook, K. R. (2007). The ribosomal protein genes and Minute loci of Drosophila melanogaster. *Genome Biol*, *8*(10), R216. https://doi.org/10.1186/gb-2007-8-10-r216

Mason, J. B., Habermehl, T. L., Underwood, K. B., Schneider, A., Brieno-Enriquez, M. A., Masternak, M. M., & Parkinson, K. C. (2022). The Interrelationship Between Female Reproductive Aging and Survival. *J Gerontol A Biol Sci Med Sci*, *77*(1), 75-83. https://doi.org/10.1093/gerona/glab252

Mathew-Steiner, S. S., Roy, S., & Sen, C. K. (2021). Collagen in Wound Healing. *Bioengineering (Basel)*, *8*(5). https://doi.org/10.3390/bioengineering8050063

Matsuoka, T., Ahlberg, P. E., Kessaris, N., Iannarelli, P., Dennehy, U., Richardson, W. D., McMahon, A. P., & Koentges, G. (2005). Neural crest origins of the neck and shoulder. *Nature*, *436*(7049), 347-355. https://doi.org/10.1038/nature03837

Mayhew, T. M., Jenkins, H., Todd, B., & Clifton, V. L. (2008). Maternal asthma and placental morphometry: effects of severity, treatment and fetal sex. *Placenta*, *29*(4), 366-373. https://doi.org/10.1016/j.placenta.2008.01.011

McCay, C. M., Crowell, M. F., & Maynard, L. A. (1935). The Effect of Retarded Growth Upon the Length of Life Span and Upon the Ultimate Body Size: One Figure. *The Journal of Nutrition*, *10*(1), 63-79. https://doi.org/https://doi.org/10.1093/jn/10.1.63

McGivern, D. R., & Lemon, S. M. (2009). Tumor suppressors, chromosomal instability, and hepatitis C virus-associated liver cancer. *Annu Rev Pathol*, *4*, 399-415. https://doi.org/10.1146/annurev.pathol.4.110807.092202

McLaughlin, T., Lamendola, C., Coghlan, N., Liu, T. C., Lerner, K., Sherman, A., & Cushman, S. W. (2014). Subcutaneous adipose cell size and distribution: Relationship to insulin resistance and body fat. *Obesity*, *22*(3), 673-680. https://doi.org/10.1002/oby.20209

McLaughlin, T., Sherman, A., Tsao, P., Gonzalez, O., Yee, G., Lamendola, C., Reaven, G. M., & Cushman, S. W. (2007). Enhanced proportion of small adipose cells in insulin-resistant vs insulin-sensitive obese individuals implicates impaired adipogenesis. *Diabetologia*, *50*(8), 1707-1715. https://doi.org/10.1007/s00125-007-0708-y

Medina-Gomez, G., Gray, S., & Vidal-Puig, A. (2007). Adipogenesis and lipotoxicity: role of peroxisome proliferator-activated receptor γ (PPARγ) and PPARγcoactivator-1 (PGC1). *Public Health Nutrition*, *10*(10A), 1132-1137. https://doi.org/10.1017/S1368980007000614

Mercer, M., Jang, S., Ni, C., & Buszczak, M. (2021). The Dynamic Regulation of mRNA Translation and Ribosome Biogenesis During Germ Cell Development and Reproductive Aging. *Front Cell Dev Biol*, *9*, 710186. https://doi.org/10.3389/fcell.2021.710186

Merheb, E., Cui, M. H., DuBois, J. C., Branch, C. A., Gulinello, M., Shafit-Zagardo, B., Moir, R. D., & Willis, I. M. (2021). Defective myelination in an RNA polymerase III mutant leukodystrophic mouse. *Proc Natl Acad Sci U S A*, *118*(40). https://doi.org/10.1073/pnas.2024378118

Merry, B. J., & Holehan, A. M. (1979). Onset of puberty and duration of fertility in rats fed a restricted diet. *J Reprod Fertil*, *57*(2), 253-259. https://doi.org/10.1530/jrf.0.0570253

Michalopoulos, G. K. (2017). Hepatostat: Liver regeneration and normal liver tissue maintenance. *Hepatology*, *65*(4), 1384-1392. https://doi.org/10.1002/hep.28988

Michels, A. A., Robitaille, A. M., Buczynski-Ruchonnet, D., Hodroj, W., Reina, J. H., Hall, M. N., & Hernandez, N. (2010). mTORC1 directly phosphorylates and regulates human MAF1. *Mol Cell Biol*, *30*(15), 3749-3757. https://doi.org/10.1128/MCB.00319-10

Mirea, A. M., Tack, C. J., Chavakis, T., Joosten, L. A. B., & Toonen, E. J. M. (2018). IL-1 Family Cytokine Pathways Underlying NAFLD: Towards New Treatment Strategies. *Trends Mol Med*, *24*(5), 458-471. https://doi.org/10.1016/j.molmed.2018.03.005

Mitani, H., Koshiishi, I., Toyoda, H., Toida, T., & Imanari, T. (1999). Alterations of hairless mouse skin exposed to chronic UV irradiation and its prevention by hydrocortisone. *Photochem Photobiol*, *69*(1), 41-46. https://www.ncbi.nlm.nih.gov/pubmed/10063799

Mohallem, R., Schaser, A. J., & Aryal, U. K. (2025). Proteomic and phosphoproteomic signatures of aging mouse liver. *Geroscience*, *47*(3), 5205-5224. https://doi.org/10.1007/s11357-025-01601-0

Moir, R. D., & Willis, I. M. (2013). Regulation of pol III transcription by nutrient and stress signaling pathways. *Biochim Biophys Acta*, *1829*(3-4), 361-375. https://doi.org/10.1016/j.bbagrm.2012.11.001

Mojiri, A., Walther, B. K., Jiang, C., Matrone, G., Holgate, R., Xu, Q., Morales, E., Wang, G., Gu, J., Wang, R., & Cooke, J. P. (2021). Telomerase therapy reverses vascular senescence and extends lifespan in progeria mice. *Eur Heart J*, *42*(42), 4352-4369. https://doi.org/10.1093/eurheartj/ehab547

Morello, G. M., Capas-Peneda, S., Brajon, S., Lamas, S., Lopes, I. M., Gilbert, C., & Olsson, I. A. S. (2024). Proper micro-environment alleviates mortality in laboratory mouse breeding induced by litter overlap and older dams. *Communications Biology*, *7*(1), 1008. https://doi.org/10.1038/s42003-024-06654-z

Morimoto, R. I. (2020). Cell-Nonautonomous Regulation of Proteostasis in Aging and Disease. *Cold Spring Harb Perspect Biol*, *12*(4). https://doi.org/10.1101/cshperspect.a034074

Moura, C. S., Lollo, P. C. B., Morato, P. N., & Amaya-Farfan, J. (2018). Dietary Nutrients and Bioactive Substances Modulate Heat Shock Protein (HSP) Expression: A Review. *Nutrients*, *10*(6). https://doi.org/10.3390/nu10060683

Müller, G., Wied, S., Dearey, E. A., & Biemer-Daub, G. (2011). Glycosylphosphatidylinositol-anchored proteins coordinate lipolysis inhibition between large and small adipocytes. *Metabolism*, *60*(7), 1021-1037. https://doi.org/10.1016/j.metabol.2010.10.007

Naesens, L., Haerynck, F., & Gack, M. U. (2023). The RNA polymerase III-RIG-I axis in antiviral immunity and inflammation. *Trends Immunol*, *44*(6), 435-449. https://doi.org/10.1016/j.it.2023.04.002

Nagasawa, H., Naito, T., & Kataoka, K. (1989). Relationship between milk composition and pup's growth in mice. *Proc Soc Exp Biol Med*, *191*(1), 78-81. https://doi.org/10.3181/00379727-191-42892

Nakao, S., Takeo, T., Watanabe, H., Kondoh, G., & Nakagata, N. (2020). Successful selection of mouse sperm with high viability and fertility using microfluidics chip cell sorter. *Scientific Reports*, *10*(1), 8862. https://doi.org/10.1038/s41598-020-65931-z

Narayan, P., & Puett, D. (2003). Luteinizing Hormone Receptor Signaling. In H. L. Henry & A. W. Norman (Eds.), *Encyclopedia of Hormones* (pp. 612-616). Academic Press. https://doi.org/https://doi.org/10.1016/B0-12-341103-3/00192-3

Nelson, R. J. (2011). *An introduction to behavioral endocrinology* (4th ed.). Sinauer Associates.

Nestle, F. O., Kaplan, D. H., & Barker, J. (2009). Psoriasis. *New England Journal of Medicine*, *361*(5), 496-509. https://doi.org/10.1056/NEJMra0804595

Neuhaus, B., Niessen, C. M., Mesaros, A., Withers, D. J., Krieg, T., & Partridge, L. (2012). Experimental analysis of risk factors for ulcerative dermatitis in mice. *Exp Dermatol*, *21*(9), 712-713. https://doi.org/10.1111/j.1600-0625.2012.01558.x

Neurath, M. F., & Finotto, S. (2011). IL-6 signaling in autoimmunity, chronic inflammation and inflammation-associated cancer. *Cytokine & Growth Factor Reviews*, *22*(2), 83-89. https://doi.org/10.1016/j.cytogfr.2011.02.003

Ni, C., & Buszczak, M. (2023). Ribosome biogenesis and function in development and disease. *Development*, *150*(5). https://doi.org/10.1242/dev.201187

Nierras, C. R., & Warner, J. R. (1999). Protein kinase C enables the regulatory circuit that connects membrane synthesis to ribosome synthesis in Saccharomyces cerevisiae. *J Biol Chem*, *274*(19), 13235-13241. https://doi.org/10.1074/jbc.274.19.13235

Nijhout, H. F., Best, J. A., & Reed, M. C. (2019). Systems biology of robustness and homeostatic mechanisms. *Wiley Interdiscip Rev Syst Biol Med*, *11*(3), e1440. https://doi.org/10.1002/wsbm.1440

Nilsson, E., & Skinner, M. K. (2024). Overview of the Reproduction of Laboratory Mice and Rats. In *Reference Module in Biomedical Sciences*. Elsevier. https://doi.org/https://doi.org/10.1016/B978-0-443-21477-6.00212-1

Nizar, N., Afriwardi, A., Yamwirsati, Y., & Arlan, A. (2021). Matrix Metalloproteinase-2, COL1A1, and COL3A1 mRNA Expression in Aponeurosis Musculus obliquus Externus Abdominis of Adult Inguinal Hernias. *Open Access Macedonian Journal of Medical Sciences*, *9 (No. A)*, 318–323. https://doi.org/10.3889/oamjms.2021.6143

Noguchi, C., Wang, L., Shetty, M., Mell, J. C., Sell, C., & Noguchi, E. (2021). Maf1 limits RNA polymerase III-directed transcription to preserve genomic integrity and extend lifespan. *Cell Cycle*, *20*(3), 247-255. https://doi.org/10.1080/15384101.2021.1874697

Norris, D. O., & Carr, J. A. (2023). *Endocrine disruption : biological basis for health effects in wildlife and humans*. Oxford University Press. https://doi.org/10.1093/oso/9780195137491.001.0001

Numata, T., Harada, K., & Nakae, S. (2022). Roles of Mast Cells in Cutaneous Diseases. *Frontiers in Immunology, 13*. https://doi.org/10.3389/fimmu.2022.923495

Oduwole, O. O., Huhtaniemi, I. T., & Misrahi, M. (2021). The Roles of Luteinizing Hormone, Follicle-Stimulating Hormone and Testosterone in Spermatogenesis and Folliculogenesis Revisited. *Int J Mol Sci*, *22*(23). https://doi.org/10.3390/ijms222312735

Office for National Statistics. (2025). *National life tables, United Kingdom: 1980–1982 to 2021–2023* (Version 2021–2023 release) Office for National Statistics. https://www.ons.gov.uk/peoplepopulationandcommunity/birthsdeathsandmarriages/lifeexpectancies/datasets/nationallifetablesunitedkingdomreferencetables

Ogrodnik, M., Miwa, S., Tchkonia, T., Tiniakos, D., Wilson, C. L., Lahat, A., Day, C. P., Burt, A., Palmer, A., Anstee, Q. M., Grellscheid, S. N., Hoeijmakers, J. H. J., Barnhoorn, S., Mann, D. A., Bird, T. G., Vermeij, W. P., Kirkland, J. L., Passos, J. F., von Zglinicki, T., & Jurk, D. (2017). Cellular senescence drives age-dependent hepatic steatosis. *Nat Commun*, *8*, 15691. https://doi.org/10.1038/ncomms15691

Oh, J., Lee, Y. D., & Wagers, A. J. (2014). Stem cell aging: mechanisms, regulators and therapeutic opportunities. *Nat Med*, *20*(8), 870-880. https://doi.org/10.1038/nm.3651

Ozawa, M., Mori, H., Endo, T., Ishikawa-Yamauchi, Y., Motooka, D., Emori, C., & Ikawa, M. (2023). Age-related decline in spermatogenic activity accompanied with endothelial cell senescence in male mice. *iScience*, *26*(12), 108456. https://doi.org/10.1016/j.isci.2023.108456

Padhiar, N. H., Katneni, U., Komar, A. A., Motorin, Y., & Kimchi-Sarfaty, C. (2024). Advances in methods for tRNA sequencing and quantification. *Trends in Genetics*, *40*(3), 276-290. https://doi.org/10.1016/j.tig.2023.11.001

Palian, B. M., Rohira, A. D., Johnson, S. A., He, L., Zheng, N., Dubeau, L., Stiles, B. L., & Johnson, D. L. (2014). Maf1 is a novel target of PTEN and PI3K signaling that negatively regulates oncogenesis and lipid metabolism. *PLoS Genet*, *10*(12), e1004789. https://doi.org/10.1371/journal.pgen.1004789

Panghiyangani, R., Soeharso, P., Andrijono, Suryandari, D. A., Wiweko, B., Kurniati, M., & Pujianto, D. A. (2020). CYP19A1 Gene Expression in Patients with Polycystic Ovarian Syndrome. *J Hum Reprod Sci*, *13*(2), 100-103. https://doi.org/10.4103/jhrs.JHRS_142_18

Panwar, V., Singh, A., Bhatt, M., Tonk, R. K., Azizov, S., Raza, A. S., Sengupta, S., Kumar, D., & Garg, M. (2023). Multifaceted role of mTOR (mammalian target of rapamycin) signaling pathway in human health and disease. *Signal Transduction and Targeted Therapy*, *8*(1), 375. https://doi.org/10.1038/s41392-023-01608-z

Park, J. L., Lee, Y. S., Kunkeaw, N., Kim, S. Y., Kim, I. H., & Lee, Y. S. (2017). Epigenetic regulation of noncoding RNA transcription by mammalian RNA polymerase III. *Epigenomics*, *9*(2), 171-187. https://doi.org/10.2217/epi-2016-0108

Park, S. U., Walsh, L., & Berkowitz, K. M. (2021). Mechanisms of ovarian aging. *Reproduction*, *162*(2), R19-R33. https://doi.org/10.1530/REP-21-0022

Partridge, L. (2010). The new biology of ageing. *Philos Trans R Soc Lond B Biol Sci*, *365*(1537), 147-154. https://doi.org/10.1098/rstb.2009.0222

Partridge, L., & Gems, D. (2002). Mechanisms of ageing: public or private? *Nat Rev Genet*, *3*(3), 165-175. https://doi.org/10.1038/nrg753

Patel, R., Moffatt, J. D., Mourmoura, E., Demaison, L., Seed, P. T., Poston, L., & Tribe, R. M. (2017). Effect of reproductive ageing on pregnant mouse uterus and cervix. *J Physiol*, *595*(6), 2065-2084. https://doi.org/10.1113/JP273350

Peleg, S., Sananbenesi, F., Zovoilis, A., Burkhardt, S., Bahari-Javan, S., Agis-Balboa, R. C., Cota, P., Wittnam, J. L., Gogol-Doering, A., Opitz, L., Salinas-Riester, G., Dettenhofer, M., Kang, H., Farinelli, L., Chen, W., & Fischer, A. (2010). Altered histone acetylation is associated with age-dependent memory impairment in mice. *Science*, *328*(5979), 753-756. https://doi.org/10.1126/science.1186088

Perrier, S., Macintosh, J., Misiaszek, A. D., Lambert, G., Guerrero, K., Tran, L. T., Muller, C. W., Pastinen, T., Maegawa, G. H. B., Thiffault, I., & Bernard, G. (2024). Novel Pathogenic Variants in POLR3K Cause POLR3-Related Leukodystrophy. *Hum Mutat*, *2024*, 8807171. https://doi.org/10.1155/2024/8807171

Pinto, C., Ninfole, E., Benedetti, A., Marzioni, M., & Maroni, L. (2021). Involvement of Autophagy in Ageing and Chronic Cholestatic Diseases. *Cells*, *10*(10). https://doi.org/10.3390/cells10102772

Piper, M. D., Selman, C., McElwee, J. J., & Partridge, L. (2008). Separating cause from effect: how does insulin/IGF signalling control lifespan in worms, flies and mice? *J Intern Med*, *263*(2), 179-191. https://doi.org/10.1111/j.1365-2796.2007.01906.x

Pluta, K., Lefebvre, O., Martin, N. C., Smagowicz, W. J., Stanford, D. R., Ellis, S. R., Hopper, A. K., Sentenac, A., & Boguta, M. (2001). Maf1p, a negative effector of RNA polymerase III in Saccharomyces cerevisiae. *Mol Cell Biol*, *21*(15), 5031-5040. https://doi.org/10.1128/MCB.21.15.5031-5040.2001

Portincasa, P., Grattagliano, I., Palmieri, V. O., & Palasciano, G. (2005). Nonalcoholic steatohepatitis: recent advances from experimental models to

clinical management. *Clin Biochem*, *38*(3), 203-217. https://doi.org/10.1016/j.clinbiochem.2004.10.014
Powers, E. T., Morimoto, R. I., Dillin, A., Kelly, J. W., & Balch, W. E. (2009). Biological and chemical approaches to diseases of proteostasis deficiency. *Annu Rev Biochem*, *78*, 959-991. https://doi.org/10.1146/annurev.biochem.052308.114844
Powers, R. W., 3rd, Kaeberlein, M., Caldwell, S. D., Kennedy, B. K., & Fields, S. (2006). Extension of chronological life span in yeast by decreased TOR pathway signaling. *Genes Dev*, *20*(2), 174-184. https://doi.org/10.1101/gad.1381406
Powers, T., & Walter, P. (1999). Regulation of ribosome biogenesis by the rapamycin-sensitive TOR-signaling pathway in Saccharomyces cerevisiae. *Mol Biol Cell*, *10*(4), 987-1000. https://doi.org/10.1091/mbc.10.4.987
Pritchard, M. T., & Apte, U. (2015). Chapter 2 - Models to Study Liver Regeneration. In U. Apte (Ed.), *Liver Regeneration* (pp. 15-40). Academic Press. https://doi.org/https://doi.org/10.1016/B978-0-12-420128-6.00002-6
Qiao, J., & Han, B. (2019). Chapter Four - Diseases caused by mutations in luteinizing hormone/chorionic gonadotropin receptor. In Y.-X. Tao (Ed.), *Progress in Molecular Biology and Translational Science* (Vol. 161, pp. 69-89). Academic Press. https://doi.org/https://doi.org/10.1016/bs.pmbts.2018.09.007
Qu, N., Xu, M., Mizoguchi, I., Furusawa, J., Kaneko, K., Watanabe, K., Mizuguchi, J., Itoh, M., Kawakami, Y., & Yoshimoto, T. (2013). Pivotal roles of T-helper 17-related cytokines, IL-17, IL-22, and IL-23, in inflammatory diseases. *Clin Dev Immunol*, *2013*, 968549. https://doi.org/10.1155/2013/968549
Rajendra, K. C., Cheng, R., Zhou, S., Lizarazo, S., Smith, D. J., & Van Bortle, K. (2024). Evidence of RNA polymerase III recruitment and transcription at protein-coding gene promoters. *Molecular Cell*, *84*(21), 4111-4124.e4115. https://doi.org/10.1016/j.molcel.2024.09.019
Raju, G. A., Chavan, R., Deenadayal, M., Gunasheela, D., Gutgutia, R., Haripriya, G., Govindarajan, M., Patel, N. H., & Patki, A. S. (2013). Luteinizing hormone and follicle stimulating hormone synergy: A review of role in controlled ovarian hyper-stimulation. *J Hum Reprod Sci*, *6*(4), 227-234. https://doi.org/10.4103/0974-1208.126285
Ramsay, E. P., Abascal-Palacios, G., Daiß, J. L., King, H., Gouge, J., Pilsl, M., Beuron, F., Morris, E., Gunkel, P., Engel, C., & Vannini, A. (2020). Structure of human RNA polymerase III. *Nature Communications*, *11*(1), 6409. https://doi.org/10.1038/s41467-020-20262-5
Rehwinkel, J., & Gack, M. U. (2020). RIG-I-like receptors: their regulation and roles in RNA sensing. *Nature Reviews Immunology*, *20*(9), 537-551. https://doi.org/10.1038/s41577-020-0288-3
Reid, K., Daniels, E. G., Vasam, G., Kamble, R., Janssens, G. E., Hu, I. M., Green, A. E., Houtkooper, R. H., & Menzies, K. J. (2023). Reducing mitochondrial ribosomal gene expression does not alter metabolic health or lifespan in mice. *Sci Rep*, *13*(1), 8391. https://doi.org/10.1038/s41598-023-35196-3
Rhea, L., & Dunnwald, M. (2020). Murine Excisional Wound Healing Model and Histological Morphometric Wound Analysis. *J Vis Exp*(162). https://doi.org/10.3791/61616
Richter, K., Haslbeck, M., & Buchner, J. (2010). The Heat Shock Response: Life on the Verge of Death. *Molecular Cell*, *40*(2), 253-266. https://doi.org/10.1016/j.molcel.2010.10.006
Ristow, M., & Schmeisser, K. (2014). Mitohormesis: Promoting Health and Lifespan by Increased Levels of Reactive Oxygen Species (ROS). *Dose*

Response, *12*(2), 288-341. https://doi.org/10.2203/dose-response.13-035.Ristow

Rodriguez-Martinez, A., & Young-Baird, S. K. (2025). Polysome profiling is an extensible tool for the analysis of bulk protein synthesis, ribosome biogenesis, and the specific steps in translation. *Mol Biol Cell*, *36*(4), mr2. https://doi.org/10.1091/mbc.E24-08-0341

Rodriques, S. G., Stickels, R. R., Goeva, A., Martin, C. A., Murray, E., Vanderburg, C. R., Welch, J., Chen, L. M., Chen, F., & Macosko, E. Z. (2019). Slide-seq: A scalable technology for measuring genome-wide expression at high spatial resolution. *Science*, *363*(6434), 1463-1467. https://doi.org/10.1126/science.aaw1219

Roy, S., Santra, S., Das, A., Dixith, S., Sinha, M., Ghatak, S., Ghosh, N., Banerjee, P., Khanna, S., Mathew-Steiner, S., Ghatak, P. D., Blackstone, B. N., Powell, H. M., Bergdall, V. K., Wozniak, D. J., & Sen, C. K. (2020). Staphylococcus aureus Biofilm Infection Compromises Wound Healing by Causing Deficiencies in Granulation Tissue Collagen. *Ann Surg*, *271*(6), 1174-1185. https://doi.org/10.1097/SLA.0000000000003053

Ruland, J., Duncan, G. S., Wakeham, A., & Mak, T. W. (2003). Differential Requirement for Malt1 in T and B Cell Antigen Receptor Signaling. *Immunity*, *19*(5), 749-758. https://doi.org/10.1016/S1074-7613(03)00293-0

Rutz, S., Eidenschenk, C., & Ouyang, W. (2013). IL-22, not simply a Th17 cytokine. *Immunol Rev*, *252*(1), 116-132. https://doi.org/10.1111/imr.12027

Ruvinsky, I., & Meyuhas, O. (2006). Ribosomal protein S6 phosphorylation: from protein synthesis to cell size. *Trends in Biochemical Sciences*, *31*(6), 342-348. https://doi.org/10.1016/j.tibs.2006.04.003

Ryu, B. Y., Orwig, K. E., Oatley, J. M., Avarbock, M. R., & Brinster, R. L. (2006). Effects of aging and niche microenvironment on spermatogonial stem cell self-renewal. *Stem Cells*, *24*(6), 1505-1511. https://doi.org/10.1634/stemcells.2005-0580

Sabatini, D. M., Erdjument-Bromage, H., Lui, M., Tempst, P., & Snyder, S. H. (1994). RAFT1: a mammalian protein that binds to FKBP12 in a rapamycin-dependent fashion and is homologous to yeast TORs. *Cell*, *78*(1), 35-43. https://doi.org/10.1016/0092-8674(94)90570-3

Sadler, T. W. (2012). *Langman's Medical Embryology* (12th ed. ed.). Wolters Kluwer Health/Lippincott Williams & Wilkins. https://nlm.nih.gov/catalog/101562744

Saghi, M., InanlooRahatloo, K., Alavi, A., Kahrizi, K., & Najmabadi, H. (2022). Intellectual disability associated with craniofacial dysmorphism due to POLR3B mutation and defect in spliceosomal machinery. *BMC Med Genomics*, *15*(1), 89. https://doi.org/10.1186/s12920-022-01237-5

Saitsu, H., Osaka, H., Sasaki, M., Takanashi, J., Hamada, K., Yamashita, A., Shibayama, H., Shiina, M., Kondo, Y., Nishiyama, K., Tsurusaki, Y., Miyake, N., Doi, H., Ogata, K., Inoue, K., & Matsumoto, N. (2011). Mutations in POLR3A and POLR3B encoding RNA Polymerase III subunits cause an autosomal-recessive hypomyelinating leukoencephalopathy. *Am J Hum Genet*, *89*(5), 644-651. https://doi.org/10.1016/j.ajhg.2011.10.003

Salas-Silva, S., Simoni-Nieves, A., Chavez-Rodriguez, L., Gutierrez-Ruiz, M. C., Bucio, L., & Quiroz, L. E. G. (2021). Mechanism of cholangiocellular damage and repair during cholestasis. *Ann Hepatol*, *26*, 100530. https://doi.org/10.1016/j.aohep.2021.100530

Sancak, Y., Thoreen, C. C., Peterson, T. R., Lindquist, R. A., Kang, S. A., Spooner, E., Carr, S. A., & Sabatini, D. M. (2007). PRAS40 is an insulin-regulated

inhibitor of the mTORC1 protein kinase. *Mol Cell*, *25*(6), 903-915. https://doi.org/10.1016/j.molcel.2007.03.003

Sargent, J. L., Koewler, N. J., & Diggs, H. E. (2015). Systematic Literature Review of Risk Factors and Treatments for Ulcerative Dermatitis in C57BL/6 Mice. *Comp Med*, *65*(6), 465-472. https://www.ncbi.nlm.nih.gov/pubmed/26678363

Sasaki, M., Ikeda, H., Yamaguchi, J., Miyakoshi, M., Sato, Y., & Nakanuma, Y. (2010). Bile ductular cells undergoing cellular senescence increase in chronic liver diseases along with fibrous progression. *Am J Clin Pathol*, *133*(2), 212-223. https://doi.org/10.1309/AJCPWMX47TREYWZG

Saul, D., Jurk, D., Doolittle, M. L., Kosinsky, R. L., Monroe, D. G., LeBrasseur, N. K., Robbins, P. D., Niedernhofer, L. J., Khosla, S., & Passos, J. F. (2023). Distinct secretomes in p16- and p21- positive senescent cells across tissues. *bioRxiv*. https://doi.org/10.1101/2023.12.05.569858

Sawaguchi, S., Suzuki, R., Oizumi, H., Ohbuchi, K., Mizoguchi, K., Yamamoto, M., Miyamoto, Y., & Yamauchi, J. (2022). Hypomyelinating Leukodystrophy 8 (HLD8)-Associated Mutation of POLR3B Leads to Defective Oligodendroglial Morphological Differentiation Whose Effect Is Reversed by Ibuprofen. *Neurol Int*, *14*(1), 212-244. https://doi.org/10.3390/neurolint14010018

Saxton, R. A., & Sabatini, D. M. (2017). mTOR Signaling in Growth, Metabolism, and Disease. *Cell*, *168*(6), 960-976. https://doi.org/10.1016/j.cell.2017.02.004

Schenk, A., Ghallab, A., Hofmann, U., Hassan, R., Schwarz, M., Schuppert, A., Schwen, L. O., Braeuning, A., Teutonico, D., Hengstler, J. G., & Kuepfer, L. (2017). Physiologically-based modelling in mice suggests an aggravated loss of clearance capacity after toxic liver damage. *Sci Rep*, *7*(1), 6224. https://doi.org/10.1038/s41598-017-04574-z

Schindelin, J., Arganda-Carreras, I., Frise, E., Kaynig, V., Longair, M., Pietzsch, T., Preibisch, S., Rueden, C., Saalfeld, S., Schmid, B., Tinevez, J. Y., White, D. J., Hartenstein, V., Eliceiri, K., Tomancak, P., & Cardona, A. (2012). Fiji: an open-source platform for biological-image analysis. *Nat Methods*, *9*(7), 676-682. https://doi.org/10.1038/nmeth.2019

Schmitt, A., Grondona, P., Maier, T., Brändle, M., Schönfeld, C., Jäger, G., Kosnopfel, C., Eberle, F. C., Schittek, B., Schulze-Osthoff, K., Yazdi, A. S., & Hailfinger, S. (2016). MALT1 Protease Activity Controls the Expression of Inflammatory Genes in Keratinocytes upon Zymosan Stimulation. *Journal of Investigative Dermatology*, *136*(4), 788-797. https://doi.org/10.1016/j.jid.2015.12.027

Schramm, L., & Hernandez, N. (2002). Recruitment of RNA polymerase III to its target promoters. *Genes Dev*, *16*(20), 2593-2620. https://doi.org/10.1101/gad.1018902

Schulte, H., Muhlfeld, C., & Brandenberger, C. (2019). Age-Related Structural and Functional Changes in the Mouse Lung. *Front Physiol*, *10*, 1466. https://doi.org/10.3389/fphys.2019.01466

Sclafani, A. M., Skidmore, J. M., Ramaprakash, H., Trumpp, A., Gage, P. J., & Martin, D. M. (2006). Nestin-Cre mediated deletion of Pitx2 in the mouse. *Genesis*, *44*(7), 336-344. https://doi.org/10.1002/dvg.20220

Scott, P. H., Brunn, G. J., Kohn, A. D., Roth, R. A., & Lawrence, J. C., Jr. (1998). Evidence of insulin-stimulated phosphorylation and activation of the mammalian target of rapamycin mediated by a protein kinase B signaling pathway. *Proc Natl Acad Sci U S A*, *95*(13), 7772-7777. https://doi.org/10.1073/pnas.95.13.7772

Segaloff, D. L., & Ascoli, M. (2013). Thyroid-Stimulating Hormone/Luteinizing Hormone/Follicle-Stimulating Hormone Receptors. In W. J. Lennarz & M. D. Lane (Eds.), *Encyclopedia of Biological Chemistry (Second Edition)* (pp. 387-391). Academic Press. https://doi.org/https://doi.org/10.1016/B978-0-12-378630-2.00324-8

Sehgal, S. N., Baker, H., & Vezina, C. (1975). Rapamycin (AY-22,989), a new antifungal antibiotic. II. Fermentation, isolation and characterization. *J Antibiot (Tokyo)*, *28*(10), 727-732. https://doi.org/10.7164/antibiotics.28.727

Selman, C. (2024). The dietary exposome: a brief history of diet, longevity, and age-related health in rodents. *Clin Sci (Lond)*, *138*(21), 1343-1356. https://doi.org/10.1042/CS20241248

Selman, C., Lingard, S., Choudhury, A. I., Batterham, R. L., Claret, M., Clements, M., Ramadani, F., Okkenhaug, K., Schuster, E., Blanc, E., Piper, M. D., Al-Qassab, H., Speakman, J. R., Carmignac, D., Robinson, I. C., Thornton, J. M., Gems, D., Partridge, L., & Withers, D. J. (2008). Evidence for lifespan extension and delayed age-related biomarkers in insulin receptor substrate 1 null mice. *FASEB J*, *22*(3), 807-818. https://doi.org/10.1096/fj.07-9261com

Selman, C., & Swindell, W. R. (2018). Putting a strain on diversity. *EMBO J*, *37*(22). https://doi.org/10.15252/embj.2018100862

Selman, C., Tullet, J. M., Wieser, D., Irvine, E., Lingard, S. J., Choudhury, A. I., Claret, M., Al-Qassab, H., Carmignac, D., Ramadani, F., Woods, A., Robinson, I. C., Schuster, E., Batterham, R. L., Kozma, S. C., Thomas, G., Carling, D., Okkenhaug, K., Thornton, J. M.,…Withers, D. J. (2009). Ribosomal protein S6 kinase 1 signaling regulates mammalian life span. *Science*, *326*(5949), 140-144. https://doi.org/10.1126/science.1177221

Selman, C., & Withers, D. J. (2011). Mammalian models of extended healthy lifespan. *Philos Trans R Soc Lond B Biol Sci*, *366*(1561), 99-107. https://doi.org/10.1098/rstb.2010.0243

Sferruzzi-Perri, A. N., Lopez-Tello, J., & Salazar-Petres, E. (2023). Placental adaptations supporting fetal growth during normal and adverse gestational environments. *Exp Physiol*, *108*(3), 371-397. https://doi.org/10.1113/EP090442

Shanley, D. P., & Kirkwood, T. B. (2000). Calorie restriction and aging: a life-history analysis. *Evolution*, *54*(3), 740-750. https://doi.org/10.1111/j.0014-3820.2000.tb00076.x

Sharma, D., & Bhartiya, D. (2022). Aged mice ovaries harbor stem cells and germ cell nests but fail to form follicles. *J Ovarian Res*, *15*(1), 37. https://doi.org/10.1186/s13048-022-00968-4

Sharma, U., Conine, C. C., Shea, J. M., Boskovic, A., Derr, A. G., Bing, X. Y., Belleannee, C., Kucukural, A., Serra, R. W., Sun, F., Song, L., Carone, B. R., Ricci, E. P., Li, X. Z., Fauquier, L., Moore, M. J., Sullivan, R., Mello, C. C., Garber, M., & Rando, O. J. (2016). Biogenesis and function of tRNA fragments during sperm maturation and fertilization in mammals. *Science*, *351*(6271), 391-396. https://doi.org/10.1126/science.aad6780

Shimizu, S., Ishino, Y., Tohyama, M., & Miyata, S. (2018). NDE1 positively regulates oligodendrocyte morphological differentiation. *Sci Rep*, *8*(1), 7644. https://doi.org/10.1038/s41598-018-25898-4

Shindo, M., Tsumura, H., Miyado, K., Kang, W., Kawano, N., Yoshida, T., Fukami, M., & Miyado, M. (2021). Similar responsiveness between C57BL/6N and C57BL/6J mouse substrains to superovulation. *MicroPubl Biol*, *2021*. https://doi.org/10.17912/micropub.biology.000375

Shook, B. A., Wasko, R. R., Mano, O., Rutenberg-Schoenberg, M., Rudolph, M. C., Zirak, B., Rivera-Gonzalez, G. C., Lopez-Giraldez, F., Zarini, S., Rezza,

A., Clark, D. A., Rendl, M., Rosenblum, M. D., Gerstein, M. B., & Horsley, V. (2020). Dermal Adipocyte Lipolysis and Myofibroblast Conversion Are Required for Efficient Skin Repair. *Cell Stem Cell*, *26*(6), 880-895 e886. https://doi.org/10.1016/j.stem.2020.03.013

Shor, B., Wu, J., Shakey, Q., Toral-Barza, L., Shi, C., Follettie, M., & Yu, K. (2010). Requirement of the mTOR kinase for the regulation of Maf1 phosphorylation and control of RNA polymerase III-dependent transcription in cancer cells. *J Biol Chem*, *285*(20), 15380-15392. https://doi.org/10.1074/jbc.M109.071639

Simmons, J., & Gallo, R. L. (2024). The Central Roles of Keratinocytes in Coordinating Skin Immunity. *J Invest Dermatol*, *144*(11), 2377-2398. https://doi.org/10.1016/j.jid.2024.06.1280

Simoni, M., Gromoll, J., & Nieschlag, E. (1997). The follicle-stimulating hormone receptor: biochemistry, molecular biology, physiology, and pathophysiology. *Endocr Rev*, *18*(6), 739-773. https://doi.org/10.1210/edrv.18.6.0320

Singh, D., Rai, V., & Agrawal, D. K. (2023). Regulation of Collagen I and Collagen III in Tissue Injury and Regeneration. *Cardiol Cardiovasc Med*, *7*(1), 5-16. https://doi.org/10.26502/fccm.92920302

Slack, C., Alic, N., Foley, A., Cabecinha, M., Hoddinott, M. P., & Partridge, L. (2015). The Ras-Erk-ETS-Signaling Pathway Is a Drug Target for Longevity. *Cell*, *162*(1), 72-83. https://doi.org/10.1016/j.cell.2015.06.023

Somasundaram, I., Jain, S. M., Blot-Chabaud, M., Pathak, S., Banerjee, A., Rawat, S., Sharma, N. R., & Duttaroy, A. K. (2024). Mitochondrial dysfunction and its association with age-related disorders. *Front Physiol*, *15*, 1384966. https://doi.org/10.3389/fphys.2024.1384966

Sornson, M. W., Wu, W., Dasen, J. S., Flynn, S. E., Norman, D. J., O'Connell, S. M., Gukovsky, I., Carriere, C., Ryan, A. K., Miller, A. P., Zuo, L., Gleiberman, A. S., Andersen, B., Beamer, W. G., & Rosenfeld, M. G. (1996). Pituitary lineage determination by the Prophet of Pit-1 homeodomain factor defective in Ames dwarfism. *Nature*, *384*(6607), 327-333. https://doi.org/10.1038/384327a0

Sriskanthadevan-Pirahas, S., Deshpande, R., Lee, B., & Grewal, S. S. (2018). Ras/ERK-signalling promotes tRNA synthesis and growth via the RNA polymerase III repressor Maf1 in Drosophila. *PLoS Genet*, *14*(2), e1007202. https://doi.org/10.1371/journal.pgen.1007202

Stábile, L. A., Mendes, C. M., Hamilton, T. R. d. S., Goissis, M. D., Alves, Á. d. M., Nichi, M., Barbosa-Moyano, H., Garcia-Gomes, M. d. S. A., Mori, C. M. C., Visintin, J. A., & Assumpção, M. E. O. D. Á. (2025). Age-related decline in behavior and reproductive health in male mice. *Scientific Reports*, *15*(1), 22366. https://doi.org/10.1038/s41598-025-08743-3

Ståhl, P. L., Salmén, F., Vickovic, S., Lundmark, A., Navarro, J. F., Magnusson, J., Giacomello, S., Asp, M., Westholm, J. O., Huss, M., Mollbrink, A., Linnarsson, S., Codeluppi, S., Borg, Å., Pontén, F., Costea, P. I., Sahlén, P., Mulder, J., Bergmann, O.,…Frisén, J. (2016). Visualization and analysis of gene expression in tissue sections by spatial transcriptomics. *Science*, *353*(6294), 78-82. https://doi.org/10.1126/science.aaf2403

Stark, M. J., Hodyl, N. A., Wright, I. M., & Clifton, V. L. (2011). Influence of sex and glucocorticoid exposure on preterm placental pro-oxidant-antioxidant balance. *Placenta*, *32*(11), 865-870. https://doi.org/10.1016/j.placenta.2011.08.010

Stearns, S. C. (1992). *The evolution of life histories*. Oxford University Press. Publisher description http://www.loc.gov/catdir/enhancements/fy0604/91034726-d.html

Table of contents only http://www.loc.gov/catdir/enhancements/fy0604/91034726-t.html
Stenkula, K. G., & Erlanson-Albertsson, C. (2018). Adipose cell size: importance in health and disease. *American Journal of Physiology-Regulatory, Integrative and Comparative Physiology*, *315*(2), R284-R295. https://doi.org/10.1152/ajpregu.00257.2017
Stocco, C. (2008). Aromatase expression in the ovary: hormonal and molecular regulation. *Steroids*, *73*(5), 473-487. https://doi.org/10.1016/j.steroids.2008.01.017
Strbo, N., Younis, S., Frasca, D., & Paganelli, A. (2025). Skin aging and immunosenescence. *Exploration of Immunology*, *5*, 1003218. https://doi.org/10.37349/ei.2025.1003218
Streeper, R. S., Grueter, C. A., Salomonis, N., Cases, S., Levin, M. C., Koliwad, S. K., Zhou, P., Hirschey, M. D., Verdin, E., & Farese, R. V., Jr. (2012). Deficiency of the lipid synthesis enzyme, DGAT1, extends longevity in mice. *Aging (Albany NY)*, *4*(1), 13-27. https://doi.org/10.18632/aging.100424
Su, K. H., & Dai, C. (2017). mTORC1 senses stresses: Coupling stress to proteostasis. *Bioessays*, *39*(5). https://doi.org/10.1002/bies.201600268
Sundberg, J. P., Brown, K., & McMahon, W. M. (1994). Chronic ulcerative dermatitis in black mice. In *In J. P. Sundberg (Ed.), Handbook of mouse mutations with skin and hair abnormalities: animal models and biomedical tools. (pp. 485–492). Bar Harbor: CRC Press*.
Sundberg, J. P., Taylor, D., Lorch, G., Miller, J., Silva, K. A., Sundberg, B. A., Roopenian, D., Sperling, L., Ong, D., King, L. E., & Everts, H. (2011). Primary Follicular Dystrophy With Scarring Dermatitis in C57BL/6 Mouse Substrains Resembles Central Centrifugal Cicatricial Alopecia in Humans. *Veterinary Pathology*, *48*(2), 513-524. https://doi.org/10.1177/0300985810379431
Takeo, M., Lee, W., & Ito, M. (2015). Wound healing and skin regeneration. *Cold Spring Harb Perspect Med*, *5*(1), a023267. https://doi.org/10.1101/cshperspect.a023267
Tamano, S., Hagiwara, A., Shibata, M. A., Kurata, Y., Fukushima, S., & Ito, N. (1988). Spontaneous tumors in aging (C57BL/6N x C3H/HeN)F1 (B6C3F1) mice. *Toxicol Pathol*, *16*(3), 321-326. https://doi.org/10.1177/019262338801600302
Tanaka, T., Narazaki, M., & Kishimoto, T. (2014). IL-6 in Inflammation, Immunity, and Disease. *Cold Spring Harbor Perspectives in Biology*, *6*(10), a016295-a016295. https://doi.org/10.1101/cshperspect.a016295
Tanaka, Y., Matsuo, K., & Yuzuriha, S. (2011). Near-Infrared Irradiation Non-thermally Affects Subcutaneous Adipocytes and Bones. *Eplasty*, *11*, e12. https://www.ncbi.nlm.nih.gov/pubmed/21408032
Tang, J., Ju, A., Li, B., Zhang, S., Gong, Y., Ma, B., Jiang, Y., Liu, H., Fu, Y., & Luo, Y. (2021). Young and Undamaged rMSA Improves the Healthspan and Lifespan of Mice. *Biomolecules*, *11*(8). https://doi.org/10.3390/biom11081191
Tao, Z., & Cheng, Z. (2023). Hormonal regulation of metabolism-recent lessons learned from insulin and estrogen. *Clin Sci (Lond)*, *137*(6), 415-434. https://doi.org/10.1042/cs20210519
Tatar, M., Kopelman, A., Epstein, D., Tu, M. P., Yin, C. M., & Garofalo, R. S. (2001). A mutant Drosophila insulin receptor homolog that extends life-span and impairs neuroendocrine function. *Science*, *292*(5514), 107-110. https://doi.org/10.1126/science.1057987

Templeman, N. M., & Murphy, C. T. (2018). Regulation of reproduction and longevity by nutrient-sensing pathways. *J Cell Biol*, *217*(1), 93-106. https://doi.org/10.1083/jcb.201707168

Terhal, P. A., Vlaar, J. M., Middelkamp, S., Nievelstein, R. A. J., Nikkels, P. G. J., Ross, J., Creton, M., Bos, J. W., Voskuil-Kerkhof, E. S. M., Cuppen, E., Knoers, N., & van Gassen, K. L. I. (2020). Biallelic variants in POLR3GL cause endosteal hyperostosis and oligodontia. *Eur J Hum Genet*, *28*(1), 31-39. https://doi.org/10.1038/s41431-019-0427-0

Tetreault, M., Choquet, K., Orcesi, S., Tonduti, D., Balottin, U., Teichmann, M., Fribourg, S., Schiffmann, R., Brais, B., Vanderver, A., & Bernard, G. (2011). Recessive mutations in POLR3B, encoding the second largest subunit of Pol III, cause a rare hypomyelinating leukodystrophy. *Am J Hum Genet*, *89*(5), 652-655. https://doi.org/10.1016/j.ajhg.2011.10.006

Thiffault, I., Wolf, N. I., Forget, D., Guerrero, K., Tran, L. T., Choquet, K., Lavallee-Adam, M., Poitras, C., Brais, B., Yoon, G., Sztriha, L., Webster, R. I., Timmann, D., van de Warrenburg, B. P., Seeger, J., Zimmermann, A., Mate, A., Goizet, C., Fung, E.,…Bernard, G. (2015). Recessive mutations in POLR1C cause a leukodystrophy by impairing biogenesis of RNA polymerase III. *Nat Commun*, *6*, 7623. https://doi.org/10.1038/ncomms8623

Thornton, M. J. (2002). The biological actions of estrogens on skin. *Exp Dermatol*, *11*(6), 487-502. https://doi.org/10.1034/j.1600-0625.2002.110601.x

Tian, K., Wang, R., Huang, J., Wang, H., & Ji, X. (2023). Subcellular localization shapes the fate of RNA polymerase III. *Cell Rep*, *42*(8), 112941. https://doi.org/10.1016/j.celrep.2023.112941

Toyoshima, S., & Okayama, Y. (2022). Neuro-allergology: Mast cell–nerve cross-talk. *Allergology International*, *71*(3), 288-293. https://doi.org/10.1016/j.alit.2022.04.002

Trefts, E., Gannon, M., & Wasserman, D. H. (2017). The liver. *Curr Biol*, *27*(21), R1147-R1151. https://doi.org/10.1016/j.cub.2017.09.019

Trier, A. M., Mack, M. R., & Kim, B. S. (2019). The Neuroimmune Axis in Skin Sensation, Inflammation, and Immunity. *J Immunol*, *202*(10), 2829-2835. https://doi.org/10.4049/jimmunol.1801473

Turowski, T. W., & Tollervey, D. (2016). Transcription by RNA polymerase III: insights into mechanism and regulation. *Biochem Soc Trans*, *44*(5), 1367-1375. https://doi.org/10.1042/BST20160062

Tynes, V. V. (2013). Behavioral Dermatopathies in Small Mammals. *Veterinary Clinics of North America: Exotic Animal Practice*, *16*(3), 801-820. https://doi.org/10.1016/j.cvex.2013.05.004

Um, S. H., D'Alessio, D., & Thomas, G. (2006). Nutrient overload, insulin resistance, and ribosomal protein S6 kinase 1, S6K1. *Cell Metab*, *3*(6), 393-402. https://doi.org/10.1016/j.cmet.2006.05.003

Upadhya, R., Lee, J., & Willis, I. M. (2002). Maf1 is an essential mediator of diverse signals that repress RNA polymerase III transcription. *Mol Cell*, *10*(6), 1489-1494. https://doi.org/10.1016/s1097-2765(02)00787-6

Urena, E., Xu, B., Regan, J. C., Atilano, M. L., Minkley, L. J., Filer, D., Lu, Y. X., Bolukbasi, E., Khericha, M., Alic, N., & Partridge, L. (2024). Trametinib ameliorates aging-associated gut pathology in Drosophila females by reducing Pol III activity in intestinal stem cells. *Proc Natl Acad Sci U S A*, *121*(4), e2311313121. https://doi.org/10.1073/pnas.2311313121

Valabhji, J., Barron, E., Pratt, A., Hafezparast, N., Dunbar-Rees, R., Turner, E. B., Roberts, K., Mathews, J., Deegan, R., Cornelius, V., Pickles, J., Wainman, G., Bakhai, C., Johnston, D. G., Gregg, E. W., & Khunti, K. (2024). Prevalence of multiple long-term conditions (multimorbidity) in England: a

whole population study of over 60 million people. *J R Soc Med*, *117*(3), 104-117. https://doi.org/10.1177/01410768231206033
Valeri, M., & Raffatellu, M. (2016). Cytokines IL-17 and IL-22 in the host response to infection. *Pathog Dis*, *74*(9). https://doi.org/10.1093/femspd/ftw111
Van Kempen, T. A., Milner, T. A., & Waters, E. M. (2011). Accelerated ovarian failure: a novel, chemically induced animal model of menopause. *Brain Res*, *1379*, 176-187. https://doi.org/10.1016/j.brainres.2010.12.064
Vanhooren, V., & Libert, C. (2013). The mouse as a model organism in aging research: usefulness, pitfalls and possibilities. *Ageing Res Rev*, *12*(1), 8-21. https://doi.org/10.1016/j.arr.2012.03.010
Vellai, T., Takacs-Vellai, K., Zhang, Y., Kovacs, A. L., Orosz, L., & Muller, F. (2003). Genetics: influence of TOR kinase on lifespan in C. elegans. *Nature*, *426*(6967), 620. https://doi.org/10.1038/426620a
Verberne, E. A., Dalen Meurs, L., Wolf, N. I., & van Haelst, M. M. (2020). 4H leukodystrophy caused by a homozygous POLR3B mutation: Further delineation of the phenotype. *Am J Med Genet A*, *182*(7), 1776-1779. https://doi.org/10.1002/ajmg.a.61600
Vihko, K. K. (1996). Gonadotropins and ovarian gonadotropin receptors during the perimenopausal transition period. *Maturitas*, *23 Suppl*, S19-22. https://doi.org/10.1016/0378-5122(96)01006-7
Wall, E. G., Desai, R., Khant Aung, Z., Yeo, S. H., Grattan, D. R., Handelsman, D. J., & Herbison, A. E. (2023). Unexpected Plasma Gonadal Steroid and Prolactin Levels Across the Mouse Estrous Cycle. *Endocrinology*, *164*(6). https://doi.org/10.1210/endocr/bqad070
Wambach, J. A., Wegner, D. J., Patni, N., Kircher, M., Willing, M. C., Baldridge, D., Xing, C., Agarwal, A. K., Vergano, S. A. S., Patel, C., Grange, D. K., Kenney, A., Najaf, T., Nickerson, D. A., Bamshad, M. J., Cole, F. S., & Garg, A. (2018). Bi-allelic POLR3A Loss-of-Function Variants Cause Autosomal-Recessive Wiedemann-Rautenstrauch Syndrome. *Am J Hum Genet*, *103*(6), 968-975. https://doi.org/10.1016/j.ajhg.2018.10.010
Wang, B., Han, J., Elisseeff, J. H., & Demaria, M. (2024). The senescence-associated secretory phenotype and its physiological and pathological implications. *Nat Rev Mol Cell Biol*, *25*(12), 958-978. https://doi.org/10.1038/s41580-024-00727-x
Wang, H., Wang, G., Banerjee, N., Liang, Y., Du, X., Boor, P. J., Hoffman, K. L., & Khan, M. F. (2021). Aberrant Gut Microbiome Contributes to Intestinal Oxidative Stress, Barrier Dysfunction, Inflammation and Systemic Autoimmune Responses in MRL/lpr Mice. *Front Immunol*, *12*, 651191. https://doi.org/10.3389/fimmu.2021.651191
Wang, J., Cui, B., Chen, Z., & Ding, X. (2022). The regulation of skin homeostasis, repair and the pathogenesis of skin diseases by spatiotemporal activation of epidermal mTOR signaling. *Front Cell Dev Biol*, *10*, 950973. https://doi.org/10.3389/fcell.2022.950973
Wang, S., Ren, J., Jing, Y., Qu, J., & Liu, G.-H. (2024). Perspectives on biomarkers of reproductive aging for fertility and beyond. *Nature Aging*, *4*(12), 1697-1710. https://doi.org/10.1038/s43587-024-00770-5
Wang, Z., Man, M. Q., Li, T., Elias, P. M., & Mauro, T. M. (2020). Aging-associated alterations in epidermal function and their clinical significance. *Aging (Albany NY)*, *12*(6), 5551-5565. https://doi.org/10.18632/aging.102946
Watt, K. E., Macintosh, J., Bernard, G., & Trainor, P. A. (2023). RNA Polymerases I and III in development and disease. *Semin Cell Dev Biol*, *136*, 49-63. https://doi.org/10.1016/j.semcdb.2022.03.027

Weaver, C. T., Elson, C. O., Fouser, L. A., & Kolls, J. K. (2013). The Th17 pathway and inflammatory diseases of the intestines, lungs, and skin. *Annu Rev Pathol*, *8*, 477-512. https://doi.org/10.1146/annurev-pathol-011110-130318

Wei, Y., Tsang, C. K., & Zheng, X. F. (2009). Mechanisms of regulation of RNA polymerase III-dependent transcription by TORC1. *EMBO J*, *28*(15), 2220-2230. https://doi.org/10.1038/emboj.2009.179

Weston, C. J., Zimmermann, H. W., & Adams, D. H. (2019). The Role of Myeloid-Derived Cells in the Progression of Liver Disease [Review]. *Frontiers in Immunology*, *Volume 10 - 2019*. https://doi.org/10.3389/fimmu.2019.00893

Williams, E. G., Pfister, N., Roy, S., Statzer, C., Haverty, J., Ingels, J., Bohl, C., Hasan, M., Čuklina, J., Bühlmann, P., Zamboni, N., Lu, L., Ewald, C. Y., Williams, R. W., & Aebersold, R. (2022). Multiomic profiling of the liver across diets and age in a diverse mouse population. *Cell Systems*, *13*(1), 43-57.e46. https://doi.org/10.1016/j.cels.2021.09.005

Williams, G. C. (1957). PLEIOTROPY, NATURAL SELECTION, AND THE EVOLUTION OF SENESCENCE. *Evolution*, *11*(4), 398-411. https://doi.org/https://doi.org/10.1111/j.1558-5646.1957.tb02911.x

Williams, L. K., Csaki, L. S., Cantor, R. M., Reue, K., & Lawson, G. W. (2012). Ulcerative dermatitis in C57BL/6 mice exhibits an oxidative stress response consistent with normal wound healing. *Comparative Medicine*, *62*(3), 166-171. https://www.ncbi.nlm.nih.gov/pubmed/22776048

Williams-Fritze, M. J., Carlson Scholz, J. A., Zeiss, C., Deng, Y., Wilson, S. R., Franklin, R., & Smith, P. C. (2011). Maropitant citrate for treatment of ulcerative dermatitis in mice with a C57BL/6 background. *Journal of the American Association for Laboratory Animal Science*, *50*(2), 221-226. https://pubmed.ncbi.nlm.nih.gov/21439216/

Willis, I. M., & Moir, R. D. (2018). Signaling to and from the RNA Polymerase III Transcription and Processing Machinery. *Annu Rev Biochem*, *87*, 75-100. https://doi.org/10.1146/annurev-biochem-062917-012624

Woiwode, A., Johnson, S. A., Zhong, S., Zhang, C., Roeder, R. G., Teichmann, M., & Johnson, D. L. (2008). PTEN represses RNA polymerase III-dependent transcription by targeting the TFIIIB complex. *Mol Cell Biol*, *28*(12), 4204-4214. https://doi.org/10.1128/MCB.01912-07

Wolf, N. I., Vanderver, A., van Spaendonk, R. M., Schiffmann, R., Brais, B., Bugiani, M., Sistermans, E., Catsman-Berrevoets, C., Kros, J. M., Pinto, P. S., Pohl, D., Tirupathi, S., Stromme, P., de Grauw, T., Fribourg, S., Demos, M., Pizzino, A., Naidu, S., Guerrero, K.,…Group, H. R. (2014). Clinical spectrum of 4H leukodystrophy caused by POLR3A and POLR3B mutations. *Neurology*, *83*(21), 1898-1905. https://doi.org/10.1212/WNL.0000000000001002

Wolff, C. A., Lawrence, M. M., Porter, H., Zhang, Q., Reid, J. J., Laurin, J. L., Musci, R. V., Linden, M. A., Peelor, F. F., 3rd, Wren, J. D., Creery, J. S., Cutler, K. J., Carson, R. H., Price, J. C., Hamilton, K. L., & Miller, B. F. (2021). Sex differences in changes of protein synthesis with rapamycin treatment are minimized when metformin is added to rapamycin. *Geroscience*, *43*(2), 809-828. https://doi.org/10.1007/s11357-020-00243-8

Won, Y. S., Kwon, H. J., Oh, G. T., Kim, B. H., Lee, C. H., Park, Y. H., Hyun, B. H., & Choi, Y. K. (2002). Identification of Staphylococcus xylosus Isolated from C57BL/6J-Nos2tm1Lau Mice with Dermatitis. *Microbiology and Immunology*, *46*(9), 629-632. https://doi.org/10.1111/j.1348-0421.2002.tb02744.x

Wu, C., Chen, D., Stout, M. B., Wu, M., & Wang, S. (2025). Hallmarks of ovarian aging. *Trends in Endocrinology & Metabolism*, *36*(5), 418-439. https://doi.org/10.1016/j.tem.2025.01.005

Wu, J. J., Liu, J., Chen, E. B., Wang, J. J., Cao, L., Narayan, N., Fergusson, M. M., Rovira, II, Allen, M., Springer, D. A., Lago, C. U., Zhang, S., DuBois, W., Ward, T., deCabo, R., Gavrilova, O., Mock, B., & Finkel, T. (2013). Increased mammalian lifespan and a segmental and tissue-specific slowing of aging after genetic reduction of mTOR expression. *Cell Rep*, *4*(5), 913-920. https://doi.org/10.1016/j.celrep.2013.07.030

Wu, L., Pan, J., Thoroddsen, V., Wysong, D. R., Blackman, R. K., Bulawa, C. E., Gould, A. E., Ocain, T. D., Dick, L. R., Errada, P., Dorr, P. K., Parkinson, T., Wood, T., Kornitzer, D., Weissman, Z., Willis, I. M., & McGovern, K. (2003). Novel small-molecule inhibitors of RNA polymerase III. *Eukaryot Cell*, *2*(2), 256-264. https://doi.org/10.1128/EC.2.2.256-264.2003

Wu, S. W., Li, L., Feng, F., Wang, L., Kong, Y. Y., Liu, X. W., & Yin, C. (2021). Whole-exome sequencing reveals POLR3B variants associated with progeria-related Wiedemann-Rautenstrauch syndrome. *Ital J Pediatr*, *47*(1), 160. https://doi.org/10.1186/s13052-021-01112-6

Wulff, B. C., & Wilgus, T. A. (2013). Mast cell activity in the healing wound: more than meets the eye? *Exp Dermatol*, *22*(8), 507-510. https://doi.org/10.1111/exd.12169

Wynn, T. A. (2008). Cellular and molecular mechanisms of fibrosis. *J Pathol*, *214*(2), 199-210. https://doi.org/10.1002/path.2277

Xu, B., Hull, A., Hill, O. N. M., Kobal, N., Urena, E., Partridge, L., & Alic, N. (2025). Loss of Pol III repressor Maf1 in neurons promotes longevity by preventing the age-related decline in 5S rRNA and translation. *PLoS Biol*, *23*(7), e3003250. https://doi.org/10.1371/journal.pbio.3003250

Yanina, I. Y., Tuchin, V. V., Navolokin, N. A., Matveeva, O. V., Bucharskaya, A. B., Maslyakova, G. N., & Altshuler, G. B. (2012). Fat tissue histological study at indocyanine green-mediated photothermal/photodynamic treatment of the skin in vivo. *J Biomed Opt*, *17*(5), 058002. https://doi.org/10.1117/1.JBO.17.5.058002

Yao, X., Huang, J., Zhong, H., Shen, N., Faggioni, R., Fung, M., & Yao, Y. (2014). Targeting interleukin-6 in inflammatory autoimmune diseases and cancers. *Pharmacology & Therapeutics*, *141*(2), 125-139. https://doi.org/10.1016/j.pharmthera.2013.09.004

Ye, J., & Lai, Y. (2025). Keratinocytes: new perspectives in inflammatory skin diseases. *Trends Mol Med*, *31*(12), 1103-1113. https://doi.org/10.1016/j.molmed.2025.03.012

Yee, N. S., Gong, W., Huang, Y., Lorent, K., Dolan, A. C., Maraia, R. J., & Pack, M. (2007). Mutation of RNA Pol III subunit rpc2/polr3b Leads to Deficiency of Subunit Rpc11 and disrupts zebrafish digestive development. *PLoS Biol*, *5*(11), e312. https://doi.org/10.1371/journal.pbio.0050312

Yeh, S., Tsai, M. Y., Xu, Q., Mu, X. M., Lardy, H., Huang, K. E., Lin, H., Yeh, S. D., Altuwaijri, S., Zhou, X., Xing, L., Boyce, B. F., Hung, M. C., Zhang, S., Gan, L., & Chang, C. (2002). Generation and characterization of androgen receptor knockout (ARKO) mice: an in vivo model for the study of androgen functions in selective tissues. *Proc Natl Acad Sci U S A*, *99*(21), 13498-13503. https://doi.org/10.1073/pnas.212474399

Yi, Y., Huang, C., Zhang, Y., Tian, S., Lei, J., Chen, S., Shi, G., Wu, Z., Xia, N., & Zhong, S. (2017). Exploring a common mechanism of alcohol-induced deregulation of RNA Pol III genes in liver and breast cells. *Gene*, *626*, 309-318. https://doi.org/10.1016/j.gene.2017.05.048

Yoo, K. S., Lim, W. T., & Choi, H. S. (2016). Biology of Cholangiocytes: From Bench to Bedside. *Gut Liver*, *10*(5), 687-698. https://doi.org/10.5009/gnl16033

Younan, G. J., Heit, Y. I., Dastouri, P., Kekhia, H., Xing, W., Gurish, M. F., & Orgill, D. P. (2011). Mast cells are required in the proliferation and remodeling phases of microdeformational wound therapy. *Plast Reconstr Surg*, *128*(6), 649e-658e. https://doi.org/10.1097/PRS.0b013e318230c55d

Young, C. W., Legates, J. E., & Farthing, B. R. (1965). PRENATAL AND POSTNATAL INFLUENCES ON GROWTH, PROLIFICACY AND MATERNAL PERFORMANCE IN MICE. *Genetics*, *52*(3), 553-561. https://doi.org/10.1093/genetics/52.3.553

Yuan, R., Hascup, E., Hascup, K., & Bartke, A. (2023). Relationships among Development, Growth, Body Size, Reproduction, Aging, and Longevity - Trade-Offs and Pace-Of-Life. *Biochemistry (Mosc)*, *88*(11), 1692-1703. https://doi.org/10.1134/S0006297923110020

Zaragoza, D., Ghavidel, A., Heitman, J., & Schultz, M. C. (1998). Rapamycin induces the G0 program of transcriptional repression in yeast by interfering with the TOR signaling pathway. *Mol Cell Biol*, *18*(8), 4463-4470. https://doi.org/10.1128/MCB.18.8.4463

Zhang, C., Zhao, S., Deng, H., Zhang, S., Wang, J., Song, X., Yu, D., Zhang, Y., & Deng, W. (2023). STAT3 promotes RNA polymerase III-directed transcription by controlling the miR-106a-5p/TP73 axis. *Elife*, *12*. https://doi.org/10.7554/eLife.82826

Zhang, J., Powell, C. A., Kay, M. K., Sonkar, R., Meruvu, S., & Choudhury, M. (2021). Effect of Chronic Western Diets on Non-Alcoholic Fatty Liver of Male Mice Modifying the PPAR-gamma Pathway via miR-27b-5p Regulation. *Int J Mol Sci*, *22*(4). https://doi.org/10.3390/ijms22041822

Zhang, K., Chen, S., Yang, Q., Guo, S., Chen, Q., Liu, Z., Li, L., Jiang, M., Li, H., Hu, J., Pan, X., Deng, W., Xiao, N., Wang, B., Wang, Z.-x., Zhang, L., & Mo, W. (2022). The Oligodendrocyte Transcription Factor 2 OLIG2 regulates transcriptional repression during myelinogenesis in rodents. *Nature Communications*, *13*(1), 1423. https://doi.org/10.1038/s41467-022-29068-z

Zhang, T., Ma, C., Zhang, Z., Zhang, H., & Hu, H. (2021). NF-kappaB signaling in inflammation and cancer. *MedComm (2020)*, *2*(4), 618-653. https://doi.org/10.1002/mco2.104

Zhang, X., Zhang, L., & Xiang, W. (2025). The impact of mitochondrial dysfunction on ovarian aging. *J Transl Med*, *23*(1), 211. https://doi.org/10.1186/s12967-025-06223-w

Zhang, Y., Bokov, A., Gelfond, J., Soto, V., Ikeno, Y., Hubbard, G., Diaz, V., Sloane, L., Maslin, K., Treaster, S., Rendon, S., van Remmen, H., Ward, W., Javors, M., Richardson, A., Austad, S. N., & Fischer, K. (2014). Rapamycin extends life and health in C57BL/6 mice. *J Gerontol A Biol Sci Med Sci*, *69*(2), 119-130. https://doi.org/10.1093/gerona/glt056

Zhang, Y., Li, Q., Rao, E., Sun, Y., Grossmann, M. E., Morris, R. J., Cleary, M. P., & Li, B. (2015). Epidermal Fatty Acid Binding Protein Promotes Skin Inflammation Induced by High-Fat Diet. *Immunity*, *42*(5), 953-964. https://doi.org/10.1016/j.immuni.2015.04.016

Zhang, Y., Zhang, L. S., Dai, Q., Chen, P., Lu, M., Kairis, E. L., Murugaiah, V., Xu, J., Shukla, R. K., Liang, X., Zou, Z., Cormet-Boyaka, E., Qiu, J., Peeples, M. E., Sharma, A., He, C., & Li, J. (2022). 5-methylcytosine (m(5)C) RNA modification controls the innate immune response to virus infection by regulating type I interferons. *Proc Natl Acad Sci U S A*, *119*(42), e2123338119. https://doi.org/10.1073/pnas.2123338119

Zhang, Z., Kruglikov, I., Zhao, S., Zi, Z., Gliniak, C. M., Li, N., Wang, M. Y., Zhu, Q., Kusminski, C. M., & Scherer, P. E. (2021). Dermal adipocytes contribute to the metabolic regulation of dermal fibroblasts. *Exp Dermatol*, *30*(1), 102-111. https://doi.org/10.1111/exd.14181

Zhang, Z., Shang, J., Yang, Q., Dai, Z., Liang, Y., Lai, C., Feng, T., Zhong, D., Zou, H., Sun, L., Su, Y., Yan, S., Chen, J., Yao, Y., Shi, Y., & Huang, X. (2023). Exosomes derived from human adipose mesenchymal stem cells ameliorate hepatic fibrosis by inhibiting PI3K/Akt/mTOR pathway and remodeling choline metabolism. *J Nanobiotechnology*, *21*(1), 29. https://doi.org/10.1186/s12951-023-01788-4

Zhao, Y., Ye, X., Dunker, W., Song, Y., & Karijolich, J. (2018). RIG-I like receptor sensing of host RNAs facilitates the cell-intrinsic immune response to KSHV infection. *Nat Commun*, *9*(1), 4841. https://doi.org/10.1038/s41467-018-07314-7

Zhao, Y., Zhao, S., Liu, S., Ye, W., & Chen, W.-d. (2025). Kupffer cells, the limelight in the liver regeneration. *International Immunopharmacology*, *146*, 113808. https://doi.org/https://doi.org/10.1016/j.intimp.2024.113808

Zhong, S., Machida, K., Tsukamoto, H., & Johnson, D. L. (2011). Alcohol induces RNA polymerase III-dependent transcription through c-Jun by co-regulating TATA-binding protein (TBP) and Brf1 expression. *J Biol Chem*, *286*(4), 2393-2401. https://doi.org/10.1074/jbc.M110.192955